

Microwave and functional materials: a novel
strategy for detecting toxic metals in polluted
freshwater

Ilaria Frau

A thesis submitted in partial fulfilment of the requirements
of Liverpool John Moores University for the degree of
Doctor of Philosophy

October 2020

Dedicated to

Irene

Abstract

Worldwide, thousands of pollutants threaten freshwater and environmental health. Therefore, toxic metals from point and diffuse sources in abandoned mining areas need to be efficiently managed and monitored.

As of yet, no method can measure toxic metals in water, *in situ* and in real-time, guaranteeing a clear picture of water quality continuously. Microwave spectroscopy has been shown to give a real-time response dependent on the sample composition as soon as a water sample interacts with the electromagnetic waves.

Consequently, this work aims to specialise microwave sensors to monitor toxic metals in mining-impacted water. Planar microwave sensors have been integrated with mixtures of materials (such as metal oxides and chelating polymers) using screen-printing technology. These novel sensing structures are defined as functionalised electromagnetic sensors (f-EM sensors). F-EM sensors, compared with uncoated sensors, were able to qualify with higher sensitivity and selectivity toxic metals (Zn and Cu) in simple lab-prepared solutions at various concentrations.

F-EM sensors were then adapted to directly probe water samples and tested in the laboratory with collected freshwater samples using the standard addition method. Data were analysed using a novel approach based on multiple peak analysis at selected frequencies. Subsequently, f-EM sensors were tested *in situ* in mining-impacted water in four polluted mining areas in the UK. The results were compared and the possibility to qualify and differentiate *in situ* polluted water was assessed.

In conclusion, a combination of various f-EM sensors, defined as an *f-EM sensor array*, is a valuable solution for monitoring and managing contaminated freshwater resources, by providing practical, rapid, *in situ* and low-cost measurements for evaluating unexpected variations in water composition.

Acknowledgements

I would like to thank the fabulous people who have supported me, professionally and personally, during this fantastic and challenging journey. Specifically, I want to offer my thanks to my Lead Supervisor, Dr Steve Wylie, for his incredible guidance, corrections, and recommendations; my Co-supervisors, Dr Patrick Byrne, for his constant help and support, and for involving me in other exciting environmental projects and Dr Jeff Cullen, for his practical assistance and valuable suggestions; and my Industrial Advisor, Prof Alex Mason, for his brilliant recommendations and knowledge sharing. An immense thank you to Prof Olga Korostynska, my former Director of Studies, who guided and taught me how to be an amazing and inventive researcher, and continues to offer me assistance to my professional life. A thank you to Dr Eduardo Cordova-Lopez, for being a patient supporter and for cheering me up during stressful times. A huge thank you to Dr Patrizia Onnis, for her precious suggestions and encouragement, and for assisting with the field measurements. I would like to thank Prof David Phipps, for being a source of inspiration and discussing novel ideas. Also, I want to thank all the researchers and technicians at LJMU who have assisted me in the Engineering and Science laboratories, including Peter Moran, Montserrat Ortoneda Pedrola, Paul Gibbons, Dave Williams, Hazel Clarke, Nicola Dempster, Robert Allen. Moreover, I would like to thank Prof Rafid Al Khaddar, Prof Ahmed Al-Shamma'a and the Doctoral Academy for their financial support to attend two international conferences. As well, I want to thank my office mates and PGR colleagues for being there with me during pleasant and tough times, and Victoria and Jo (from the Doctoral Academy), for providing the very productive writing sessions. Last but not least, I want to thank my beloved parents and Irene for their continual support; Silvia, for her encouragement and friendship; my amazing friends and the researchers from the University of Cagliari, who believes in me unconditionally. Finally, a huge thank you to my lovely Graham, who supported me during these hard writing months, with patience, endless love and understanding. A sincere thank you to you all!

Table of Contents

List of figures	ix
List of tables.....	xviii
List of acronyms and abbreviations	xx
List of symbols and notations	xxiii
Chapter 1 Introduction	1
1.1 Background information.....	1
1.2 Mining areas and pollution.....	2
1.2.1 Abandoned mines and the freshwater environment.....	5
1.2.2 European and UK overview.....	8
1.2.3 Problem statement.....	10
1.3 Purpose of this study	11
1.3.1 Novelty.....	11
1.3.2 Aim and objectives	12
1.4 Chapters overview	13
Chapter 2 State-of-the-art and new trends: toxic metal analysis	16
2.1 Current methods for metal detection	16
2.1.1 Water samples collection and physicochemical parameters.....	17
2.1.2 Laboratory-based analytical detection techniques.....	19
2.1.2.1 ICP-OES.....	20
2.1.2.2 ICP-MS	21
2.1.2.3 AAS.....	22
2.1.2.4 Advantages and disadvantages.....	23
2.2 Novel strategies and frontiers for toxic metal analysis	24
2.2.1 Electrochemical methods.....	25
2.2.1.1 Stripping voltammetry	27
2.2.1.2 Potentiometry	28
2.2.1.3 Lab-on-a-chip.....	29
2.2.2 Optical sensors	29
2.2.2.1 Fibre optic sensors	29
2.2.2.2 Fluorescent colorimetric sensors.....	30
2.2.2.3 UV-Vis Spectrophotometer.....	31
2.2.3 Biosensors.....	31
2.2.4 X-Ray Fluorescence.....	32
2.2.5 Near-Infrared Diffuse Reflectance Spectroscopy	33
2.2.6 Examples of commercially available sensing devices.....	33
2.2.7 Summary of limitations	34

2.3 Novel trend: microwave spectroscopy as a potential solution	35
Chapter 3 Microwave spectroscopy	37
3.1 Introduction	37
3.2 The electromagnetic spectrum.....	37
3.2.1 Overview of EM Sensing.....	39
3.3 Microwave sensing.....	40
3.3.1 Microwave principle	41
3.3.2 Microwave measurements	42
3.3.3 High adaptability: current research and applications.....	45
3.3.4 Sensing structures	45
3.4 Microwaves and water.....	46
3.4.1 Microwave rotational spectroscopy	46
3.4.2 Microwave analysis of liquids	49
3.4.2.1 Resonant cavities.....	50
3.4.2.2 Planar sensors.....	52
3.4.3 Impedance measurements at low-frequencies	54
3.4.4 Degraded sensitivity and lack of selectivity	55
3.4.5 Progress and challenges	56
3.5 Materials integration.....	58
3.5.1 Materials	59
3.5.1.1 Inorganic materials.....	60
3.5.1.2 Chelating polymers	61
3.5.2 Depositional methods	62
3.5.2.1 Thick-film technology.....	62
3.6 F-EM sensors.....	63
3.6.1 Proof of concept.....	64
3.6.2 Project progression and choices.....	64
Chapter 4 Research methodologies.....	65
4.1 Introduction	65
4.2 F-EM sensors development.....	66
4.2.1 Screen-printed coatings.....	66
4.2.2 Paste mixture and coatings development.....	68
4.2.2.1 Functionalised Ag eight-pair IDE on microscope slides	69
4.2.2.2 Functionalised Au eight-pair IDE on PTFE substrate (f-EM sensors)	71
4.2.3 Thicknesses measurements	76
4.3 Water samples	77
4.3.1 Lab-samples	77

4.3.2 Field samples	78
4.3.3 Physicochemical parameters.....	79
4.3.4 Effective concentration evaluation using certified methods.....	79
4.4 Measurements.....	82
4.4.1 Optical measurements.....	82
4.4.2 Low-frequency impedance measurements.....	83
4.4.2.1 Gold-plated sensor on sample	84
4.4.2.2 “Crocodile clips”	86
4.4.2.3 F-EM sensors	88
4.4.3 Microwave measurements	89
4.4.3.1 Small sample volume onto sensor.....	91
4.4.3.2 Adaptation for <i>in situ</i> measurements	94
4.4.3.2.1 Submerged sensor in water.....	94
4.4.3.2.2 Adapted standard addition method.....	96
4.4.3.2.3 Portable VNAs and <i>in situ</i> trial measurements	97
4.4.3.2.4 Slug injection trial	99
4.5 Coatings characterisation	100
4.5.1 Repeatability and Reproducibility	100
4.5.2 SEM and EDS.....	101
4.5.3 Adsorption experiment	102
4.6 Data analysis.....	103
4.6.1 Statistical features and performance evaluation	104
4.6.2 Signal analysis: curve fitting.....	105
4.6.3 Lorentzian peak fitting function	107
4.6.4 Standard addition method: analysis	108
4.7 Summary	109
Chapter 5 Results and discussion (phase 1): f-EM sensors and simple metal water solutions	110
5.1 Introduction	110
5.1.1 Proof of concept: microwave spectroscopy and toxic metals.....	111
5.1.2 Preface: developed and tested f-EM sensors	116
5.1.3 Required features	120
5.2 Lacquered sensors and Pb ions.....	120
5.2.1 Analysis, results and discussion	121
5.2.1.1 Absorbance.....	121
5.2.1.2 Impedance responses.....	122
5.2.1.3 Microwave responses	123

5.2.1.4 Comparisons between optical, impedance and microwave responses ...	125
5.3 β -Bi ₂ O ₃ based coatings and Zn ions	126
5.3.1 Analysis, results and discussion	127
5.3.1.1 Absorbance of Zn samples	128
5.3.1.2 Impedance responses.....	129
5.3.1.2.1 Zn samples.....	129
5.3.1.3 Microwave responses	131
5.3.1.3.1 F-EM sensors: coating's effect.....	134
5.3.1.4 Summary of optical, electrical and microwave measurements.....	138
5.3.1.5 Interaction between β -Bi ₂ O ₃ and Zn	140
5.3.1.5.1 Time responses using microwave and impedance measurements...	140
5.3.1.5.2 Adsorption experiment	142
5.3.1.5.3 EDS and SEM analysis.....	143
5.3.1.5.4 Recovery time.....	144
5.4 Chelating polymers based coatings and Cu detection	145
5.4.1.1 Absorbance of Cu samples.....	148
5.4.2 L-CyChRu based coating and Cu ions.....	149
5.4.2.1 Analysis, results and discussion.....	150
5.4.2.1.1 Impedance responses	151
5.4.2.1.2 Microwave responses	153
5.4.2.1.3 Summary of optical, impedance and microwave measurements....	156
5.4.3 L-CyChBCZ based coatings and Cu ions	156
5.4.3.1 Analysis, results and discussion.....	157
5.4.3.1.1 Microwave responses	157
5.4.4 Interaction of Cu with coatings based on chelating polymers	159
5.4.4.1 Durability and degradability	161
5.5 Metal oxides based coatings	163
5.6 Summary of the main findings	163
5.6.1 Lacquered sensors and Pb ions	163
5.6.2 β -Bi ₂ O ₃ based coatings and Zn ions	164
5.6.3 Chelating polymers based coatings and Cu detection	164
5.7 Overall summary and implications.....	165
Chapter 6 Results and discussion (phase 2): submerged f-EM sensors and mining-impacted waters.....	168
6.1 Introduction	168
6.1.1 Samples from mining-impacted freshwaters	169
6.1.1.1 Wemyss mine	171

6.1.1.2 Parys Mountain mining district.....	172
6.1.1.3 Nant y Mwyn mine.....	173
6.1.1.4 Leadhills mine.....	173
6.1.2 Chapter overview.....	174
6.2 Summary of materials and methods.....	175
6.2.1 Analysed samples and SAM.....	175
6.2.2 Measurements.....	175
6.2.3 Data analysis.....	176
6.3 Results and discussion: submersible microwave sensors.....	177
6.3.1 400 μ L method vs immersed sensors.....	177
6.3.2 Uncoated sensors and SAM.....	177
6.3.3 L-CyChBCZ coatings, standard addition method and field samples.....	181
6.3.3.1 C and R at low-frequencies.....	181
6.3.3.2 Uncoated and coated sensors: a comparison.....	184
6.3.3.3 ZVA 24 vs miniVNA tiny.....	186
6.3.3.3.1 Impedance correspondences.....	188
6.3.3.4 Lorentzian-peak function.....	190
6.3.3.5 Cu vs Zn.....	193
6.3.3.6 Time responses, SEM and EDS analysis.....	195
6.3.3.7 Feasibility of differentiating mining-water samples.....	198
6.3.3.8 Interferences from other factors.....	201
6.4 Summary of the main findings.....	203
6.5 Overall summary and implications.....	203
Chapter 7 Results and discussion (phase 3): <i>in situ</i> field trials and multiple f-EM sensors.....	206
7.1 Introduction.....	206
7.2 Brief recapping of materials and methods.....	206
7.2.1 f-EM sensor array.....	207
7.2.2 In situ trial measurements.....	207
7.3 Results and discussion: characterise polluted waters using multiple f-EM sensors.....	208
7.3.1 F-EM sensors: general laboratory comparisons.....	209
7.3.2 In situ analysis of polluted freshwater.....	212
7.3.2.1 Wemyss mine.....	213
7.3.2.1.1 First in situ trial measurement at Wemyss mine.....	214
7.3.2.2 Parys Mountain mining district.....	215
7.3.2.2.1 In situ trial at Parys Mountain mining district.....	216

7.3.2.3 Nant y Mwyn mine.....	219
7.3.2.3.1 In situ measurements using multiple f-EM sensors.....	221
7.3.2.4 Leadhills mine.....	225
7.3.2.5 Other <i>in situ</i> trial measurements	226
7.3.2.5.1 Results from a slug injection trial.....	226
7.3.3 Comparisons between mining-impacted water.....	229
7.3.3.1 <i>In situ</i> measurements comparisons: an overview.....	230
7.3.3.1.1 Uncoated sensors	230
7.3.3.1.2 F-EM sensors based on β -Bi ₂ O ₃ coatings.....	231
7.3.3.1.3 F-EM sensors based on L-CyChBCZ coatings.....	232
7.3.3.1.4 Lacquered sensors	233
7.3.3.1.5 F-EM sensors based on ITO coatings.....	234
7.3.3.2 Laboratory comparisons.....	235
7.3.3.3 Summary of <i>in situ</i> measurements	236
7.4 Discussion of overall results and implications	237
7.4.1 Future strategies for effective applicability	239
7.5 Overall summary and implications.....	240
Chapter 8 Conclusions	241
8.1 Limitations of the research	243
8.2 Recommendations for future research.....	243
8.2.1 Study of interferences	244
References.....	245
Appendix 1	265
Appendix 2a	266
Appendix 2b.....	267
Appendix 2c	268
Appendix 2d.....	269
Appendix 3.....	270
Appendix 4.....	271
Appendix 5a	272
Appendix 5b.....	273
List of publications.....	274
Journal articles.....	274
Book Chapters	274
Conference Proceedings	274
Awards	275

List of figures

Figure 1.1 An example of a mining area: Parys Mountain mine site (Anglesey, UK)	3
Figure 1.2 Example of a drainage adit in the Montevecchio Mine district (South-West Sardinia, Italy).....	5
Figure 1.3 Leachate from tailings heaps in Nant y Mwyn lead mine (Central Wales, UK)	6
Figure 1.4 Afon Goch River (Parys Mountain mine, Anglesey, UK)	9
Figure 1.5 Example of a functionalised electromagnetic wave sensor (f-EM sensor)....	12
Figure 2.1 Manual sample collection (a) and automatic sampler collecting programmed samples (b)	17
Figure 2.2 Example of <i>in situ</i> physicochemical parameters measurements: EC using a multi-parameters meter (a), pH using a pH meter (b) and multi-parameter probe, AQUAREAD (c).....	18
Figure 2.3 An ICP-OES at LJMU	20
Figure 2.4 An ICP-MS at LJMU.....	22
Figure 2.5 An AAS at LJMU	23
Figure 2.6 Example of research fields for water quality monitoring focused on toxic metal detection	25
Figure 2.7 ASV principle	27
Figure 2.8 Schematic image of the biosensors developed by Eltzov et al (2015) (adapted figure).....	32
Figure 2.9 Available toxic metals analysers for on-site monitoring: HM3000 form Trace ₂ O (a); PDV6000 plus from MODERN WATER (b); Nanotek2000 from Lubsun Co (c)	34
Figure 3.1 The Electromagnetic Spectrum (adapted from 2005 SURA).....	38
Figure 3.2 Scheme of EM waves propagation showing electric (E_f) and magnetic (H_f) field	39
Figure 3.3 Sketch of measurement set-up and output (S_{11} and S_{21}).....	43
Figure 3.4 Example of raw output data as a reflection coefficient from a VNA: magnitude, phase, Smith and polar	44
Figure 3.5 Examples of sensing structures for various applications within the RFM group at LJMU	46
Figure 3.6 Scheme of the polar orientation of the water molecules with the EM field at microwave frequency and molecules rotation.....	47
Figure 3.7 Example of ion hydration spheres	48
Figure 3.8 Example (group 1, period 1 in the periodic table) and their association with ionic radius, conductivity and hydration radius	48
Figure 3.9 Example of connection between analyser and sensing structure: coaxial cable and connectors (N-type and SMA)	49
Figure 3.10 Example of cylindrical and rectangular resonant cavities	51

Figure 3.11 Example of flexible and rigid planar EM sensors	52
Figure 3.12 Example of measurement set-up for a planar sensor integrated with a microfluidic system and LUT (a); its side (b) and top view (c) ((Vélez et al, 2019) modified).....	54
Figure 3.13 a DSS-SRR (a) developed and tested (b) for ethanol and DW mixtures which show improvement in sensitivity with resonance frequency shift (c) (modified from Benkhaoua et al (2016)).....	57
Figure 3.14 3D ball and stick structure model (on the top) and its sketched model (on the bottom) for L-cysteine (a) and chitosan with copper ion (b) generated and verified using Chem 3D	61
Figure 4.1 Required materials for the development of f-EM sensors: a screen-printer (1); a mesh with stencil (2); a paste mixture (3); a planar sensor (4); an oven (5) and SMA connectors and a soldering station (6).....	68
Figure 4.2 Paste mixture preparation process: specific weight of the material in powder form (a); addition of the binder (b) and addition of some drops of solvent which results in a printable paste mixture (example using β -Bi ₂ O ₃ based paste mixture)	69
Figure 4.3 Example of developed Ag IDE screen-printed on microscope slides (a) using silver paste ready-made (b) and mesh with the eight-pair IDE stencil (c).....	70
Figure 4.4 Example of some successful screen-printed coating on Ag eight-pair IDE onto microscope slides, showing their front and back view	70
Figure 4.5 Scheme with size of an Au eight-pair IDE sensor (mm) showing its front view (a), 3D view (b) and a picture of it (c)	71
Figure 4.6 Au eight-pair IDE with a PCB lacquered coating	72
Figure 4.7 Scheme of an f-EM sensor based on β -Bi ₂ O ₃ which shows the coatings (=thick film) dimension (a) and the picture of the final product with a sample holder and a soldered SMA connector.....	73
Figure 4.8 Scheme (a) and a picture of f-EM sensors based on L-CyChRu (b)	74
Figure 4.9 Scheme (a) and picture (b) f f-EM sensors based on an L-CyChBCZ coating	74
Figure 4.10 Scheme of the ITO based coating and its underlying nonconductive coating (a) and a picture of the final product (b)	75
Figure 4.11 Screen-printed f-EM sensors based on M10.....	76
Figure 4.12 Equipment used for measuring the coating thickness: an electronic micrometer (a), a vernier caliper (b) and a surface profiler (c).....	76
Figure 4.13 Example of metals standard solutions prepared under fume cupboard using 50 mL volumetric flasks (a) reading the bottom of the concave meniscus (b); then, they were placed in high-density polyethylene bottles (c).....	78
Figure 4.14 ICP-MS (a) and ICP-OES (b) at LJMU equipped with auto-samplers	80
Figure 4.15 Example of colour strips for Cu screening analysis, John's Copper (a); a read test strip is immersed in water (b) and the Cu concentration is assessed by visual colour matching (c)	81

Figure 4.16 UV-Vis Spectrophotometer and its output as absorbance spectrum at 200-1000 nm.....	83
Figure 4.17 Experimental set-up: an LCR bridge and labVIEW software interface with a bespoke coaxial probe (a) (assembled with an FR4 circuit board as shown in (b), back view, and (c), front view) measuring using a gold-plated sensing with two electrodes (rods) a water sample (400 μ L), held in place by a specific holder (as magnified in (d)) (modified from <i>Frau et al (2019a)</i>)	86
Figure 4.18 Configuration of "crocodile clips measurements" for measuring the repeatability and reproducibility of the Ag-IDE screen-printed on microscope slides (a), connected through crocodile clips (R&S HZ184 Kelvin measurable cables) elevated by a developed platform (b), connected to an LCR bridge for measuring C and R using a LabVIEW software as data acquisition (c)	87
Figure 4.19 Example of functionalised IDE connected to an LCR through crocodile clips, specifically with coatings based on l-cysteine (a), l-cysteine, chitosan and ruthenium oxide (b) and on Indium tin oxide chitosan and pyrrole, with an under-layer of dielectric material (c)	87
Figure 4.20 Uncoated (a) and functionalised IDE on microscope slides with a 400 μ L sample held in place by a specific holder (b).....	88
Figure 4.21 Example of f-EM sensor based on β -Bi ₂ O ₃ connected to the LCR bridge..	89
Figure 4.22 Scheme of the interaction principle between an incident wave produced by a VNA which interacts with a sample placed on a sensing structure and generates a reflected signal (as S ₁₁ response) at specific frequencies which is a spectrum.....	90
Figure 4.23 Configuration of S ₁₁ measurements using a Rohde and Schwarz ZVA 24 VNA using an uncoated and various f-EM sensors with 400 μ L of sample onto each one held in place by a bespoke holder	91
Figure 4.24 IDE sensors and measurements of pH calibration solutions (a), at pH 4 (b), 7 (c) and 10 (d).....	92
Figure 4.25 Portable VNAs that were tested in laboratory using the 400 μ L method onto the sensor: a ZVL13 VNA (a), a picoVNA (b), a miniVNA tiny (c) and a MS2024A VNA (d)	93
Figure 4.26 F-EM sensors embedded in 50 mL centrifuge tube lids, adapted for <i>in situ</i> measurements and correspondences of the same sensors using the 400 μ L method, described in the previous section. The f-EM sensors that are shown in this figure, from left to right, are: uncoated and based on β -Bi ₂ O ₃ , L-CyChBCZ, ITO, M10 and lacquered	95
Figure 4.27 Experimental configuration adopted for submerging the waterproofed f-EM sensor and its structure with screwable parts (a) in water sample using a VNA configured with an additional coaxial cable, a retort stand for holding the sensor in place (b) and its close-up (c).....	96
Figure 4.28 Set-up measurements using a miniVNA tiny allowing S ₁₁ measurements at one port configuration (DUT), operating via USB connection to a laptop using VNA/J software (a), and another connected using a USB OTG to a smartphone using the blueVNA software (b).....	98

Figure 4.29 Example of <i>in situ</i> measurements in two mining areas in the UK, using a laptop (a) and a smartphone (b) as output device	98
Figure 4.30 Evaluation of the feasibility to measure “unexpected” variation in a parameter (NaCl in this case) in freshwater and the return to the baseline level.....	100
Figure 4.31 Screen-printed coatings (25×40 mm) onto microscope slides, specifically β - Bi_2O_3 (a) and L-CyChBCZ based coatings (b) and their absorbance measurements using a UV-Vis spectrophotometer (c)	101
Figure 4.32 SEM, EDS and their outputs.....	102
Figure 4.33 Experimental adsorption experiment for β - Bi_2O_3 (a) and L-CyChBCZ based coatings (b) coatings with respectively Zn and Cu solutions at various concentrations	103
Figure 4.34 Schematic example of Gaussian, Voigtian and Lorentzian profiles, which identify peaks’ shapes	106
Figure 4.35 Flow diagram which shows the data analysis approach and peak selection	108
Figure 5.1 Resonant cavity connected to a VNA (a) that was used as proof of concept for measuring Pb water solutions and the linear correlation identified for changes in concentration (0-100 mg/L) at two specific frequencies, 415 MHz and 2.45 GHz (b) (modified from Frau et al (2018a))	112
Figure 5.2 Spectral response comparison between a resonant cavity (a) and planar Au eight-pair IDE sensors (b) measuring Pb solutions: the major spectral changes depending on the metal concentrations (0-100 mg/L) are identified at the same frequencies, 415 MHz and 2.45 GHz	114
Figure 5.3 Example of microwave response which shows the comparable response for the same concentration (1-100 mg/L) of Pb and Zn	115
Figure 5.4 Spectral response for low Zn concentration (0-1 ppm) measured with an Au eight-pair IDE sensors which shows the infeasibility to detect with acceptable sensitivity the concentrations <1 ppm at three frequencies, namely 0.82, 1.27 and 2.45 GHz.....	115
Figure 5.5 Partial cross-section of an f-EM sensor with a sample on it held in place by a specific holder which shows the propagation of the EM field through each part of the sensing structure and sample, showing the two components, electric and magnetic lines (adapted from Frau et al (2019a))	118
Figure 5.6 Developed and tested f-EM sensors	119
Figure 5.7 Average absorbance spectrum of various lead solutions in 200–350 nm range measured with a UV–Vis spectrophotometer (a); linear correlations for the absorbance and Pb concentration at two wavelengths, namely 247 and 300 nm (b).....	122
Figure 5.8 Spectral responses for C (a) and R (b) and Pb solutions (0-100 mg/L) at low frequencies (20-200,000 Hz); linear correlations between C and Pb concentration at two discrete frequencies (30 Hz and 6 kHz) (c) and between R and Pb concentration at 180 Hz and 200 kHz (d)	123
Figure 5.9 Microwave spectral response (average) captured with a lacquered IDE sensor at 0.01–15 GHz frequency range for each sample concentration of Pb. The red rectangle highlights the area in which the spectra variate due to the diverse Pb concentration	

- (magnified in b). Specifically, at the frequency range between 2.30–2.65 GHz two specific frequencies are evidenced, namely 2.40 and 2.49 GHz (peak), where there are strong linear correlations between reflection coefficient (S_{11}) and Pb concentration (c) 124
- Figure 5.10 Absorbance for Zn samples in the wavelength range between 200-350 nm (a) and their linear correlations for low concentrations (0.1, 0.5 and 1 mg/L) at 218 nm (b) and for high concentrations (10, 50 and 100 mg/L) at 240 nm (c) and 300 nm (d)..... 129
- Figure 5.11 Spectral response for capacitance (C) (a), resistance (R) (b) and Zn solutions at low frequencies (20 Hz – 3 kHz); their enlargement in the frequency range 200-600 Hz (indicated by the arrows in a and b) for C (c) and R (d) is shown for a clearer view of the selected frequency with a logarithmic scale for displaying also the Zn concentration < 1 mg/L 130
- Figure 5.12 Power correlation between resistance (R) (expressed in logarithmic scale) and Zn concentration (in black) at 500 Hz; and linear correlation between capacitance (C) and Zn concentration (in red) at 250 Hz. Both parameters are measured with a LCR meter 131
- Figure 5.13 Spectral responses in the frequency range 0.1-3.2 GHz for Zn water solutions (0-100 mg/L) measured using an uncoated sensor (a) and an f-EM sensor based on β - Bi_2O_3 based coating with a thickness of 40 μm where are marked three amplitude shifts for each one, namely at 0.502, 1.26 and 2.46 GHz for the uncoated sensor and at 0.502, 1.26-1.35 and 2.46 GHz 133
- Figure 5.14 Change in S_{11} of microwave spectra for Zn solutions measured with a f-EM sensor with 60 μm of β - Bi_2O_3 based coating (a) and the linear correlation between S_{11} and Zn concentration (in logarithmic scale for showing 0.1 and 0.5 mg/L of Zn) at two discrete frequencies and a frequency range, namely 599 MHz, 2.56 GHz (peak) and 1.57-1.68GHz 134
- Figure 5.15 Spectral response for the peak identified at around 1.2 GHz (which shifts due to the coating's thickness) for uncoated (a) and f-EM sensors with 40 μm (b) and 60 μm (c) of β - Bi_2O_3 base coating which show the improvement of this last coating to better distinguish between Zn concentrations between 0 and 1 mg/L 136
- Figure 5.16 Variation in microwave response for uncoated and coated sensors with 40 μm and 60 μm of β - Bi_2O_3 base coating which shows the sensitivity improvement for Zn concentration between 0.1 and 1 mg/L 137
- Figure 5.17 Example of the average of absorbance spectra showing the repeatability and reproducibility of the coating for paste prepared and printed during diverse days..... 137
- Figure 5.18 Timeline responses for 30 minutes for Zn solutions measured with a β - Bi_2O_3 based thick film (60 μm), screen-printed onto Ag-IDE measuring C at 150 Hz (a), and screen-printed onto Au microwave sensors, measuring C at 150 Hz (b) and S_{11} responses at 2.53 GHz (c)..... 142
- Figure 5.19 Schematisation of a partial cross-section of the f-EM sensor illustrating the sorption of Zn onto the sensing layer (a); SEM image of the coating after the sorption reaction with the Zn ions (with highlighted particle size) and its elemental spectra (c) and elemental weight % (d) of the coating after the adsorption 144
- Figure 5.20 Recovery sensor time measured examples that show the spectral variation by time after the sample is taken off from the coating and allowed to dry, showing that after

about 100-150 seconds the response returns to the baseline (defined as "air" spectrum) for both C (a) and S ₁₁ measurements (b and c)	145
Figure 5.21 Materials in power form, namely l-cysteine, chitosan and ruthenium oxide (4:4:1) (a) were mixed with a binder and a solvent to develop a screen-printable paste (L-CyChRu) to print using a screen-printer (c) onto planar sensing substrates.....	147
Figure 5.22 Example of C variation by time using a coating screen-printed on Ag-IDE based on a mixture of chelating polymers for selective detection of Cn, Pb and Zn....	148
Figure 5.23 Absorbance spectra for Cu water solutions (0-100 mg/L) (a) and comparison between 10 ppm between Cu, Zn and Pb. Linear correlation at 218 nm for low Cu concentrations (0-1 mg/L) (c) and at 240 (d) and 300 nm (e) for high concentrations of Cu (1-100 mg/L)	149
Figure 5.24 Set-up of the impedance and microwave measurements using L-CyChRu based coatings using respectively an LCR programmable bridge connected to a coated Ag-IDE screen-printed on microscope slide (a) (magnified in b) connected through crocodile clips and a ZVA 24 connected with coaxial cables to uncoated and f-EM sensors (c) (magnified in d) (Frau et al, 2018c).....	151
Figure 5.25 Capacitance spectra of Cu solutions (0-50 mg/L) between 30 and 500 Hz (a) and their magnification for low Cu concentrations (0-5 mg/L) at 30-250 Hz (b) using an Ag-IDE covered with an L-CyChRu based coatings	152
Figure 5.26 Linear correlations for C and Cu concentrations (0-50 mg/L) by time (at 30, 300 and 600 seconds) and the focus on low concentrations, 0-5 mg/L (b), at 150 Hz .	153
Figure 5.27 S ₁₁ responses between 0.01 and 8 GHz of Cu solutions (0-50 mg/L) using uncoated (a) and f-EM sensors based on L-CyChRu coatings (b), and the magnification of the peak produced respectively at 1.26 GHz and 1.37 GHz. The f-EM sensor is able to separate better low Cu concentrations (< 1 mg/L)	154
Figure 5.28 correlations by time (30, 300 and 600 sec) for the peak at 1.26 GHz using uncoated sensors (a) and at 1.35 GHz using the f-EM sensors with L-CyChRu (b). Slope, hence sensitivity comparison for Cu at low concentration (0-1 mg/L) at 600 sec (c) ..	155
Figure 5.29 Spectral response for Cu solutions using f-EM sensor based on L-CyChBCZ extracted at 1 (dash lines), 5 (dot lines) and 10 minutes (solid lines) (a), where the highlighted areas show the best linear correlations at 1.4-1.5 GHz and 2.3 GHz (b), with an improvement in sensitivity ($\Delta 0.19$ dB for every mg/L) compared with uncoated sensors ($\Delta 0.03$ dB for every mg/L)(c) for Cu concentrations 0-1 mg/L	159
Figure 5.30 SEM image of the L-CyChRu coating (a) and its elemental composition after the interaction with Cu samples (b) and scheme of the probable chelation between Cu ions and chelating polymers (c)	161
Figure 5.31 Visual comparison of durability between f-EM sensors based L-CyChRu and L-CyChBCZ, respectively after 1 h (a vs d), 24 h (b vs e) and 72 h (c and f).....	162
Figure 6.1 Adapted map from Environment Agency (2008) which shows catchments at risk from non-coal (in blue) and coal (in black) mines. The four mining areas, specifically Wemyss mine, Nant y Mwyn mine, Parys Mountain mine (Wales, UK) and Leadhills mine (Scotland, UK), from where mining-impacted freshwater samples were tested, are highlighted with yellow stars	171

Figure 6.2 Example of polluted streams in the UK from where samples were collected and tested in the laboratory and <i>in situ</i> using microwave spectroscopy: Nant Cwmnewyddion (a), Afon Goch (b), Nant y Bai (c) (Wales) and Wanlock Water (d) (Scotland).....	174
Figure 6.3 Schematisation of the approach used in this chapter: 1) sensors were adapting for directly probing the water; 2) water samples (lab-prepared and collected from impacted mining areas) were spiked with Cu and Zn solutions using the SAM; 3) measurements were performed using non-portable (ZVA 24) and portable VNAs (miniVNA tiny); 4) Spectral responses were characterised using Lorentzian peak function; 5) statistical featured were evaluated (such as R^2 , sensitivity, Q,) and compared between diverse samples	176
Figure 6.4 Comparison example of spectral response measured using the 400 mL sample volume onto the sensor or the submersible f-EM sensor using both uncoated and coated sensors with L-CyChBCZ based coating	177
Figure 6.5 Spectral responses between 0.01 and 2 GHz for “unknown” Cu (UNK3 as 3 mg/L) solution and for “unknown” Zn (UNK0.2 as 0.2 mg/L) solutions (b) using uncoated sensors submerged in 40 mL of each water sample.	178
Figure 6.6 Magnification of the peak located at 440 MHz for the “unknown” Cu and Zn (UNK3 and UNK0.2) samples spiked with Cu and Zn solutions (highlighted in Figure 6.5 respectively in a and b); their calibration plots are shown in c and d respectively, where the effective concentration corresponds to the intercept of the curve.....	179
Figure 6.7 Capacitance (C) (a) and resistance (R) (b) plots measured using a LCR bridge and functionalised IDE with L-CyChBCZ based coatings for a collected polluted sample, FA, doped with the SAM	182
Figure 6.8 Linear correlations for capacitance (a) and resistance (b) with FA samples spiked with Cu at 1 kHz (in blu) and 150 Hz (in green)	183
Figure 6.9 Comparison between spectral responses measured using uncoated sensors (a) and f-EM sensors with L-CyChBCZ based coating (b) for FA samples spiked with continual additions of +1.25 mg/L of Cu concentration; the solid pink arrows in b compare the sensing response with a and the dashed violet arrows show the coating effect.....	185
Figure 6.10 Spectral response for FA series measure with the miniVNA tiny in the frequency range 0.01-2.5 GHz (a) and its magnifications at three resonant peaks: at 0.04 GHz (b), at 0.47 GHz (c) and 0.91-0.98 GHz (d)	187
Figure 6.11 Example of S_{11} output and impedance correspondences responses (R, X, Z) for a sample (FA+5.00 mg/L of Cu) measured using the miniVNA tiny	189
Figure 6.12 Impedance measurement, as R (a), X (b) and Z (c), for FA+ samples series performed using the miniVNA tiny and f-EM sensors based on L-CyChBCZ coatings; their linear correlations are shown respectively in (d), (e) and (f).....	190
Figure 6.13 Example of the Lorentzian peak fitting function for the sample “FA+1.25 mg/L of Cu” showing an example of overlapped peaks (modified from Frau et al (2020))	191
Figure 6.14 Summary of peak-parameters for FA sample spiked with the SAM, as peak centre, x_c , (a), FWHM, w, (b), area, A, (c) and height, H, (d) of the peaks determined by fitting the spectral responses with Lorentzian function with underlined points using orange-dotted-circles, orange and grey arrows (modified from Frau et al (2020))	193

Figure 6.15 Selected peak features (w (a) and H (b)) which show the comparison between Cu and Zn solutions; linear correlations for peaks 1 and 2 and H are shown in (c) and (d) (modified from Frau et al (2020)	195
Figure 6.16 S_{11} (a), C and R (b) measurement by time demonstrating that within 10 minutes the measurements reach a stability	196
Figure 6.17 Scanning electron micrograph of the SEM image (a) and EDS analysis showing the weight percentage of the elemental composition of the L-CyChBCZ coating after the interaction with a Cu solution, on the IDE (b and c)	196
Figure 6.18 Recovery time of the sensor after being washed returning to its baseline level within 2/2.5 minutes.....	198
Figure 6.19 Real-mine water samples (FA, MR, NC, PM) output analysed using f-EM sensors based on L-CyChBCZ based coatings with SD	199
Figure 6.20 Peak properties (xc, w, H, A) comparison at peaks 1, 2, 3, 4, 5, and 6 (respectively shown in graphs a, b, c, d, e and f) which were identified for 4 collected water samples (FA, MR, NC, PM).....	201
Figure 6.21 Example of spectral changes measured for the pH calibrations solution (pH= 4, 7, 10) (a) and variations in spectral responses for a 10 ppm Cu&Zn sample (1:1) due to T variation (8.2 to 19.5°C) measured every 30 minutes using a f-EM sensor based on an L-CyChBCZ coating	202
Figure 7.1 Comparison between sensing responses using multiple microwave sensors (uncoated (UNC), f-EM sensors based on β -Bi ₂ O ₃ , L-CyChBCZ, lacquer, ITO coatings) for DW (dotted line), FA (dashed line) and FA+5ppm of Cu (solid line) samples (a). Magnification of selected frequency range and peaks (p) number identification: 0.01 to 0.65 GHz (b); 0.6 to 1.05 GHz (c); 0.9 to 1.7 GHz; and 1.4 to 2.2 GHz. For straightforwardness, curves have the same colour as the represented coated sensor....	211
Figure 7.2 Comparison between L-CyChBCZ (solid line) and UNC (dashed line) sensors focusing on describing when the reflection coefficient S_{11} is similar at peaks 1 and 2; and comparison between DW and tap water (TW).....	212
Figure 7.3 Example of <i>in situ</i> trials performed in Wemyss mine areas for FA sample using three f-EM sensors based on ITO, lacquered and β -Bi ₂ O ₃ (a and b) and for diverse samples (MR, FA and NC) using the same sensor (ITO)	215
Figure 7.4 Example of <i>in situ</i> measurement for the PM (adit) sample using a lacquered sensor	217
Figure 7.5 <i>In situ</i> measurements at Parys Mountain mining district in Nov 2019 using a combination of f-EM sensors at PM-1 and PM-2 sites, two highly polluted water samples located in the mining area	218
Figure 7.6 Comparison between PM-1 (a) and PM-2 (b) samples analysed <i>in situ</i> using an f-EM sensor array with mean and SD from 0.01 and 2 GHz; each sensor, UNC (c), β -Bi ₂ O ₃ (d) and ITO (e) was able to distinguish between these two samples at three frequencies	219
Figure 7.7 Example of <i>in situ</i> measurements probing the sensors directly in water (a and b) using various f-EM sensors, such as uncoated (c) and based on ITO (d) and β -Bi ₂ O ₃ (e) for assessing the f-EM sensor array principle in the real environment	220

Figure 7.8 Spectral response for the NYB-1 (solid line) and NYB-2 (dashed line) measurement water sites using a f-EM sensor based on β -Bi ₂ O ₃ coating (orange) and a f-EM sensor based on an L-CyChBCZ coating (gold). The respective arrows show the spectral change from higher to lower polluted sample (NYB-1 is more polluted than NYB-2).....	222
Figure 7.9 Comparisons between NYB-1 (black) and NYB-2 (red) <i>in situ</i> measurements with SD using the f-EM sensor based on β -Bi ₂ O ₃ (a) and L-CyChBCZ (b).....	223
Figure 7.10 Reflection coefficient spectral response and SD using various f-EM sensors (as f-EM sensor array) for <i>in situ</i> measurements of the sample NYB-2 using a miniVNA tiny	224
Figure 7.11 Peak parameters, xc (a), w (b), A (c) and H (d) analysed using a Lorentzian peak fitting function of the S ₁₁ responses of <i>in situ</i> measurement of the NYB-2 site using a miniVNA tiny. As the previous graph, colours in the graph corresponds to “coatings colour” (except for M10)	225
Figure 7.12 <i>In situ</i> response for WW-1 and WW-A using various sensors.....	226
Figure 7.13 Results from an experimental trial of a slug injection of NaCl using a lacquered sensors probing the Nant Cwmnewyddion water measured every 5 seconds for 1,625 sec (27 minutes), demonstrating the feasibility of measuring <i>in situ</i> and in real-time the variation in a water parameter (a); the variation in the S ₁₁ response at 0.565 GHz by time and its return to the baseline once the concentration decrease (b).....	228
Figure 7.14 <i>In situ</i> comparisons between different areas using uncoated sensors probing the water (a) and their peak parameters comparisons at peak 1 (b) and 2 (c).....	230
Figure 7.15 <i>In situ</i> measurements comparison using f-EM sensors based on β -Bi ₂ O ₃ coatings in various sites (a and b) and their peaks parameters comparisons at peak 1 (c) and 2 (d)	232
Figure 7.16 <i>In situ</i> analysis comparisons using f-EM sensors based on L-CyChBCZ coatings (a and b) and their peaks parameters (c and d)	233
Figure 7.17 <i>In situ</i> analysis using a lacquered sensor (a) and the description of the peak 1 (b)	234
Figure 7.18 Sensing output of the f-EM sensor based on ITO for <i>in situ</i> measurements (a and b) and peaks features comparisons (c and d).....	235

List of tables

Table 1.1 UK EQS for some metals and sulphates in surface water and global range concentrations from waters impacted by historical deep metal mining.....	7
Table 1.2 Zn, Cu and Pb average concentration ranges in some water impacted by non-coal mines in Europe and in the UK	10
Table 2.1 Summary of the performance of the “gold standard methods” for toxic metal analysis.....	23
Table 2.2 Simple comparison of promising techniques for on-site and <i>in situ</i> monitoring of toxic metals in water	35
Table 3.1 Example of resonant cavities and their tested application for LUT measurements.....	51
Table 3.2 Example of planar structure and their tested application for water liquid analysis	53
Table 3.3 Example of IDE sensors for low-frequencies impedance measurements	55
Table 4.1 Summary of the successful paste mixtures which describes the acronym of the developed coating, the percentage of the added binder, the percentage of each material and their CAS number.....	72
Table 4.2 Summary of cost of equipment for microwave spectroscopy using the measurement configurations, equipment and materials used in this work.....	93
Table 4.3 Comparisons of curve fitting function performances, using Gaussian, Lorentzian and Voigtian profiles	106
Table 5.1 Summaries of statistical features for Pb ions and optical, impedance and microwave measurements, using a resonant cavity, IDE sensors and lacquered IDE sensors	125
Table 5.2 pH and EC of the Zn solutions.....	130
Table 5.3 Summary of statistical features obtained for optical, electrical and microwave measurements of Zn water sample	138
Table 5.4 Estimation of the percentage of adsorption between β -Bi ₂ O ₃ based film and Zn solutions (0-100 mg/L) after 5 and 10 minutes	143
Table 5.5 pH and EC of the prepared and analysed Cu solutions.....	151
Table 5.6 Linear correlation (R^2), CV in % and sensitivity for Cu samples (0-1 mg/L) using optical, electrical and microwave methods combined with f-EM sensors.	156
Table 6.1 Summary of statistical information for 3 identified peaks (at frequency <1 GHz) using uncoated (UNC) and f-EM sensors based on L-CyChBCZ (f-EM) for a mine-water sample (Frongoch adit, FA) spiked with Cu using the SAM. The better performance of the f-EM sensor at peak 2 is highlighted with numbers in bold.....	186
Table 6.2 Comparison of statistical features between VNAs (ZVA 24 and miniVNA tiny) using F-EM sensors based on L-CyCHBCZ coatings	188
Table 6.3 Metal concentrations and physicochemical parameters for the four samples collected in two mining areas in Wales (UK).	198

Table 7.1 Variation of EC and S_{11} signal by time due to change in salt <i>in situ</i> and in real-time and the return to the baseline spectrum. NaCl was successively measured by applying conversion equations.....	228
---	-----

List of acronyms and abbreviations

A	Area (of the peak)
AAS	Atomic Absorption Spectroscopy
Ag	Silver
AMD	Acid mine drainage
Aq	Aqueous form (dissolved in water)
ARD	Acid rock drainage
As	Arsenic
ASV	Anodic stripping voltammetry
Au	Gold
β -Bi ₂ O ₃	Beta bismuth (III) Oxide
BCZ	Bismuth cobalt zinc oxide
Bi	Bismuth
Bi ₂ O ₃	Bismuth (III) Oxide
C	Capacitance
CD	Carbon dot
CE	Counter electrode
CSSR	Complementary split-ring resonators
Cu	Copper
Cu ²⁺	Copper ion
CuFeS ₂	Chalcopyrite (copper iron sulphide mineral)
CuS	Covellite (copper sulphide mineral)
CRM	Certified reference material
CV	Coefficient of variation
CWA	Clean water act (US legislation body)
dB	Decibel
DEFRA	Department for Environment, Food & Rural Affairs
DL	Detection limit
DPV	Differential pulse voltammetry
DSS-SRR	Double sided-spiral split-ring resonator
DW	Deionised water
E	Energy
EC	Electrical conductivity
EDS	Energy Dispersive X-ray Spectroscopy
E _f	Electric field
EIS	Electrochemical Impedance Spectroscopy
EM	Electromagnetic
EQS	Environmental quality standards
Fe ²⁺	Iron ion (reduced)
Fe ³⁺	Iron ion (oxidised)
Fe(OH) ₃	Ferric Oxide (solid form, “precipitate”)
FeS ₂	Pyrite (iron sulphide mineral)
f-EM sensor	Functionalised electromagnetic wave sensor

FT-IR	Fourier-transform infrared spectroscopy
FWHM	Full width half maximum
g	Gaseous form
H	Peak height
H ⁺	Hydrogen ion (acidity)
H _f	Magnetic field
H ₂ O	Water
HCl	Hydrochloric acid
HFO	Hydrous Ferric Oxides
HNO ₃	Nitric acid
ICP-OES	Inductively coupled plasma optical emission spectrometry
ICP-AES	Inductively coupled plasma atomic emission spectroscopy
ICP-MS	Inductively coupled plasma mass spectrometry
IDE	Interdigitated electrode (or interdigital electrodes)
IMWA	International Mine Water Association
ISE	Ion selective electrode
ITO	Indium Tin Oxide
LCR	Inductance (L), capacitance (C), Resistance (R)
L-CyChBCZ	L-cysteine – chitosan - Bismuth Cobalt Zinc oxide
L-CyChRu	L-cysteine – chitosan - Ruthenium oxide
LJMU	Liverpool John Moores University
LSV	Linear sweep voltammetry
M10	Aquaminal material (mostly metal oxides mixture)
MUT	Material under test
NaCl	Sodium chloride
NAMD	Net alkaline mine drainage
NIDRS	Near-infrared diffuse reflectance spectroscopy
O ₂	Oxygen
OTG	On-the-go (UBS)
RE	Reference electrode
RFM	Radio Frequency and Microwave
RSD	Relative standard deviation
Pb	Lead
Pb ²⁺	Lead ion
PbS	Galena (lead sulphide mineral)
PCA	Principal component analysis
PHEs	Potentially harmful elements
PLS	Partial least square
PTEs	Potentially toxic elements
PTFE	Polytetrafluoroethylene
PVB	Polyvinyl butyral
QDs	Quantum dots
R	Resistance
RE	Reference electrode

RFM	Radio Frequency & Microwave
s	Solid form
S_{11}	Reflection coefficient (standing for $ S_{11} $ in this work)
S_{21}	Transmission coefficient
SAM	Standard addition method
SD	Standard deviation
SDS	Safety data sheet
SEM	Scanning Electron Microscope
SO_4^{-2}	Sulphate (dissolved in water)
SRR	Split Ring Resonator
SWV	Square wave voltammetry
SWASV	Square-wave anodic stripping voltammetry
T	Temperature
TDS	Total dissolved solids
TW	Tap water
UNC	Uncoated (sensor)
UK TAG	UK Technical Advisory Group (on the WFD)
US EPA	Environmental protection agency (United States)
VNA	Vector Network Analyser
w	Full width at half maximum (FWHM)
WE	Working electrode
WFD	Water Framework Directive (EU legislation body)
X	Reactance
xc	Peak center
XRF	X-Ray Fluorescence
Y	Admittance
Z	Impedance
Zn	Zinc
Zn^{2+}	Zinc ion
ZnS	Sphalerite (Zinc sulphide mineral)

List of symbols and notations

dB	decibel
Ω	ohm
Φ	grain size
F	Farad
n	nano
k	kilo
ε_A	absorptivity / molar attenuation coefficient of the species
ε'	real part of the permittivity
ε''	imaginary part of the permittivity
ε_0	permittivity of free space
ε_{eff}	effective dielectric constant
ε_{par}	relative complex permittivity of the particle under test
ε_W	relative permittivity of water
ε_r	relative permittivity
μ_r	relative permeability
v_f	volume fraction
ω	operational frequency
$ S_{11} $	reflection coefficient magnitude (designated as S_{11})
mg/L	milligrams per litre (as ppm)
$\mu\text{g/L}$	micrograms per litre (as ppb)
Hz	hertz
kHz	kilohertz (10^3 Hz)
MHz	megahertz (10^6 Hz)
GHz	gigahertz (10^9 Hz)
THz	terahertz (10^{12} Hz)
ZHz	zettahertz (10^{21} Hz)
mW	milliwatt
ppm	parts per million (as mg/L)
ppb	parts per billion (as $\mu\text{g/L}$)
ppt	parts per trillion (as ng/L)
Pa s	pascal seconds
V	voltage
J	joule
λ	wavelength
c	speed of light
f	frequency
Γ	gamma (return loss or reflection coefficient)
sec	seconds
min	minutes
t	tonnes

Chapter 1 Introduction

1.1 Background information

Freshwater is an indispensable resource, but it is limited in quantity and quality. Water management is becoming increasingly challenging owing to factors such as climate change, overexploitation and contamination from both point and diffuse sources due to agricultural and industrial activities (Nordstrom, 2009). Legislation to protect the environment first appeared in the early 1970s, when the European Community and the United States made water quality a priority with the First Environmental Action Programme (European Communities, 1973; European Parliamentary Research Service (EPRS), 2018) and the Federal Water Pollution Control Act, respectively. Since then, several EU and US directives were introduced to prevent, monitor, reduce, control and remediate pollution of river basins in Europe and worldwide. Currently, the most important pieces of related water legislation are the European Union Water Framework Directive (EU WFD, 2000/60/EU) and the United States Environmental Protection Agency Clean Water Act (US EPA CWA). They aim to assure good water quality by controlling and limiting contaminants to established standards that are regularly revised (Brack et al, 2017).

Inorganic metals pose a substantial risk to almost half of the water bodies recently monitored in Europe. One of the major causes of their dispersion in freshwater bodies is due to the exploitation of sulphide minerals for the extraction of valuable metals. These include potentially toxic metals, such as zinc (Zn), copper (Cu), lead (Pb) and cadmium (Cd) which are not degraded by normal biogeochemical cycles and can move from one environmental sector to another (Ali et al, 2019). They are also accumulated in living organisms including human organs through the food chain (Byrne et al, 2012).

The “*heavy metals*” denomination, widely used by many researchers and industries for describing potentially toxic inorganic elements is NOT used in this thesis. This definition generally includes proper metals and semimetals (metalloids), such as Zn, Cu, Cd, Pb, As and Hg, but it is considered confusing by the International Mine Water Association (IMWA) as it includes elements that are not *heavy* nor a *metal*, such as arsenic (Duffus, 2002; Wolkersdorfer, 2008). They are more correctly denominated as potentially harmful elements (PHEs), potentially toxic elements (PTEs), trace metals and toxic metals. In this work, Cu, Zn, Pb, Cd, etc. are referred to as *toxic metals*.

1.2 Mining areas and pollution

Mining activities have been an important contributor to global wealth but mineral extraction disfigures the landscape and generates huge quantities of waste materials rich in potentially toxic metals. They can severely impact the ecosystem and be detrimental to human health (Wolkersdorfer, 2008).

The metalliferous veins from which the metals of interest are extracted in non-coal metal mines are mostly sulphide minerals, such as galena (PbS, lead sulphide), sphalerite (ZnS, zinc sulphide), pyrite (FeS₂, iron sulphide) and chalcopyrite (CuFeS₂, copper iron sulphide). They are quarried in open pits (removing the surface layer), underground mines (through horizontal tunnels, shafts) or both (Figure 1.1). The valuable metals were commonly separated using grinding, leaching and electrolysis. The waste materials derived from the extraction of the valuable metals, defined as “gangue”, were deposited in waste rock dumps or abandoned in river beds. They are still highly rich in potentially toxic materials, which are mobilised in the environment. These waste materials have varied granulometry, which determines the potential for the toxic elements to be

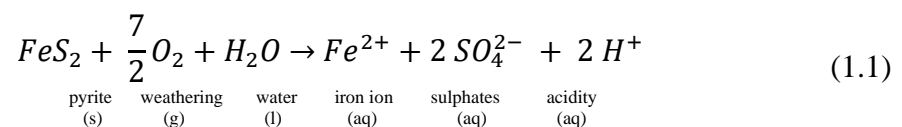
dispersed. The smaller the granulometry (e.g. fine tailings), the higher the exposed surface is to weathering.



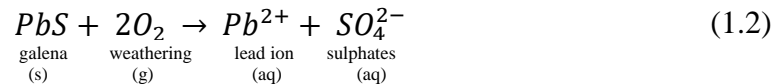
Figure 1.1 An example of a mining area: Parys Mountain mine site (Anglesey, UK)

The major mechanism associated with the mobilisation of metal ions in mining areas is the oxidation and consequent hydrolysis of sulphide minerals, exposed by mining activity that increases the surface area exposed to weathering and the consequent release of metals (Johnson, 2003).

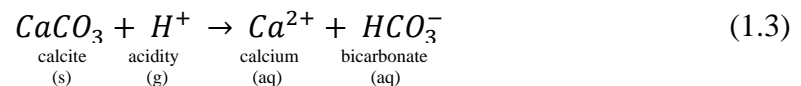
This process, which is typically called acid mine drainage (AMD) or acid rock drainage (ARD), leads to the dispersion of metal ions in water bodies with high sulphate concentrations and low pH levels (acidic water), well described by the oxidation and dissolution of pyrite (formula 1.1) (Younger et al, 2002):



Discharges are not only highly acidic, but they can also be circumneutral. This mainly depends on the following two factors. The first is the ore mineralization itself, as the oxidation of other sulphide minerals (e.g. galena, sphalerite) do not produce acidity (formula 1.2). This process is known as net-alkaline mine drainage (NAMD).



The second is the neutralisation of the acidity caused by calcium carbonate (if present in the embedding rock) (formula 1.3).



Generally, the ionic metal form is considered the most toxic, although other weak complexed species (oxides, hydroxides, and sulphates) and organic colloidal phases are also cause for concern. The metal ionic form and its precipitation or sorption to other phases are related to the pH, the sorbate identity and its concentration, and the sorbent composition, etc (Smith, 1999).

Besides, pollution by extracting agents is another serious problem. For example, the extraction of Au from host minerals is achieved by cyanidation, and the cyanide (CN⁻, highly toxic) and other waste material are stocked in tailings impoundment (Da Pelo et al, 2009).

Therefore, adequate monitoring and accurate assessment are required to minimise the environmental risk posed by both acidic and neutral mine drainage from active and abandoned mining sites all over the world.

1.2.1 Abandoned mines and the freshwater environment

Surface water is the preferential dispersion route of these toxic elements even at considerable distances from their source, and several reactions occur in the watershed with the consequent possibility of polluting drinking water supplies. Pollution sources are mainly grouped into two categories: point and diffuse sources. Point sources are mostly *drainage adits* (Figure 1.2), which are groundwater that rises after the pumping used for the mining activity has stopped (Environment Agency, 2008). Diffuse sources are mainly due to leaching from deposits of waste materials (Figure 1.3) either piled up in heaps, along river beds or buried (Perkins et al, 2016). These toxic metals sources are not always easily identified as metals mobilisation depends on environmental conditions, such as stream flux, changes in pH and riverbed materials (Cidu et al, 2011; Gozzard et al, 2011).



Figure 1.2 Example of a drainage adit in the Montevecchio Mine district (South-West Sardinia, Italy)

Mobilised metals can also be transported from headwater catchments to coastal areas (Mayes et al, 2013).

Several natural attenuation processes also influence the dispersion of metal ions. For example, the bioprecipitation process of hydrozincite is responsible for the natural reduction of Zn in stream water (Medas et al, 2012); the adsorption of metals on Hydrous Ferric Oxides (HFO) generated by changes in pH (Smith, 1999); natural wetlands or biogeochemical barriers which attenuate the metal concentrations in freshwater systems (De Giudici et al, 2017; Dean et al, 2013).



Figure 1.3 Leachate from tailings heaps in Nant y Mwyn lead mine (Central Wales, UK)

The most common metals that are related to mining areas are zinc (Zn) copper (Cu), lead (Pb) and cadmium (Cd), and excessive concentrations can be harmful to living organisms (Byrne et al, 2012). They are also called *trace metals*, due to their toxicity and presence in the environment at generally low concentrations ($\mu\text{g/l}$ range to few mg/l). Consequently, global and European legislation has established environmental quality standards (EQS), as “safe concentrations” of toxic metals in freshwater. Table 1 reviews

the EQS established by the UK Technical Advisory Group on the EU WFD (UK TAG) (UK Technical Advisory Group on the Water Framework Directive, 2008) and US EPA (Environmental Protection Agency) (United States Environmental Protection Agency, 1986) for Zn, Cu, Pb, Cd and sulphates, as well as the metal concentration range for polluted rivers in mining areas worldwide. Pb and Cd are itemised in the priority list for their elevated toxicity at nano levels (Agency for Toxic Substances and Disease Registry, 2017). Besides, in some mining-impacted area, the “baseline” metal level is already above the EQSs, despite the extraction activities. Recently, the Department for Environment, Food & Rural Affairs (DEFRA) has reconsidered standard values by evaluating the pollution above the baseline metal concentration, especially for Zn, recognising the importance of local baseline variability (Department for Environment Food & Rural Affairs, 2014; Hudson et al, 2018).

Their bioavailability is regulated by several physical and chemical factors, such as temperature, pH and consequent differential adsorption, phase association, thermodynamic equilibrium, and complexation kinetics (Tchounwou et al, 2012).

Table 1.1 UK EQS for some metals and sulphates in surface water and global range concentrations from waters impacted by historical deep metal mining

Toxic metals and sulphates	UK EQS (mg/L) for inland and other surface water (Environment Agency, 2011)	US EPA EQS (mg/l) for freshwater (acute and chronic) (United States Environmental Protection Agency, 1986)	Global concentration ranges in polluted mining surface water (mg/L) (Byrne et al, 2012)
Lead (Pb)^a	0.0072 ^b	0.0015-0.065 ^c	<0.0072->12
Zinc (Zn)	0.008-0.125 ^c	0.059-0.210 ^c	<0.008->420
Copper (Cu)	0.001-0.028 ^c	0.017-0.034 ^c	<0.001->240
Cadmium (Cd)^a	< 0.00008 – 0.00025 ^{bc}	0.00066-0.0018 ^c	<0.00008->2.6
Sulphates (SO₄)	400	250	<400->16,000

^apriority substances (by ATSDR);

^bdissolved concentration (<0.45 µm);

^cdepending on the annual mean concentration of CaCO₃;

There are many examples where waste from the mining industry has posed a risk to water resources and to animal and human health. In 2015, a failure of the Fundão and Santarém mine tailings dams in Minas Gerais, Brazil, caused the release of 62 million m³ of sediment

and water. This cut off potable water supplies, blanketed more than 650 km of rivers, and flowed into the Atlantic Ocean. In January 2019, another tailing dam collapsed in the same area. Another example is the accident in the Gold King Mine, Colorado, where the water and tailings from the mine spilt into Cement Creek which was turned bright yellow during the attempted remediation. The Rio Tinto Mining district in Spain, which has been working for more than 5,000 years, has polluted more than 90 km of rivers with an extremely high concentration of metals and low pH (<3): 8.1% of the dissolved Zn flux in the global rivers comes from the Rio Tinto (Hudson-Edwards, 2016). Numerous attempts at reclaiming mining areas have not been completely efficient, because not effective studies nor consideration of detailed research carried out by Universities. An example is Baccu Locci mine in Italy, where the remediation solved the problem related with the reduction of acidity and Pb concentration, without considering that the increase of pH determines a higher dispersion of As (Ardau et al, 2013).

1.2.2 European and UK overview

Europe was one of the most productive mining regions in the world. Each country still suffers from water metal pollution problems caused by past mining activity which include rising mine waters (which sometimes intercept important aquifers), and surface water pollution arising from the discharges of spoil heaps (Wolkersdorfer & Bowell, 2005; Wolkersdorfer et al, 2012). In England and Wales alone, there are 4,923 abandoned metal mines (Mayes et al, 2010) which pollute water bodies. 9 % of rivers in England and Wales, and 2 % in Scotland, carry some of the biggest discharges of metals such as zinc, copper, lead and cadmium to the seas around Britain, failing targets for good chemical and ecological status established by WFD. For instance, Table 1.2 summarises some examples of polluted water in mining areas with high Zn, Cu and Pb concentration for

some selected countries in Europe (Spain, Italy, Finland, Norway, North Macedonia, Germany) as well as in the United Kingdom, mostly Wales. Generally, in England and Wales, the pH of water is mostly circumneutral (6.5-7.5), as pyrite based mineralisations are sporadic (Mayes et al, 2010). An exception is Parys Mountain mine, where the ore is based on chalcopyrite, galena and sphalerite, with abundant pyrite forms a unique deposit in the UK, which produces very acidic conditions, pH of 2-3 in the river basin (Boult et al, 1994) (Figure 1.4).



Figure 1.4 Afon Goch River (Parys Mountain mine, Anglesey, UK)

Table 1.2 Zn, Cu and Pb average concentration ranges in some water impacted by non-coal mines in Europe and in the UK

	Country	Mining district	Zn (mg/L)	Cu (mg/L)	Pb (mg/L)	Reference
Europe*	SP	Rio Tinto	56-420	24-240	0.1-2.4	(Hudson-Edwards et al, 1999)
	IT	Montevecchio	0.25-1,200	0.21-3.4	0.56-3.60	(Cidu et al, 2011)
	FI	Luikonlahti	1.6-4.1	0.003-0.5	-	(Wolkersdorfer & Bowell, 2005)
	NO	Løkken	30-50	5-10	-	
	NM	Zletovo	0.06-26.11	0.03-1.05	<0.03-0.08	(Alderton et al, 2005)
	GE	Kupferschiefer	0.41-1.05	0.080-0.360	0.06-0.08	(Bozau et al, 2017)
UK	Force Crag Mine		0.21-2.95	-	0.005-0.097	(Jarvis et al, 2019)
	Parys Mountain Mine		1-10	0.01-3.0	-	(Dean et al, 2013)
	Cwm Rheidol Mine		13.5	-	0.75	(Mayes et al, 2009)
	Afon Twymyn		0.01-1.7	<0.030	0.01-0.4	(Byrne et al, 2013)
	Nant y Bai Lead Mine		0.5	-	0.28	(Natural Resources Wales, 2014)
	Parc Lead-Zinc Mine		0.27-0.34	-	0.38-2.60	(Gao & Bradshaw, 1995)

*(SP – Spain; IT – Italy; FI – Finland; NO - Norway; NM – North Macedonia; GE - Germany)

1.2.3 Problem statement

It is difficult to identify, characterise and quantify point and diffuse sources of toxic metals in polluted mining areas. As previously explained, metal ions are not “static” but are involved in reactions between water, solid phases and organisms under different geochemical and hydrological settings in addition to human actions (Byrne et al, 2012). Currently, water resources in a watershed require sampling at different locations and consequent laboratory analysis of these samples. Existing laboratory-based methods are able to detect ppb range levels of metals in multi-metal water samples, but they are expensive, bulky and off-line. This allows the determination of pollution of a particular site at a particular moment, but it is not enough for evaluating the impact assessment or efficient remediation strategy; it is necessary to enable a more detailed exploration of metal dynamics (Jarvis et al, 2019). Moreover, laboratory-based analysis is not applicable for an early warning of an unexpected variations in water composition. Also, to apply efficient remediation strategies it is necessary to monitor their effect continuously once they are in place, as well as taking account of seasonal variation (Mayes et al, 2009).

Consequently, it is necessary to develop low-cost sensing systems for *in situ* monitoring of water resources to minimise the environmental risk posed by mine drainage from both active and abandoned mining complexes (Altenburger et al, 2015).

1.3 Purpose of this study

The purpose of the current PhD project is to develop and test a novel real-time sensing platform based on functionalised electromagnetic wave sensors (f-EM sensors) (Figure 1.5) for the *in situ* detection of toxic metals in water.

Microwave spectroscopy can continuously detect changes in material properties. This work has investigated the possibility of using microwave spectroscopy as a solution to detect toxic metals in water.

Early experiments that were performed using already developed planar sensors at LJMU demonstrated the possibility to detect changes in the concentration of Zn, Cu and Pb . The technique needed improvement, however, to detect smaller changes in metal content (< 1 mg/L) and to distinguish between similar toxic metals. Consequently, this PhD project has investigated the integration of functional materials on planar electromagnetic (EM) sensors to improve the performance of microwave spectroscopy for monitoring toxic metals in water.

1.3.1 Novelty

The novelty of this PhD project is the research and development of innovative f-EM sensors. For the first time, planar microwave sensors, which were already developed at LJMU, were integrated with screen-printed thick films based on combinations of various materials using screen-printing technology.

The novelty of this work is supported by peer-reviewed papers that are published in international journals and conference proceedings of work presented at various international conferences.

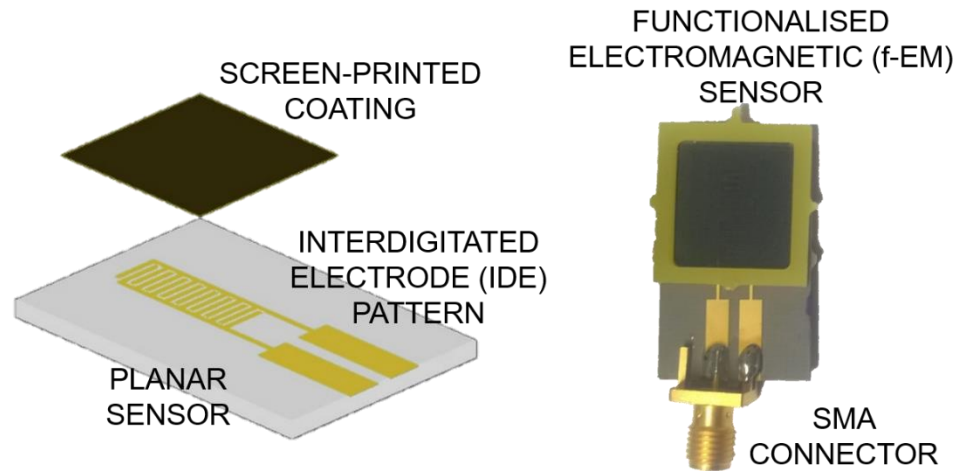


Figure 1.5 Example of a functionalised electromagnetic wave sensor (f-EM sensor)

1.3.2 Aim and objectives

This PhD project aims to research and develop a novel real-time sensing system, based on microwave spectroscopy and f-EM sensors, for detecting the presence and concentration of toxic metals in polluted water in real-time, and for generating a more specific response between similar toxic metals.

The objectives for accomplishing the aim of this work are:

- O1)** Evaluate the improved performance of various developed f-EM sensors, in the laboratory, which are based on selected functional materials, for detecting the concentration of single metal solutions (Pb, Zn and Cu) using microwave and low-frequency impedance measurements, and comparing the response with uncoated sensors;

O2) Investigate the microwave response of adapted f-EM sensors when directly probing water samples collected from mining-impacted areas in the UK, which were processed using the standard addition method;

O3) Test multiple f-EM sensors for more specific characterisation of the water samples and perform field trials in four mining-impacted waters in the UK to evaluate the feasibility of *in situ* monitoring using microwave spectroscopy.

The specific objectives are restated and expanded at the beginning of each of the *Results and Discussion* chapters, 5, 6 and 7, which correspond respectively to O1, O2 and O3.

1.4 Chapters overview

This section describes the structure of this thesis by chapter.

Chapter 1 outlines the problem associated with mining areas and the consequent pollution of water resources, particularly related to the dispersion of toxic metal in freshwater. Limits related to current methods for metal analysis are introduced and the need for developing a sensing system that can monitor toxic metals *in situ* and in real-time is explained. Consequently, the approach and the solution proposed in this work is introduced by explaining the aim, novelty and objectives.

Chapter 2 describes both the established methods and novel trends for monitoring toxic metals in water. The chapter is divided into three parts: the first part describes the “gold standard techniques” able to analyse metal ions in water, with a focus on their advantages, and disadvantages. The second part describes the ongoing research that is taking place for solving the problem of lack of *in situ* monitoring, with a small indication of what is

available on the market. Finally, the third introduces microwave spectroscopy and f-EM sensors as a possible solution.

Chapter 3 defines the technology in use, specifically microwave spectroscopy: the required theory, the interaction with water, its potential and its limitation. It introduces the principle and the approaches other researchers are taking to detect “materials” in the environment. Then, other research carried out around the globe is critically investigated. The emphasis is then moved on to the novel methodologies that are used for improving the performance of microwave spectroscopy for specific purposes, mainly focusing on the material integration. Finally, the choices of the research approach used in this work are justified by consulting relevant past and up-to-date literature.

Chapter 4 describes the research methodology. Firstly, coating preparation and the development of the f-EM sensors are explained. Then, sample preparation and collection are described. This is followed up by a description of the measurement set-up for the tests carried out, which included optical, low-frequency impedance and microwave measurements, and the description of how the sensing system was adapted for *in situ* analysis. Coating characterisation techniques before and after metal interaction with functional materials are then described. Finally, it is explained how the spectral responses are investigated for evaluating the sensing performance.

Chapter 5, 6, and 7 present results and findings. **Chapter 5** describes results for small volume analysis (400 μL) of simple water samples, such as Zn, Cu and Pb solutions at various concentrations, using uncoated and f-EM sensors, with coatings based on diverse material mixtures. Specifically, these coatings are based on a mixture of chelating polymers (l-cysteine and chitosan) and metal oxides ($\beta\text{-Bi}_2\text{O}_3$, M10, ITO, RuO, BiCoZnO). Results are analysed, compared and discussed.

Chapter 6 delineates the response of various f-EM sensors for more complex water samples. It also describes results for the strategies adopted for *in situ* monitoring (e.g. immersed sensors in water, portable VNAs, etc). Two novel approaches for microwave sensing are described: i) the standard addition method for metal analysis and ii) the multiple peaks and multiple parameter analysis (x_c , f_0 , FWHM, H, A) using Lorentzian fitting functions.

Chapter 7 presents results for experimental *in situ* field testing using various f-EM sensors and a portable VNA in mining-impacted waters from selected mining areas in the UK (e.g Parys Mountain, Wemyss and Nant y Mwyn mines). The concept of using an *f-EM sensor array* is presented for providing a more specific response, especially for multi-metal solutions with complex matrices.

Finally, **Chapter 8** concludes the thesis, summarising the main findings.

Chapter 2 State-of-the-art and new trends: toxic metal analysis

2.1 Current methods for metal detection

Current techniques that are able to detect toxic metals accurately in water are destructive bulky laboratory-based machines, which require sample collection, preparation, expensive consumables, time and highly trained staff (Priya et al, 2017). However, their biggest limitation is the inability to give a specific, real-time *in situ* response. Gold standard methods provide off-line monitoring, low-frequency data sampling and delays between sampling and availability of the results. This limits the ability to characterise point and diffuse sources related to metal dynamics when environmental conditions change, and to detect an unexpected change in toxic metal pollution as soon as it happens. Consequently, worldwide researchers are working on developing novel techniques able to identify and distinguish toxic metal ions both qualitatively and quantitatively *in situ*. Specifically, it is interesting to notice that there is an enormous difference between on-site and *in situ* measurements. Explicitly, on-site means that the system is portable, although the probe cannot be immersed directly in the water, samples need to be collected and prepared; instead, *in situ* means the sensor is probing in water, and the sample is not collected (Holmes et al., 2018).

This thesis describes the novel research of a method for toxic metal detection which is an application that has not found a tangible and practical solution up until now.

This chapter describes i) the “gold standard techniques” used for metals analysis in water, and ii) the progress in other research areas for *in situ* monitoring, with a particular focus on their potential and limitations.

2.1.1 Water samples collection and physicochemical parameters

Nowadays, the characterisation of polluted mining-impacted water is evaluated by expansive and time-consuming campaigns, with consequent costly laboratory analysis. Samples are collected manually at a specific site, in a particular moment, with specific environmental conditions (Figure 2.1a). The problem of sampling rate at a specific site can be addressed using auto-sampling equipment (Figure 2.1b) which can collect samples when there are variations in environmental conditions (e.g. daily or flow variation). They are programmed to collect a fixed water volume at specific time intervals (e.g. every few hours or every few days). However, this can still introduce errors into measurements if samples are left in the field for too long before collection and reduce one's ability to determine a significant event because of the sampling frequency and consequent analysis.



Figure 2.1 Manual sample collection (a) and automatic sampler collecting programmed samples (b)

Sampling is always also accompanied by *in situ* measurements of other parameters, such as conductivity (EC), pH and temperature (T) (Figures 2.2a, b and c). These physicochemical parameters are “labile”, as they are liable to change between the field and the laboratory where the samples are processed and analysed. The EC can be an indirect measure of pollution: generally, a sample with a higher EC and lower pH, will

be more polluted than a sample with a lower EC and higher pH. However, this is not always true, as a high EC can be also generated by a high bacterial charge. Consequently, physicochemical parameters are necessary for the first evaluation of variations related to other environmental conditions that can influence metal dynamic.

After samples are collected, they are processed. Generally, an aliquot is filtered to 0.45 μm for evaluating the dissolved toxic metal component; another one is measured as unfiltered, generally considered as total, particulate and complexed (oxides, complexed with organic matter, etc.) (De Giudici et al, 2019). Then, samples are acidified, using 1-2% v/v of nitric acid (HNO_3) or hydrochloric acid (HCl) to i) preserve trace metals in solution and ii) avoid or reduce precipitation.



Figure 2.2 Example of *in situ* physicochemical parameters measurements: EC using a multi-parameters meter (a), pH using a pH meter (b) and multi-parameter probe, AQUAREAD (c)

Several other technologies have been recently developed as alternatives to traditional grab sampling and laboratory analysis. In Colorado, Chapin (2015) and his research group from the U.S. Geological Survey developed a water sampler, the MiniSipper, able to acidify, filter samples and grab water samples with high frequency, thanks to its capacity to collect up to 250×5 mL samples. This uses gas bubbles to separate a small volume of samples (for ICP-MS analysis) in a long tubing coil. This new approach is advantageous

for detecting an unexpected event (due to its capability to collect samples with high frequency), for the capacity to prepare samples directly on-site for analysis in the laboratory, and for improving our understanding of the geochemical response to temporally variable processes. However, this is not able to solve the high costs of laboratory analysis. Also, a long period between samples collection and analysis in the laboratory can result in alteration of samples composition due to chemical, biological, and physical reactions (Radovanović et al, 2019).

2.1.2 Laboratory-based analytical detection techniques

The accredited laboratory-based techniques for detecting toxic metals in water include inductively coupled plasma – optical/atomic emission spectrometry (ICP-OES/ICP-AES), inductively coupled plasma - mass spectrometry (ICP-MS) and atomic absorption spectroscopy (AAS) (Morton et al, 2009). These methods are highly sensitive and selective, although they need sample preparation, trained staff, expensive disposable equipment and gas for running experiments (Lu et al, 2003).

Spectroscopy and spectrometry do not describe the same method and the terms are not interchangeable. Spectroscopy studies how electromagnetic radiations, at any frequency, interact with the matter and produces a specific spectrum. Spectrometry can be considered as a method of studying spectra. This is not necessarily as intensity as a function of frequency. For instance, atomic absorption spectroscopy studies the absorption of light by a particular element at a specific wavelength; while mass spectrometry spectra plot intensity versus mass (Todoli & Mermet, 2008a).

2.1.2.1 ICP-OES

ICP-OES (Figure 2.3) and ICP-AES have been used for the last few decades and represent the same technology and method. This technology was introduced and developed in the mid-1960s and is still one of the most widely used techniques for analysing cations in a water sample. The principle behind it is the interaction with a plasma and electromagnetic radiation. The sample enters a chamber and is ionised with argon gas through a torch at high temperature (10,000°C). Then, the mixture gas emits photons which are collected by a lens. The photodetector converts the excited wavelengths to an electrical signal, which is processed by a computer (Cidu, 1996). In ICP-OES, the ions are excited by a vertical plasma, emitting photons that are separated on the basis of their emission wavelengths. ICP-OES is able to detect more than 60 elements simultaneously, but it is not able to detect concentrations in the ppt range. Its main disadvantage is the potential of interferences in the spectral response and a high-volume gas installation (argon) in a laboratory. It is used for analysis of water with more total dissolved solids (TDS), with a tolerance up to 30%, by comparison with ICP-MS (up to 0.2%).



Figure 2.3 An ICP-OES at LJMU

Running ICP-OES samples requires specialised lab staff with technical expertise for samples preparation using analytical solvents, calibration, assessment of the

measurements using certified reference materials (CRM) and maintenance (Eddaif et al, 2019).

2.1.2.2 ICP-MS

The ICP-MS (Figure 2.4) is the dominant technique to detect trace metal concentrations in water. This technique combines the plasma coupling technology with a mass spectrometer system, which separates the ions based on their mass-to-charge ratios, allowing a higher sensitivity of metal ion detection (in the ppt range). This method suffers from interferences, caused by the matrix, the reagents, and the plasma gases, but they can be identified and corrected. ICP-MS combines the plasma coupling technology with mass spectrometry, allowing the determination of trace elements in the ppt range with a wider dynamic range than ICP-OES. Moreover, it is able to measure the isotopic elemental concentrations in liquids. It can detect a larger number of elements (82) simultaneously compared with the ICP-OES, and requires a lower sample volume (a few mL depending on the programme, and on how many elements and repetitions are required). Appropriate configurations must be applied by a skilled specialist, as it is more difficult to use than the ICP-OES. The maintenance cost is also 2 to 3 times higher than an ICP-OES, and it requires the use of an internal standard in the analysed samples, which is a small volume of a rare element not found in the analysed water (e.g. rhodium, Rh). The operation and purity reagent cost are also much higher (Cidu, 1996; Todoli & Mermet, 2008b).



Figure 2.4 An ICP-MS at LJMU

2.1.2.3 AAS

The AAS is a spectroscopic technique and it is used for single toxic metal analysis determination. The principle is based on the absorption of optical radiation (light) at specific wavelengths, by metal ions and their concentration is described by the Beer-Lambert Law. The sample under test is first converted to an aerosol by a flame atomizer, and mixed with a gas (e.g. acetylene) in a spray chamber. Then it is irradiated and the resulting light is passed through a monochromator which separates the specific wavelength for the single element under test. The specific absorbed radiation is distinguished by a detector and the elemental concentration is quantified (Fernández et al, 2019). It is a quick low-cost method, but it is not generally used for analysing toxic metals in water from mining areas as the water is complex and polluted by several toxic metals simultaneously. Consequently, it is not convenient to run a single analysis for each pollutant on each sample, despite being much cheaper than the two ICP described earlier.



Figure 2.5 An AAS at LJMU

2.1.2.4 Advantages and disadvantages

In summary, these gold standard methods for toxic metal analysis present several advantages, including high sensitivity, high precision, low detection limit (DL) (lower for ICP-MS and AAS), and the opportunity to detect many trace metals simultaneously (ICP-OES and ICP-MS). Their performances are compared in Table 2.1.

Table 2.1 Summary of the performance of the “gold standard methods” for toxic metal analysis.

	ICP-OES	ICP-MS	AAS
Sample separation	plasma that excited atoms, which emit photons	plasma which generates cations	flame atomizer
Ion detection	wavelength of emitted light	mass-to-charge ratio	wavelength of absorbed light
DL in the	ppb range	ppt range	ppb range
Multi-metal analysis	YES	YES	NO
Sample preparation	YES	YES	YES
<i>In situ</i>	NO	NO	NO
N of elements detected	73	82	>70
Extra	higher TDS tolerance	+ isotopic analysis	
Cost	£ 30,000 - 50,000	£ 150,000 - 250,000	£ 15,000 - 40,000

However, they also have several drawbacks: they are expensive, they require a constant supply of costly chemicals, reference materials are required to ensure the quality of the

results obtained and well-trained staff are essential for performing the multi-step sample preparation and analytical procedures. Also, only total metal concentration can be determined, while speciation data is only possible with complex extraction and separation techniques. The biggest disadvantage is the impossibility of being used *in situ* and real-time at remote sites and to detect the immediate effects of accidental or unexpected contamination events. Considering the limitation of the current gold standard methods, a more suitable technique, that is able to monitor toxic metals in polluted water is required (Li et al, 2018).

2.2 Novel strategies and frontiers for toxic metal analysis

The emergent drive for water quality has increased the demand for devices to monitor the presence of toxic metals in water (Korostynska et al, 2013b). Meeting the requirements set by the EU WFD requires research and development of novel strategies for effectively monitoring freshwater resources (Brack et al, 2017). Traditional grab and automatic sampling with consequent laboratory analysis limit the ability to quantify the correct concentration of selected toxic metals, and to evaluate their behaviour in particular environmental conditions, which can determine accidental pollution events. Consequently, the requisite of on-line systems to monitor polluted water has sparked the development of remote detection and monitoring systems. Considering its importance, attention to *in situ* monitoring systems is increasing, and researchers and industries around the globe are working on finding affordable and effective sensing technologies that can guarantee a rapid response through continuous measurements (O'Flynn et al, 2010).

In this section, current trends and interesting innovations in water quality monitoring are discussed. Researchers must develop appropriate smart sensors and sensor systems that

will be able to survey freshwater, with a particular focus on toxic metals monitoring, as no current sensing system can be integrated as a part of a national water security monitoring network (Mukhopadhyay & Mason, 2015). During the last two decades, technologies for analysing water quality have evolved, with the aim of offering the advantages of operational surveillance and early warning *in situ*. Modern approaches are based on different methods for on-site monitoring including electrochemical, optical and biosensors (Figure 2.6).

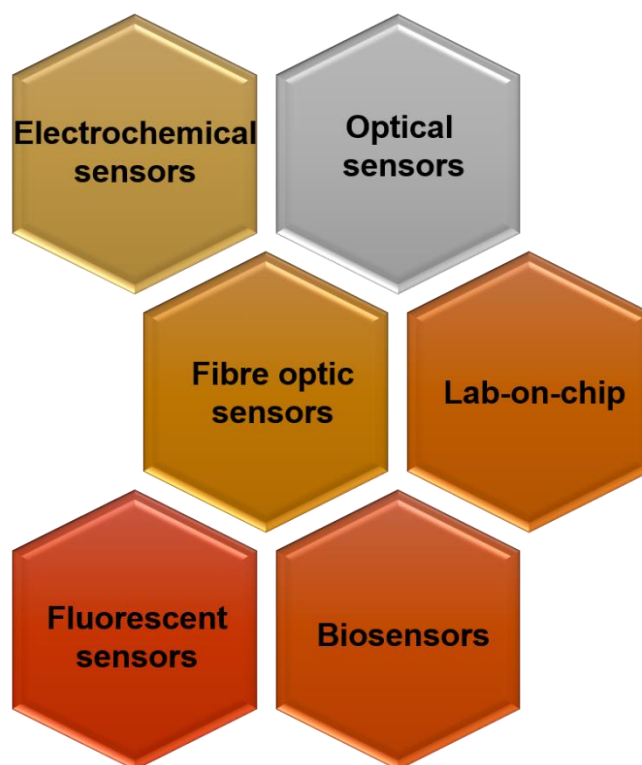


Figure 2.6 Example of research fields for water quality monitoring focused on toxic metal detection. Although they suffer from limitations, these sensing technologies are addressing the challenge of producing portable devices with a rapid response (Varun & Daniel, 2018).

2.2.1 Electrochemical methods

Electrochemical methods are considered the only current sensing systems with high sensitivity and that can be adapted and adopted for on-site monitoring (Tesarova et al,

2009). They are low-cost and give a rapid response. They comprise three parts: 1) an electrochemical sensing system; 2) electrochemical detecting instrument; 3) an electrolyte. The detection device is usually composed of three electrodes: a working electrode (WE), reference electrode (RE), and counter electrode (CE). The modification of the surface of the WE allows the specific identification of selected metal ions (Lu et al, 2018). Metal cations are reduced on the working electrode surface and transfer electrons, which generate a measurable signal. The principle is based on the quantification of the metal ions under test depending on a variation in electrical parameters, such as resistance, potential, current, or the current-voltage curve.

These methods present several advantages, such as high sensitivity, accuracy, and speciation determination, although they tend to have low selectivity (Pujol et al, 2014). Commercially available electrochemical devices are capable of on-site monitoring (as they can be portable) but they require sample collection, which makes them unsuitable for continuous *in situ* measurements (probing the water) and for detecting variations in water contamination.

Current research to detect more specifically diverse metal ions is ongoing (Li et al, 2018). Electrochemical analysis can be categorised as voltammetry or potentiometry, but the only electrochemical method, which offers high sensitivity and can guarantee on-site monitoring, is voltammetry. Moreover, the evaluation and modification of the material of the surface of the WE is a constant research area for improving the sensitivity and selectivity (Lu et al, 2018). For example, Bansod et al (2017) integrated several biosensor electrodes for improving the sensitivity.

2.2.1.1 Stripping voltammetry

Stripping voltammetry consists of two essential steps. The first one is the pre-concentration, which is determined by i) the Faraday reaction, which reduces the metals to zero-valent metals and with the application of a negative potential specific for particular metals which are attracted on the WE surface; or by ii) the adsorption and complex formation between specific ligands and metal cations, which reduce them to zero-valent metals. The second step is the dissolution, and it is carried out by anodic stripping voltammetry (ASV), stripping the electrode potential to the anodic direction to obtain a specific output (current, in A) for a particular voltage (V) for specific metal ions and materials on the WE surface (Figure 2.7). The application of a potential difference using selected materials allows the determination of a specific metal.

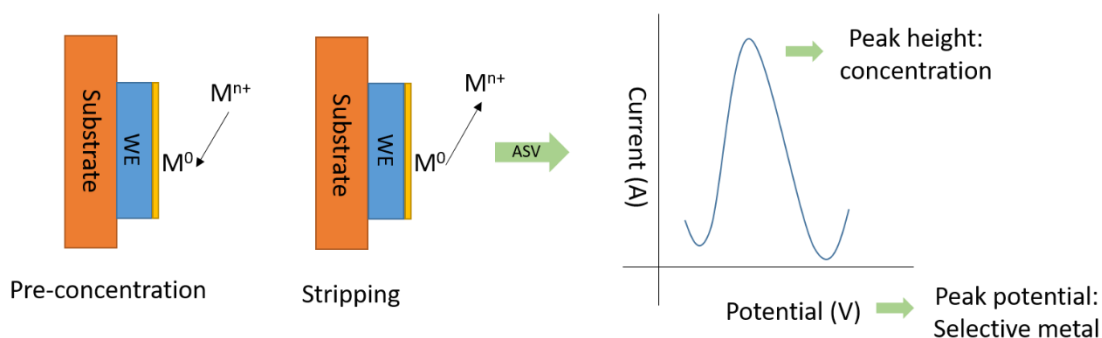


Figure 2.7 ASV principle

Depending on the “time waveforms” that are produced by the diverse materials, the most common voltammetry techniques are classified as cyclic voltammetry, square wave voltammetry (SWV), linear sweep voltammetry (LSV), and differential pulse voltammetry (DPV). Between these, DPV and SWV have the lowest detection limit (Li et al, 2018; Lu et al, 2018).

Several research projects have been carried out using a large number of different materials and variations. Among the most recent, Holmes et al (2019) reviewed work on metal

analysis using voltammetric analyses for *in situ* measurements of free metals in water. Ismail et al (2019) have experimented with the direct simultaneous determination of Pb and Cd using the square wave adsorptive stripping voltammetric (SWASV) technique using a composite electrode based on carbon graphite and lanthanum impregnated zeolite. The reported work showed high selectivity for samples of single metal ions or mixtures of up to 3 metal ions, but analysis of mixtures consisting of more than 3 metal ions as well as freshwater samples are still of great challenge. Electrochemical based techniques can guarantee sensitivity, as they have a low detection limit, even though they need sample pre-concentration, and they can enable on-site analysis and not *in situ* continuous monitoring. The most important issue is that the electrode surface does not guarantee long-term stability and reusability because of absorbing compounds, or oxidation (Shimizu et al., 2019).

2.2.1.2 Potentiometry

Ion-selective electrodes (ISEs) convert the activity of ions dissolved in a solution to electrical potential. Depending on the material on their membrane, these are mainly categorised into three groups: polymeric, polycrystalline and glass membrane ISEs. Only the target ions pass through the membrane. They are selective, low cost and portable for *in situ* monitoring. They are also promising in terms of miniaturisation and integration into standalone sensing units (Tang et al, 2018), but they are only able to detect a single pre-selected metal ion at a time, and they have limited durability. Also, they also suffer from interferences from other ions and potential drift after a period of time.

Parat & Pinheiro (2015) developed the ISIDORE probe based on the Donnan membrane technique, that was able to determine free Zn, Cd and Pb concentration in freshwater. This was also promising for *in situ* monitoring, but they did not proceed with this aim.

2.2.1.3 Lab-on-a-chip

Novel research is evaluating the integration of microfluidic processors and voltammetry with the aim to miniaturise the device for toxic metal detection. This is based on microchips, hence as 'lab-on-a-chip'. They are manufactured at low-cost (as they can be paper-based (Nie et al, 2010)) and with a diameter of a few centimetres, they are portable. Lab-on-chip can enable chemical reactions and can be made to communicate with a smartphone app (Li et al, 2018). Wooseok et al (2011) describe a polymer lab-on-chip sensor for on-site Pb (II) detection using SWASV. It claims reusability, an environmentally friendly electrode, as it replaces mercury and bismuth, and has high repeatability and a low DL.

2.2.2 Optical sensors

Optical sensors are capable of identifying the presence of toxic metals at specific wavelengths in water using conventional methods, such as absorption, reflection or luminescence spectrometry. These sensors can be disposable, such as test strips, or by using optical fibres, capillary-type devices and fluorescent compounds (Oehme & Wolfbeis, 1997), but, they suffer from poor selectivity, high DL and reversibility. As with electrochemical sensors, optical devices can also be integrated with lab-on-chip (microfluidic) devices.

2.2.2.1 Fibre optic sensors

Fibre optic sensors can give fast and accurate responses. Optical fibres consist of cores and claddings with a different reflection index. They are connected to a light source and a light beam travels through it and produces an optical response of the target. The monitoring of toxic metals simultaneously in water was not investigated fully until recent

years. Lately, Kopitzke & Geissinger (2014) have developed a novel optical fibre sensor array with the inclusion of a fluorescent compound for Cu and Zn detection which gives fast and accurate results (RSD 10%), with high sensitivity and selectivity (DL of sub-ppm). Further, Halkare et al (2019) experimented with the integration of bacteria (*E.coli B40*) on nanoparticles, and obtained a fast response (10 min) with a much lower DL (0.5 ppb) for transitional metals, although the selectivity was only proven by comparing Cd and Hg, which are chemically quite different.

2.2.2.2 Fluorescent colorimetric sensors

During the last decades, fluorescent sensors have become more popular than absorbance ones, due to higher sensitivities to the direct measurement of light intensity, instead of through the medium. Fluorescent sensors have been developed and tested for toxic metal analysis. For instance, Jiao et al (2019) developed a novel fluorescent sensor array integrating quantum dots (QDs) for Cu, Ag, Cd detection obtaining a unique fluorescent response. Responses were sifted for selectivity and sensitivity using principal component analysis (PCA) with high sensitivity (30 ng/L). Also, Yarur et al (2019) have described the detection capability for Co, Fe, Pb and Hg in the blue and red fluorescent band using carbon dots (CDs). Guo et al (2019) developed a highly sensitive and selective chemosensor for distinguishing Cu from other metals.

For improving the selectivity of metal detection, Huang et al (2019) have recently developed a simple and effective *electronic tongue*, as a colorimetric sensor array using dithizone, for distinguishing 15 different metal ions.

2.2.2.3 UV-Vis Spectrophotometer

In analytical laboratories, UV-Vis spectrophotometer can detect substances (mostly molecules) in water by simply measuring the absorbance and transmittance at specific wavelengths (~200-1000 nm). To adapt this simple method to toxic metal analysis, metal ions would need to be complexed using specific agents. Even though this method is very simple and low cost, it is mostly used for single metal analysis and high metal concentration. Recently, Zhou et al (2019) have experimented a novel method for simultaneously measuring Zn, Cu and Ni using UV-Vis spectrometry without separation steps, by integrating radio spectra derivatives and algorithms that use measurements over time and produce an estimation of unknown concentrations. Although this can detect ppm concentrations, it is problematic for both on-site and *in situ* monitoring.

2.2.3 Biosensors

During recent years, biosensors have been widely investigated for detecting toxic metals in water. They are constituted by the integration of sensitive biological components, such as enzymes, nucleic acids, bacteria, antibodies, antigens, etc. on a sensing structure (Long et al, 2013). These biological elements, interact or bind with a specific analyte under test. Their main advantage is the ability to measure bioavailability (Kim et al, 2020). The transducer can be optical, electrochemical or electroluminescent for example. Eltzov et al (2015) have produced a new portable whole-cell biosensor for detecting water toxicity. The prototype is integrated with two systems: non-disposable (optoelectronic instrumentation) and disposable (bioluminescent bacteria immobilised in calcium alginate matrix pads) parts (Figure 2.8).

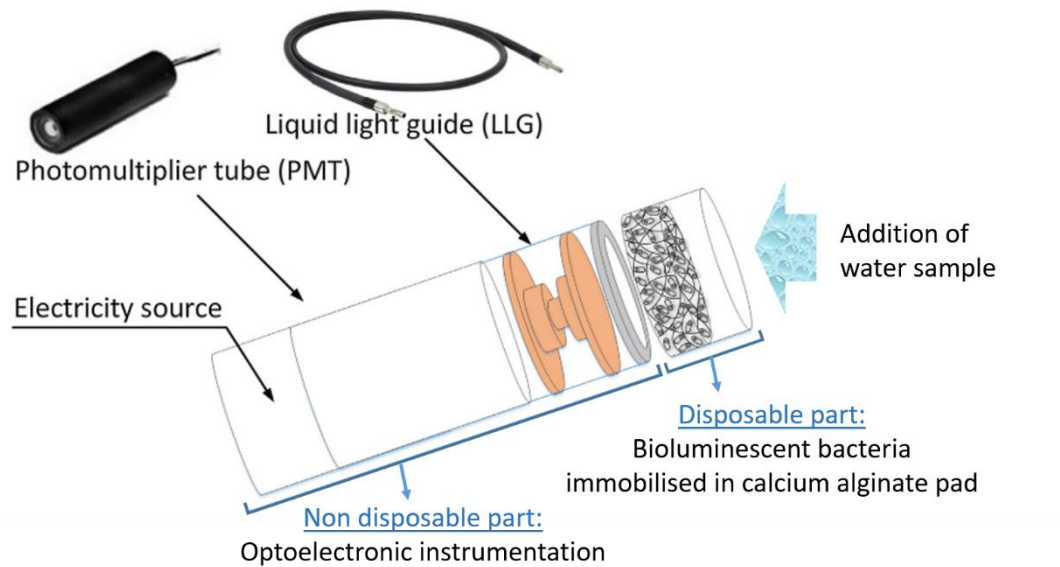


Figure 2.8 Schematic image of the biosensors developed by Eltzov et al (2015) (adapted figure)

Different toxic pollutants, including Cu and Zn, were detected with the prototype in the laboratory and on-site. The findings have shown a highly sensitive response to some of the tested contaminants. This device is attractive due to its ease of maintenance, measuring procedures, portability and sensitivity. Although its sensitivity (ppm range) is too high for detecting Cu and Zn in mining-impacted waters, it is disposable, and feasible for on-site monitoring, but not for *in situ*. As an alternative, Lukyanenko et al (2019) have developed another biosensor integrated with a disposable microfluidic chip for Cu detection (DL = 2.5 mg/L, so relatively high), with the aim of future integration for unexpected pollution in water.

2.2.4 X-Ray Fluorescence

Recently, X-Ray Fluorescence (XRF) spectroscopy has been identified as a potential portable method for detecting toxic metals in water on-site. This method involves using X-rays to excite the electrons from the inner level, which release energy in fluorescence form when they decay down. Although it has a higher DL than laboratory-based ICP

methods, it does not need sample preparation or dilution, and can be used in the field with a wider dynamic range (Pearson et al, 2018).

2.2.5 Near-Infrared Diffuse Reflectance Spectroscopy

Another technique described by Iqbal et al (2017) is promising for on-line monitoring of toxic metals in water. This method is based on near-infrared diffuse reflectance spectroscopy (NIDRS) and chemometric detection. This is a rapid and cost-effective technique, although it requires a large sample volume (1 L), and has poor selectivity, which can be in part overcome by applying partial least square (PLS) regression models.

2.2.6 Examples of commercially available sensing devices

Despite the large amount of research that is currently being carried out for toxic metal analysis, a sensing device does not exist yet that is able to monitor, *in situ* and continuously, metal pollution in water. During the last decade, only a few instruments have been commercially available for toxic metal detection on-site, but not *in situ*, limiting the possibility of detecting an unexpected change in metal concentration. The existing methods are mostly based on voltammetry analysis, so they need sample preparation (pre-concentration) and are limited in terms of simultaneous multi-metals *in situ* monitoring. Among the few commercial products, the most efficient portable systems are the Metalyser® Portable HM1000 and HM3000 (from Trace₂O, Figure 2.9a), the PDV 6000 plus (from MODERN WATER, Figure 2.9b), the Nanotek2000 (from Labsun Co, Figure 2.9c) and HM-3000P (from Skyray Instruments), which are based on voltammetry principles (Modern Water, 2012). Thus, they have a low DL (ppb), can be used on-site but not *in situ*, need sample preparations and are not able to detect multi-metals simultaneously (only 2 metals simultaneously) in 5-10 minutes (Cases-Utrera et al, 2015).

Besides, these instruments are large and arguably too expensive to be deployed as part of a monitoring network. Some other available portable cheap option is given by analysers based on the colorimetric principle (Barton et al, 2016). The indicator-based colorimetric Visual Dip& Read Test Stripes (from SanSafe) are an example, as they are cheap, disposable, semi-quantitative and give a quick response, although they are able to detect only a few individual metals selectively, including As, Pb, Fe and Cu, or the sum of multiple-metals, such as *Water Metals Check*, which can detect Cu, Co, Zn, Ni, Pb etc. As it is based on a colour evaluation comparison, it can be different for each examiner, but they are still a valuable option for field pre-screening.

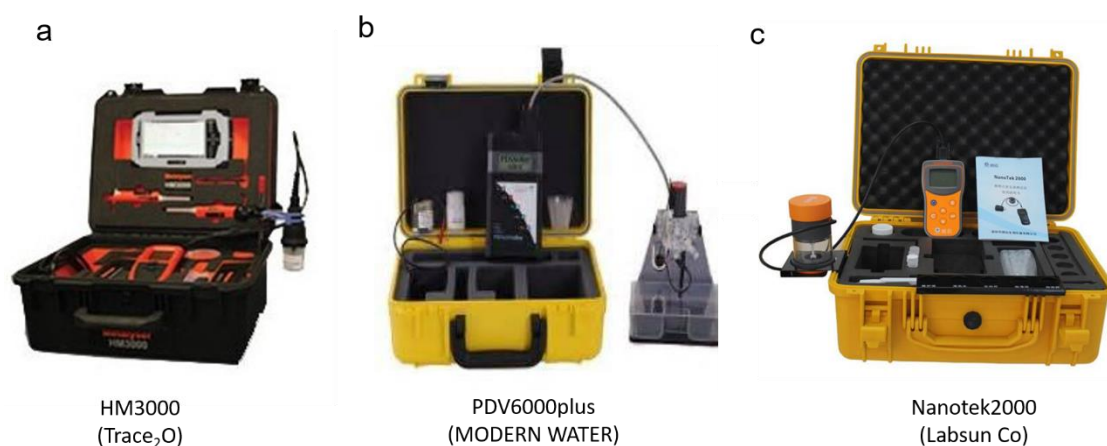


Figure 2.9 Available toxic metals analysers for on-site monitoring: HM3000 form Trace₂O (a); PDV6000 plus from MODERN WATER (b); Nanotek2000 from Labsun Co (c)

2.2.7 Summary of limitations

No single system available today can fully meet the need to determine, in real-time, the composition of water to the desired sensitivity level and cost for long-term monitoring of water bodies affected by metal mine drainage. Current methods suffer from the limitations that are summarised in Table 2.2. The wording “weak, in progress” in the column *multi-metal analysis* means that some recent research has shown the differentiation between

two or three metals but the method itself cannot perform multi-metal analysis, and more research and development is necessary.

Selective and sensitive methods (ICPs and AAS) require sample collection, problematic sample handling and are laboratory-based; voltammetry and potentiometry techniques are not selective enough and also require pre-concentration, so they can be used on-site but not *in situ*. Biosensors and fibre optic sensors are promising, but more research and improvement is necessary for *in situ* continuous monitoring.

Table 2.2 Simple comparison of promising techniques for on-site and *in situ* monitoring of toxic metals in water

Detection method	Sample preparation	Multi-metal analysis	On-site	<i>In situ</i>	DL
ICP-OES	YES	YES	NO	NO	ppb
ICP-MS	YES	YES	NO	NO	ppt
AAS	YES	NO	NO	NO	ppb
Voltammetry	YES	weak, in progress	YES	NO	ppt
Potentiometry	YES	NO	YES	weak, in progress	ppb
Fibre optic	YES	weak, in progress	YES	weak, in progress	ppb
Fluorescent	YES	weak, in progress	YES	NO	ppt
UV-Vis	YES	NO	NO	NO	ppm
Biosensors	NO	weak, in progress	YES	weak, in progress	ppm
XRF	NO	weak, in progress	YES	NO	ppm
NIDRS	YES	weak, in progress	YES	weak, in progress	ppm

2.3 Novel trend: microwave spectroscopy as a potential solution

Despite the many technological advances, significant work is still needed for the continuous evaluation of toxic metals pollution in water. Microwave spectroscopy is highly adaptable because of the different configurations of the sensing structure. It is promising for *in situ* continuous monitoring as it can guarantee an immediate specific response as soon as the EM waves are in contact with a material under test (MUT). This

methodology offers the potential to reduce costs by combining wireless sensing systems and consequently offering continuous monitoring *in situ*.

For this reason, this research project focuses on the development and testing of a novel real-time sensing system, operating at microwave frequencies, for detecting toxic metals at low concentrations in mining-polluted waters.

The next chapter describes in more detail the principle, current research carried out using this technology, and the adopted strategies for improving its sensitivity and selectivity.

Chapter 3 Microwave spectroscopy

3.1 Introduction

Using EM waves at microwave frequencies for sensing purposes is an active research approach with potential for commercialisation. This novel sensing approach has several advantages, including non-invasiveness, non-destructiveness, immediate response when the EM waves are in contact with a MUT, low-cost and power, providing the opportunity to guarantee continuous monitoring of freshwater resources.

Ongoing research on microwave spectroscopy has recently demonstrated the ability to detect changes in many materials, thanks to the adaptability of the sensing structure. Although, it suffers from lack of specificity, sensitivity and selectivity. Therefore, more research is needed to specialise this fascinating novel technology for addressing environmental problems, such as water quality monitoring. Initial experimental work shows that the method was not able to distinguish between similar pollutants in water. Consequently, this thesis investigates novel strategies for specialising this technology to detect low concentrations of various toxic metals in water.

3.2 The electromagnetic spectrum

The EM spectrum (Figure 3.1) is characterised in bands from low frequency (100 kHz) and high wavelength (10 km) to high frequencies (1 ZHz) and low wavelength (1 pm).

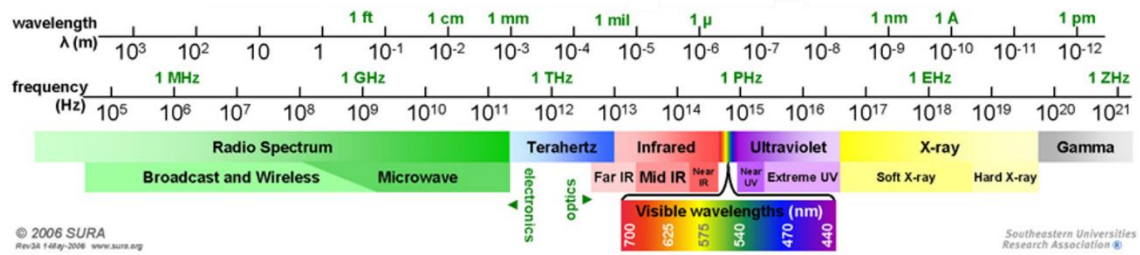


Figure 3.1 The Electromagnetic Spectrum (adapted from 2005 SURA)

Electromagnetic waves travel through a vacuum at the speed of light. They are made by two components: an electric field (E_f) and a magnetic field (H_f) which oscillate perpendicular to one another and perpendicular to the propagation direction (Figure 3.2). EM waves propagate with a harmonic configuration and the wavelength λ corresponds to the distance between the peaks of two consecutive cycles. Equation 3.1 describes the λ of EM wave with frequency (f) travelling in a vacuum (relative permittivity, $\epsilon_r = 1$) at the speed of light (c).

$$\lambda = \frac{c}{f} \quad (3.1)$$

If EM waves propagate in a medium with an ϵ_r and relative permeability (μ_r) higher than 1, the speed will be reduced according to Equation 3.2.

$$\lambda = \frac{c}{\sqrt{\epsilon_r \mu_r} f} \quad (3.2)$$

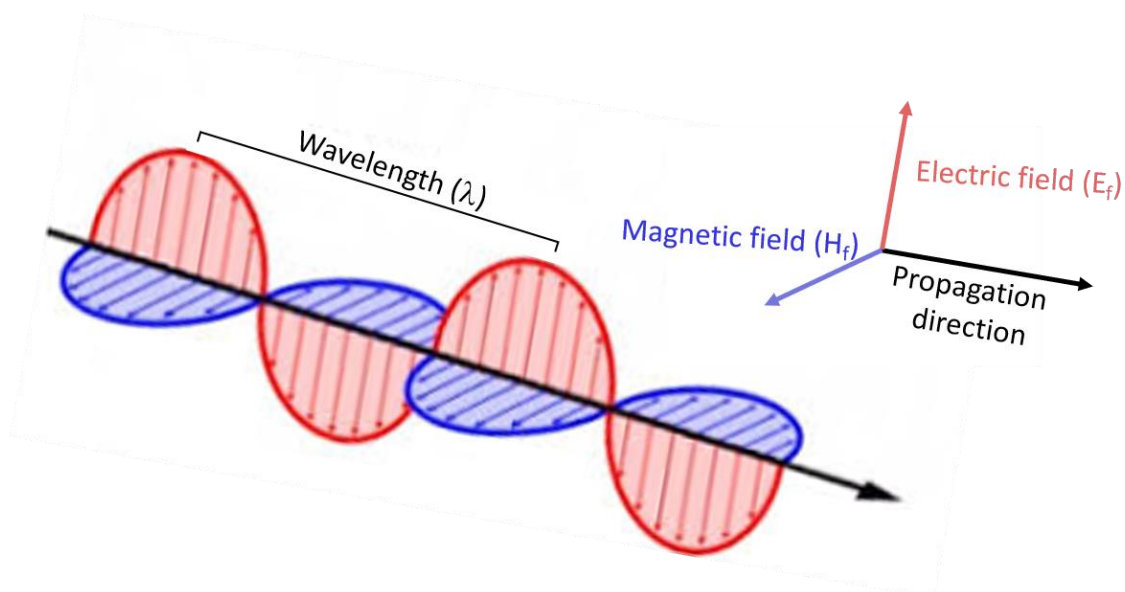


Figure 3.2 Scheme of EM waves propagation showing electric (E_f) and magnetic (H_f) field

The energy of the EM radiation is defined by Equation 3.3, where E is energy (J), h is Planck's constant (6.62×10^{-34} Js) and f is the frequency of the electromagnetic wave (Hz).

$$E = hf \quad (3.3)$$

Generalising, the bands at lower frequencies than 100 GHz (microwave radiations) are considered electronic and are generally described using frequency. More energetic bands such as optics are described in wavelengths. Terahertz (as Raman spectroscopy, between 150 GHz and 6 THz) sit between the electronic and optic regions.

3.2.1 Overview of EM Sensing

Spectroscopy methods are widely used in analytical chemistry. The absorption or transmission of the EM radiation at specific frequencies or wavelengths can be related to the structure or concentration of a gas, liquid or solid material. For sensing, specific spectroscopy methods are used depending on i) the frequency or wavelength; ii) the form of the material under test; iii) the sensing purpose, as ionic, elemental composition, molecular determination. The nature of the interaction depends on the energy of the

radiation. Analysing the EM spectrum from high to low energies, gamma and X-ray radiation break chemical bonds; ultraviolet radiations cause transitions between electronic energy states within a molecule; infrared and Raman cause internal vibrations within the molecule; and microwaves causes molecules to rotate. The microwave output is similar to other spectra that are measured, but it operates at a lower frequency range and low energy.

3.3 Microwave sensing

Microwave radiation forms part of the EM spectrum between 1 and 100 GHz. Microwave sensing technology is a developing approach which has been used for real-time and non-destructive measurements.

The domestic microwave oven operates at a specific frequency (2.45 GHz) with a high-power electron tube (magnetron), which generates and emits the EM energy (Laverghetta, 2005). The sensing principle that is currently under investigation and can measure changes in materials properties operates at low power (0 dBm as 1 mW) and over a broad range of frequencies.

During the last 3 decades, microwave spectroscopy for liquid sensing has been investigated. However, measurements of liquids are complex and not fully understood, as the rotation is hindered by intermolecular forces, and the bandwidths are much greater. The microwave is an oscillating electromagnetic field and if the molecule is polar, the microwave field can couple with the molecular dipole and cause it to rotate, but rotation is hindered so the molecule cannot re-orientate fast enough to follow the field reversals exactly. Thus it loses energy which appears as heat. Basically, there are two components to consider: i) the dielectric permittivity and 2) the dielectric loss (Jilani et al, 2012).

3.3.1 Microwave principle

The principle of microwave spectroscopy is based on the singular interaction between incident waves at specific frequencies and the analyte presented to the sensing structure. The change in the spectral response at specific frequencies depends on variations in permittivity and/or conductivity, which can be linked to the composition and concentration of the measured solution. Conductivity alone is not sufficient to explain the variations in complex permittivity (Li et al, 2019). Accordingly, permittivity (ϵ_r) as defined in Equation 3.4 relates to a material's ability to transmit an electric field and is a complex value which varies with changing frequency and temperature, and accounts for both the energy stored by a material (ϵ'), which indicates the ability to be polarised by the external electric field, and any losses of energy that occur (ϵ''), which quantifies the efficiency with which the electromagnetic energy is converted to heat.

$$\epsilon_r = \epsilon' - j\epsilon'' \quad (3.4)$$

The response of the sensor manifests itself as a resonant frequency change or an attenuation of the signal (Korostynska et al, 2013a). Different materials have diverse permittivities, and a mixture has a permittivity value, which depends on the permittivity of each component and its structure (Nyfors, 2000). The correlation of the permittivity of a material with its composition can indicate the properties of the material, with a consequent identification of the changes in the material's parameter.

The Maxwell-Garnett model describes the effective dielectric constant (ϵ_{eff}) for a dielectric medium such as water, which includes conducting particles, as it is described by Equation 3.5:

$$\epsilon_{eff} = \epsilon' + \frac{3vf(\epsilon_{par} - \epsilon_w)}{\epsilon_{par} + 2\epsilon_w} \quad (3.5)$$

where ε_w is the relative permittivity of water; ε_{par} is the relative complex permittivity of the particle under test, and vf is the volume fraction of the particles. Then, the ε_{par} is described by Equation 3.6:

$$\varepsilon_{par}(\omega) = \varepsilon'_{par} - j\varepsilon''_{par} = \varepsilon'_{par} - j\frac{\sigma_{par}}{\omega\varepsilon_0} \quad (3.6)$$

where ε'_{par} and ε''_{par} are the real and imaginary part of the permittivity of the particle; σ_{par} is the conductivity of the particle; ε_0 is the vacuum dielectric constant; and ω is the operational frequency (Abrahamyan et al, 2019).

By analysing how the characteristic details of an EM spectrum in the MHz-GHz frequency range vary upon properties of the analyte presented to the sensing structure, such as conductivity and permittivity, the change in the signal can be linked to the type and amount of sample under test.

3.3.2 Microwave measurements

The principle of using microwave spectroscopy is based on the interaction of electromagnetic waves with the tested sample through a sensing structure. The measurement is based on the unique interaction between EM waves at microwave frequencies and a sample. The source is a Vector Network Analyser (VNA), which provide a stimulus at low power (< 1 mW), and monitors the response as S-parameters (S_{nn} , Scattering parameters), which use matched loads (50 Ω) to characterise EM behaviour. A VNA can be configured with one or two-ports (Figure 3.3). A one-port configuration (S_{11} measurement) measures the reflection coefficient (return loss or Γ) of a MUT, which depends on how much the incident wave propagates through, or is reflected by the sample. Two-port configuration (S_{21} measurement) allows the measurement of the transmission coefficient, which depends on how much EM power

propagates from one port (port 1) through the MUT and is received at the second port (port 2). This configuration allows the determination of both transmitted and reflected signals. S-parameters vary with frequency.

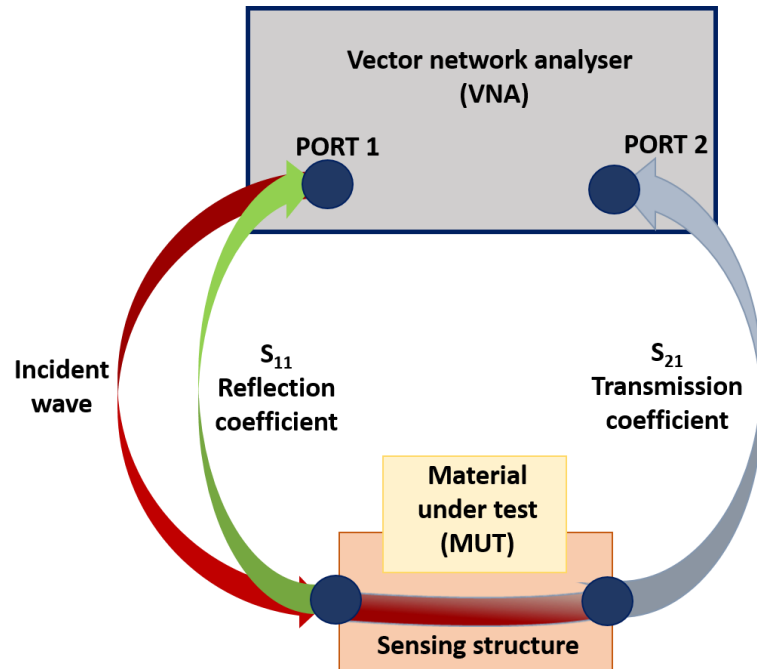


Figure 3.3 Sketch of measurement set-up and output (S_{11} and S_{21})

This method is very attractive for its non-invasiveness and non-destructiveness, its low cost and its immediate response. The output can be displayed as magnitude, phase angle, Smith chart or polar (Figure 3.4). The output has an amplitude and a phase, so is a vector quantity. Amplitude (reflection coefficient magnitude, $|S_{11}|$) is shown as a spectral response in dB (y-axis) versus frequencies (x-axis) and represents the amount of energy that is absorbed at that specific frequency. Summarising, they all describe the variation of the response at specific frequencies due to the permittivity of the MUT. At low frequencies, these are described using impedance (Z) measurements, comprising resistance (R) and reactance (X) (Equation 3.7).

$$|Z| = \sqrt{R^2 + X^2} \quad (3.7)$$

As the frequency increases, voltage and current become harder to define because the wavelength becomes small compared to the circuit dimensions. The reflection coefficient magnitude ($|S_{11}|$, described as S_{11} in this work) then becomes a more useful representation. A reflection coefficient of 0 dB represents a mismatch (100% reflection); a S_{11} of $-\infty$ dB is a perfect match (0% reflection/100% transmission).

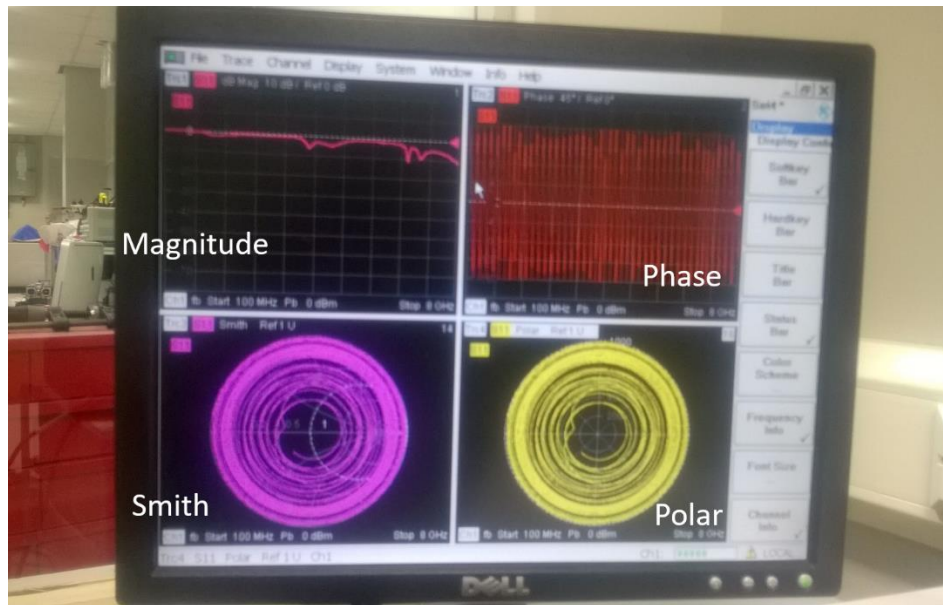


Figure 3.4 Example of raw output data as a reflection coefficient from a VNA: magnitude, phase, Smith and polar

By investigating the EM spectral response, it is possible to identify specific variations related to the MUT. Although, the response is also dependent on variations in other parameters, such as temperature, density, pressure, that can be overcome by understanding the causes and interferences in the output signal.

In a simple case of two components in an MUT, it is possible to presume the variations in S_{11} which are related to one of the two components (Nyfors, 2000). Although, if the sample under test is complex and variations are related with more constituents in the sample, more research and deeper signal analysis are necessary for clearer identification. The simultaneous existence of multiple variables such as temperature, density, moisture, structure, will affect the microwave response.

3.3.3 High adaptability: current research and applications

Microwave spectroscopy can give an immediate response as soon as a sample is in contact with the EM through a sensing structure. This technology has many advantages as it is non-invasive, non-destructive and inexpensive, which makes it highly adaptable for a wide range of materials. For these reasons, microwave spectroscopy is receiving increasing interest across a variety of applications. In many fields, including for water quality, as was extensively described in the previous chapter, existing methods are not able to give an immediate response as they require sample preparation.

Consequently, microwave spectroscopy has emerged in recent years as a novel monitoring technique in the food industry (Mason et al, 2016), healthcare (Wang, 2018), sports science (Greene et al, 2019), built environment (Heifetz et al, 2017), structural analysis (Zarifi et al, 2018a), and water quality control (Korostynska et al, 2014a).

3.3.4 Sensing structures

One reason that makes this method highly adaptable is the various physical forms that the sensing structure can take: resonant cavities, waveguides, horn antennas, flexible and planar resonant sensors depending on the form of MUT. Figure 3.5 illustrates some examples of these sensing devices and their application within the Radio Frequency & Microwave (RFM) group at LJMU. Specifically, flexible sensors were used for measuring blood lactate and glycogen variations during physical activity (Greene et al, 2019; Mason et al, 2018a) (Figure 3.5a), horn antennas for measuring moisture and steel reinforcement content or failure in concrete blocks (Kot et al, 2017) (Figure 3.5b) resonant cavities for oil validations (Figure 3.8c) and planar sensors for water quality monitoring (Figure 3.5d).

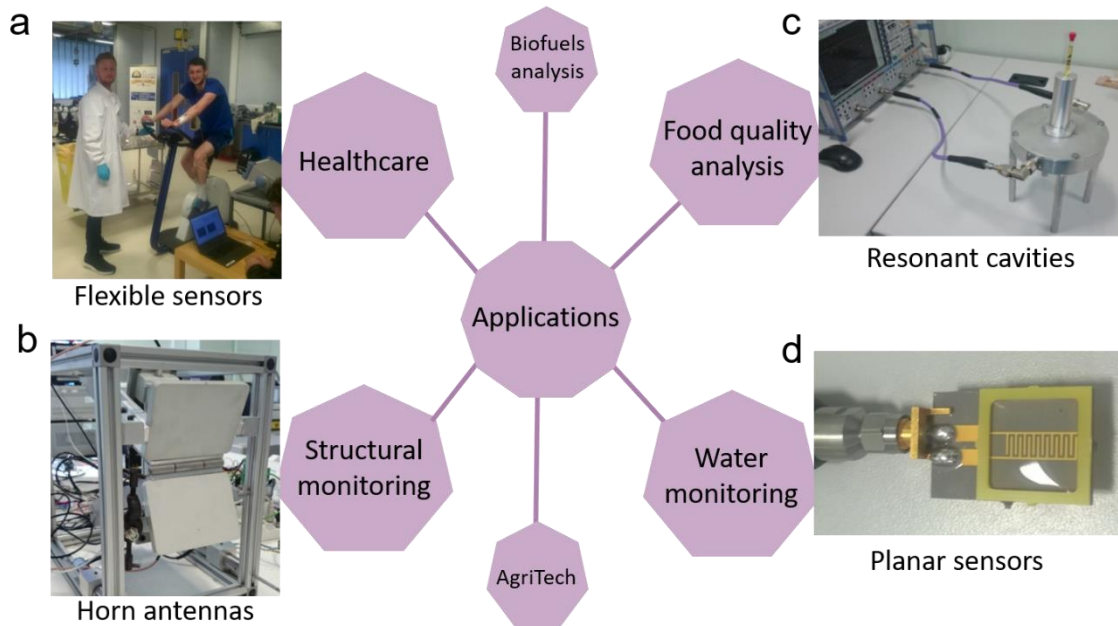


Figure 3.5 Examples of sensing structures for various applications within the RFM group at LJMU

For the analysis of liquids, waveguides and horn antennas are not generally suitable, so resonant cavities and planar sensors, are more common.

The next section describes the principle of the interaction between EM radiation at microwave frequencies and water.

3.4 Microwaves and water

3.4.1 Microwave rotational spectroscopy

Water molecules are polar, as they have a partial minus in the oxygen atom and a partial plus in the hydrogen atoms (Figure 3.6). The partial dipoles tend to align with the electric field and so the water molecules rotate. This dipolar moment depends on i) the charge separation and ii) distance between the effective charges (Hrubesh, 1973). In the gas phase, molecules are small and “free”, so they follow the “polar” microwave radiation quite easily. The water dipole attempts to continuously reorient in the electromagnetic radiation's oscillating electric field, but in the liquid phase, they are packed by hydrogen

bonding. Consequently, when a molecule tries to rotate, there is an opposite force because the hydrogen bonds try to stop it rotating. The net result is that the water cannot follow the applied field perfectly which leads to vibration rather than rotation with a consequent loss of energy which appears as heat.

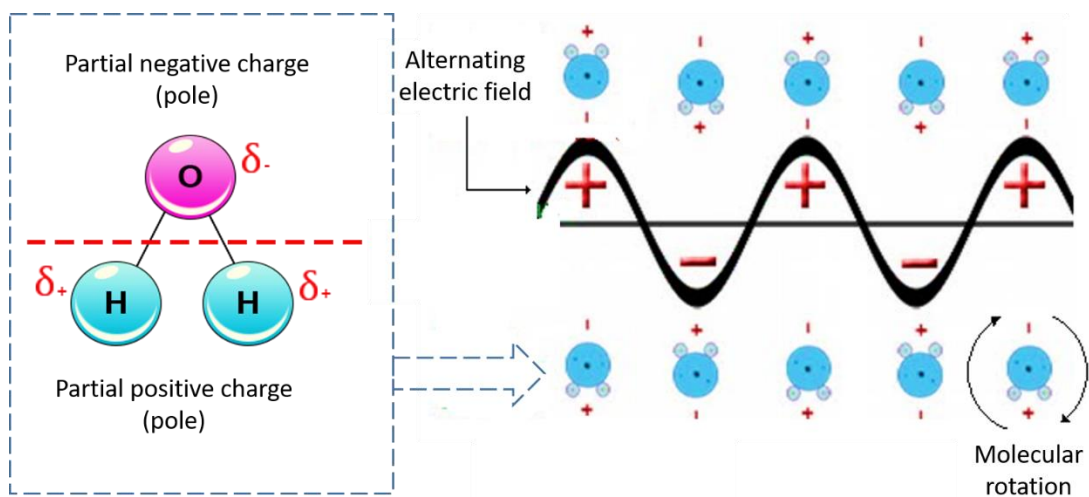


Figure 3.6 Scheme of the polar orientation of the water molecules with the EM field at microwave frequency and molecules rotation

It is also important to consider the interaction between the microwave radiation and charged ions in water. Generally, ions collect water molecules (polar) around themselves, due to their positive charge (Figure 3.7). Water molecules that are attached directly form the 1st hydration sphere where water molecules are ordered (inner hydration shell). Then, other molecules are attached to them, by hydrogen bonds and form the 2nd hydration sphere (outer hydration shell), and water molecules are semi-ordered. It is possible to go to X number of hydration spheres and exterior water is randomly distributed (bulk water). The attraction becomes weaker when the water molecules are more distant from the ion and less attracted. Hence, the molecules on the outside of the cluster are very much more weakly attracted than those closer to the metal ion. The bulk water will constantly interchange water molecules with the hydration sphere.

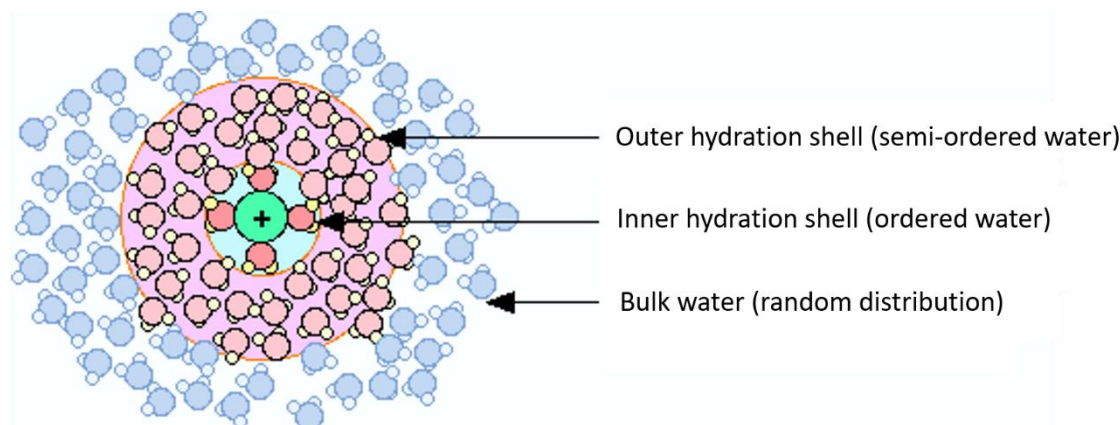


Figure 3.7 Example of ion hydration spheres

The size of the hydration radius for free ions depends on i) the charge and ii) the ionic radius. This is because the conductivity increases as the ionic radius increases (Figure 3.8). For hydrated ions, it is the other way around: the hydration radius increases as the ionic radius decreases.

Another mechanism that influences the microwave adsorption of ions in water is the ionic charge mechanism. As soon as the microwave radiation interacts with cations and/or anions in water solution, will tend to move in the direction of the electric field. The field is in constant polarity, so the ions are oscillating backwards and forwards.

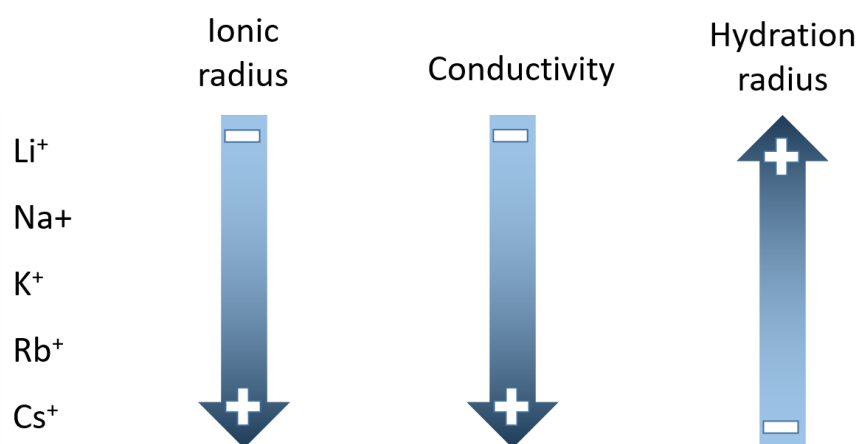


Figure 3.8 Example (group 1, period 1 in the periodic table) and their association with ionic radius, conductivity and hydration radius

The presence and concentration of specific pollutants is related to changes in complex permittivity of the solution (e.g. dielectric permittivity and conductivity) which determine

specific changes in the spectral response. The movement of the ions removes energy from the electric field, so in terms of the complex permittivity it effectively increases the ϵ'' term (refer to Equation 3.6). If the frequency (ω) is very high, the ions will not react quickly enough to generate any significant losses. This is why saltwater has a similar transparency at visible wavelengths to deionised water. Even metals stop being conductors at high frequencies, so silver cannot be used as a mirror to reflect x-rays like it can for longer optical wavelengths.

3.4.2 Microwave analysis of liquids

During the last few decades, research has been carried out to measure liquid materials using microwave spectroscopy. Considering the variability of the sensing structures, the most successful experiments for detecting a mixture of diverse liquids (e.g. oil and water) or target particles in liquids were obtained using resonant cavities and planar sensors. Figure 3.9 shows the common connections tools between the sensing devices and the VNA. Commonly, a flexible coaxial cable is used for connecting the VNA with a sensing structure. Generalising, N-type connectors are used for connecting the coaxial cable to a resonant cavity; SMA connectors, which are smaller, are soldered to planar sensors.

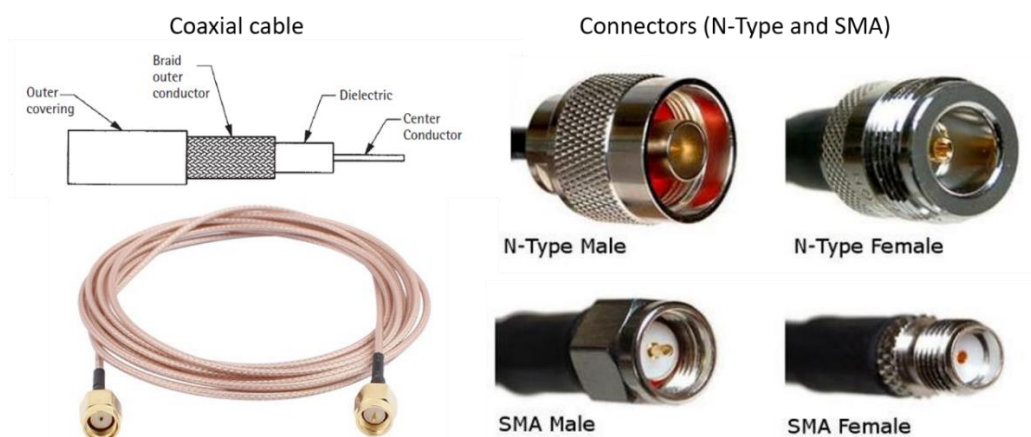


Figure 3.9 Example of connection between analyser and sensing structure: coaxial cable and connectors (N-type and SMA)

Current research (Kapilevich & Litvak, 2007) has demonstrated the possibility of identifying the presence, and quantifying the concentration, of specific components in water including a mixture of water and other liquids (e.g. water and alcohol, water and fuel).

A good sensing device must meet 4 criteria (Benkhaoua et al, 2016):

- 1) a small sensor size and consequently to operate at sub-GHz frequency range;
- 2) a high Q-factor, for reducing measurement errors;
- 3) a good linearity of sensing;
- 4) a good sensitivity.

3.4.2.1 Resonant cavities

Cavities resonate when the wavelength of the excitation within the cavity coincides with the cavity's dimensions. This wavelength will change if a sample with a different permittivity is placed inside the cavity (Teng et al, 2017). They enable non-contact measurements, as liquid samples in plastic or glass containers with known dimensions and properties, can be inserted into the cavity. Figure 3.10 shows an example for cylindrical (left side) and rectangular cavities (right side) and their N-type connectors, where the sample containers are respectively in glass and plastic.

Several experiments have shown resonant cavities to be able to detect the presence and concentration of various materials. Table 3.1 summarises some examples of work that has been performed for measuring composition and concentration of liquid materials.

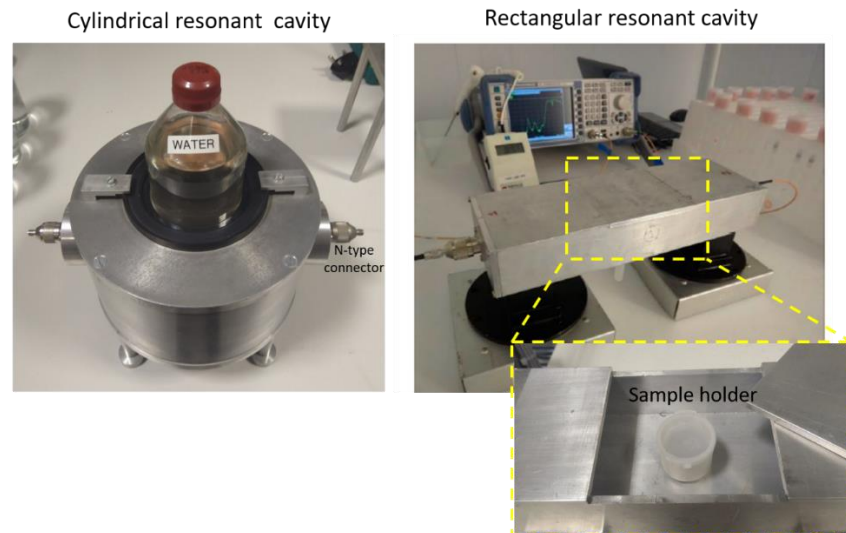


Figure 3.10 Example of cylindrical and rectangular resonant cavities

Table 3.1 Example of resonant cavities and their tested application for LUT measurements

Sensing structure	Specification	Tested LUT	C/NC ^a	References
Resonant cavity	Cylindrical	Water hardness (Ca ⁺⁺)	NC	(Teng et al, 2017)
Resonant cavity	Cylindrical	Nitrates	NC	(Cashman et al, 2017)
Resonant cavity	Cylindrical	Silver material	NC	(Ateeq et al, 2017)
Resonant cavity	Cylindrical	NaCl, KMnO ₄ , methanol	NC	(Kapilevich & Litvak, 2007)
Resonant cavity	Cylindrical	Gas-liquid two-phase flow regime	NC	(Oon et al, 2016)
Resonant cavity	Rectangular	Drip loss	NC	(Mason et al, 2016)
Resonant cavity	Rectangular	Nitrates and sulphites	NC	(Gennarelli & Soldovieri, 2013)
Substrate Integrated Waveguide Re-Entrant Cavity	+ microfluidic system	acetone and water	NC	(Wei et al, 2018)

^aC = contact measurement; NC= non-contact measurements

Despite the success of using resonant cavities for liquid measurements, they are not practical for *in situ* monitoring of polluted freshwater. A possible solution to this problem is the fluidic channels where the water sample is pumped through the sensor, as in the substrate integrated waveguide developed by Wei et al (2018) for acetone and water mixtures. Recently, Andria et al (2019) designed and modelled a coaxial structure for the real-time measurement of water-in-fuel for the automotive field.

3.4.2.2 Planar sensors

Between the numerous possible resonant structures, planar sensors have the potential to give high sensitivity and accuracy (Rahman et al, 2017). They have the advantages of small size, robustness, and low-price fabrication. They are light and practical for *in situ* and continuous monitoring. They can be rigid (Korostynska et al, 2014a) or flexible (Nag et al, 2019b) and soldered with SMA connectors (Figure 3.11), for connecting to a coaxial cable.

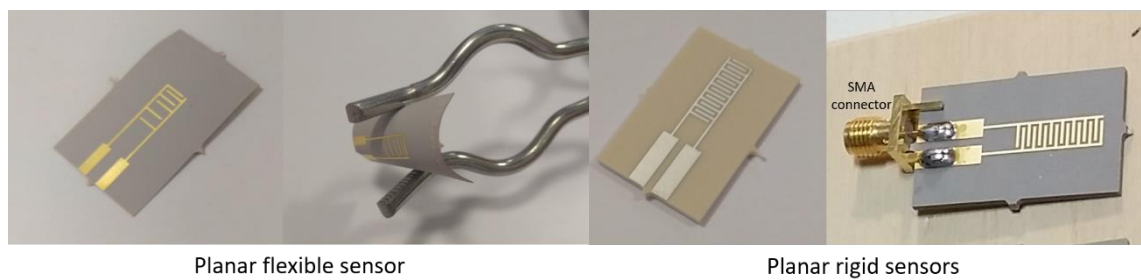


Figure 3.11 Example of flexible and rigid planar EM sensors

During the last few years, several planar microwave sensors with different conformations have been developed and tested for diverse liquid sample compositions in deionised water (DW) and various mixtures, for both qualitative and quantitative concentration measurements. Some examples are summarised in Table 3.2. They can work both in contact with an LUT or non-contact, for example integrating a fluidic system which pumps water onto the sensor using a small tube (Vélez et al, 2019) (Figure 3.12). Another example of non-contact measurement is provided by Wiltshire & Zarifi (2019), who embedded the resonators with a 3D microfluidic channel for a closer contact with the LUT. Summarising, most of the tested microwave resonant structures (both resonant cavities and planar sensors) were tested for nitrates, chlorides, and various alcohol mixtures, among others. So, the feasibility to quantify various particles in water and matrix components (e.g. water, oil, alcohol) at specific frequencies of the EM spectrum, has been demonstrated.

Table 3.2 Example of planar structure and their tested application for water liquid analysis

Sensing structure	Specification	Tested LUT	C/NC ^a	References
Coplanar waveguide	with interdigital capacitor-loaded electric-LC resonators	Nitrate and Phosphate	C	(Harnsoongnoen et al, 2018)
Planar multiband sensor	Split Ring Resonators (SSRs)	Glyphosate (herbicide)	NC	(Castillo et al, 2018)
Planar sensor	Double side split-ring resonator (DSS-SRR)	Alcohols and water	NC	(Benkhaoua et al, 2016)
Planar sensor	Complementary Split Ring Resonator (CSRR)	Water and ethanol	NC	(Chuma et al, 2018)
Planar sensor	E&C shape	Glycogen	NC	(Greene et al, 2019)
Flexible planar sensor	IDE	NaCl KCl MnCl CuCl	C	(Korostynska et al, 2014b)
Planar sensor	IDE	Tetraselmis suecica	C	(Moejes et al, 2018)
Planar sensor	IDE	Lincomycin and Tylosin Antibiotics	C	(Mason et al, 2018b)
Planar sensor	Double quadratic-shape	Ag nanoparticles in DW	NC	(Abrahamyan et al, 2019)
Planar resonator	with 3D printed channel	ethanol and DW	NC	(Wiltshire & Zarifi, 2019)
Planar sensor	IDE + microfluidic	DW and alcohol; DW and NaCl	NC	(Kilpijärvi et al, 2019)
dumbbell defect ground structure (DGS) sensor	+ microfluidic	NaCl	NC	(Vélez et al, 2019)

^aC = contact measurement; NC= non-contact measurements

Between planar sensing structures, Korostynska et al (2012) confirmed the action of a novel planar sensor with a sensing element consisting of interdigitated electrodes (IDE, also defined as interdigital by other researchers) metal patterns (silver, gold and/or copper) for water analysis, initially observing changes in the microwave part of the EM spectrum analysing air, deionised water and tap water in contact with the sensing structure. Then, Mason et al (2018b) and Moejes et al (2018) demonstrated the ability to detect respectively Lincomycin and Tylosin antibiotics and Tetraselmis suecica using gold (Au) eight-pair IDE sensors.

IDE planar sensors and contact measurements were selected because, as evaluated and confirmed by Vélez et al (2019), this was the sensor which shows the highest sensitivity for comparing various salts in water.

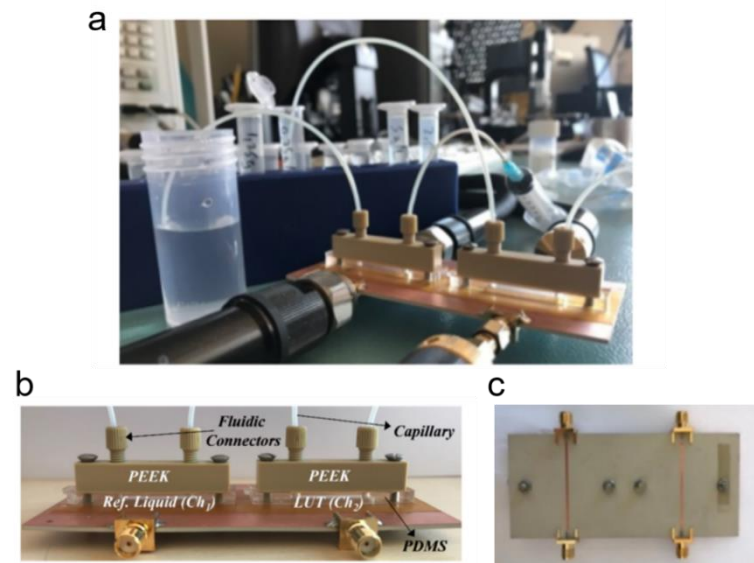


Figure 3.12 Example of measurement set-up for a planar sensor integrated with a microfluidic system and LUT (a); its side (b) and top view (c) ((Vélez et al, 2019) modified)

3.4.3 Impedance measurements at low-frequencies

IDE sensors have also been successfully used for liquid characterisation at low frequencies using impedance measurements (Z , R , C , X) by applying a small AC signal at different frequencies (Islam & Mukhopadhyay, 2017). As for microwave measurements, changes in impedance measurements in materials can be associated with ionic compositions and their concentration. Between sensing surfaces, planar IDE sensors were successfully used for analysing contaminants (*Escherichia coli* and phosphates) in water, as shown in Table 3.3. Key advantages of IDE structures include i) one-side access to the LUT; ii) control of the signal strength by changing the number and spacing of, and between, the fingers; iii) the possibility of spectroscopy measurements through a large range of frequencies, and iv) the convenience of integration of sensitive coatings (Mamishv et al, 2004).

Table 3.3 Example of IDE sensors for low-frequencies impedance measurements

Sensing structure	Specification	Tested LUT	C/NC ^a	References
Planar sensors	IDE + antibody	Escherichia coli O157:H7	C	(Wang et al, 2015)
Planar sensors	IDE	Phosphates	C	(Nag et al, 2019a)

^aC = contact measurement; NC= non-contact measurements

3.4.4 Degraded sensitivity and lack of selectivity

Microwave spectroscopy is an attractive option for detecting changes in materials in a non-invasive manner, at low-cost with the option of portability and rapid measurements. This strategy, however, suffers from a deficiency of specificity, related to low sensitivity (Δ dB related with small changes in material) and selectivity (diverse spectral response for similar pollutants) (Gennarelli & Soldovieri, 2013; Zarifi & Daneshmand, 2016). Some of the disadvantages are also related to the capability to detect minor changes in the MUT which are not related to the changes in the target analyte, such as temperature and density (Al-Kizwini et al, 2013; Buchner et al, 1999). Consequently, i) researching the causes of every change, ii) assessing how to correct them and iii) investigating new strategies for improving the specificity of the measurements are fundamental steps for the application of this technology in real-world environments.

There has been increasing research and development on understanding and improving the sensing performance of microwave spectroscopy for a deeper analysis of specific pollutants and small concentration changes related to them. Also, changes in the shape pattern of the sensing structure are not able to improve the performance of required sensitivity and selectivity of pollutants (Salim et al, 2018). The bigger problem remains the detection of more than two pollutants at low concentrations, as the aim of this project is to overcome these limitations by applying novel strategies.

3.4.5 Progress and challenges

During the last decade, research has been carried out to improve the sensing performance using microwave spectroscopy. Despite signs of progress in the field, understanding the microscopic polarization interaction between particular substances can help to develop a high-performance sensor for more specific characterisation, there are no answers for the specific response at distinct frequencies for the singular interaction between a substance and the microwaves (Li et al, 2019).

Novel strategies are being adopted to improve the sensitivity and selectivity using microwave spectroscopy, but no one has yet demonstrated the feasibility to distinguish low concentrations of similar substances, such as Cu and Zn. Amirian et al (2019) simulated the feasibility to detect between pure liquid materials, such as ethanol, ammonia, benzene, pentene using a novel sensor design and mathematical approach. Harnsoongnoen et al (2018) demonstrated the discrimination of organic and inorganic materials using planar sensors and principal component analysis (PCA); and the following year between phosphorus and nitrate using a similar approach (Harnsoongnoen et al, 2019). Other researchers are using machine learning features for selecting and distinguishing a target material (Cashman et al, 2017; Kot et al, 2018). Benkhaoua et al (2016) demonstrated an improvement in sensitivity using a DSS-SRR (Figure 3.13a and b) for methanol and ethanol % in DW, with a larger shift in resonant frequency due to the concentration of the EM field in the IDE (Figure 3.13c). Mason et al (2018b) adopted a combined sensor approach using microwave analysis, with optical and impedance measurements for a more selective and sensitive determination of antibiotics, to achieve a high sensitivity.

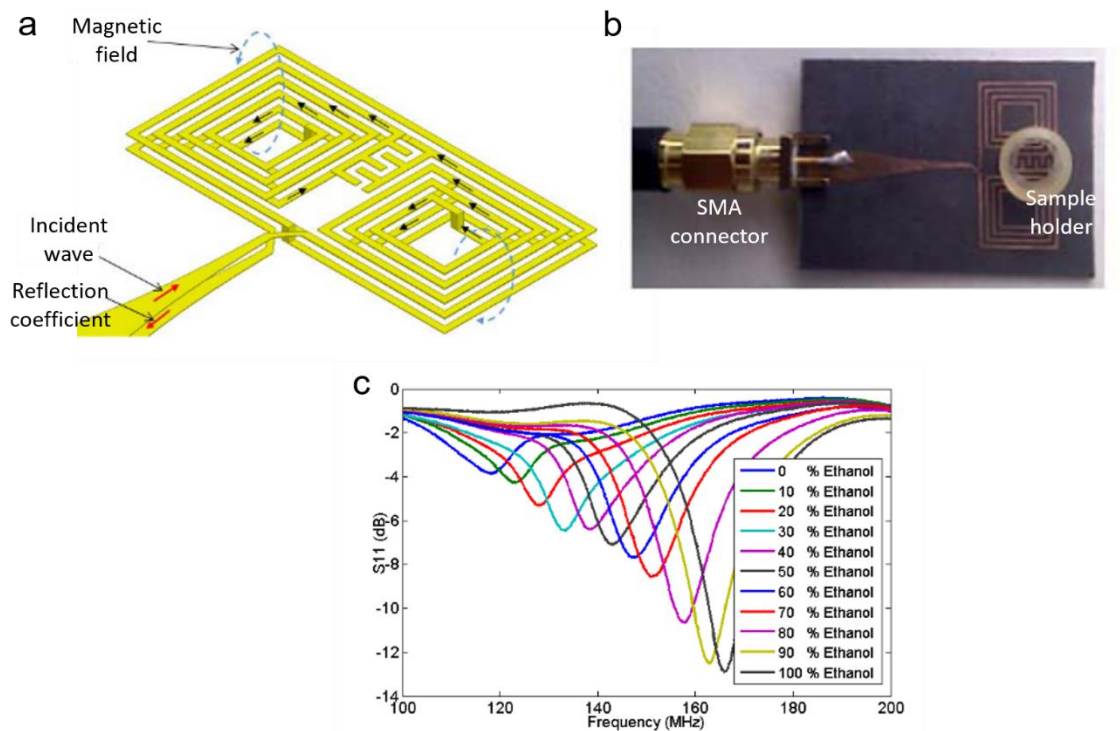


Figure 3.13 a DSS-SRR (a) developed and tested (b) for ethanol and DW mixtures which show improvement in sensitivity with resonance frequency shift (c) (modified from Benkhaoua et al (2016))

Nonetheless, the selectivity and sensitivity are a limitation for microwave spectroscopy.

Therefore, novel strategies need to be adopted for changing the spectral signal. An attractive recent approach is the integration of sensing materials onto the sensing structure, which has been experimented using electrochemical impedance spectroscopy (EIS) and IDE sensors (Afsarimanesh et al, 2018) using diverse coatings thicknesses and gas sensing (Li et al, 2019). Planar sensors are an attractive option for the implementation of materials, such as thin and thick films or microfluidic structures (Zarifi & Daneshmand, 2016).

High sensitivity, selectivity, fast response, recovery time, low hysteresis and long term stability (Adhikari et al, 2019) are the requirements for a novel sensing system able to monitor *in situ* toxic metals in water at low cost. Consequently, further improvement in sensitivity and selectivity are essential steps for liquid sensing, especially in complex mixtures (Zarifi et al, 2016).

3.5 Materials integration

The synergy between microwave sensing technology and chemical materials is providing interesting advantages in the field of quality monitoring for adapting this method to a specific purpose and it is consequently a promising area of research and development.

For a sensing platform to deliver high sensitivity and selectivity, the integration of interface materials on planar sensors is a novel, attractive approach for microwave and impedance spectroscopy (Azmi et al, 2017; Ebrahimi et al, 2014; Zarifi et al, 2018b). This has been recognised as being able to improve both resolution and specificity (Chen et al, 2012).

The principle is based on two processes: the sensing process, where the target analyte interacts, via physical or chemical interaction, with the material on the sensing structure; and the transduction process, where the interaction between EM waves, material and sample generate a particular signal (Li et al, 2019). This can be determined by non-contact measurements, where the sensing materials integrated on the sensing structure change their physical properties; or with the direct contact between the material and the analyte under test, which changes the permittivity of each component, and the consequent overall complex permittivity changes. The improvement can be associated with the increase of material thickness as well as the composition itself (Chen et al, 2012).

The principle of using distinct chemical material and the interaction with selected analytes is based on the variation in electrical properties (as capacitance, resistance, impedance, etc) and the consequent change in complex permittivity. By evaluating and understanding the functionalised sensor characteristic due to this, it is possible to obtain higher sensitivity and selectivity for a specific purpose, particularly in this research project to detect pollution of metals in surface water.

3.5.1 *Materials*

Progress has been made in the last decade in developing chemo-sensors using mostly optical and electrochemical techniques. These can recognise specific metal ions using synthetic, natural and biological receptors (Aragay et al, 2011), zeolites, inorganic oxides (Sen Gupta & Bhattacharyya, 2011), organic polymers, biological materials (Cui et al, 2015) carbon-based materials (Wanekaya, 2011) and hybrid ion-exchangers (Chatterjee & SenGupta, 2011). The interaction between the material and metal ions is the base for accredited optical and electrochemical sensing systems for detecting small concentrations in water. Usually, the specific interaction involves ionic, covalent or non-covalent bonds. Between them, non-covalent bonds, such as hydrogen bonding, van der Waals forces and π - π interaction electrostatic forces (Aragay et al, 2011), were considered the more appropriate for the integration with planar sensors and microwave spectroscopy, as these interactions are reversible. In addition, other materials and strategies, such as precipitation, ion exchange and adsorption, which are mostly used for the removal of toxic metals from wastewater, have also been investigated, as the “trapped” metals in/on specific materials can generate a change in the spectral response. Of these, adsorption is predominant. Its advantages are regeneration, low cost and easy handling (Awual, 2019). It is mostly used for natural wastes (e.g. agricultural by-products), metal nanoparticles, metal oxides, polymer-based composites and carbon-based materials. Chelating polymers are also widely used for metal ion removal or detection, thanks to their hydroxyl and amine groups, which are reactive with specific metal ions (Koneswaran & Narayanaswamy, 2009). Moreover, they are able to improve the specificity especially when mixed with metal oxides (Graunke et al, 2018). Recently, the integration of mixtures of various functional materials and the development of metamaterials (artificially made

electromagnetic materials) is taking place for specifying a particular detection/removal technique (Chen et al, 2012).

This work has, for the first time, investigated mixtures of conductive materials, metal oxides and chelating polymers for the purpose of improving the specificity of microwave spectroscopy for water quality monitoring.

3.5.1.1 Inorganic materials

Among these functional chemical compounds, inorganic oxide compositions are considered to be advantageous, owing to their strong adsorption and rapid electron transfer kinetic (Gumpu et al, 2015; Sen Gupta & Bhattacharyya, 2011). Inorganic materials have attracted considerable attention owing to their low cost, compatibility, and strong adsorption of toxic metal ions (Cui et al, 2015). For instance, zinc oxide (ZnO) nanoparticles are well known for their strong adsorption for Cu and Pb ions (Bhatia et al, 2017).

Recently, a number of approaches make use of Bi-based electrodes (Švancara et al, 2010), which have largely replaced the mercury electrode in electrochemistry for the detection of trace metals due to their low toxicity, excellent resolution of neighbouring peaks, and their low limit of detection toward metals ($<0.1 \mu\text{g/L}$) (Serrano et al, 2013). The modification of graphite screen-printed electrodes with a bismuth oxide (Bi_2O_3) precursor has been shown in several experiments to have superior sensing characteristics toward metals compared to Bi bulk electrodes (Hwang et al, 2008; Kadara et al, 2009). Also, the *nano* forms such as nanoparticles, nanowires, nanotubes, nanochannels, graphene, etc. have been widely investigated for their capability of increasing the surface area compared with bulky materials, both as electrode modification and material integration in stripping analysis and ion-selective detection (Aragay & Merkoçi, 2012).

3.5.1.2 Chelating polymers

Functional organic chemical materials have also been used for increasing the sensitivity and selectivity toward a specific pollutant. Chelating polymers have largely been used for the removal and analysis of toxic metals in water. They contain ligand groups which are capable of attractive interactions between two or more binding sites from the same ligand group and a single specific ion (e.g. hydroxyl and amine groups). Multi-dentate ligands are abundantly used to create complexes with metal ions, thanks to the chelation between them and metal cations. A large number of organic polymers which chelate with metals ions have been successfully tested, as L-cysteine and chitosan (schematised respectively in Figure 3.14a and b) (Cui et al, 2015; Verma & Gupta, 2015)

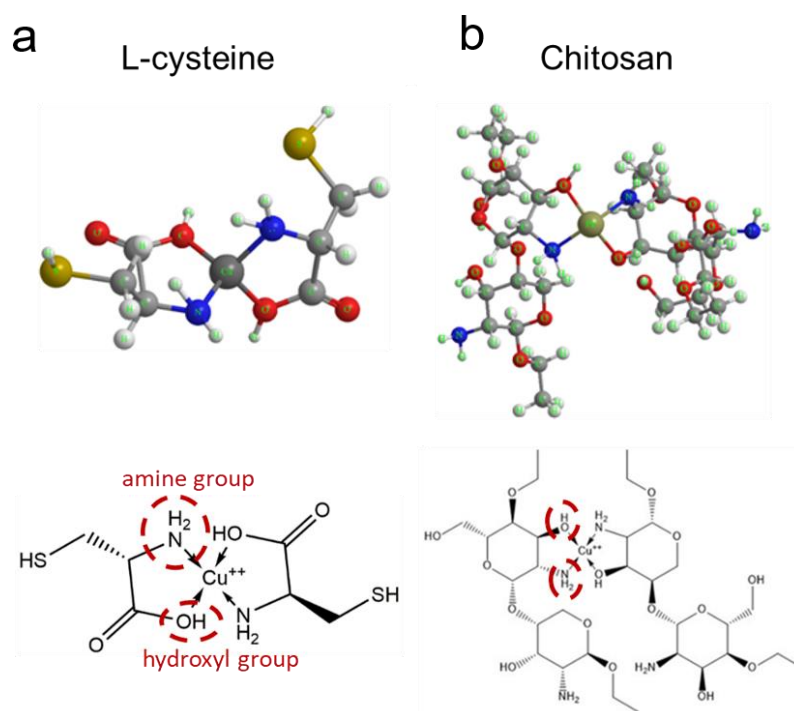


Figure 3.14 3D ball and stick structure model (on the top) and its sketched model (on the bottom) for L-cysteine (a) and chitosan with copper ion (b) generated and verified using Chem 3D

Research shows an improvement in performance thanks to the integration of chitosan for toxic metals detection and sorption. For example, Niu et al (2019) used functionalised cotton fibre with chitosan for the improved adsorption of Cu and Pb from aqueous solutions; Munim et al (2020) integrated chitosan and cellulose to improve the adsorption

capacity. The mixture of chitosan with other materials, such as ZnO, polypyrrole (Hassanein et al, 2017), ITO, (Verma & Gupta, 2015) shows improvement in the metal sorption. Likewise, l-cysteine and other material mixtures have been highly utilised for toxic metal interaction (Guang & Kim, 2008; Koneswaran & Narayanaswamy, 2009; Priya et al, 2017).

3.5.2 Depositional methods

Integrating materials onto microwave sensors is a novel strategy for microwave sensing. The most efficient techniques that can be used for IDE planar sensors' functionalisation are i) spin coating for the development of thin-film ($>0.1 \mu\text{m}$) (Nag et al, 2015; Teka et al, 2016); and ii) screen-printing technology for the development of thick films ($\sim 10\text{--}100 \mu\text{m}$). Between these two, screen-printing was selected because of its main advantage of printing a combination of different materials onto the same substrate (Kohl et al, 2014).

3.5.2.1 Thick-film technology

The goal of a cheap, sensitive and selective device to monitor metal-impacted water is achievable by the integration of chemical coatings and planar sensors using screen-printing technology (Ferrari & Prudenziati, 2012). Screen-printing is a technique where a viscous ink ($0.1\text{--}10 \text{ Pa s}$) based on functional materials is set in a screen blocking layer with a stencil (a negative of the image to be printed), which defines an open area of the mesh. A squeegee is moved across the screen and the ink passes through the mesh and a thick film is created (Prudenziati & Hormadaly, 2012). It is more compatible with the high-viscosity paste mixtures ($0.5\text{--}5 \text{ Pa s}$) as it helps to dispense the correct amount of material onto the substrate (Leng et al, 2019). Thick film is a generic term in electronics in which specific formulated pastes are applied onto a ceramic or insulating substrate using a definite

pattern. Designing functionalised sensors with the best-suited architecture will help to increase the selective identification of multi-metal ions and other pollutants simultaneously present in water. Screen-printed electrodes coupled with specific sensing materials are an attractive option for adapting diverse sensing systems to a particular purpose (Ferrari & Prudenziati, 2012). The screen-printing technique has been used to integrate a thick film onto microwave planar sensors and increase, by chemical or physical reaction, the sensitivity, specificity and selectivity between the EM waves and the toxic metal ions. Thick films are rugged, reproducible, inexpensive and have also been identified as useful for remote monitoring systems (Ferrari & Prudenziati, 2012; Kohl et al, 2014).

In this work, several materials were selected, prepared and screen-printed on planar sensors for testing with toxic metal ions in water. This can be achieved not only with the adoption of the appropriate mix of materials but also by choosing the right thickness of the film and sensor geometry (Igreja & Dias, 2006; Reimhult & Höök, 2015).

3.6 F-EM sensors

By functionalising planar sensors with certain sensitive materials using screen-printing technology, it is possible to obtain the desired sensitivity and/or selectivity to one or more specific analyte in water. Accordingly, such work has the foundations for developing new methods, based on EM sensors and functional chemical materials, capable of determining metal content in abandoned mining areas, both qualitatively and quantitatively. These sensors are defined in this work as functionalised electromagnetic sensors (f-EM sensors). This research is mostly based on the practical experimentation of novel thick-film on planar IDE sensors, which were designed, developed and tested with polluted water samples prepared in the laboratory and mining-impacted waters.

3.6.1 Proof of concept

A proof of concept that demonstrated the feasibility of detecting Pb^{+2} ions in DW using microwave spectroscopy and a resonant cavity was provided by Korostynska et al (2016). Considering its impracticability for *in situ* monitoring, this work initially demonstrated the detection of Pb^{+2} ions using planar sensors at high concentration (1-100 mg/L). These concentrations were very high compared with the typical concentrations in mining-impacted water. Other experiments demonstrated poor selectivity between Pb, Zn and Cu at concentrations just below and above the EQS established by the EU WFD or the US EPA. Consequently, this work investigated the possibility to detect and distinguish low toxic metal (Cu, Zn and Pb) concentrations by developing and testing f-EM sensors.

3.6.2 Project progression and choices

The progression of the work was determined by 1) the achievements and 2) the limitations that were identified by performing specific experiments (summarised in Appendix 1 through a smart chart). Microwave spectroscopy using planar sensors for measuring toxic metals in water were not able to detect low range metal concentrations (<1 mg/L) or distinguish between similar toxic ions with $^{2+}$ charge (Zn, Cu and Pb), which generated a very similar electromagnetic response. Therefore, f-EM sensors were developed and tested to improve the features of selectivity and sensitivity. This implies the possibility of simultaneously analysing multi-metal solutions at low concentrations, to continuously detect, in real-time, water quality and to overcome the limits of lab methods.

Therefore, the integration of EM sensors with functional chemical materials and screen-printed technology was demonstrated to be a promising approach for giving a distinctive microwave response for different multi-metal solutions, with particular focus on the detection of toxic metal ions in the surface water of mining-impacted areas.

Chapter 4 Research methodologies

4.1 Introduction

In this work, novel planar EM sensors operating at microwave frequencies with and without a functionalised coating (f-EM sensors) were designed, manufactured and tested in the engineering laboratories at LJMU using screen-printing technology, a high-resolution optical microscope and a series of low and high frequency analysers. The f-EM sensor material, pattern, composition of the functional layer, and operational parameter determination, were analysed for features linked to selectivity and sensitivity. Optical, electrical, and microwave properties of water metal solutions were detected at separate frequency ranges of the EM spectrum, using a range of low and high-frequency signal generators such as VNAs, LCR (L= inductance; C= capacitance; R= resistance) bridge and UV-Vis Spectrophotometer. The coatings were analysed using a Scanning Electron Microscope (SEM) with Energy Dispersive Spectroscopy (EDS).

Initially, the prototypes were assessed with single elements standards (Pb, Zn and Cu) over a range of concentrations (0-100 mg/L), before moving on to more complex multi-element solutions. For validation purposes, water solutions were first analysed using conventional methodologies for the detection of metal concentration, ICP-OES and/or ICP-MS and colorimetric low-cost single metal visual dip & colour test strips.

Afterwards, natural samples of water with different matrices and complex compositions were collected from mining areas around the UK and analysed in the laboratory using uncoated and f-EM sensors. Several strategies were used to adapt the sensing system for *in situ* monitoring, including waterproofing the connectors and the use of portable VNAs. This sensing system was then tested in the field in four mining areas in the UK: three in Wales and one in Scotland. Considering the infeasibility of having a metal composition comparison on-site, a first assessment of the pollution severity was evaluated *in situ*

measuring physicochemical parameters (pH, EC and T) alongside the samples acquisition. For a more specific composition characterisation, collected water samples were analysed in the laboratory using ICP-MS and a VNA.

Data were imported, analysed and summarised by graphs, correlation curves, statistical analysis and numerical methods, using mostly Excel, CurveExpert and OriginPro 9.0.

This chapter describes in detail the research methodology that was developed for this PhD research project. In the following three results chapters (Chapter 5, 6 and 7), a short introduction describes specific materials and methods that were used for particular results.

4.2 F-EM sensors development

This project included experimentation for the first time, on the integration of thick films (10-100 μm) onto planar EM sensors which operate at microwave frequencies (10 MHz – 15 GHz) for detecting toxic metals in water. Gold eight-pair IDE sensors on polytetrafluoroethylene (PTFE) substrate (dielectric material) were selected as the starting sensor. These sensors were previously developed by other researchers at LJMU. Among various planar sensors, IDEs were selected for this project because of their good response for metal concentration in water. Uncoated sensors and f-EM sensors were developed and tested with water samples in the engineering laboratories of LJMU.

4.2.1 Screen-printed coatings

This work investigated the integration of materials onto the planar sensing structure to improve sensitivity (detect metal concentration below and above the EQS established by the EU WFD), selectivity (distinguish diverse but similar compounds in water) and specificity. As described in the previous chapter, various inorganic metal oxides and

chelating polymers were selected to be integrated onto microwave sensors using screen-printing technology.

Screen printing technology is an attractive depositional method. Its main advantage is the possibility of screen-printing a mixture of materials onto a flat substrate. This is possible because the paste mixture is prepared in the laboratory.

The following apparatus were used for developing the f-EM sensors (Figure 4.1):

- (1) a screen-printer;
- (2) a mesh with a stencil;
- (3) a paste mixture;
- (4) a planar sensor;
- (5) an oven;
- (6) SMA connectors and a soldering station.

The process is based on the deposition of a mixture of material onto planar sensors using a screen-printer. The paste mixture goes through a stencil (which is the negative of the desired shape, square 2×2 cm) on a mesh to a planar sensor thanks to a squeegee on a mechanical arm. Then, f-EM sensors are placed in an oven (130-180°) for curing between each printed layer. Finally, SMA connectors are soldered to the f-EM sensors for allowing measurements using VNAs.

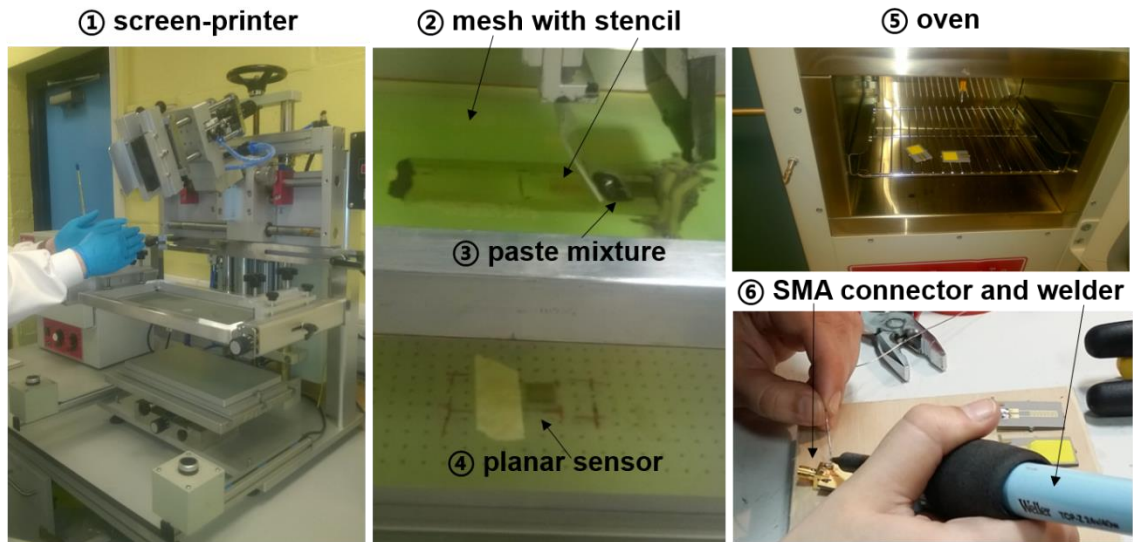


Figure 4.1 Required materials for the development of f-EM sensors: a screen-printer (1); a mesh with stencil (2); a paste mixture (3); a planar sensor (4); an oven (5) and SMA connectors and a soldering station (6)

4.2.2 Paste mixture and coatings development

To attain a paste mixture of the desired viscosity (0.1–10 Pa s), three components are required:

- (1) one or more principal functional materials;
- (2) an organic binder;
- (3) an organic volatile solvent.

These last two components work as a matrix for developing the correct viscosity of paste to be printed over the planar sensors. During this PhD project, several material combinations were prepared and tested.

A specific weight of the principal functional materials (in powder form) was mixed with 7-8% of a polyvinyl butyral (PVB), namely Butvar B98 (Sigma-Aldrich B0154) (an organic binder) and a few drops of ethylene glycol butyl ether (Sigma-Aldrich 579556) (an organic volatile solvent). Figure 4.2 shows an example of paste preparation from bismuth (III) oxide powder to screen-printable form. This was the first material to be

developed as *a proof of concept* of f-EM sensors and have been published by Frau et al (2017).

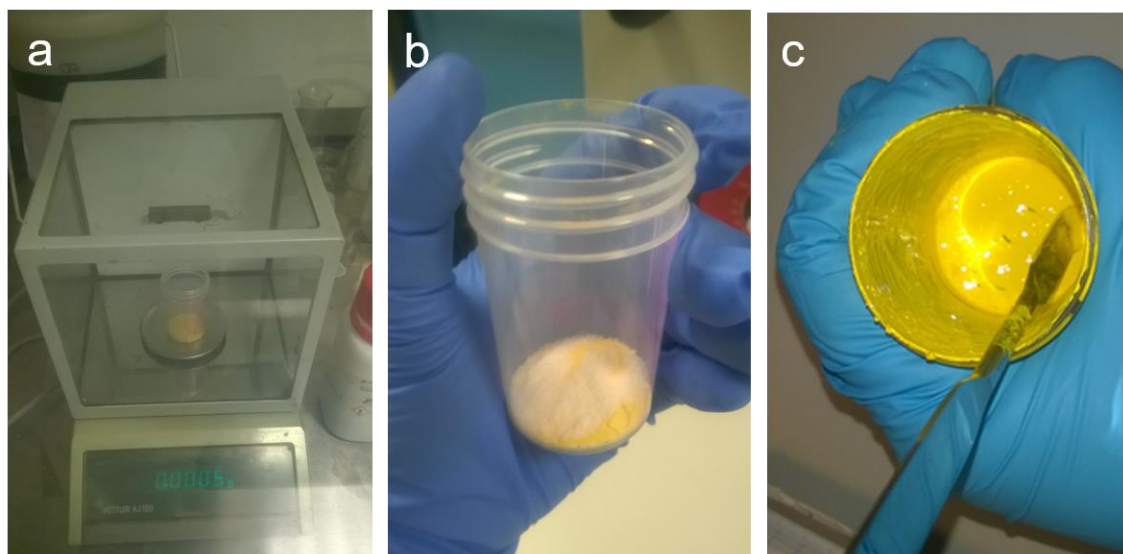


Figure 4.2 Paste mixture preparation process: specific weight of the material in powder form (a); addition of the binder (b) and addition of some drops of solvent which results in a printable paste mixture (example using β - Bi_2O_3 based paste mixture)

The developed paste mixtures were printed using a semi-automatic screen printer (Super Primex) onto:

- (1) **Ag eight-pair IDEs** that were screen-printed on microscope slides;
- (2) **Au eight-pair IDE on PTFE substrate** (microwave sensors) which are named f-EM sensors throughout the thesis.

The materials that were used in this project were carefully handled using the safety data sheet (SDS) of each product as a reference.

4.2.2.1 Functionalised Ag eight-pair IDE on microscope slides

For a pre-development and pre-characterisation, 8-pair IDEs were screen-printed onto microscope slides (Figure 4.3a) using ready-made silver pastes (Dupont 5064H (Figure 4.3b) and Heraeus LCT3410 conductors) and an IDE stencil on a mesh (Figure 4.3c).

Initial repeatability and reproducibility of the IDEs were evaluated by impedance measurements (C, R, Z).

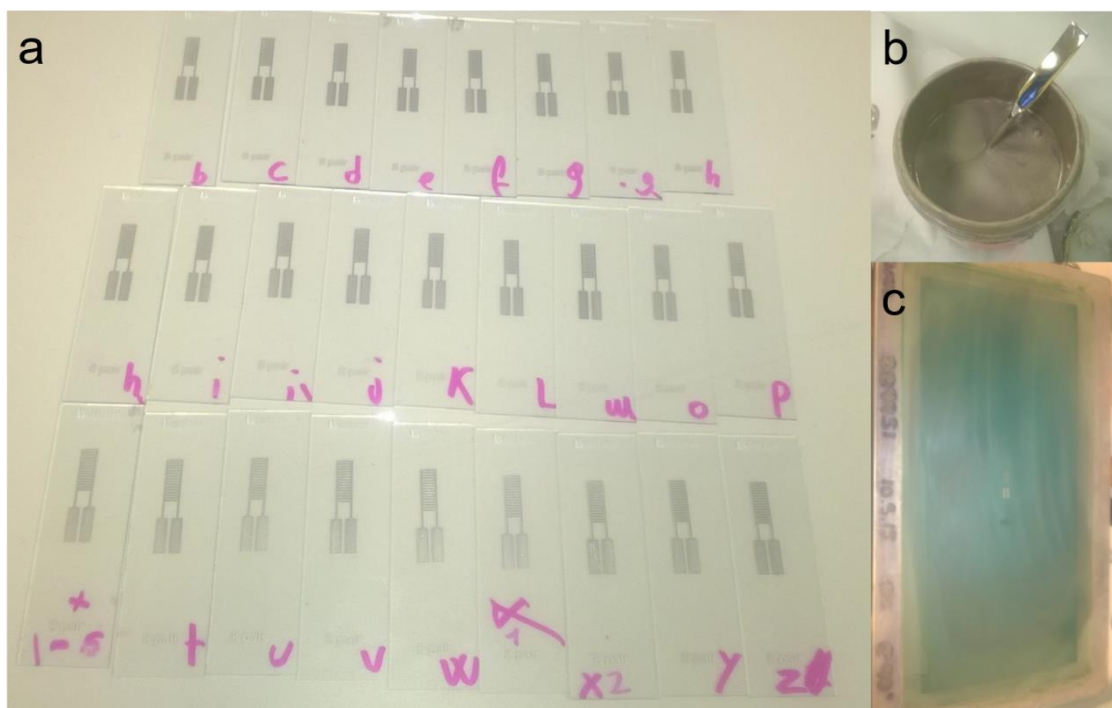


Figure 4.3 Example of developed Ag IDE screen-printed on microscope slides (a) using silver paste ready-made (b) and mesh with the eight-pair IDE stencil (c)

Coatings based on singular materials and mixtures using various percentages of the functional materials were screen-printed on top of these electrodes (Figure 4.4).

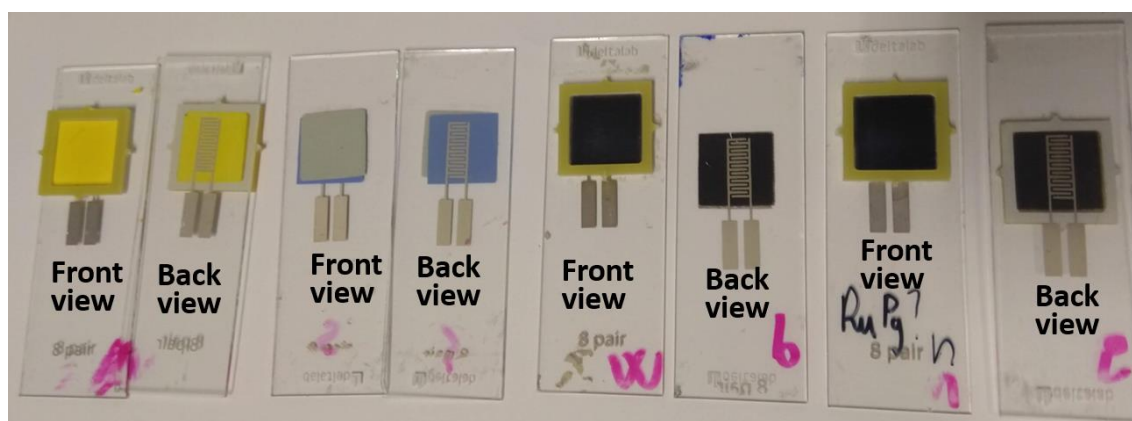


Figure 4.4 Example of some successful screen-printed coating on Ag eight-pair IDE onto microscope slides, showing their front and back view

This was done to inexpensively evaluate their printability, reproducibility, and their initial interaction between the coating material and toxic metals in water.

4.2.2.2 Functionalised Au eight-pair IDE on PTFE substrate (f-EM sensors)

The successful paste mixtures were then screen-printed onto Au eight-pair IDE microwave sensors on PTFE substrates (Figure 4.5a, b and c) which were fabricated by an external manufacturer. The layout and dimensions of the eight-pair IDE pattern sensor is shown in Figure 4.5a. Gold was used as the conductive metal material for both the bottom layer, which acted as a ground plane, and the top pattern to maintain chemical neutrality when the device is placed in contact with the analyte solution. The thickness of the Au layers was 35 μm . The microwave sensor was designed on a 1.5 mm thick PTFE substrate. A distinct feature of IDE type sensors is their higher sensitivity to change close to the sensor surface, which reduces the variation due to the external environment (Korostynska et al, 2014b).

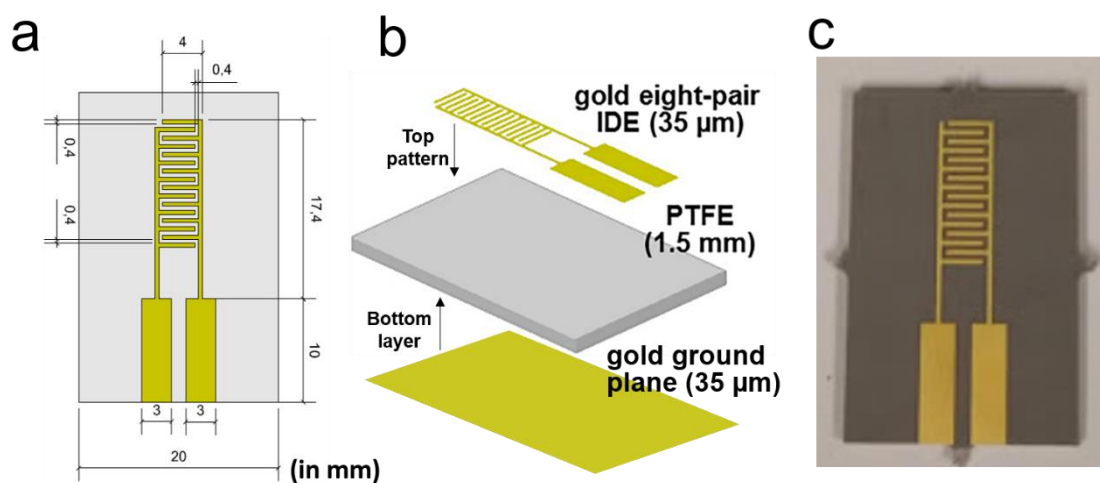


Figure 4.5 Scheme with size of an Au eight-pair IDE sensor (mm) showing its front view (a), 3D view (b) and a picture of it (c)

Initially, some sensors were also covered with a PCB lacquer spray coating (Figure 4.6) for electrical circuit protection and to avoid oxidation of the gold electrodes.



Figure 4.6 Au eight-pair IDE with a PCB lacquered coating

Table 4.1 summarises the most successful of the developed paste mixtures based on combinations and percentage of metal oxides (bismuth (III) oxide, ruthenium (IV) oxide, indium tin oxide, M10) and chelating polymers (l-cysteine and chitosan).

Table 4.1 Summary of the successful paste mixtures which describes the acronym of the developed coating, the percentage of the added binder, the percentage of each material and their CAS number

Name of the produced coating	% Butvar B98 ^a	Materials composition	CAS No.
β-Bi₂O₃	7.5 wt. %	100% Bismuth (III) oxide	1304-76-3
L-CyChRuO	7.5 wt. %	45% L-Cysteine 45% Chitosan 10% Ruthenium (IV) oxide	50-90-4 9012-76-4 12036-10-1
L-CyChBCZ	7.7 wt. %	40% L-Cysteine 40% Chitosan 20% Bismuth cobalt zinc oxide	50-90-4 9012-76-4 1853117-98
ITO	6.5 wt. %	100% Indium tin oxide (ITO) (with Polymer dielectric as an underlying layer)	50926-11-9 LTD5301 (Haereus)
M10	7.2 wt. %	100% PalPower M10 (AQM) ^b , based mostly on: 58% Magnesium oxide (MgO), 22% Silicon dioxide (SiO ₂), 14% Iron (III) oxide (Fe ₂ O ₃)	7439-95-4

^a% of the total;

^bpredominantly a mixture of metal oxides;

Specifically, their assigned name, characteristics and curing temperature and time are as follows:

- **β -Bi₂O₃**: bismuth (III) oxide nanopowder $90 < \Phi < 210$ nm particle size, characterised by tetragonal phase and space group P 421 c (114), (Sigma-Aldrich 637017) was used as the principal material. The thickness of the β -Bi₂O₃ based films (Figure 4.7a and b) was increased using multiple screen-printing, with the final coatings having either 4 or 6 layers printed, with suitable curing of the layers in an oven at 170° C for 1 hour between each print.

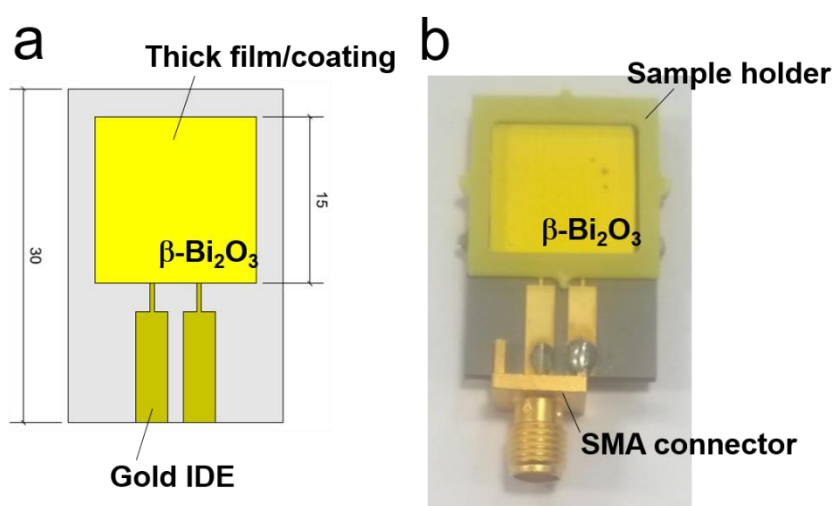


Figure 4.7 Scheme of an f-EM sensor based on β -Bi₂O₃ which shows the coatings (=thick film) dimension (a) and the picture of the final product with a sample holder and a soldered SMA connector

- **L-CyChRu**: Planar EM sensors were functionalised with two chelating polymers, chitosan and l-cysteine, as well as a resistive metal oxide, ruthenium (VI) oxide (4:4:1) (Sigma-Aldrich 168149, 448869 and 238058) (Figure 4.8a and b). The thickness of the L-CyChRu based thick film was increased using multiple screen-printing, with suitable curing of the layers in an oven at 150° C for 1 hour between each print.

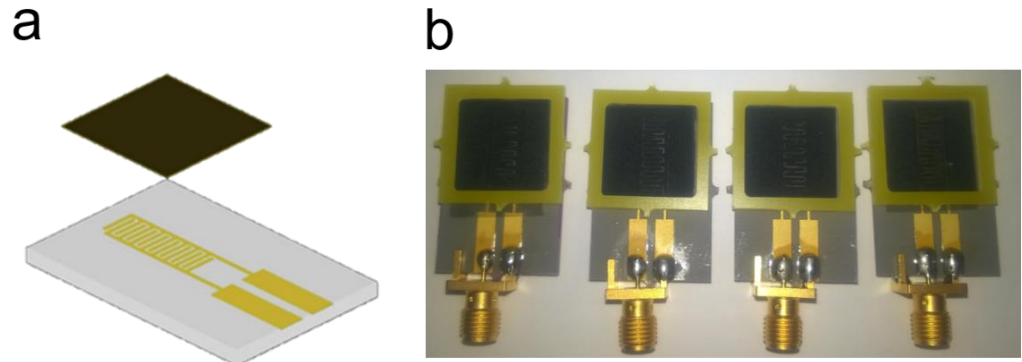


Figure 4.8 Scheme (a) and a picture of f-EM sensors based on L-CyChRu (b)

- **L-CyChBCZ:** the L-CyChBCZ based mixture is based on three materials: l-cysteine, chitosan, and bismuth cobalt zinc oxide with a proportion of 4:4:2 (Sigma-Aldrich 168149, 448869 and 631930) (Figure 4.9a and b). The particle size of this material in nanopowder form is <math><100\text{ nm}</math>. Each printed layer was cured in an oven at

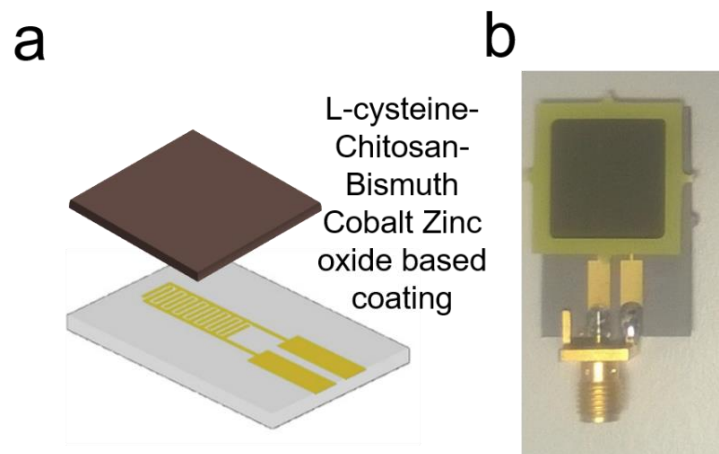


Figure 4.9 Scheme (a) and picture (b) f f-EM sensors based on an L-CyChBCZ coating

- **ITO:** The indium tin oxide (ITO) paste mixture with the appropriate viscosity was prepared by mixing indium tin oxide ($\text{In}_2\text{O}_3/\text{SnO}_2$) nanopowder, 30 nm particle size (Sigma Aldrich, 790346). This paste was prepared under a HEPA filtered hood, due to the particle size. The f-EM sensors based on ITO were previously screen-printed with a non-conductive material ($\sim 40\ \mu\text{m}$) (Heraeus, LTD5301) to

avoid short circuit; then they were screen-printed with the ITO paste ($\sim 40 \mu\text{m}$) (Figure 4.10a and b).

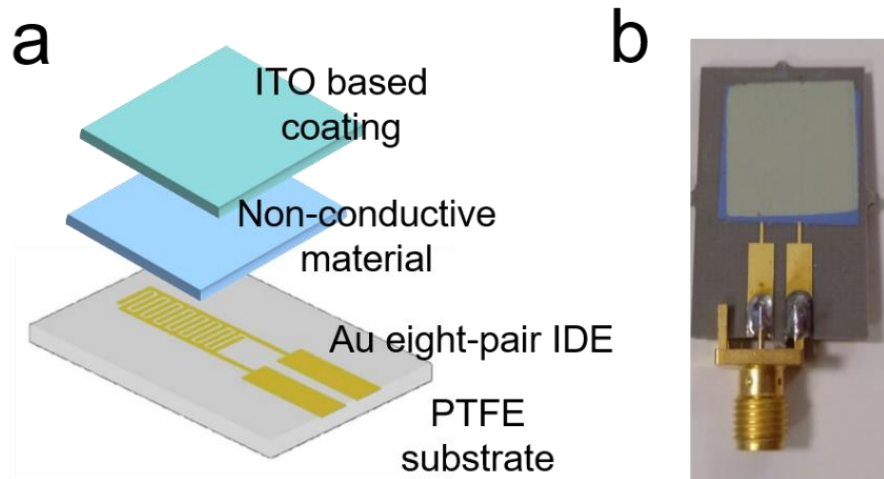


Figure 4.10 Scheme of the ITO based coating and its underlying nonconductive coating (a) and a picture of the final product (b)

- M10:** PalPower M10 is a material that has been recently developed by Aquaminerals (AQM) (Finland) for removing toxic metals from wastewater. It consists mostly of a magnesium and iron oxides based adsorbent and has been developed to remove Cu and Zn from wastewater, with subsequent recovery of the material in other forms, such as covellite (CuS) after hydrometallurgical treatment (Gogoi et al, 2018; Takaluoma et al, 2018). This material was kindly received from Esther Takaluoma, who described its successful experiments for Cu removal at the ICARD Conference in September 2018, Pretoria, South Africa (Takaluoma et al, 2018). In addition, she prepared for my experiments an appropriate granulometry to allow screen-printing (100-500 nm), for testing with the IDE sensors (Figure 4.11).

The F-EM sensors were soldered to SMA connectors for connecting the sensors to the VNAs.

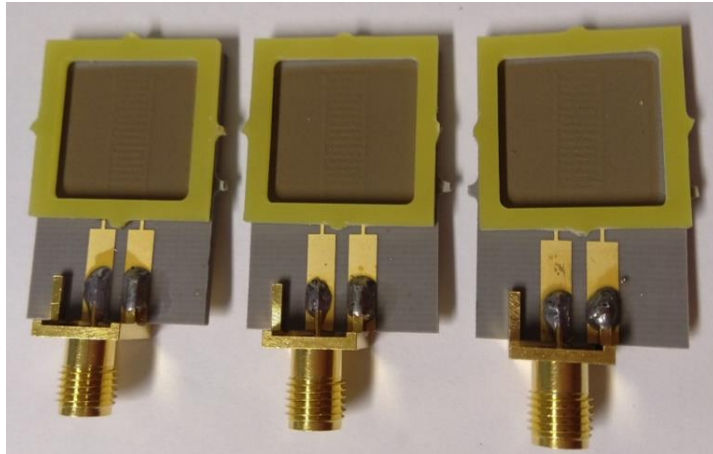


Figure 4.11 Screen-printed f-EM sensors based on M10

4.2.3 Thicknesses measurements

The thickness of the coatings was increased by multiple screen-printing, with suitable curing of the layers in an oven between each print. The final thickness of the coatings was measured using an electronic micrometer (TESA Micromaster) (Figure 4.12a), a digital vernier caliper (AOS Absolute Digimatic) (Figure 4.12b) and a surface profiler (Taylor Hobson – Form Talysurf 120) (Figure 4.12c) at LJMU.

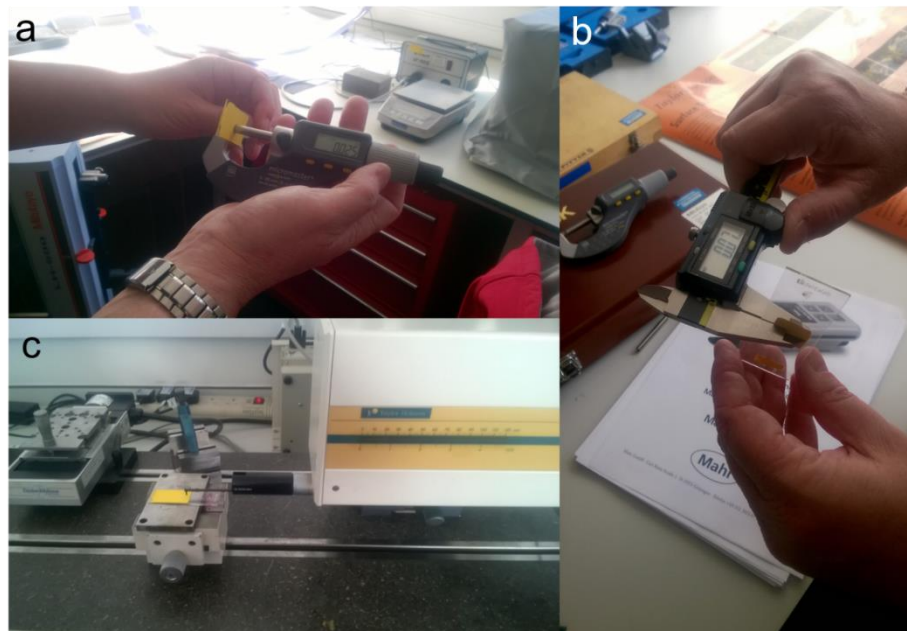


Figure 4.12 Equipment used for measuring the coating thickness: an electronic micrometer (a), a vernier caliper (b) and a surface profiler (c)

4.3 Water samples

In this work, water samples with elevated metal concentrations (mostly Pb, Zn and Cu) were prepared in the laboratory and then tested using microwave spectroscopy to evaluate the feasibility of detecting these pollutants with the required sensitivity and selectivity. After the analysis of simple laboratory-prepared water solutions, more complex water samples were analysed in the laboratory, including samples collected from mining-impacted freshwater in the UK. For all the samples, physicochemical parameters (pH, EC, T) were measured. The effective concentrations of the samples were measured using ICP-OES and ICP-MS and using a rapid qualitative screening of the metal concentration based on colorimetric test strips.

4.3.1 Lab-samples

Initially, samples with different Zn, Pb and Cu concentrations (0-100 mg/L) were accurately prepared in a fume cupboard by diluting a precise volume of ICP standard stock solution of singular metals in DW. The precise volume for preparing the desired concentration was evaluated using equation 4.1:

$$V_1 = \frac{C_2 \times V_2}{C_1} \quad (4.1)$$

where V_1 is the volume to take from the stock (in mL); C_1 is the stock solution concentration (in mg/L); C_2 represents the final desired concentration (mg/L); and V_2 denotes the volume of the final desired solution (in mL). The stock solutions of Pb, Zn and Cu were 1,000 ppm ICP standard solution certified (from Sigma-Aldrich, respectively 41318, 18562 and 68921). Water samples were accurately prepared by diluting the V_1 specific for the desired sample concentration in a 50 mL volumetric flask

(Figure 4.13a), reading the bottom of the concave meniscus (Figure 4.13b). Then, they were placed in high-density polyethylene bottles (Figure 4.13c). DW samples were prepared and then analysed for measuring the background signal and for evaluating any contamination that may occur during sample preparation or collection.

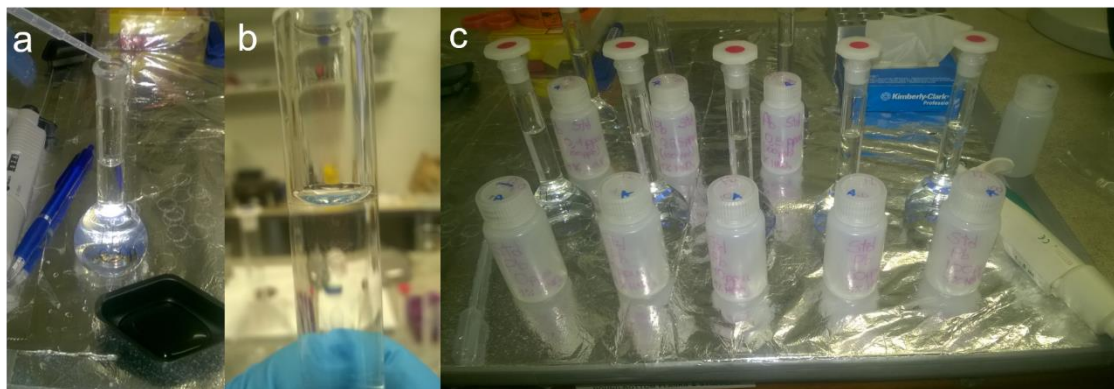


Figure 4.13 Example of metals standard solutions prepared under fume cupboard using 50 mL volumetric flasks (a) reading the bottom of the concave meniscus (b); then, they were placed in high-density polyethylene bottles (c)

Subsequently, samples based on mixtures of metals were prepared and tested, as samples created by additions and dilution, for evaluating the capability to detect small (<1 mg/L) concentration variation.

4.3.2 Field samples

Following the testing of “simple” laboratory-prepared samples (e.g. mono-metal polluted), mining-impacted water was sampled and analysed. Specifically, several freshwater samples were collected from four polluted mining areas in the UK: three in Wales and one in Scotland. These mining areas are:

1. Wemyss Mine (Mid Wales, UK);
2. Parys Mountain mining district (Anglesey, North Wales, UK);
3. Nant y Mwyn Mine (Mid Wales, UK)
4. Leadhills (Scotland, UK)

These areas and their samples are described in Chapter 6. Consequently, some *in situ* measurements using the same sample location were performed and the results are described in Chapter 7.

4.3.3 Physicochemical parameters

Physicochemical parameters which are fleeting, such as electrical conductivity (EC), pH and temperature, were measured after appropriate calibration using a multi-parameter meter (model PCE-PHD 1, PCE Instruments). The EC was calibrated using a standard solution of 1,413 $\mu\text{S}/\text{cm}$, which was corrected for temperature; the pH was calibrated using pH calibration solutions 4, 7 and 10. The temperature was also constantly monitored using a digital and a non-contact infrared thermometer (model TM-902C Lutron and 830-T2 Testo, respectively). Moreover, samples with distinct temperatures, pH and EC were analysed to evaluate their effect on the change of the microwave spectral responses. EC and pH can be an indication of water quality, as described in Chapter 1,

4.3.4 Effective concentration evaluation using certified methods

The metal concentration of the laboratory-prepared and collected samples was analysed using an ICP-MS, model 7900 Agilent Technologies (Figure 4.14a) (for low concentrations of cations), and an ICP-OES, model iCAP 6500 Duo Thermo Scientific (for high concentrations, major cations and/or higher metal concentrations) (Figure 4.14b), both equipped with an auto-sampler. Samples for ICP analysis were acidified to 1% v/v with high purity (>67%) HNO_3 .

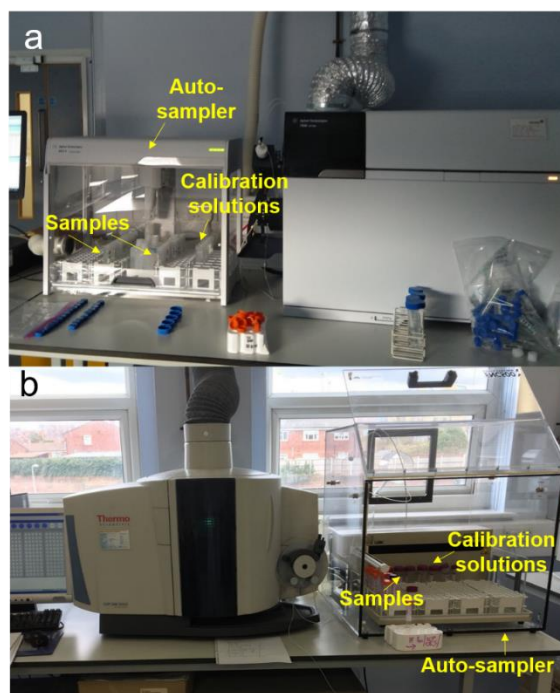


Figure 4.14 ICP-MS (a) and ICP-OES (b) at LJMU equipped with auto-samplers

For these analyses, calibration solutions at various concentrations (depending on the concentrations on the analysed samples) were prepared and measured to develop a calibration curve. The detection limit (DL) for chemical analysis was calculated at 10 times the standard deviation of the blank solutions. In addition, a certified reference material (CRM), namely EP-H-3 (Matrix Reference Material *EnviroMAT* Drinking water, high, SCP SCIENCE 140-025-032) was prepared (1:100 dilution of the stock solution in deionised water) and analysed to determine the accuracy of the measurements using equation 4.3. The accuracy represents the agreement in percentage between the mean of the *measured value* with the *theoretical value* for a quantity, and indicate how much the measured result deviates from the *true value*.

$$Accuracy = \frac{\text{measured value} - \text{theoretical value}}{\text{theoretical value}} \% \quad (4.3)$$

The precision (coefficient of variation (CV) or relative standard deviation (RSD)) indicates the repeatability of the data. It is evaluated using equation 4.4, and it represents

the standard deviation (SD) over the mean of the *measured value* multiplied by 100, are widely used to evaluate the precision of the measurement.

$$\text{Precision} = \frac{SD}{\text{measured value}} \% \quad (4.4)$$

Unfortunately, there was not the possibility to compare the microwave sensing response with certified methods for on-site or *in situ* monitoring of metals. Some collected samples were analysed using water quality test strips, a screening colorimetric technique by SanSafe (US PATENT #6541269) for selective qualitative Cu measurements (John's Copper, 481142, Figure 4.15a) and for semiquantitative contamination checking of multi-metals in drinking water (Cu^{2+} , Zn^{2+} , Cd^{2+} , Ni^{2+} , Pb^{2+} , etc.) (Water Metals Check, 481309-6). The procedure is simple: 1) a test strip is dipped into a 200 mL water sample for 30 seconds with constant back and forth motion (Figure 4.15b); 2) after removing, to shake the strip once for removing the excess of water; 3) to match the colour with the provided chart within 60 seconds for semi quantification of Cu (Figure 4.15c). Although this method is not highly precise, it gives an indication of the contamination level of Cu and total metal pollution. These test strips are developed for analysing drinking water, which has a higher tolerance limit compared with freshwater EQS (e.g. US EPA recommends 1.3 ppm for Cu as the safe limit compared with 0.034 ppm for freshwater).

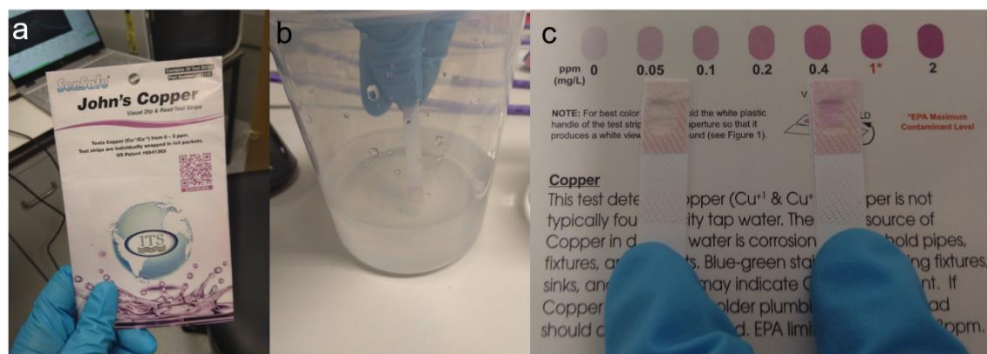


Figure 4.15 Example of colour strips for Cu screening analysis, John's Copper (a); a read test strip is immersed in water (b) and the Cu concentration is assessed by visual colour matching (c)

4.4 Measurements

The principle of using microwave spectroscopy is based on the interaction of the scattering parameters at microwave frequencies with a solution under test, and the output response as a spectral signal can be linked to the presence and concentration of specific metals in water. As described in the previous chapter, the changes in the spectral output can also be related to changes in impedance parameters, such as R, C, X. Accordingly, laboratory-prepared and collected mining-impacted water samples were analysed in parallel using i) optical, ii) low-frequency impedance, and iii) microwave measurements at separate frequency ranges of the EM spectrum. The impedance and microwave analysis were performed using uncoated and coated sensors. The impedance (capacitance (C) in F, and resistance (R) in Ω) and the microwave (reflected coefficient (S_{11}) in dB) properties of the water samples were measured using uncoated microwave sensors and f-EM sensors based on various combinations of materials. Each solution was tested 5 times using each of these three techniques to assess repeatability. Rapid and continuous measurements were performed for evaluating the feasibility to monitor real-time metal variations in water. Moreover, the application of the standard addition method using microwave spectroscopy was carried out for the first time. Measurements were performed in an air-conditioned environment at a constant temperature of 19-20°C to minimise outside influences.

4.4.1 *Optical measurements*

UV-Vis spectrophotometry was used for measuring changes in the optical absorbance of water solutions at various concentrations, as a combined measurement of water pollution. The UV-Vis absorption spectrum can be considered an optical signature of a water sample due to the absorption of electromagnetic radiation at high frequencies, in the ultraviolet

(185– 400 nm) and visible (400–800 nm) spectral region. This technique is described by the Beer-Lambert law, which models the attenuation of light properties as it crosses a sample (Mason et al, 2018b). The law is described by equation 4.5:

$$A = \varepsilon_A lc \quad (4.5)$$

where A is the absorbance, ε_A is the absorptivity (or molar attenuation coefficient) of the attenuating species ($M^{-1} \text{ cm}^{-1}$), c is the sample's concentration in molarity (M), and l is the path length in cm.

Practically, the absorbance of a solution is directly proportional to the concentration of the absorbing species in the solution and the path length. The absorbance of samples was analysed by measuring approximately 3.5 mL of the water solutions in plastic cuvettes (759170, BrandTech) and analysed with a UV-Vis Spectrophotometer (Jenway 7315) at the wavelength range 200-1000 nm (Figure 4.16).

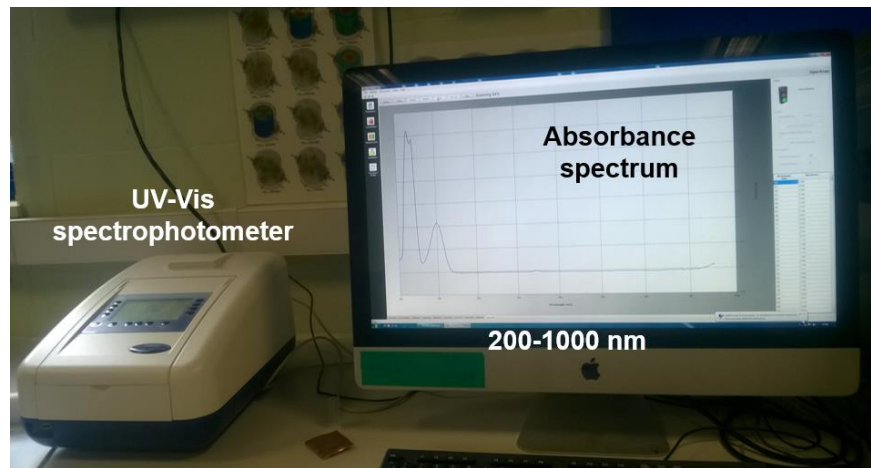


Figure 4.16 UV-Vis Spectrophotometer and its output as absorbance spectrum at 200-1000 nm

4.4.2 Low-frequency impedance measurements

The impedance properties of the samples, using coated IDEs on microscope slides, and f-EM sensors were measured using a HAMEG 8118, which is a programmable LCR bridge

(L= inductance; C= capacitance; R= resistance), that was configured in a different manner depending on the purpose. Parameters, including resistance (R) and capacitance (C) were measured between 20 Hz and 200 kHz. Capacitance and resistance measurements can detect changes in materials.

The LCR meter made use of various connectors and/or sensing structure for sample and sensors characterisation. Specifically, three configurations were used for specific purposes:

1. **Gold-plated sensor:** for impedance measurements of water samples with various metal compositions and concentrations;
2. **“Crocodile clips”:** i) for measuring the IDE and coating repeatability and reproducibility; ii) for monitoring the interaction between coatings (screen-printed on Ag IDE) and metal water solutions;
3. **F-EM sensors:** i) for measuring f-EM sensors’ repeatability; ii) for measuring the impedance variation of the f-EM sensors based on the interaction with metals;

Between these, the main purpose of using impedance measurement was the initial characterisation of coating materials and water solution interaction using “crocodile clips” for inexpensive coatings development and the decision-making process of materials to screen-print for producing f-EM sensors to use for microwave measurements. Operational modes, such as impedance parameter selection, frequency range and/or single frequency by time, were selected using a bespoke LabVIEW software interface connected to a desktop computer for data acquisition.

4.4.2.1 Gold-plated sensor on sample

Metal water solutions (Pb, Cu, Zn) at various concentrations (0-100 mg/L) were analysed at a frequency range of 20 Hz to 200 kHz. The LCR programmable bridge (Figure 4.17a)

was configured with a bespoke coaxial probe assembled on an FR4 circuit board (Figure 4.17b and c) terminating with a parallel capacitor with a constant 1.00 V open circuit voltage via a LabVIEW software interface. A gold-plated sensing structure (Figure 4.17d) with two electrodes was immersed in 400 μL of sample volume, held in place by a customised holder integrated onto a microscope slide. The sensing structure was a parallel plate capacitor and it was used for measuring C (in F) and R (in Ω) of metal solutions by measuring the relative change in dielectric constant. The electrodes were two gold-plated rods with a length of 4 mm and a diameter of 0.76 mm, with 4 mm separation between them. Considering that the measurements were performed using a parallel capacitor, it was possible to measure the variation in the relative permittivity of the water sample under test using, which for an ideal conductor is represented by equation 4.6:

$$C = \frac{\pi \epsilon_0 \epsilon_r}{\ln \frac{d}{r}} L \quad (4.6)$$

where C is the capacitance in F; ϵ_0 is the permittivity of free space; ϵ_r is the relative permittivity (dielectric constant) of the material between the plates, in this case, a polluted water sample; L is the rod length in metres; d is the separation distance (in metres) between the two rods; and r is the radius of the rod in metres (Mason et al, 2018b).

Considering that for these measurements the configuration was kept constant, the only variable is the relative permittivity. Consequently, it is possible to estimate the variation in F of diverse water samples at various concentrations, which reveals the dielectric constant change. Other variations were kept at a minimum, such as the temperature of the samples and the volume. The capacitance values were repeatedly measured ($n=5$) for the whole range of frequencies for the prepared water solutions.

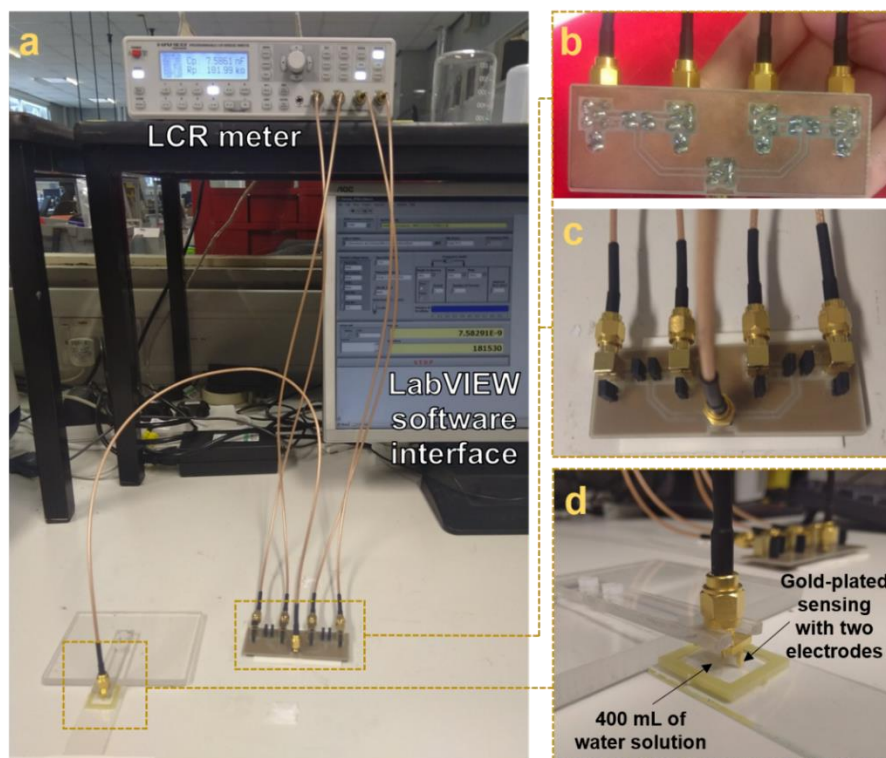


Figure 4.17 Experimental set-up: an LCR bridge and labVIEW software interface with a bespoke coaxial probe (a) (assembled with an FR4 circuit board as shown in (b), back view, and (c), front view) measuring using a gold-plated sensing with two electrodes (rods) a water sample (400 μ L), held in place by a specific holder (as magnified in (d)) (modified from *Frau et al (2019a)*)

4.4.2.2 “Crocodile clips”

IDEs were screen-printed on microscope slides to reduce development costs, and used for initial coatings tests (durability, degradability, change in impedance measurements, time responses, etc) for measuring mining-impacted water using microwave spectroscopy. An eight-pair IDEs were screen-printed to the slides, which were then covered with the coatings previously described.

The repeatability and reproducibility of the IDEs was evaluated by measuring the C and R response for multiple IDEs. The experiment was configured by placing each slide (Figure 4.18a) onto a bespoke platform, for assuring repeatability of the measurements, and connected using “crocodile clips” (R&S HZ184 Kelvin measurable cable)

(Figure 4.18b). C and R were measured between 30 Hz and 200 kHz using the LCR bridge using the LabVIEW software interface (Figure 4.18c).

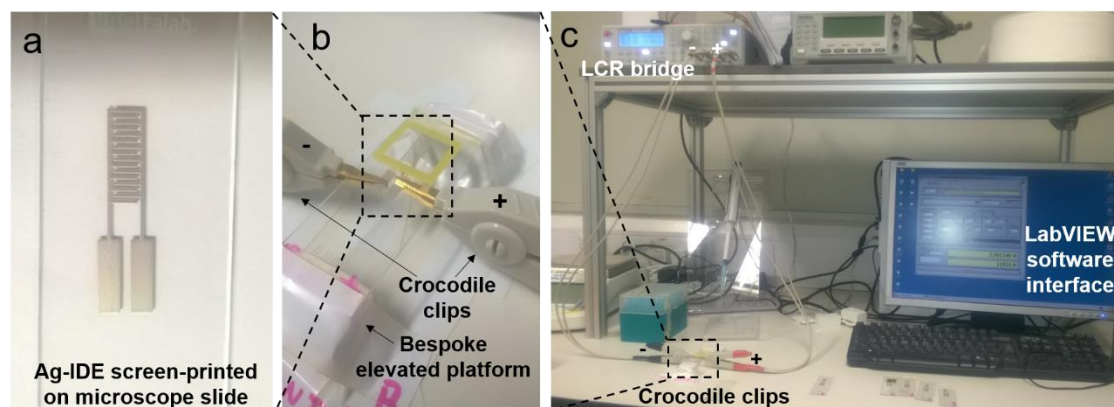


Figure 4.18 Configuration of "crocodile clips measurements" for measuring the repeatability and reproducibility of the Ag-IDE screen-printed on microscope slides (a), connected through crocodile clips (R&S HZ184 Kelvin measurable cables) elevated by a developed platform (b), connected to an LCR bridge for measuring C and R using a LabVIEW software as data acquisition (c)

The coated IDEs were measured in the same manner. Multiple IDEs (3-5) screen-printed with the same coating composition and thickness were tested. Figure 4.19 illustrates examples of the functionalised IDEs with coatings including l-cysteine (Figure 4.19a), l-cysteine with chitosan and ruthenium oxide (Figure 4.19b), and indium tin oxide with chitosan and pyrrole. An underlying layer of insulating material was used to avoid short circuits (Figure 4.19c).

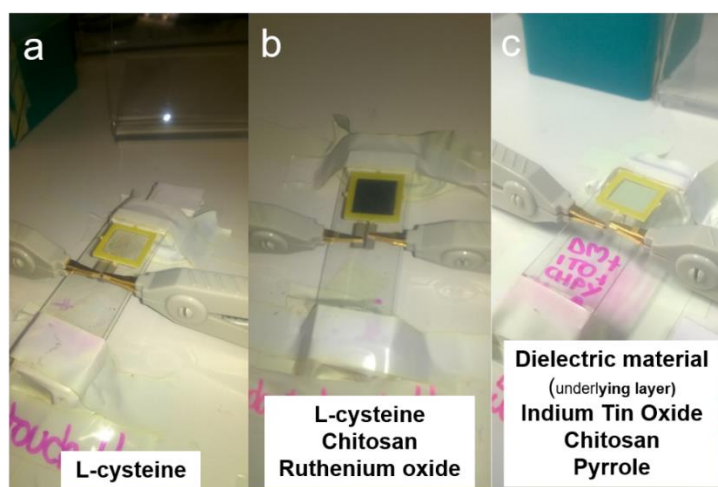


Figure 4.19 Example of functionalised IDE connected to an LCR through crocodile clips, specifically with coatings based on l-cysteine (a), l-cysteine, chitosan and ruthenium oxide (b) and on Indium tin oxide chitosan and pyrrole, with an under-layer of dielectric material (c)

The measurements were also repeated for IDEs with a sample under test to understand the variation in impedance parameters due to the interaction between the coating materials and the metal ions in the water solution. For these measurements, 400 μL of water solution were placed on uncoated (Figure 4.20a) and coated IDEs (Figure 4.20b).

Specific frequencies were then selected for time measurements, based either on the greatest R^2 and/or higher sensitivity, or using a compromise between them. Measuring the changes in impedance by time makes it possible to estimate the interaction time, such as the adsorption or chelation, of the metal ions on the surface of the coating materials. Water solutions were tested for 30 minutes using various functionalised IDE sensors. The output was extracted every 30 seconds.

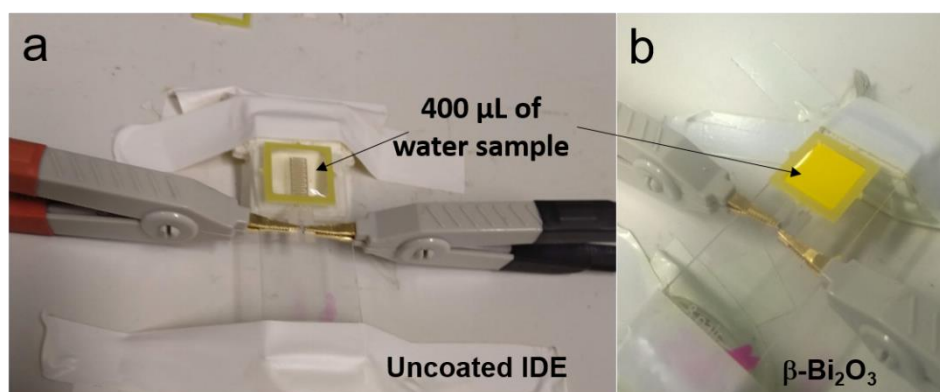


Figure 4.20 Uncoated (a) and functionalised IDE on microscope slides with a 400 μL sample held in place by a specific holder (b)

Spectra measured with the IDE sensor were recorded for air and several concentrations (0-100 mg/L) of Zn, Pb and Cu to evaluate the differences in output between the coatings for different samples.

4.4.2.3 F-EM sensors

The best paste mixtures were screen-printed onto microwave sensors for developing the f-EM sensors. The capacitance (C) of some of the f-EM sensors were measured to evaluate the repeatability. Their interaction with samples was measured with a bespoke

coaxial probe as shown in Figure 4.21 over the full frequency range, with 400 μl of sample volumes. Once the frequency response was analysed, two frequencies were selected to determine the variation in capacitance over 30 minutes, with measurements every 5 seconds. This was performed to assess the reaction between the coated sensors and metal solutions.

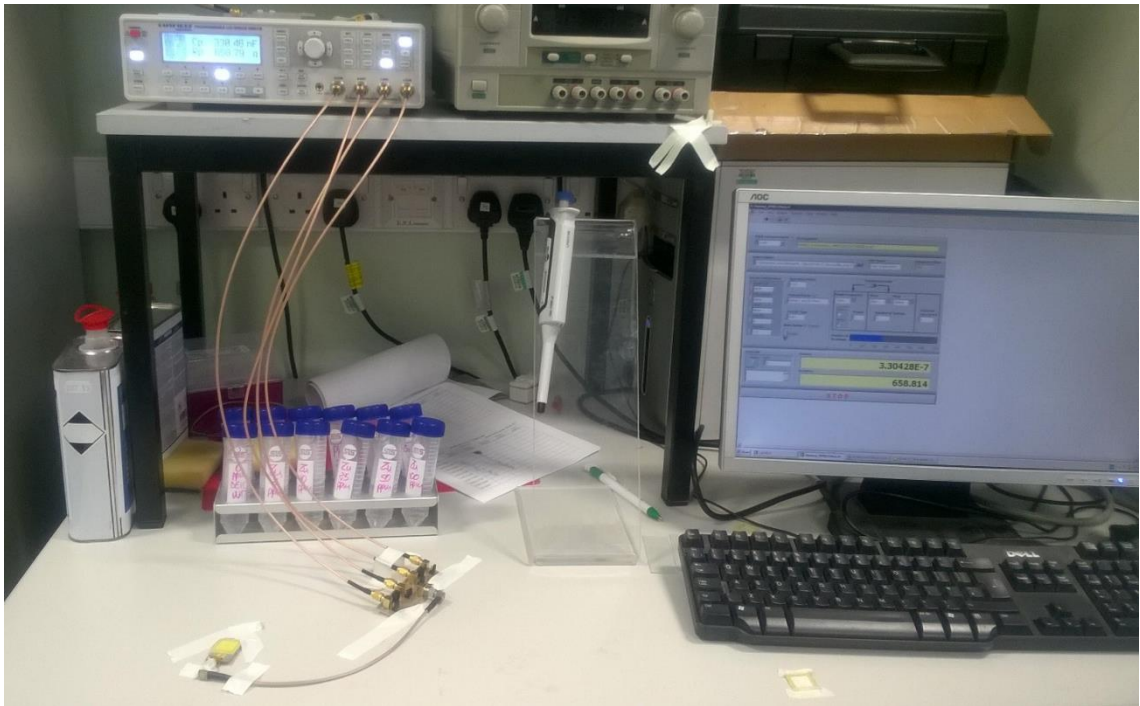


Figure 4.21 Example of f-EM sensor based on $\beta\text{-Bi}_2\text{O}_3$ connected to the LCR bridge

4.4.3 Microwave measurements

The principle of microwave spectroscopy is based on the interaction between incident waves, produced by a VNA, and a water sample in contact with a sensing structure. In this work, the VNA used a one-port configuration for S_{11} measurements of the reflected spectral response at specific frequencies, as illustrated in Figure 4.22. The uncoated and f-EM sensors were used for measuring laboratory-prepared and collected mining-impacted water samples. The purpose of using f-EM sensors is to obtain a more specific spectral response for diverse sample compositions due to the specific physical or chemical

interaction which changes the complex permittivity of the system and allows a more sensitive and selective response.

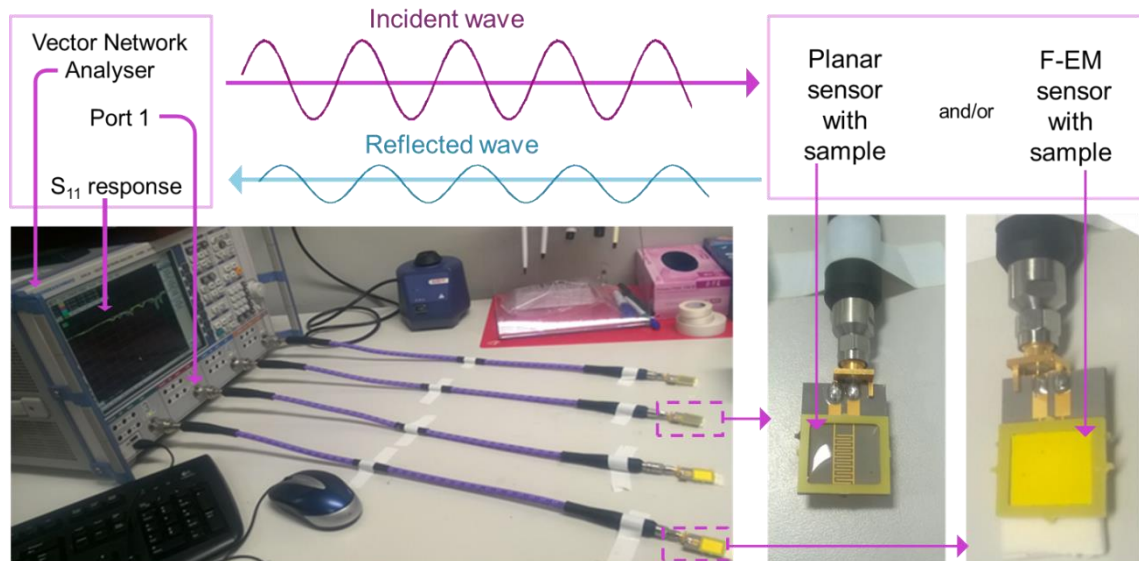


Figure 4.22 Scheme of the interaction principle between an incident wave produced by a VNA which interacts with a sample placed on a sensing structure and generates a reflected signal (as S_{11} response) at specific frequencies which is a spectrum

Initially, microwave sensors, both uncoated and coated, were connected to a Rohde and Schwarz ZVA 24 VNA via a coaxial cable and SMA type connectors wired with the sensors. All the equipment was specified for 50Ω impedance and was calibrated using a ZV-Z235 calibration kit following the manufacturer standard protocol. The microwave reflection coefficient (S_{11}), between 10 MHz and 15 GHz (with 60,000 discrete points), was measured using the VNA by way of two configurations:

1. **Small sample volume onto sensor:** for assessing the microwave response of metal solutions with various compositions and concentrations;
2. **Adaptation for *in situ* measurements:** for probing the sensing structure directly in water to allow *in situ* measurements.

The interaction between water solutions and the excitation of the sensors at microwave frequencies emits an electromagnetic field, which interacts with the solutions presented to the sensor to enable the determination of the composition and concentration.

4.4.3.1 Small sample volume onto sensor

The reflection coefficient magnitude for small volume water samples was measured with a one-port configuration by connecting both the uncoated and f-EM sensors to a Rohde and Schwarz ZVA 24 VNA through coaxial cables (Figure 4.23).

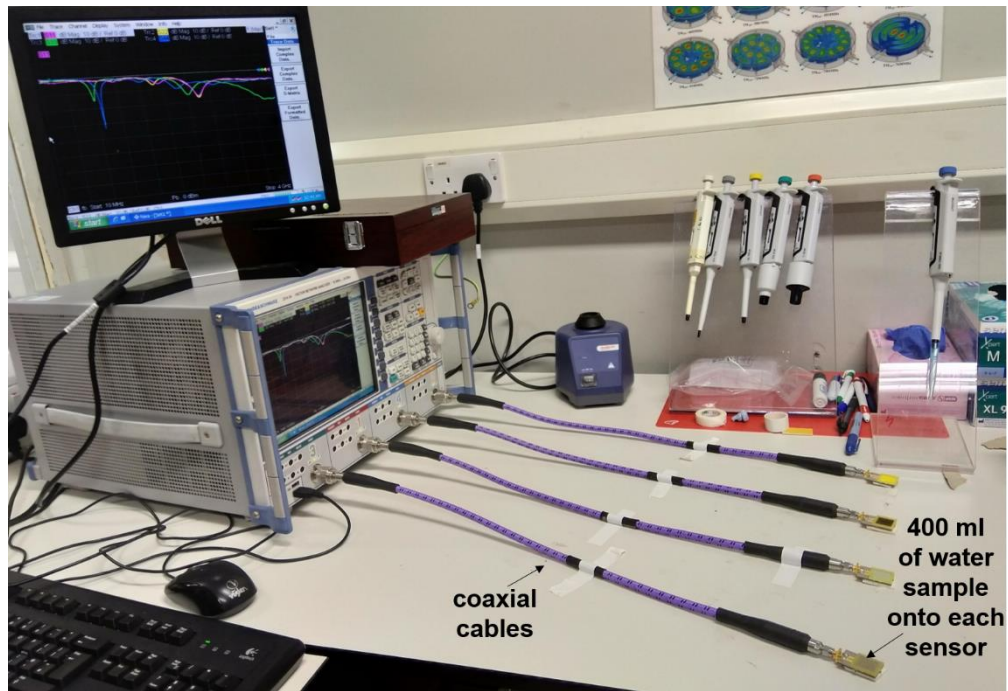


Figure 4.23 Configuration of S_{11} measurements using a Rohde and Schwarz ZVA 24 VNA using an uncoated and various f-EM sensors with 400 μL of sample onto each one held in place by a bespoke holder

The responses measured with the f-EM sensors, were compared with the uncoated sensors for evaluating the variation of the spectral response and the improvement of the sensing performance for specific sample compositions. For each measurement ($n=5$), 400 μL of laboratory-prepared water samples and samples which were collected in mining-impacted freshwater were dispensed onto the sensor using a pipette, with the solution held in place by a manufactured well.

After data analysis, the frequency range of the measurements (0.01-15 GHz) was reduced to focus on the best-selected frequencies. Time measurements (every 30 seconds) were also repeated for measuring the feasibility of continuous measurements and the time interaction between each coating and the metals in the water sample under analysis.

Variations in the microwave responses were also analysed for other parameter changes, such as T and pH (Figure 4.24) to demonstrate that the measured changes could be related to the metal composition and concentration and not other factors that influence microwave responses.

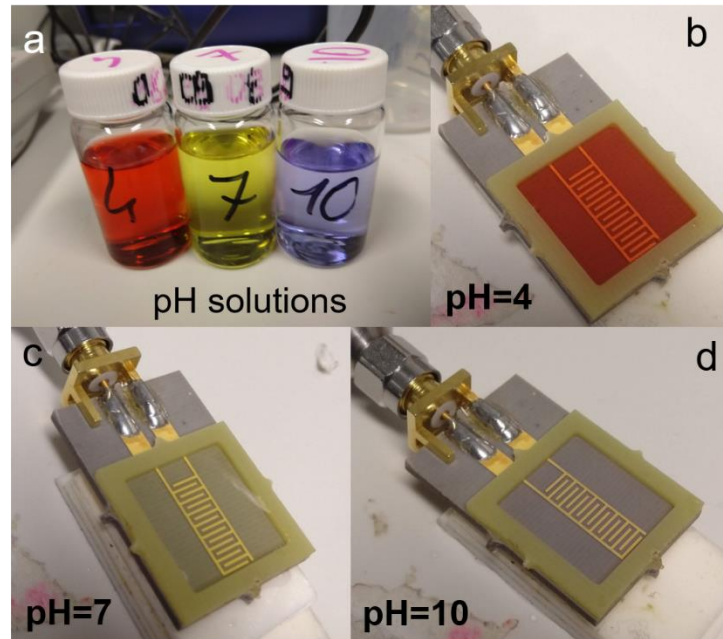


Figure 4.24 IDE sensors and measurements of pH calibration solutions (a), at pH 4 (b), 7 (c) and 10 (d). Consequently, the response for water samples using this configuration was compared with other portable VNAs, such as a ZVL13 VNA (9 kHz – 12 GHz, Rohde and Schwarz) (Figure 4.25a), a PicoVNA™ 106 (300 kHz – 6 GHz, pico technology) (Figure 4.25b), a MS2024A VNA Master (2 MHz – 4 GHz, Anritsu) (Figure 4.25c) and a miniVNA tiny (Mini Radio Solutions, 1 MHz – 3 GHz) (Figure 4.25d), to assess the feasibility to perform some on-site or *in situ* testing in mining-impacted freshwater. The cost of the equipment used in this work for performing microwave measurements using f-EM sensors and water sample is shown in Table 4.2. Although some VNAs, such as the ZVA24 and ZVL13, are costly, inexpensive options are available once the resonant frequencies are identified. In addition, compact measurements instruments can be developed for a total cost of ~ £50.

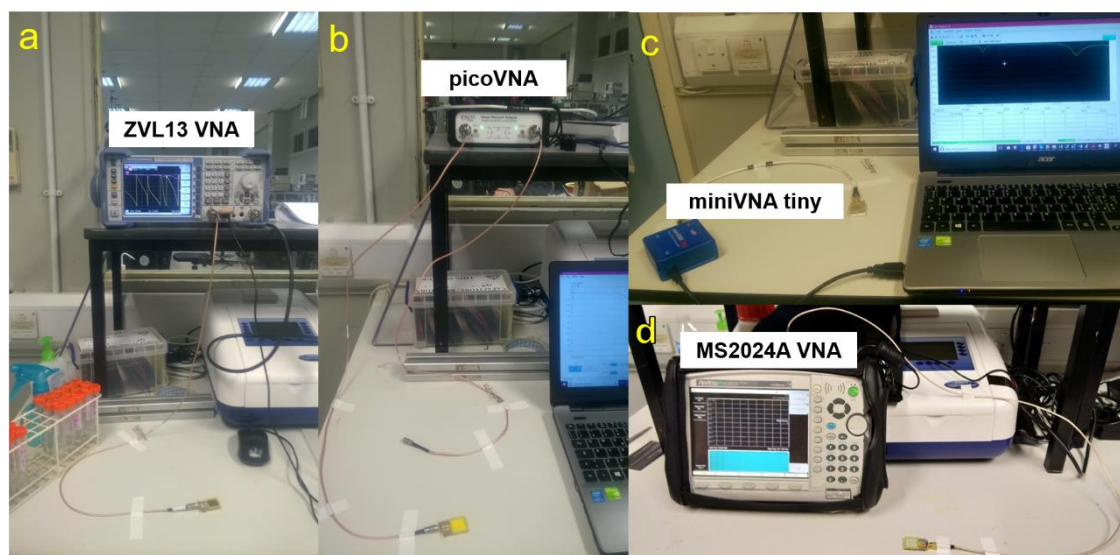


Figure 4.25 Portable VNAs that were tested in laboratory using the 400 μ L method onto the sensor: a ZVL13 VNA (a), a picoVNA (b), a miniVNA tiny (c) and a MS2024A VNA (d)

Table 4.2 Summary of cost of equipment for microwave spectroscopy using the measurement configurations, equipment and materials used in this work

Product	Brand / Supplier	Model / material	Cost
VNA	Rohde & Schwarz	ZVA24 Frequency range: 10 MHz to 24 GHz	~ £150,000
VNA	Rohde & Schwarz	ZVL13 Frequency range: 9 kHz to 13.6 GHz	~ £27,000
VNA	Anritsu	MS2024A Frequency range: 2 MHz to 4 GHz	~ £6,000
VNA	Pico technology	PicoVNATM 106 Frequency range: 300 kHz to 6 GHz	~£ 4,200
VNA	mini Radio Solutions	miniVNA tiny Frequency range: 1 MHz to 3 GHz	~ £400
Planar sensors		Gold eight-pair interdigitated electrode on PTFE substrate	~ £2-5
SMA Edge connector	JOHNSON	Coaxial Connector, Straight Jack, Solder, 50 ohm, Beryllium Copper	~ £1.5
Coatings	Chemicals (mostly) from Sigma-Aldrich Functionalisation (x10 printing)	chelating polymers	~ £0.02 - 0.5
Coatings	Chemicals (mostly) from Sigma-Aldrich Functionalisation (x10 printing)	metal oxides	~ £0.05 - 2
Sample	Sigma- Aldrich	Toxic metal (Cu, Zn, Pb) - standard solution	~ £0.5 - 2

4.4.3.2 Adaptation for *in situ* measurements

Microwave sensors were adapted for directly probing the water for *in situ* monitoring. Recently, also, Reyes-Vera et al (2019) developed a submersible permittivity sensor for liquid monitoring.

Summarising, for reaching the purpose of performing *in situ* trials:

1. sensors were adapted for directly probing the water;
2. the measurements of the increase in metal concentrations were performed continuously using the standard addition method for complex water matrix analysis;
3. portable VNAs were tested for assessing the comparable response and then some *in situ* experimental work was performed.

The following sub-section briefly describes the specific adaptations to perform *in situ* measurements.

4.4.3.2.1 Submerged sensor in water

The uncoated and f-EM sensors were waterproofed using a thermoplastic adhesive, consisting of ethylene-vinyl acetate (EVA) and terpene-phenol resin (TPR) (internal part), and silicone (external part) and embedded in 50 mL centrifuge tube lids. Figure 4.26 shows the uncoated and f-EM sensors that were developed and adapted for *in situ* monitoring during this PhD project. The figure illustrates the sensors with the waterproofed connectors and their correspondence with the sensors for “small sample volume” analysis.

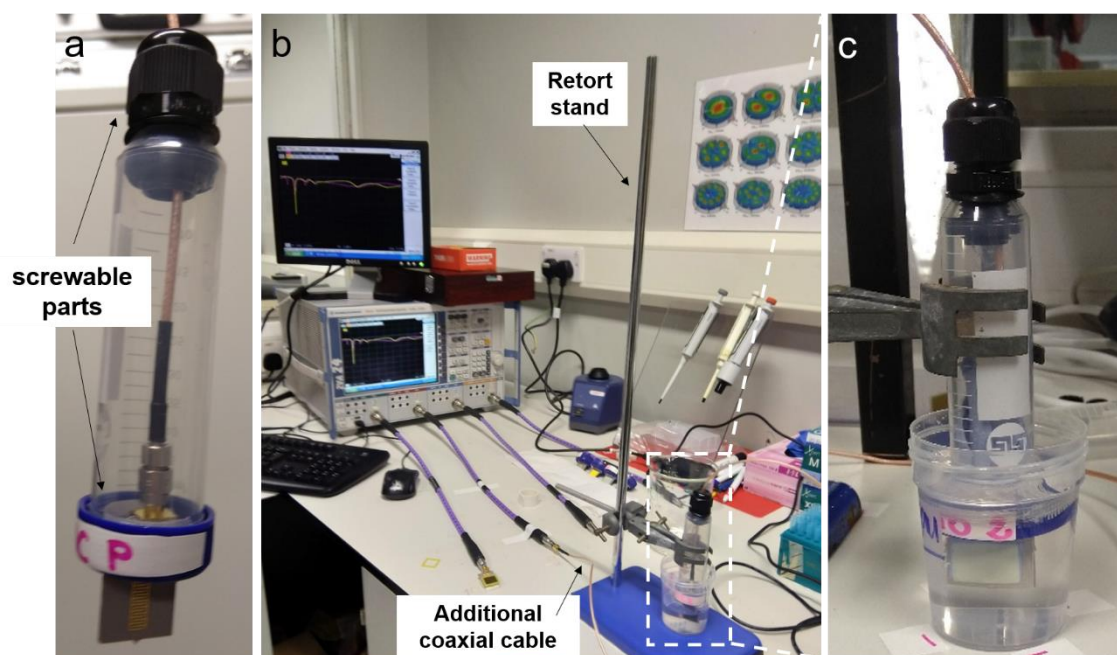


Figure 4.27 Experimental configuration adopted for submerging the waterproofed f-EM sensor and its structure with screwable parts (a) in water sample using a VNA configured with an additional coaxial cable, a retort stand for holding the sensor in place (b) and its close-up (c)

4.4.3.2 Adapted standard addition method

The standard addition method (SAM) is a quantitative method for determining the concentration of a specific analyte in an unknown and complex aqueous solution. The principle is based on the addition of the pollutant under test by multiple small and equal volumes to minimise the matrix effect which can interfere with the target analyte signal (Bader, 1980). It is particularly important in the areas of instrumental methods, such as spectrophotometry, atomic absorption (AA) and electrochemistry, especially when complex matrices are analysed (Harris, 2007). Using a linear calibration range, the response signal is directly proportional to the concentration (Bruce & Gill, 1999). In this PhD project, the SAM has been utilised with microwave spectroscopy for the first time for processing both laboratory-prepared and collected water samples from impacted mining areas. The samples were spiked by a continuous standard addition of 1 mL of 100 mg/L Cu and Zn solutions into a 40 mL sample. This corresponded to an increase of 1.25

mg/L in Cu and Zn concentration. The change in S_{11} response was monitored continuously.

4.4.3.2.3 Portable VNAs and *in situ* trial measurements

After assessing the possibility to detect changes in metal concentration in water by submerging microwave sensors in water, the EM response using portable VNAs was analysed for *in situ* trial measurements. Between the available cheap and portable VNAs (previously illustrated in Figure 4.25), a low-cost miniVNA tiny (Mini Radio Solutions) was selected to perform *in situ* measurements, due to its simplicity and practicability. First, it was tested in the laboratory by submerging the sensors in water samples. The miniVNA tiny is capable of sweeping between 1 MHz and 3 GHz with unit dimensions of approximately 80×80×35 mm. It has an SMA style connection on one face for DUT and DET (equivalent to one-port and two-port configuration, respectively) and a USB connection on the rear. It operates via the USB connection, requiring 5V, and can be connected to either a laptop/computer (Figure 4.28a) or a smartphone (using a USB On-the-go (OTG)) (Figure 4.28b). Data acquisition software, *VNA/J* for Microsoft using laptop connection, and *blue VNA* for Android with smartphone connection, both freely available, allow S_{11} measurements as well as R, X and $|Z|$. In addition, it was able to save continuously the data response every 5-10 seconds. The frequency range of this small, cheap and portable VNA corresponds to the resonant frequencies that were identified for detecting changes in metal concentration using the sensor submerged in a 40 mL water sample.

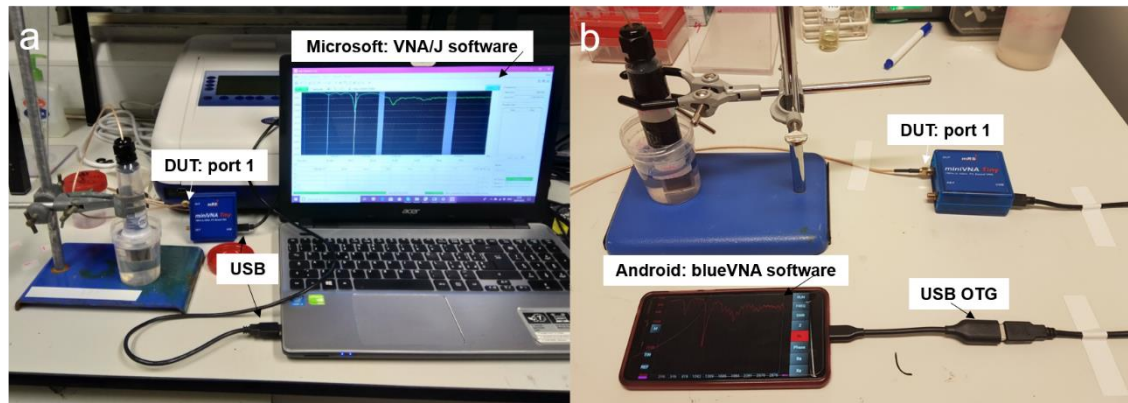


Figure 4.28 Set-up measurements using a miniVNA tiny allowing S_{11} measurements at one port configuration (DUT), operating via USB connection to a laptop using VNA/J software (a), and another connected using a USB OTG to a smartphone using the blueVNA software (b)

Figure 4.29 shows two examples of *in situ* measurements: in Nant Cwmnewyddion, Wemyss Mine, (Mid Wales, UK) using a laptop as the output device (Figure 4.29a) and in a drainage adit, Parys Mountain mining district (North Wales, UK), using a smartphone as the output device (Figure 4.29b).



Figure 4.29 Example of *in situ* measurements in two mining areas in the UK, using a laptop (a) and a smartphone (b) as output device

Measurements of mining-impacted water were performed to assess i) the prospect for quantifying metal concentrations *in situ* using various f-EM sensors and ii) the stability of the sensing response with the river flow.

4.4.3.2.4 Slug injection trial

The ability to detect an unexpected change in freshwater and then return to the baseline level could not be investigated by injecting toxic metals into natural water, so it was evaluated using *slug injections* of sodium chloride (NaCl) as a tracer, used usually for flow measurements evaluations. The tracer is injected into the stream as a near-instantaneous slug (Moore, 2004), named “slug injections” (De Giudici et al, 2019; Onnis et al, 2018) or salt gulp-injection dilution gauging (Hudson et al, 2018; Jarvis et al, 2019). A certain amount of salt (e.g. 100-500 g depending on the flow) is mixed in a specific water volume (e.g. 10 L of the same surveyed stream water) in a bucket and injected in a point along the stream. Then, the tracer concentration is measured at a downstream point (e.g. 30-100 m), where the tracer has become uniformly mixed with the streamflow. Equations based on the mass balance principle are then applied to calculate the stream discharge (Moore, 2004).

The feasibility to detect continuously the change in microwave spectrum with the NaCl and then return to its baseline spectrum was investigated (during fieldwork carried out by Onnis et al (2018)) using the miniVNA tiny and a lacquered sensor, connected via USB to a laptop, and extracting data every second (Figure 4.30).



Figure 4.30 Evaluation of the feasibility to measure “unexpected” variation in a parameter (NaCl in this case) in freshwater and the return to the baseline level

4.5 Coatings characterisation

Coatings and their interaction with metals in water were analysed by measuring changes in impedance (C and R) at low frequency and microwave parameter (S_{11}) at high frequencies. More analyses of optical, morphological and compositional properties of the coatings were performed for their characterisation before and after water interaction. Moreover, an adsorption experiment was performed for assessing the interaction between coatings and various metal concentrations.

4.5.1 Repeatability and Reproducibility

The repeatability and reproducibility of the thick film was measured through the absorbance of the film which was screen-printed on microscope slides using a larger stencil (25×40 mm) prepared on different days (Figure 4.31a and b). These measurements were performed with a UV-Vis Spectrophotometer (Jenway 7315) in an unusual

approach: placing the coating on the right side of the “cuvette container” and measuring the repeatability of the absorbance at specific wavelengths (Figure 4.31c).

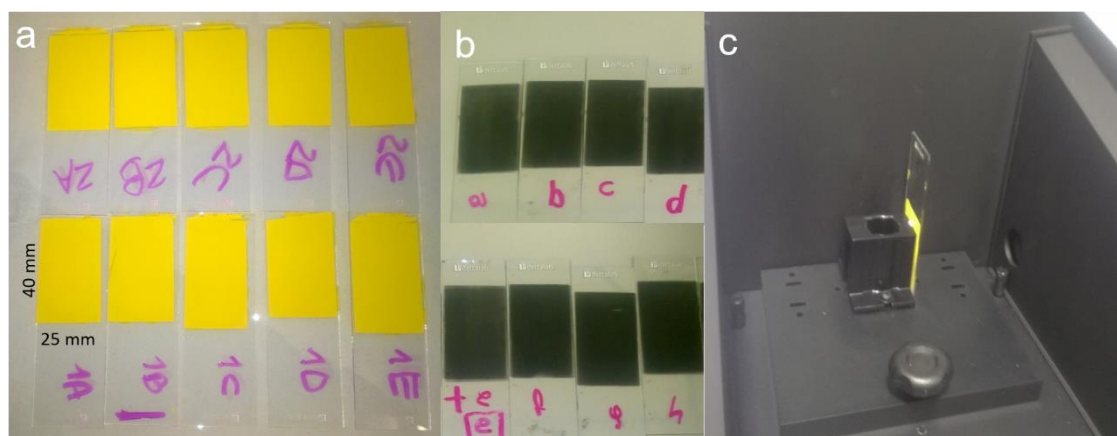


Figure 4.31 Screen-printed coatings (25×40 mm) onto microscope slides, specifically β - Bi_2O_3 (a) and L-CyChBCZ based coatings (b) and their absorbance measurements using a UV-Vis spectrophotometer (c)

4.5.2 SEM and EDS

Morphological properties of the coatings were measured, before and after the interaction with toxic metals, using a Scanning Electron Microscope (SEM), model FEI - Quanta 200. The elemental composition in % of the coatings was then analysed with an Energy Dispersive Spectroscopy (EDS, model INCA-X-act, Oxford Instruments), connected to the SEM (Figure 4.32).

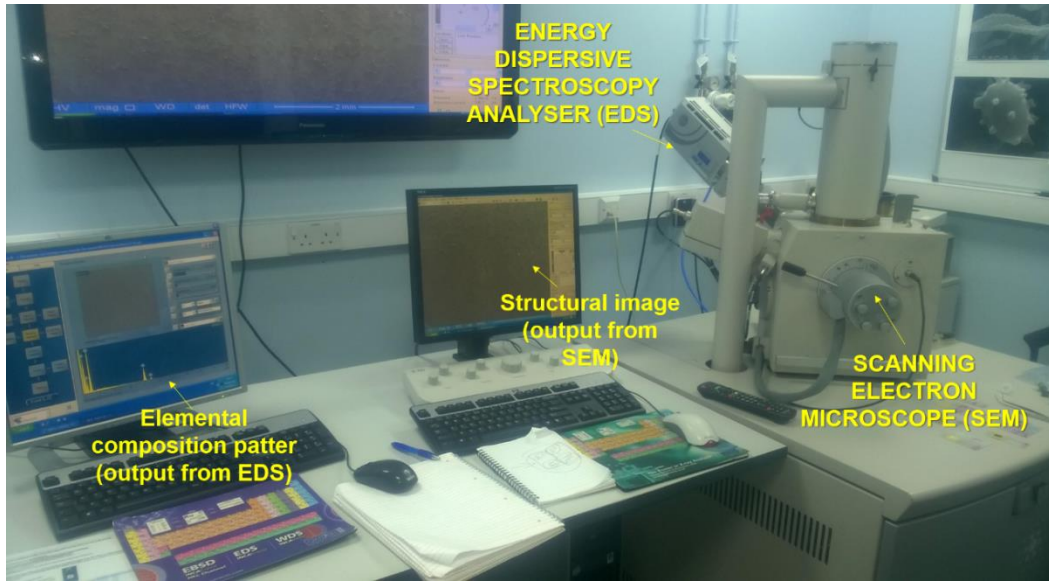


Figure 4.32 SEM, EDS and their outputs

4.5.3 Adsorption experiment

The percentage of adsorption between adsorbent (coating material) and adsorbate (metal ion) was estimated by measuring the difference of the initial concentration of each metal solution and the concentration after the adsorption, by modifying the procedure described by Dada et al (2012) for simulating the capability of the coating to adsorb metal ions. This was experimented for evaluating the adsorption of Zn and Cu ions onto respectively β - Bi_2O_3 and L-CyChBCZ based coating (Figure 4.33). Specifically, 0.02 g of the thick film (printed on a microscope slide) was put in a plastic container with 20 ml of each metal solution (0, 1, 10, 50, 100 mg/l). The concentrations in the solution after the adsorption were measured after 5, 10 and 30 minutes.

The percentage of adsorption was evaluated using equation 4.7:

$$\% \text{ adsorption} = \frac{C_i - C_e}{C_i} \times 100 \quad (4.7)$$

where C_i is the metal concentration before the adsorption and C_e is the metal concentration after the adsorption.

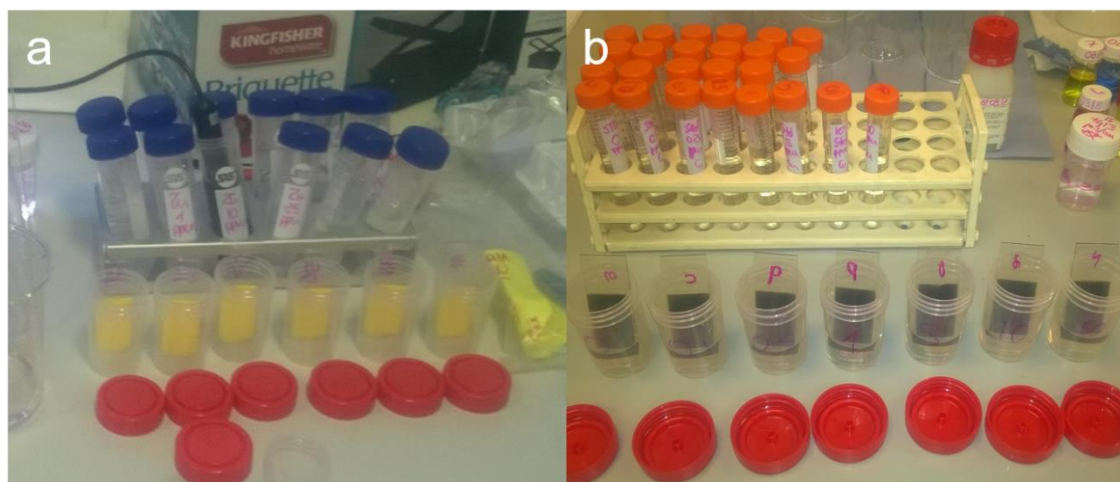


Figure 4.33 Experimental adsorption experiment for β - Bi_2O_3 (a) and L-CyChBCZ based coatings (b) coatings with respectively Zn and Cu solutions at various concentrations

4.6 Data analysis

The sensing output from optical, impedance and microwave measurements is a spectrum, with peaks and troughs, both are defined as peaks in this thesis. The response of coated IDEs and f-EM sensors was compared with the uncoated versions, for evaluating the benefit of using these novel sensing devices for higher sensitivity and selectivity of polluted mining-impacted water. Results obtained using the described approach were used as an indicator of metal content. They were analysed using Excel, OriginPro9, and CurveExpert Basic. By studying the impedance and microwave responses at specific frequencies, it is possible to evaluate correlations with distinct toxic metals. Moreover, the response of multiple peaks and/or multiple f-EM sensors (defined as f-EM sensor array) was combined for achieving a more specific response, considering that the resonant peaks that were identified at specific frequencies are different comparing the response of different f-EM sensors for various analysed water solutions. This is due to both the different matrix of the analysed samples and different analysed metals, which interact with the materials of the coating and change the physical properties.

4.6.1 Statistical features and performance evaluation

Best-fit curves for different Pb, Zn and Cu concentrations at specific frequencies of the EM spectrum were evaluated by comparing responses between uncoated and f-EM sensors, analysing various parameters, including the R^2 (the square of the Pearson correlation coefficient), the coefficient of variation (CV), which is the ratio of the standard deviation (SD) to the mean, the sensitivity for every 1 mg/L changes of Cu, the limit of detection (LOD) and the quality factor of the peaks (Q-factor). Specifically, the R^2 is used for evaluating the correlation (mostly linear) between the spectral response (e.g. S_{11} value in dB) at specific frequencies with the concentration (mg/L) of the metal under test. This allows the development of a calibration curve for evaluating the “unknown” concentration of a sample under test. For example, as with all the established methods (e.g. ICP-OES), it is necessary before every analysis to prepare a calibration curve using standard solutions at concentrations which represent the range of the analysed unknown sample.

The CV is used to evaluate the precision of the sensing response and this is achieved by performing repetitive measurements (x 5-10) of the same sample. The sensitivity describes how much the signal changes for a small increase (e.g. for each mg/L) in metal concentration. It is equivalent to the slope of the calibration curve attained as S_{11} versus metal concentration (Rahman et al, 2018). The LOD represents the smallest concentration that can be detected by the instrument. This was evaluated, as described by Salim & Lim (2018), using equation 4.8 which describes the smallest concentration of a toxic metal that can be detected.

$$LOD = 3.3 \times \frac{(SD \text{ of blank response})}{(\text{slope of calibration curve})} \quad (4.8)$$

The Q-factor (Q) was found using equation 4.9:

$$Q = \frac{f_0}{f_{3dB}} \quad (4.9)$$

where f_0 is the centre of the peak and f_{3dB} is the half-power bandwidth. A higher Q-factor represents a better result, as it implies a lower attenuation rate.

Considering that the microwave response in the frequency range studied in this work consists of multiple peaks at specific frequencies, the analysis of these described parameters for multiple resonant peaks can improve the specificity of the sensing response. Consequently, spectra were analysed in their entirety using peak functions.

4.6.2 Signal analysis: curve fitting

The microwave spectral responses for the polluted water samples consist of a combination of peaks. For more accurate identification of a specific metal in the water sample under test, the full-spectral-response was analysed by fitting the S_{11} responses using peak functions. This enabled the determination of multiple features for each individual peak, such as area, centre and height of the peaks, and to analyse multiple peaks simultaneously. Moreover, if the peaks are superimposed, curve fitting is the best way to isolate the peaks and define their specific characteristic (Meier, 2005).

In the first instance, various metal solutions were analysed and the S_{11} responses were fitted using symmetric profiles, such as Gaussian, Lorentzian and Voigtian (a convolution between them). A schematic illustration of these profiles is shown in Figure 4.34.

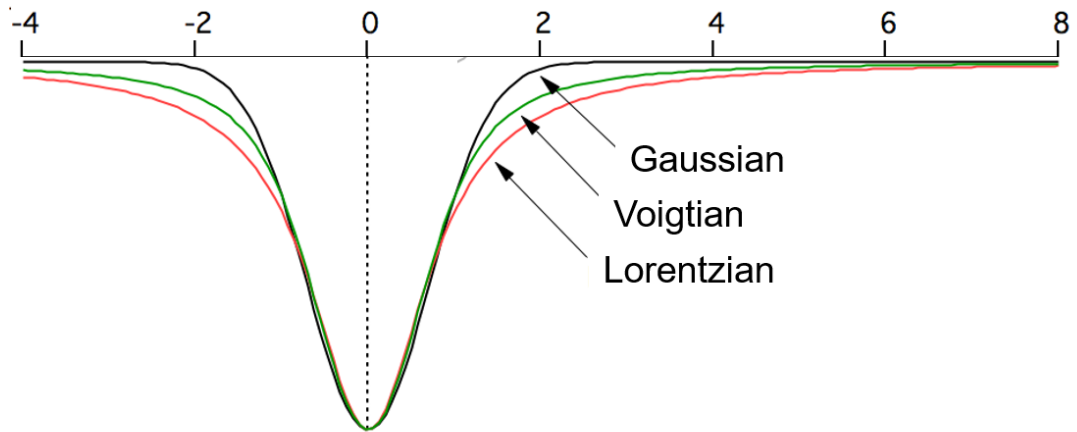


Figure 4.34 Schematic example of Gaussian, Voigtian and Lorentzian profiles, which identify peaks' shapes

The most accurate peak fitting results were achieved, as highlighted in bold green in Table 4.2, with the Lorentzian function for both the R^2 and Chi-square, which represents the adherence of the moulded cumulative fit peak and the goodness of fit. Lorentzian peaks have a far wider tail than Gaussian ones, so are more representative to the peak shapes obtained with microwave spectroscopy.

Table 4.3 Comparisons of curve fitting function performances, using Gaussian, Lorentzian and Voigtian profiles

	Gaussian	Lorentzian	Voigtian
R^2	0.96±0.02	0.99±0.01	0.97±0.01
Reduced Chi-sqr	0.27±0.08	0.06±0.03	0.18±0.08

The Lorentzian peak function used is given in equation 4.10:

$$y = y_0 + \frac{2A}{\pi} \times \frac{w}{4(x - x_c)^2 + w^2} \quad (4.10)$$

where y_0 is the offset; x_c is the centre of the peak; w is the FWHM (full width at half maximum) and A is the area of the peak. Consequently, the S_{11} responses for the tested samples were fitted with the Lorentzian peak fitting function and multiple peak analyses were performed.

4.6.3 Lorentzian peak fitting function

The Lorentzian peak fitting function was applied to the mean of 5 measurements of each sample that was analysed, allowing both the determination of multiple peaks and the peaks parameters. It was performed using the function “Analysis > Peaks and Baseline > Peak Analyser” in OriginPro9. Then, Fit peaks (Pro) goal was selected with the baseline as maximum, which is then removed. After this, the peak filtering setting is selected by height, and manually corrected. Fit control then allows Lorentzian to be selected as the peak type, the curve is fitted until it converges and the peaks parameters are determined. The fit is considered successful when the $R^2 > 0.99$ and a Chi-Sqr tolerance value of 10^{-6} was reached.

Summarising, the analysis of the raw data and the selection of the peaks is illustrated in the flow chart in Figure 4.35. First of all, the mean, the SD and the CV are evaluated. The data with a $CV > 5\%$ are not considered, as the response is not repeatable. Then, the spectra for diverse samples are compared. Samples with the same metal (e.g. Cu) at various concentrations (between 0 and 10 mg/L) are used to identify the resonant frequency and the sensitivity. For these, the peaks that produce a higher sensitivity, Q-factor and R^2 , lower CV and LOD are selected. Samples with diverse metals (e.g. Cu and Zn) and the same concentrations are compared to evaluate the selectivity. The different S_{11} response at various peaks is used mostly to evaluate the selectivity. For this purpose, it is useful to analyse various peaks and their parameters by applying the Lorentzian peak fitting function, for evaluating the “pattern recognition” of a particular metal and assessing more differences at multiple peaks between similar metals.

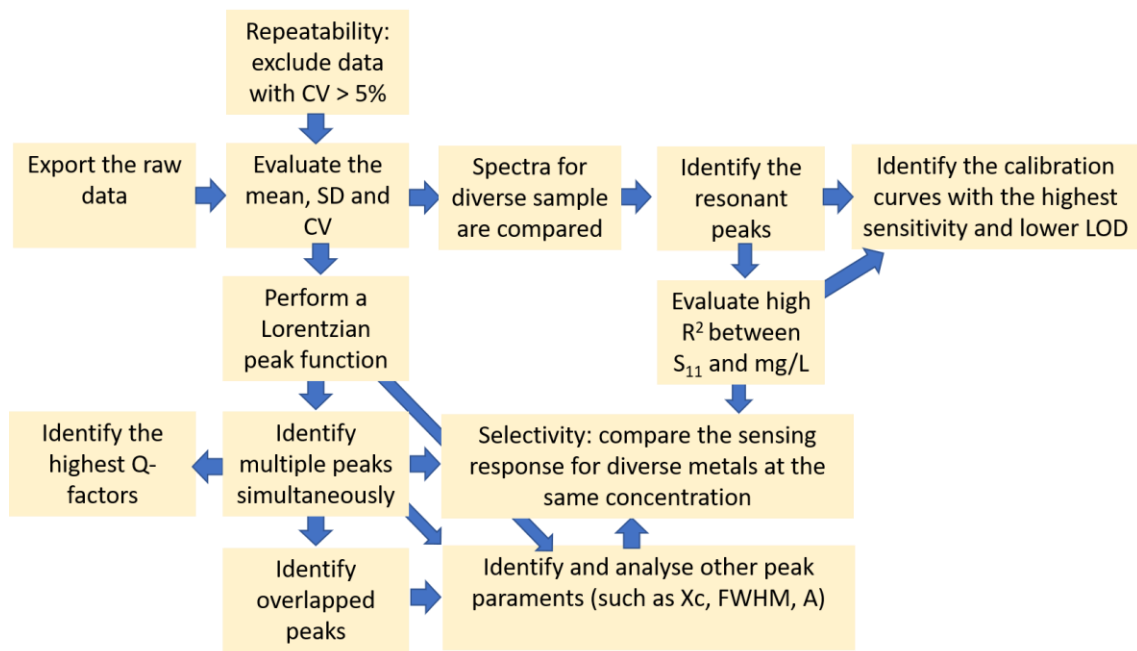


Figure 4.35 Flow diagram which shows the data analysis approach and peak selection

4.6.4 Standard addition method: analysis

The results from the experimental work performed using the SAM were analysed. The S_{11} response of the blank response (the DW signal) was subtracted and the linear regression was then plotted. The concentration of the unknown sample is determined using the slope and the intercept, which corresponds to the point at which the calibration plot crosses zero on the x-axis. Equation 4.11 was applied for each addition:

$$\frac{C_x}{C_x + C_s} = \frac{S_{11 \text{ for } x}}{S_{11 \text{ for } x+s}} \quad (4.11)$$

where C_x and $C_x + C_s$ are respectively the concentrations of the pollutant without and with the standard addition; and $S_{11 \text{ for } x}$ and $S_{11 \text{ for } x+s}$ are the S_{11} measurement of the solution alone and with the standard addition, respectively.

4.7 Summary

The novel methodology described in this chapter was developed and experimented for the first time. Several new strategies were adopted to generate new results in the research of microwave spectroscopy and the detection of toxic metals in polluted water. The most relevant are the following:

- Microwave and low-frequency impedance measurements were researched to detect toxic metals at low concentrations in water;
- Planar microwave sensors were functionalised with unique thick films using screen-printed technology;
- Sensors were adapted for directly probing water samples for *in situ* analysis;
- The standard addition method was used with microwave spectroscopy;
- The spectral responses were analysed in their entirety using Lorentzian peak-fitting functions;
- Microwave sensors and portable VNAs were tested *in situ* in mining-impacted freshwater.

The next three chapters will describe the major results that were found during this research project. Specifically:

- **Chapter 5:** describes the responses using uncoated and coated sensors for simple water samples;
- **Chapter 6:** describes results for multi-metal samples and collected mining-impacted water;
- **Chapter 7:** describes results using multiple f-EM sensors and *in situ* measurements.

Chapter 5 Results and discussion (phase 1): f-EM sensors and simple metal water solutions

5.1 Introduction

The objective of this chapter (O1) is to research and develop f-EM sensors based on various functional materials for detecting single metal samples (Pb, Zn and Cu) at low metal concentrations and ascertaining the improvement of the microwave sensing performance; specifically:

- evaluating the feasibility of planar interdigitated electrodes (IDE) sensors for qualification and quantification of toxic metals in water;
- developing lacquered sensors and f-EM sensors based on β -Bi₂O₃, chelating polymers and metal oxides using microwave and low-frequency impedance measurements, and comparing the response with uncoated sensors;
- assessing the interaction between toxic metals and coating materials.

Previously, it was acknowledged that the use of microwave resonators, in the form of a resonant cavity, as a sensing structure for detecting Pb water solutions, was feasible (Korostynska et al, 2016). But this was not practical for *in situ* monitoring because of its bulk. Planar sensors were therefore selected and tested as they are more suitable for *in situ* monitoring. Initial experiments demonstrated that planar sensors (Au eight-pair IDE) were also able to detect vast changes of Pb concentrations (0, 1, 10, 50 and 100 mg/L), which are not representative of the common metal concentration of mine water (0-5 mg/L). Indeed microwave spectroscopy suffers from a lack of specificity, especially sensitivity (measure changes in small concentration) and selectivity (distinguish between metal ions).

This chapter describes the results that were obtained from measuring single metal water samples using uncoated and various f-EM sensors by i) combining the response between optical, low-frequency impedance and microwave measurements; ii) using the method of

placing a small volume of single metal laboratory-prepared water samples onto sensors; and iii) summarising the main findings which are the bases for the next chapters which describe multi-metal mining-impacted waters.

5.1.1 Proof of concept: microwave spectroscopy and toxic metals

A proof of concept using microwave spectroscopy for detecting metal ions, namely Pb ions, was attained by part of my supervisory team and presented at the 16th International Multidisciplinary Scientific GeoConference (SGEM) 2016, using a resonant cavity connected to a VNA and a data processing, measuring the reflection coefficient S_{11} (Korostynska et al, 2016). The successful action of the resonant structure demonstrates the real-time ability to detect changes in Pb concentration (0, 1, 10, 50 and 100 mg/L), placed in 50 mL centrifuge tubes, with a good linear correlation, with $R^2=0.9527$ and $R^2=0.9017$ respectively at two frequencies, 415 MHz and 2.45 GHz after processing of the raw data. This experiment demonstrates the feasibility to have an inexpensive real-time detection of Pb at various concentrations as soon as the EM waves interact with the water sample under test.

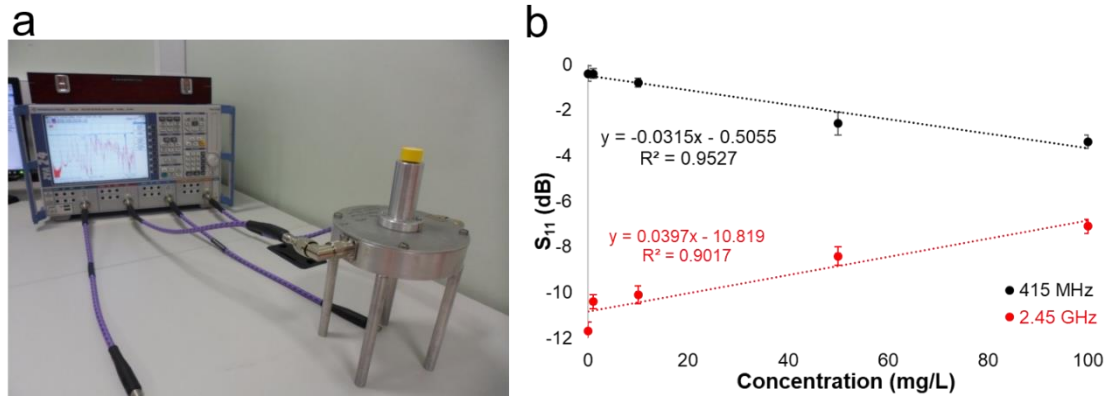


Figure 5.1 Resonant cavity connected to a VNA (a) that was used as proof of concept for measuring Pb water solutions and the linear correlation identified for changes in concentration (0-100 mg/L) at two specific frequencies, 415 MHz and 2.45 GHz (b) (modified from Frau et al (2018a))

This experiment gives the conviction that the microwave spectrometry is an attractive option for surveying, with minimal operation cost, toxic metals in water. Although, the resonant cavities are not very practical for adaptation to *in situ* monitoring, planar sensors offer a good alternative due to their robustness, low price fabrication and weight, reproducibility and practicability. Additionally, the design of microwave planar printed patterns can be tailored to suit particular applications, coupled with reliability and cost-efficiency (Korostynska et al, 2014b). Planar sensors were used in this work for measuring changes in the EM sensing response due to the different composition and/or concentration of the water samples. Consequently, Pb water solutions were measured using planar sensors, for evaluating the ability of small resonant structures to detect changes in material composition.

Korostynska et al (2012), confirmed the action of a novel microwave sensor for water analysis, observing changes in the microwave part of the electromagnetic spectrum analysing air, deionised water and tap water using a flexible planar Ag IDE sensor, demonstrating the action of planar sensors for water analysis.

Consequently, in this project, planar Au eight-pair IDEs onto PTFE substrates were tested with metal water solutions at various concentrations for evaluating the feasibility to detect

in real-time metal concentration variation. Initially, these planar Au eight-pair IDE sensors were tested with Pb water solution (0, 1, 10, 50 and 100 mg/L). The response for the microwave sensor is given in dB and demonstrates a shift in amplitude corresponding at different frequencies to the concentration of Pb in each sample. Figure 5.2 shows the comparable response obtained using the resonant cavity (Figure 5.2a) (that is not adaptable for *in situ* analysis) and the planar Au eight-pair IDE sensors (Figure 5.2b) where a small volume of sample (400 μ L) was set onto the sensor using a micropipette. The resonant peaks in the spectral responses were identified at the same frequencies (0.415 and 2.45 GHz) with a similar reflection coefficient magnitude S_{11} , with a higher dB for the planar sensor. In addition, with the planar sensor, another peak at 1.27 GHz was produced as soon as the water sample was placed in contact with the EM spectrum which was related to the Pb concentration.

After each measurement, responses returned to the original position (air spectra), confirming that the developed resonant cavity and microwave sensors are reliable and reusable, and thus a sustainable solution for continuous water quality monitoring. As the concentrations used in this experiment were too high, smaller concentrations were consequently investigated for the real metal concentration of toxic metals that can be commonly found in mining-impacted water.

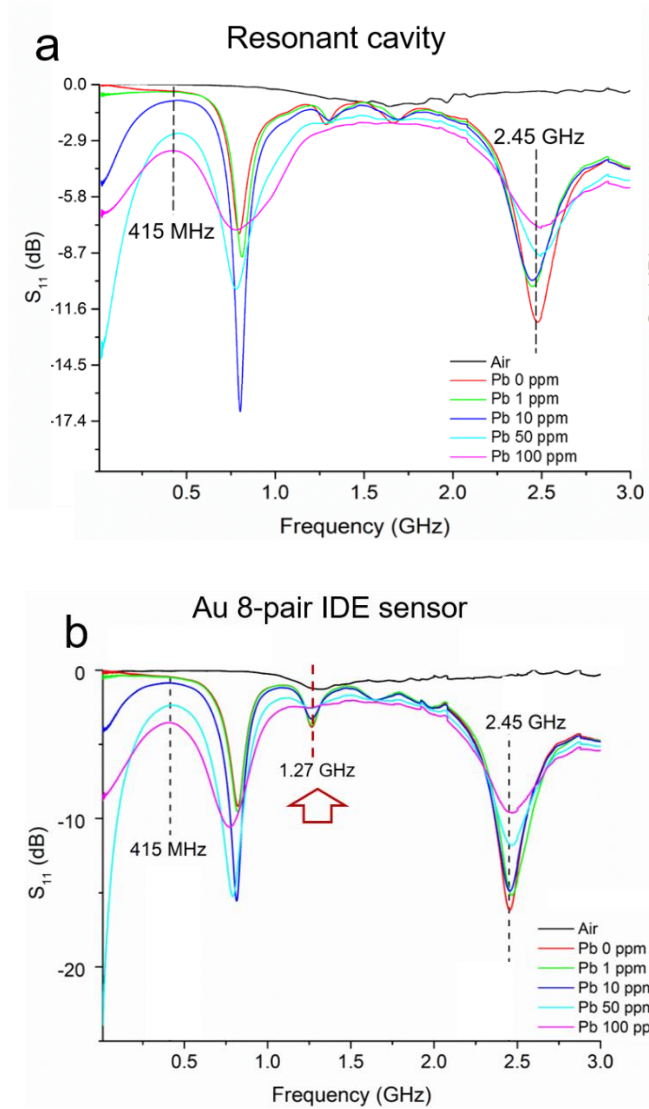


Figure 5.2 Spectral response comparison between a resonant cavity (a) and planar Au eight-pair IDE sensors (b) measuring Pb solutions: the major spectral changes depending on the metal concentrations (0-100 mg/L) are identified at the same frequencies, 415 MHz and 2.45 GHz

It was assessed by both literature and preliminary laboratory experiments, that it was infeasible to distinguish between similar toxic metals (e.g. Pb and Zn) (Figure 5.3) and to detect small changes in a metal concentration (<1 mg/L) (Figure 5.4). Specifically, the spectral response for the same concentrations (1-100 mg/L) of Pb and Zn is very similar, as is shown in Figure 5.3. Only the resonant peak at 2.45 GHz is able to slightly distinguish Pb and Zn solutions at 1 mg/L. Although, this is not the only limitation to deal with.

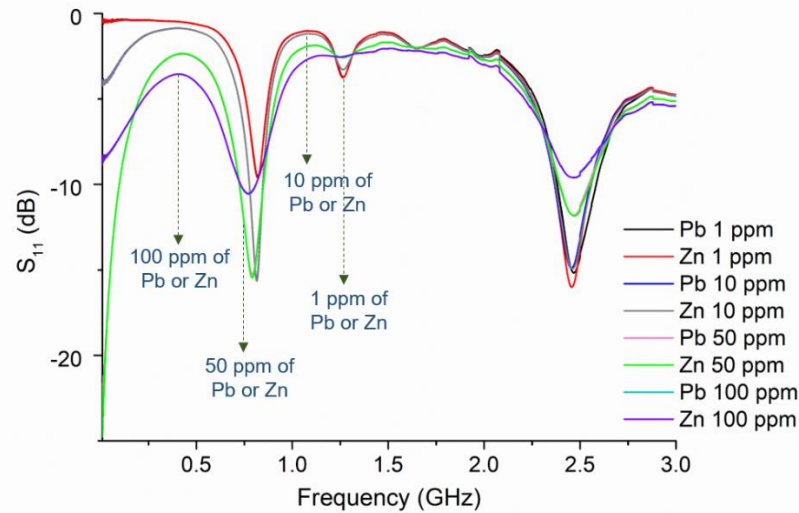


Figure 5.3 Example of microwave response which shows the comparable response for the same concentration (1-100 mg/L) of Pb and Zn

Microwave spectroscopy is not able to differentiate with enough sensitivity (dB variation), between low metal concentrations, such as between 0 and 1 mg/L, as is shown in Figure 5.4. The spectral response using planar IDE sensors was not able to distinguish metal concentrations between 0 and 1 ppm, in all three resonant frequencies (0.82, 1.27 and 2.45 GHz) which were identified as able to distinguish Pb and Zn concentrations between 1 and 100 mg/L.

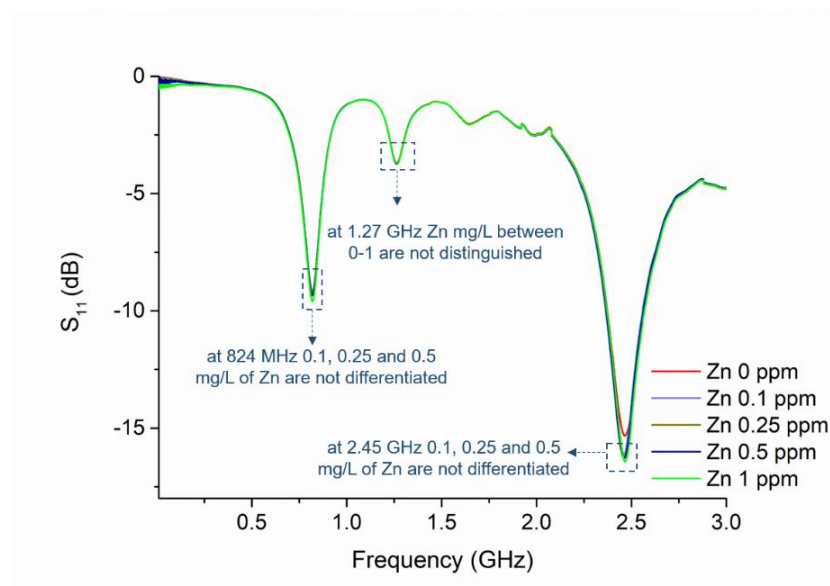


Figure 5.4 Spectral response for low Zn concentration (0-1 ppm) measured with an Au eight-pair IDE sensors which shows the infeasibility to detect with acceptable sensitivity the concentrations <1 ppm at three frequencies, namely 0.82, 1.27 and 2.45 GHz

This was also verified by changing the pattern of the sensing electrodes, as it is a limitation of microwave sensing (Li et al, 2019) and novel strategies are aiming to face this challenge to distinguish more specifically between low concentrations of similar materials (Zarifi et al, 2018b).

Puangngernmak & Chalermwisutkul (2014) are the only researchers who have also experimented the detection of toxic metals (Cu, Zn and Ni) in water with concentrations of 1, 10, 100 and 1000 mg/L using an open-ended coaxial structure and a VNA. They demonstrated the detection of these metals at frequencies lower than 2 GHz and the differentiation of these metals between 2 and 3 GHz. Notwithstanding, they have shown the differentiation of only high concentrations (100 mg/L) of these metals, resulting in not being adequate for the detection of these metals in impacted-mining waters.

After having evaluated the possibility of measuring changes in metal concentrations using low-cost planar IDE sensors and having assessed the comparable response obtained with the resonant cavity, these sensors were selected as “base sensors”. These sensors were then functionalised for producing the f-EM sensors with paste mixtures based on suitable materials that were chosen in the literature.

5.1.2 Preface: developed and tested f-EM sensors

The development of f-EM sensors as a solution was driven by the awareness of changing the microwave signal response due to the interaction between the toxic metals in a water sample, the coating material and the EM waves. Initial research and development of the coating to be screen-printed onto the planar sensors consisted on evaluating:

1. the paste mixture preparation;
2. the printability of the coatings;
3. the repeatability;

4. the stability and low dissolution with the water samples;
5. the effective change in microwave and impedance response due to the physical or chemical interaction between the coating and the toxic metals.

For subsequent successful testing and development, the coatings need to fulfil these requirements. Several materials and coating that were initially tested were not selected for consequent experimentation. For example: the PVC as binder was not able to generate a smooth paste that could have been screen-printed; the polypyrrole was not printable because of its grain dimension; some mixtures (e.g. ITO and L-cysteine) were not repeatable and generated a diverse signal (capacitance) for coatings with the same thickness; the mixture of β -Bi₂O₃ and chitosan was not stable and dissolved when in contact with water solutions.

A scheme of the EM propagation, comprising electric and magnetic lines, in an f-EM sensor (a functionalised Au IDE onto a PTFE substrate) measuring a toxic metal water solution is illustrated in Figure 5.5. A water sample in contact with the EM waves through a sensing structure, held in place by a specific holder, produces a spectral response which depends on the composition of the sample under test. This spectral response is related to the properties of the sample, such as conductivity and permittivity. The integration of materials in the form of a thick film (described also as *coating* in this thesis) onto the sensing pattern, adds a new element to sense, which changes the value of the complex permittivity itself, generating a variation on the spectral signal. Moreover, the physical or chemical interaction between the toxic metals (presented in the water sample) in contact with the material (onto the sensing pattern) determines a change in the permittivity, with a consequent variation in spectral response (Bernou et al, 2000). Summarising, the permittivity of each component of the sensing structure (sensor, coating and their

materials), the interaction between coating and water sample, and the EM propagation, determine a variation in the spectral response.

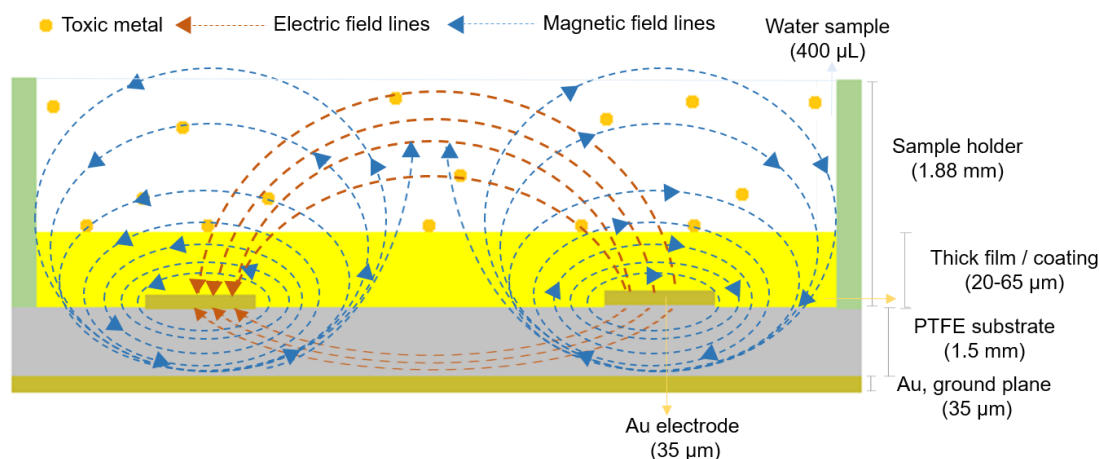


Figure 5.5 Partial cross-section of an f-EM sensor with a sample on it held in place by a specific holder which shows the propagation of the EM field through each part of the sensing structure and sample, showing the two components, electric and magnetic lines (adapted from Frau et al (2019a))

Considering the inability to detect the permittivity of the coating and its variation due to the interaction with toxic metals because of the absence of appropriate equipment, other impedance parameters, such as capacitance and resistance were analysed as pre-characterisation of the coating, considering that they are an indirect measure of the permittivity. Thick films based on various material compositions and thicknesses were initially screen-printed onto Ag electrodes, in turn, screen-printed on microscope slides for an inexpensive initial characterisation of the interaction between the materials and the metal ions using an LCR bridge. Initially, singular and mixtures of various materials on IDE printed on microscope slides were characterised evaluating their stability, durability and performance, as changes in C and R which are possibly related with the interaction with toxic metals presented in a sample under test. Therefore, these initial assessments allowed selecting which mixture of materials to screen-print onto microwave sensors for measuring changes in metal concentration in polluted water using microwave spectroscopy.

The following sensors and f-EM sensors (Figure 5.6) were developed and tested:

- Uncoated and lacquered sensors;
- F-EM sensors based on $\beta\text{-Bi}_2\text{O}_3$;
- F-EM sensors based on chelating polymers, which comprehend L-CyChRu and L-CyChBCZ based coatings;
- F-EM sensors based on metal oxides, which comprehend ITO and M10 based coatings.

Additionally, other measurements and experiments were performed for evaluating the effective metal interaction with the coatings, time responses, repeatability and stability of the measurements.

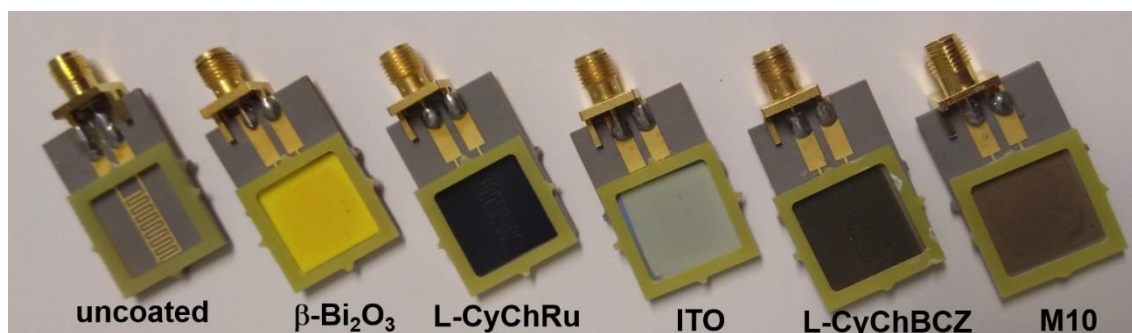


Figure 5.6 Developed and tested f-EM sensors

F-EM sensors based on these materials were used to measure more specifically changes in water properties that can be associated with increases or decreases in metal content in water. In this chapter, the results that were obtained with specific coatings and selected metals are described. Specifically, the lacquered sensors were tested with Pb solution, the $\beta\text{-Bi}_2\text{O}_3$ with Zn solutions and the sensors based on the chelating polymers with Cu solutions. The metal oxides based sensors gave a similar response to the $\beta\text{-Bi}_2\text{O}_3$. So, their response is described in Chapter 7, as they were tested with complex solutions.

This chapter describes the response of some f-EM sensors with simple single metal solutions, in addition to the integration of optical and impedance measurements and other

measurements, such as SEM and EDS analysis. All responses were compared with the results that were obtained using the uncoated sensors.

5.1.3 Required features

Sensing and transducing the microwave spectral response of the concentration of various metals in water requires addressing specific features. The magnitude reflection coefficient S_{11} and the related impedance measurements which were measured using uncoated and f-EM sensors were assessed with a series of statistical features. In this chapter, data processing for comparing the performance at specific frequencies between coated and uncoated sensors, the main descriptive statistics that were considered are the R^2 , CV and the sensitivity, between response parameters (in dB, Ω , F for example) and metal concentrations at specific frequencies. Clearly, better performance is represented by i) a high R^2 , preferably if linear correlation; ii) a lower CV, which indicates a high precision and repeatability of the measurements; and iii) a higher sensitivity, which represents a bigger spectral variation for a small change in concentration. The responses were analysed for satisfying these features, although on particular occasions, such as for specific concentration ranges at specific peaks, it was necessary to find a compromise between high R^2 and high sensitivity.

Coatings, based on low-cost materials for mass production, were initially characterised for printability, reproducibility and stability. Then the interaction between toxic metals and coating materials with time was investigated.

5.2 Lacquered sensors and Pb ions

The feasibility to detect metal ions using planar sensors was assessed during the first month of this project using a resonant cavity and Au eight-pair IDE sensors, which gave

a comparable response. An initial attempt was made to modify the sensing structure response and by adding a PCB lacquer coating spray. The purpose was to avoid oxidation of the sensors during *in situ* monitoring.

5.2.1 Analysis, results and discussion

In these opening experiments, PCB lacquered microwave sensors were developed and tested with five Pb solutions (0, 1, 10, 50, 100 mg/L) dissolved in DW. These solutions were acidified with 1% v/v of HNO₃ (analytical grade, 67%). Spectrum responses for four properties (absorbance, capacitance, resistance, and reflection coefficient S₁₁) at three frequency ranges of the electromagnetic spectrum were monitored and analysed. For optical and electrical microwave, properties of lead solutions were detected at separate frequency ranges of the EM spectrum.

5.2.1.1 Absorbance

Absorbance spectra between 200 and 350 nm (UV) are shown in Figure 5.7a, and represent the only area of the measured optical spectra where significant variation in absorbance occurred with varied Pb concentrations. The chemical information given by an absorption spectrum is contained in the position and intensities of the absorption band. It is visible that the absorbance is related to the Pb concentration, particularly at the 300 nm peak. Linear correlations at two wavelengths, 247 and 300 nm, are shown in Figure 5.7b, with high correlation in both cases (R^2 equals 0.9757 and 0.9869, respectively). Further experiments disproved the ability to detect metal ions using simple optical measurements at these wavelengths for unfiltered samples, demonstrating that isolated metal ions cannot be read using a UV-Vis spectrophotometer.

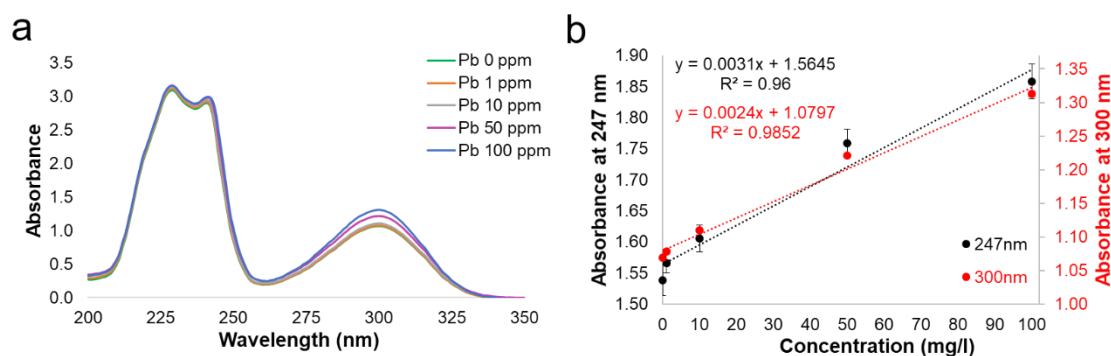


Figure 5.7 Average absorbance spectrum of various lead solutions in 200–350 nm range measured with a UV–Vis spectrophotometer (a); linear correlations for the absorbance and Pb concentration at two wavelengths, namely 247 and 300 nm (b)

5.2.1.2 Impedance responses

Capacitance and resistance results of the water samples were used for an initial evaluation of the possibility to detect changes in Pb concentration using impedance measurements. C and R spectral responses at low frequency for Pb samples (0–100 mg/L) are shown in Figure 5.8a and b. The correlations between C (in F), R (in Ω) and Pb content (in mg/L) are illustrated, respectively, in Figure 5.8c and d. It is clear that these parameters changed with the Pb concentration. It is notable how the C increases with the metal concentration increases, while the R decreases. Best-fit curves for different Pb concentrations at specific frequencies of the EM spectrum were evaluated using the coefficient of determination (R^2), equal to the square of the Pearson correlation, which corresponds to the covariance of two variables divided by the product of their standard deviations.

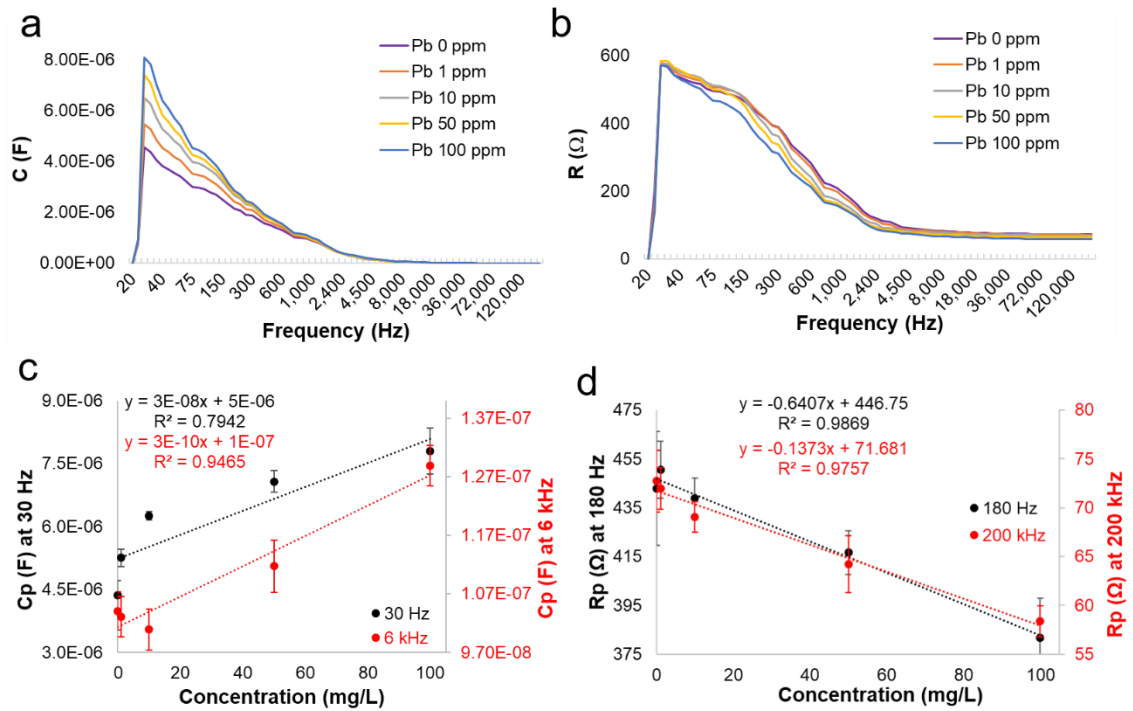


Figure 5.8 Spectral responses for C (a) and R (b) and Pb solutions (0-100 mg/L) at low frequencies (20-200,000 Hz); linear correlations between C and Pb concentration at two discrete frequencies (30 Hz and 6 kHz) (c) and between R and Pb concentration at 180 Hz and 200 kHz (d)

In addition, a compromise was found between responses with higher correlation and lower sensitivity, and lower R^2 and higher sensitivity, considered as parameter variation. Summarising, high linear correlation with Pb concentration was identified for both parameters: for C, where $R^2 = 0.79$ at 30 Hz and $R^2 = 0.95$ at 6 kHz (Figure 5.8c); for R, with $R^2 = 0.9869$ at 180 Hz and $R^2 = 0.9757$ at 200 kHz (Figure 5.8d).

5.2.1.3 Microwave responses

The microwave spectrum in the frequency range 500 MHz-15 GHz obtained by measurements with the lacquered IDE sensor is shown in Figure 5.9a. During the measurements, significant pronounced resonant peak shifts were noticed when the different samples were placed in contact with the sensor pattern. This shift was more evident when the samples had a higher concentration of Pb. This is clearly visible in several parts of the spectrum, in particular between 300 MHz and 3 GHz. The shift in the

spectrum with the best linear correlation among the Pb samples was in the frequency range of 2.3-2.65 GHz (shown in the red rectangle in Figure 5.9a and magnified in Figure 5.9b). The correlations between reflected power and Pb concentration in each of 60,000 points of the frequency range 10 MHz – 10 GHz, were calculated with the square of Pearson's correlation using Excel. In this way, it was found that the best correlation was at 2.40 GHz with $R^2=0.9982$ ($R^2=0.978$ in the peak at 2.49 GHz) (Figure 5.9c).

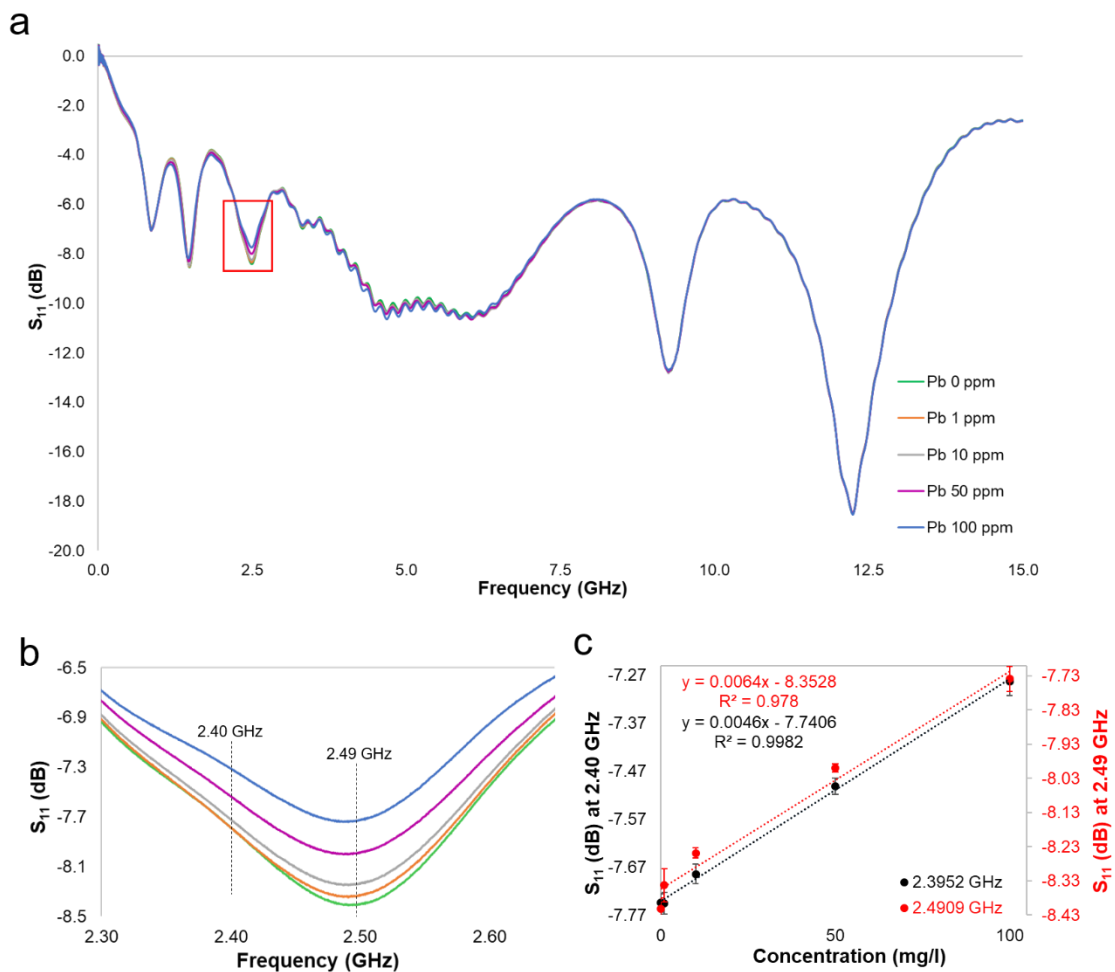


Figure 5.9 Microwave spectral response (average) captured with a lacquered IDE sensor at 0.01–15 GHz frequency range for each sample concentration of Pb. The red rectangle highlights the area in which the spectra variate due to the diverse Pb concentration (magnified in b). Specifically, at the frequency range between 2.30–2.65 GHz two specific frequencies are evidenced, namely 2.40 and 2.49 GHz (peak), where there are strong linear correlations between reflection coefficient (S_{11}) and Pb concentration (c)

Results confirmed the ability of the lacquered IDE sensors to quantify the Pb concentration in DW, as changes in spectrum signal at specific frequencies of the

electromagnetic spectrum. Shifts in the resonant frequencies were noticed when different lead solutions were placed in direct contact with the EM field through the sensing structure, and the return to the baseline spectrum (air response, as was shown in Figure 5.2) demonstrating the possibility of continuous monitoring. Consequently, investigating more microwave spectroscopy and applying novel strategies for improving its performance for the determination of various toxic metals at lower concentration (<1 mg/L) using microwave spectroscopy, is a promising alternative to traditional grab-sampling and laboratory-based analyses.

5.2.1.4 Comparisons between optical, impedance and microwave responses

Statistical features, namely R^2 , sensitivity, and CV (expressed in % for comparing the features between different methods) for Pb solutions between 0 and 100 mg/L obtained by measuring optical, impedance and microwave techniques are compared in Table 1. The CV was < 5%, which is considered the acceptable standard for most of the analytical methods.

Table 5.1 Summaries of statistical features for Pb ions and optical, impedance and microwave measurements, using a resonant cavity, IDE sensors and lacquered IDE sensors

Properties	Frequency/ Wavelength ^a	R^2	Sensitivity ^b	Max CV (%)	Average CV (%)
Absorbance	247 nm	0.96	0.0031	1.5 %	1.5 %
Absorbance	300 nm	0.9852	0.0024	0.3 %	0.3 %
Capacitance	30 Hz	0.7942	30 nF	3.7 %	3.7 %
Capacitance	6 kHz	0.9465	0.3 nF	3.3 %	3.3 %
Resistance	180 Hz	0.9869	-0.64 Ω	3.6 %	3.7 %
Resistance	200 kHz	0.9757	-0.14 Ω	3.9 %	3.9 %
S₁₁ (resonant cavity)	415 MHz	0.9527	-0.0315 dB	1.9 %	1.5 %
S₁₁ (resonant cavity)	2.45 GHz	0.9017	0.0397 dB	2.1 %	1.4%
S₁₁ (IDE sensor)	415 MHz	0.9864	-0.03415 dB	0.4 %	0.3 %
S₁₁ (IDE sensor); peak	2.45 GHz	0.9692	0.0593 dB	0.4 %	0.3 %
S₁₁ (lacquered IDE sensor)	2.40 GHz	0.9982	0.0046 dB	0.4 %	0.3 %
S₁₁ (lacquered IDE sensor); peak	2.50 GHz	0.9780	0.0064 dB	0.4 %	0.3 %

^aabsorbance is expressed in wavelength; ^bfor changes in every 1mg/L of Pb concentration;

Also, microwave responses using a resonant cavity, an uncoated IDE sensor and lacquered sensors are described. Microwave measurement reflects better, and more

specifically changes which are related with metals in water than absorbance and impedance measurements at low-frequency, due to the production of resonant peaks at specific frequencies. Between these parameters, the uncoated sensors showed an improved sensitivity in the most pronounced peak, if compared with the results obtained using the resonant cavity and the lacquered sensor. Although, the lacquered sensors are protected from oxidation by the lacquer, which can be advantageous for the continuous monitoring of water resources. The most pronounced peak (at 2.50 GHz) which was able to distinguish diverse Pb concentration slightly shifted to higher frequencies, due to the thickness and to the change of dielectric properties of the complex sensing structure. In addition, other consequent experiments demonstrated that the different spectral shape and the lower sensitivity that was obtained with the lacquered sensor and Pb sample was also caused by the fact that these samples were acidified with 1% of HNO₃.

The results discussed above have been published by Frau et al (2018a).

Accordingly, consequent experiments were performed using non-acidified samples, for 1) obtaining higher sensitivity and 2) performing real-time measurements avoiding sample preparation. These experiments gave the basis to work on improving the features of these sensing systems to simultaneously analyse a range of metals at low concentrations, allowing for continuous *in situ* monitoring, thus solving the limitations of lab-based technologies.

5.3 β -Bi₂O₃ based coatings and Zn ions

Summarising from the previous chapters, among materials that can be integrated onto sensors for performance improvement, inorganic oxide compositions are considered to be most advantageous. During the last decade, a number of approaches have made use of Bi-based electrodes for the detection of toxic metals at trace concentrations (Švancara et al,

2010). In this section, results using f-EM sensors based on bismuth (III) oxide coatings are illustrated. These sensors were the first developed and tested f-EM sensors for measuring Zn water solutions. This was the first time that β -Bi₂O₃ in nanopowder form ($90 < \Phi < 210$ nm particle size) was used as the principal material for developing a paste mixture to integrate in the form of a thick film onto microwave planar sensors for water quality analysis.

The first toxic metal that was tested in this project using f-EM sensors was Zn, considering its potential adsorption on bismuth (III) oxide and its lower toxicity compared with the others metals and its higher EQS in freshwater. Also, Zn is one of the most abundant toxic metals that is present with high concentrations in mining-impacted catchments in the UK and worldwide (Gozzard et al, 2011).

In this subchapter, results for novel f-EM sensors based on β -Bi₂O₃ based coatings, with two thickness 40 and 60 μ m, are described for measuring Zn ions in water.

5.3.1 Analysis, results and discussion

In this section, optical, impedance and microwave analyses were performed for Zn water solutions using uncoated and novel f-EM sensors. Summarising from the methodology chapter, three series of microwave sensors were developed and tested with Zn water samples:

1. a series was left uncoated;
2. a series of sensors was functionalised with β -Bi₂O₃ based film with 4 printed layers (40 μ m);
3. another series was functionalised with β -Bi₂O₃ based film with 6 layers (60 μ m).

Repeatability and reproducibility were measured and confirmed using the absorbance of the screen-printed coatings on microscope slides with β -Bi₂O₃ based paste mixtures.

In this section, results for the analysis of seven laboratory water samples of Zn at different concentrations (0, 0.1, 0.5, 1, 10, 50, 100 mg/L) were prepared and measured using:

- a UV-Vis Spectrophotometer, measuring the absorbance;
- a LCR bridge, measuring C and R;
- a ZVA 24, measuring the reflection coefficient S_{11} , adding a small sample volume (400 μL);

Initial characterisation of the coating, its interaction with Zn solutions at various concentrations, its durability, reaction and recovery time were initially assessed by low-frequency impedance measurements for thick films screen-printed on top of Ag eight-pair electrodes that have been screen-printed onto microscope slides for an inexpensive development. Morphological properties and elemental composition were analysed before and after Zn detection using SEM and EDS analysers. Summarising, the interaction between the Zn and the coating materials was assessed by:

- C, R and S_{11} time measurements, to analyse the reaction and recovery time;
- SEM and EDS analysis;
- By evaluating the adsorption between coatings and Zn samples at various concentration.

Then, responses were analysed and they are illustrated in the following subsections.

5.3.1.1 Absorbance of Zn samples

The absorbance for Zn samples at low (0.1, 0.5 and 1 mg/L) and high concentrations (10, 50 and 100 mg/L) is shown in Figure 5.10a, for wavelengths between 200 and 350 nm, which was selected from the full range (200-1,000 nm) as more representative of the variation in Zn concentration. Specific wavelengths were selected to measure the correlation between absorbance and Zn solutions.

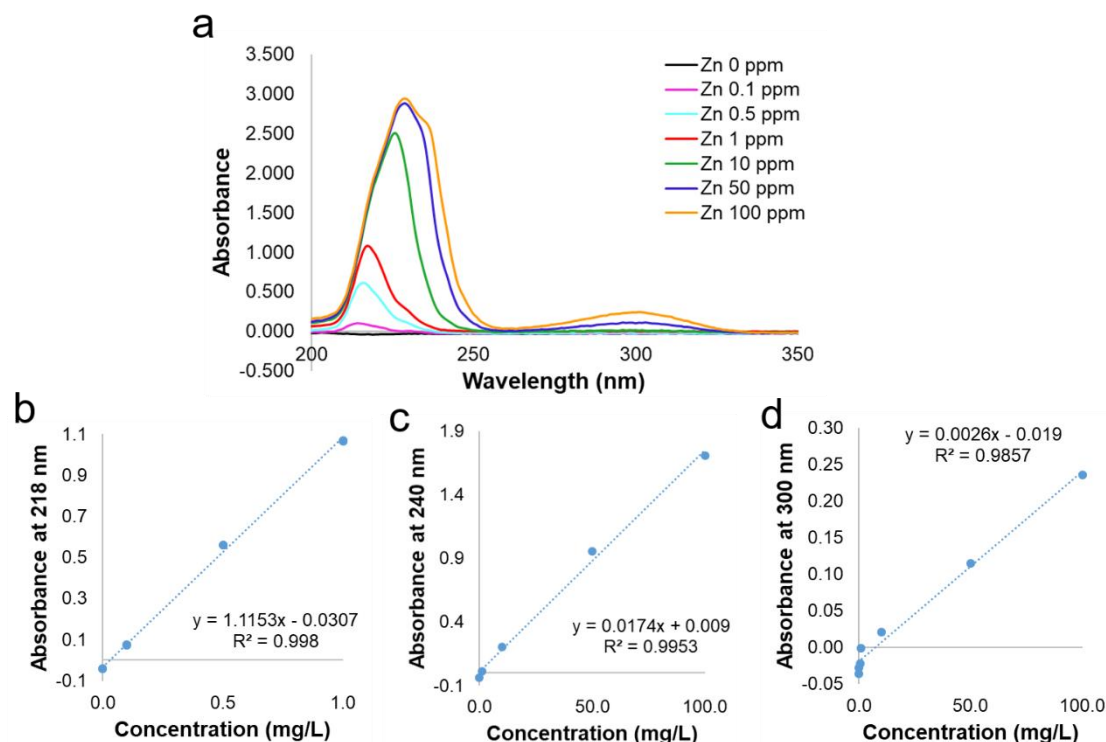


Figure 5.10 Absorbance for Zn samples in the wavelength range between 200-350 nm (a) and their linear correlations for low concentrations (0.1, 0.5 and 1 mg/L) at 218 nm (b) and for high concentrations (10, 50 and 100 mg/L) at 240 nm (c) and 300 nm (d)

Specifically, 218 nm was selected for Zn concentrations at low concentration (0-1 mg/L) and absorbance, which shows a high correlation ($R^2=0.99$) (Figure 5.10b); likewise, 240 and 300 nm were selected for high linear correlation between high Zn concentrations (1-100 mg/L) and absorbance. Although, the variation of the absorbance (sensitivity) at 218 nm for low concentrations (1.1Δ of absorbance for each 1 mg/L) is much higher than the one measured for high concentrations ($\Delta 0.017$ and 0.0026 of absorbance for each mg/L).

5.3.1.2 Impedance responses

5.3.1.2.1 Zn samples

Spectral responses for capacitance and resistance at the investigated frequencies (20 Hz – 3 kHz) for Zn concentrations 0-100 mg/L are illustrated in Figures 5.11a and b: it is notable how the capacitance and resistance reflect an inverted behaviour.

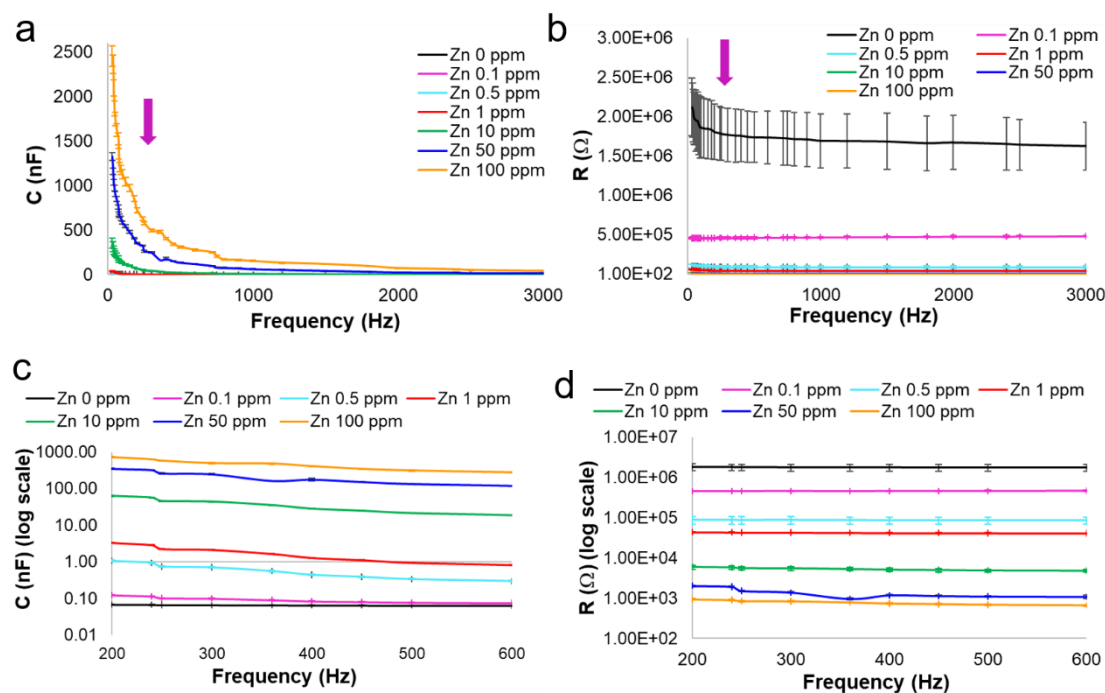


Figure 5.11 Spectral response for capacitance (C) (a), resistance (R) (b) and Zn solutions at low frequencies (20 Hz – 3 kHz); their enlargement in the frequency range 200-600 Hz (indicated by the arrows in a and b) for C (c) and R (d) is shown for a clearer view of the selected frequency with a logarithmic scale for displaying also the Zn concentration < 1 mg/L

The capacitance increases as the Zn concentration and the EC increase (Table 5.2), conversely the resistance and pH decrease. Moreover, the C decreases moving towards higher frequencies, while the R remains stable. The part of the spectrum that shows a higher relation between these two parameters and Zn concentration was identified between 200 and 600 Hz (magnified respectively in Figures 5.11c and d). Low-frequency electrical measurements were able to detect changes in Zn concentration. The capacitance measurements show a good linear correlation with Zn concentration at 250 Hz, with $R^2 = 0.9991$.

Table 5.2 pH and EC of the Zn solutions

Zn solutions (mg/L)	pH	EC (mS/cm)
0	7.36	0.0021
0.1	5.71	0.0141
0.5	4.26	0.0711
1	3.78	0.1313
10	2.60	1.326
50	1.99	6.53
100	1.97	13.06

Otherwise, the resistance and Zn concentration are correlated with a power trend with $R^2 = 0.9468$ at 500 Hz. Figure 5.12 shows these two electrical parameters where Zn concentration is expressed with a logarithmic scale to permit to distinguish also a calibration curve under 1 mg/L (0.1 and 0.5 mg/L).

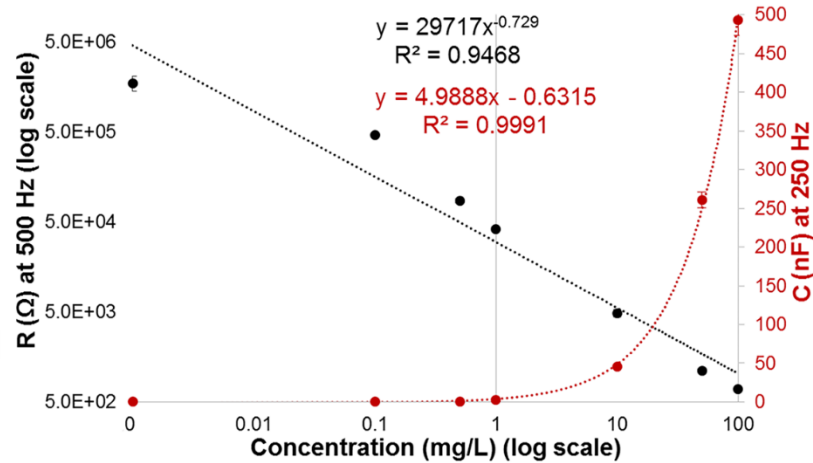


Figure 5.12 Power correlation between resistance (R) (expressed in logarithmic scale) and Zn concentration (in black) at 500 Hz; and linear correlation between capacitance (C) and Zn concentration (in red) at 250 Hz. Both parameters are measured with a LCR meter

5.3.1.3 Microwave responses

Results, obtained with f-EM sensors based on β -Bi₂O₃ thick film with diverse thicknesses, show how the S_{11} spectra were dependent on the presence and concentration of Zn at various concentrations in water. The spectral microwave response for the microwave technique with uncoated and coated sensors demonstrates a shift in signal amplitude at specific frequencies, which corresponds to the different concentrations of Zn tested. During the measurements, significant resonant peak shifts were noticed for the different concentrations of Zn samples as soon as they were in contact with the EM field through the sensing structure. Figure 5.13a, b and 5.14a illustrate the S_{11} magnitude respectively of the uncoated microwave sensor and f-EM sensors coated with 40 and 60 μm of β -Bi₂O₃ based thick film in contact with various Zn concentration solutions. The distinct feature is the change in the resonant peak amplitude, clearly visible in several parts of the

spectrum, especially between 100 MHz and 3.2 GHz, with the amplitude decreasing with increasing Zn concentration, for peaks at frequency < 1 GHz, and increasing for peaks identified > 1 GHz. A number of resonant peaks can be identified to serve as an indicator of the Zn content in a solution. The microwave spectra are different for each Zn solution at various concentrations with the most pronounced resonant peaks, indicating higher sensitivity, at around 2.5 GHz for all the sensors used. Figure 5.14b shows two frequencies and a frequency range (599 MHz, 2.56 and 1.57-1.68 GHz) at which good correlations (respectively $R^2=0.9993$, $R^2=0.9318$ and $R^2=0.9466$) with Zn concentration (expressed with a logarithmic scale to permit to distinguish also 0.1 and 0.5 mg/L of Zn) and S_{11} occur, using the 60 μm $\beta\text{-Bi}_2\text{O}_3$ based sensor.

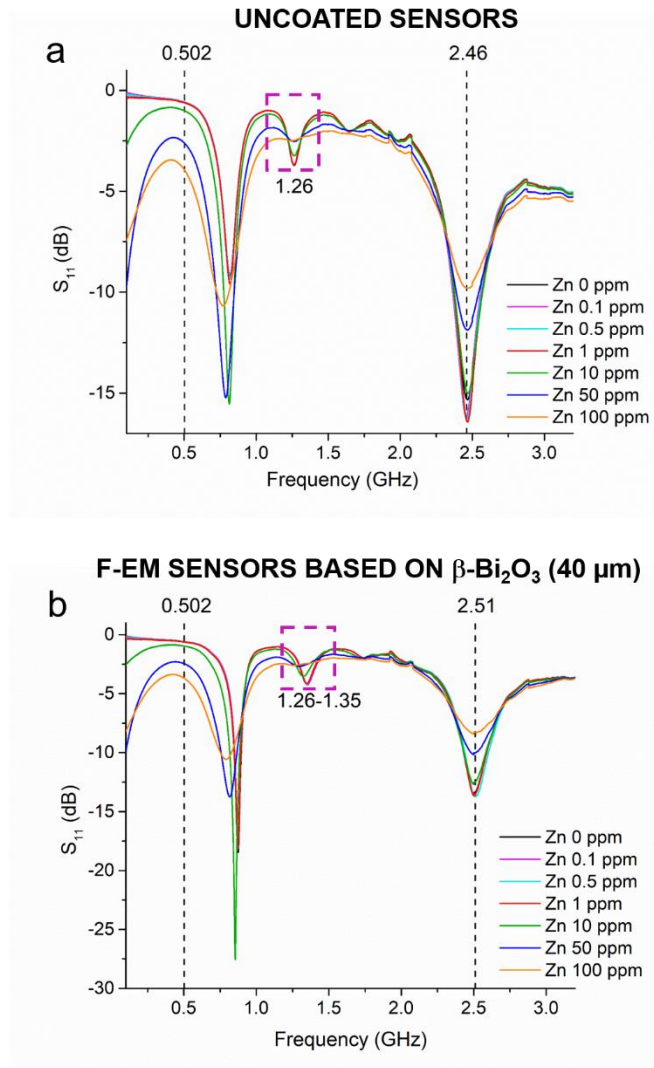


Figure 5.13 Spectral responses in the frequency range 0.1-3.2 GHz for Zn water solutions (0-100 mg/L) measured using an uncoated sensor (a) and an f-EM sensor based on β - Bi_2O_3 based coating with a thickness of $40 \mu\text{m}$ where are marked three amplitude shifts for each one, namely at 0.502, 1.26 and 2.46 GHz for the uncoated sensor and at 0.502, 1.26-1.35 and 2.46 GHz

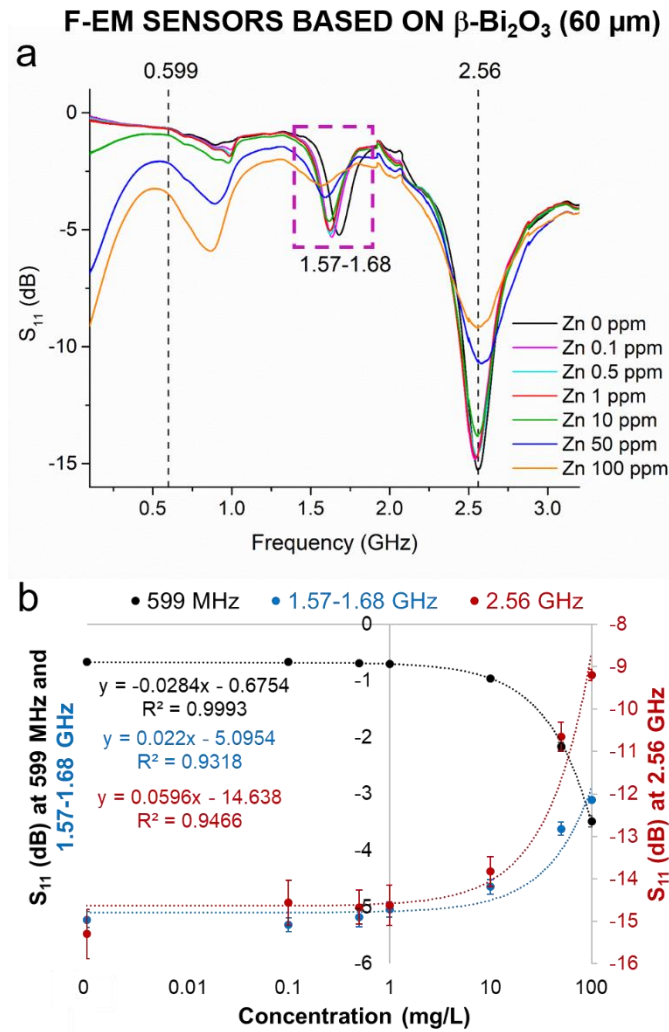


Figure 5.14 Change in S_{11} of microwave spectra for Zn solutions measured with a f-EM sensor with 60 μ m of β -Bi₂O₃ based coating (a) and the linear correlation between S_{11} and Zn concentration (in logarithmic scale for showing 0.1 and 0.5 mg/L of Zn) at two discrete frequencies and a frequency range, namely 599 MHz, 2.56 GHz (peak) and 1.57-1.68GHz

5.3.1.3.1 F-EM sensors: coating's effect

In the f-EM sensors, the electromagnetic wave propagates in both the substrate on which gold IDE are printed, and the top β -Bi₂O₃ based thick film. Therefore, the overall propagation will depend on the permittivity of each component in the system, such as a substrate permittivity and its thickness, and on the sensitive material permittivity, which will change with the interaction of the zinc with the sensitive layer. The response changes due to the effect of the β -Bi₂O₃ based thick film have been compared with the uncoated sensors noting significant differences. This functionalisation enhances the sensor performance significantly leading to a higher sensitivity compared to the bare IDE

electrode, particularly around 1.5 GHz for Zn detection between 0.1 and 1 mg/L, important for detecting Zn just above and below the EQSs.

The effect of the β -Bi₂O₃ based thick film produced an overall shift toward higher frequencies, probably due to the decreasing of the dielectric constant and the coating thickness (Patil & Puri, 2010). Notably, with the uncoated sensor, the peak was at 2.46 GHz (Figure 5.13a); with the functionalised sensor (40 μ m) at 2.51 GHz (Figure 5.13b); and with the functionalised sensor (60 μ m) at 2.56 GHz (Figure 5.14a). An interpretation of the obtained results suggests a change in dielectric properties due to the thickness of the coating (Chen et al, 2012; Patil & Puri, 2010).

A higher R^2 (=0.9993) is identified at 599 MHz and measured with the 60 μ m β -Bi₂O₃ based film. Nevertheless, the linear correlation is higher, the sensitivity is slightly smaller than that measured at 502 MHz with the uncoated sensor (respectively 0.0028 and 0.0035 change in S_{11} for every 100 μ g/L change of Zn concentration). Possibly, this is due to a permittivity change of the sensitive coating that induces a decrease in the resonant response at the peak, causing a reduction of the amplitude to the signal (Bernou et al, 2000).

Additionally, with the coated sensors, the change in the resonant peak amplitude was accompanied by a gradual shift in the frequency between distinct Zn concentrations, which increases with thickness. Specifically, the uncoated sensor had a resonant peak at 1.26 GHz (Figure 5.15a); the sensor with 40 μ m thickness of β -Bi₂O₃ based film manifests a frequency shift for 0-100 mg/L Zn concentrations between 1.26 to 1.35 GHz (Figure 5.15b); with 60 μ m, the shift is more pronounced, recognised at 1.57-1.68 GHz (Figure 5.15c). Notably, for higher Zn concentration solutions, the peak is set at lower frequencies, at 1.57 GHz for 100 mg/L and 1.63 GHz for 0.1 mg/L.

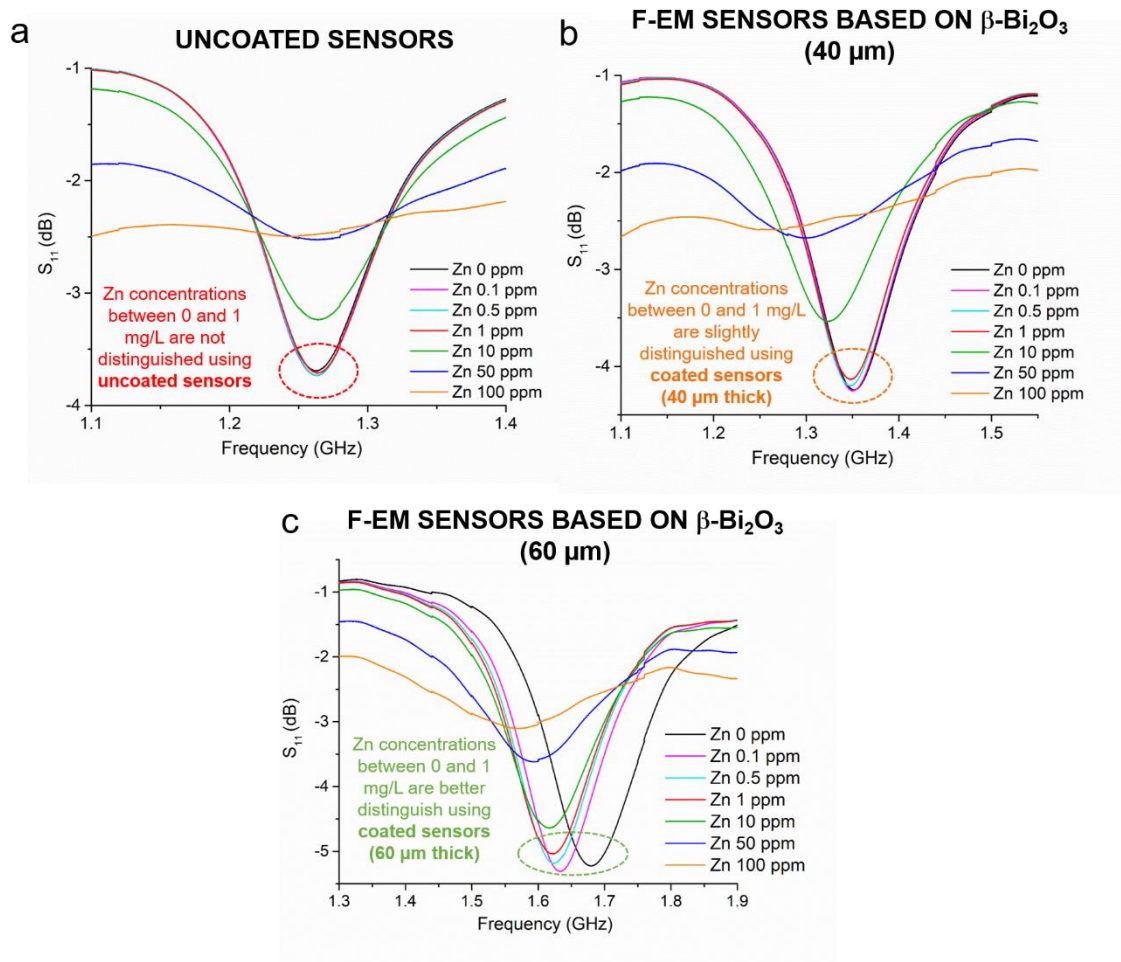


Figure 5.15 Spectral response for the peak identified at around 1.2 GHz (which shifts due to the coating's thickness) for uncoated (a) and f-EM sensors with 40 μ m (b) and 60 μ m (c) of β -Bi₂O₃ base coating which show the improvement of this last coating to better distinguish between Zn concentrations between 0 and 1 mg/L

These responses are probably due to the effect of a permittivity variation of the sensitive chemical layer (Ferrari & Prudenziati, 2012). As described by Bernou et al (2000), the electromagnetic wave propagates in each component in the system.

Due to the shift in both amplitude and frequency, the sensor performance is improved with the β -Bi₂O₃ based film for all Zn concentrations. Of particular importance is the different response for low concentrations (100 and 500 μ g/L) important for detecting the Zn level in freshwater superior to the EQSs (> 125-210 μ g/L) or identifying small variations above the "baseline" polluted level. Consequently, there is an increase of sensitivity, which is represented by a higher slope, due to this shift in both amplitude and

frequency, passing from 1.4×10^{-3} (uncoated sensor), 1.8×10^{-3} ($40 \mu\text{m}$ coating) to 2.2×10^{-3} ($60 \mu\text{m}$ coating) change in S_{11} (ΔdB) for every $100 \mu\text{g/L}$ change of Zn concentration (Figure 5.16).

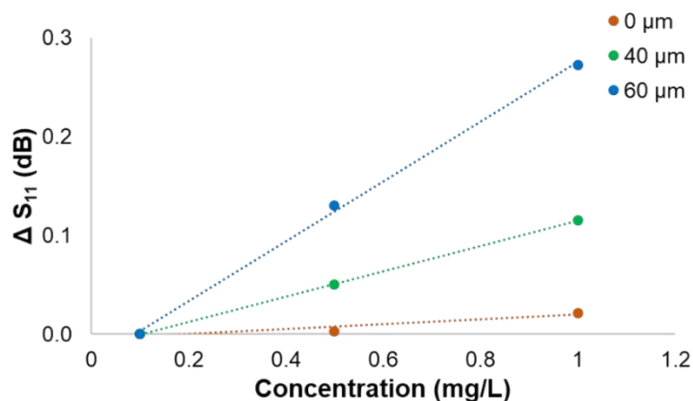


Figure 5.16 Variation in microwave response for uncoated and coated sensors with $40 \mu\text{m}$ and $60 \mu\text{m}$ of $\beta\text{-Bi}_2\text{O}_3$ base coating which shows the sensitivity improvement for Zn concentration between 0.1 and 1 mg/L

Furthermore, the $\beta\text{-Bi}_2\text{O}_3$ based coatings are stable, repeatable and reproducible, as confirmed by absorbance spectra measurements of the screen-printed coating on microscope slides screen-printed with paste mixtures prepared during diverse days (Figure 5.17).

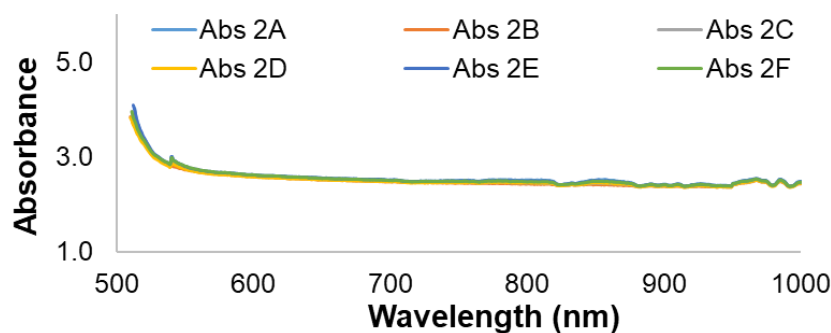


Figure 5.17 Example of the average of absorbance spectra showing the repeatability and reproducibility of the coating for paste prepared and printed during diverse days

5.3.1.4 Summary of optical, electrical and microwave measurements

Results obtained measuring the Zn solutions at different concentration with the techniques previously described are summarised in Table 5.3, which shows R^2 , sensitivity (for each 100 $\mu\text{g/L}$ of Zn concentration) and CV in % in order to demonstrate the repeatability and reproducibility of the measurements. Summarising, absorbance response was able to distinguish Zn concentrations between 0-1 mg/L at 218 nm and higher concentrations than 1 mg/L at 240 nm. Capacitance and resistance measurements were able to distinguish Zn concentrations at low and high concentrations, where low frequencies (250-500 Hz) were selected for quantifying Zn solutions for their higher sensitivity compared with higher frequencies (500-20,000 Hz). Although comparing the spectral response between electrical (Figures 5.11a and b) and microwave measurements (Figure 5.13a, b and 5.14a), it is notable that microwave multi-peak spectra offer a more specific characterisation of the water samples under test with their high spectral resolution using 60,000 distinct points. Contrariwise, low-frequency capacitance and resistance responses gave a less specific signature, considering their “flat” profile, giving a less specific signature for detecting variations in a water sample under test.

Table 5.3 Summary of statistical features obtained for optical, electrical and microwave measurements of Zn water sample

Properties	Frequency/wavelength	R^2	Sensitivity ^a	CV (%)
Absorbance	at 218 nm	0.998	0.1115	1.5 %
Absorbance	at 240 nm ^b	0.995	0.0017	1.5 %
Capacitance	at 250 Hz	0.9991	0.5 nF	2.5 %
Resistance	at 500 Hz	0.9468 ^c	119.9 Ω	2.5 %
Reflection coefficient (S_{11}) - uncoated IDE sensor	at 502 MHz	0.9914	0.0035 dB	0.6 %
	at 1.26 GHz ^b	0.8377	0.0014 dB	0.6 %
	at 2.46 GHz (peak)	0.9563	0.0065 dB	1.1 %
Reflection coefficient (S_{11}) – functionalised IDE sensor (4 layers, 40 μm)	at 511 MHz	0.9915	0.0032 dB	1.3 %
	1.26-1.35 GHz ^b	0.8301	0.0018 dB	1.1 %
	at 2.51 GHz (peak)	0.9682	0.0054 dB	2.1 %
Reflection coefficient (S_{11}) – functionalised IDE sensor (6 layers, 60 μm)	at 599 MHz	0.9993	0.0028 dB	1.8 %
	1.57-1.68 GHz ^b	0.9318	0.0022 dB	2.0 %
	at 2.56 GHz (peak)	0.9466	0.0069 dB	2.8 %

^afor every 100 $\mu\text{g/L}$ change of Zn concentration; ^bfor Zn concentrations 0-1 mg/L; ^cpower correlation;

Generally, using microwave spectroscopy, at the most pronounced peak produced, the sensitivity is higher, but measuring Zn solutions, the CV in % is higher (representing a lower precision) and R^2 is lower than at other selected frequencies. However, the CV was $< 2.8\%$ for all performed measurements, which indicates that the measurements are precise and repeatable. Consequently, it is advantageous to find an appropriate compromise depending on the particular analysed condition. For instance, using the f-EM sensors with $60\ \mu\text{m}$ of $\beta\text{-Bi}_2\text{O}_3$ based coatings, it is advantageous for detecting Zn concentrations between 0 and 1 mg/L at the frequency range 1.57-1.68 GHz. The response at other two peaks (at 0.5-0.6 and 2.46-2.56 GHz) is more useful for detecting concentrations between 1 and 100 mg/L using both uncoated and f-EM sensors. The improvement of capacitive sensors due to material integration onto IDE sensors was demonstrated also by Liu et al (2019) for humidity sensing; and by Bahoumina et al (2017), with the integration of sensitive material onto flexible microwave sensors deposited by injecting printing technology, for harmful gas sensing due to frequency shifts on the output.

Bi_2O_3 is a high dielectric material, which determines a variation in spectral response shifting to higher frequencies and increasing the H_f intensity on the surface of the microwave sensing structure. Although, the effective dielectric constant cannot be evaluated, as it is not a pure material, it is mixed with binders for creating the paste mixture with the right consistency to be printed. The relationship between permittivity and resonant frequency variations using a thick film based on $\alpha\text{-Bi}_2\text{O}_3$ onto a microstrip patch antenna, at higher frequencies (8-12 GHz), was evaluated for the first time by Patil & Puri (2010), demonstrating that the thickness of the coating influences the microwave response, with an input impedance which decreases with the increase in thickness. In this

work, a comparable behaviour, where resonance frequency shifts towards high frequencies end, was observed.

Despite the large amount of ongoing research carried out into using microwave technology, more research is necessary for developing microwave sensors able to detect toxic metal ions at the required sensitivity. Due to the difficulty in finding other microwave sensors measuring Zn in the literature, the resolution (considered as the smallest change that a sensor can detect) of the f-EM sensor described in this work is compared with other diluted solutions of DW. As recently reported by Vélez et al (2019), the f-EM sensor based on β -Bi₂O₃ is the one that “exhibits an extremely good resolution (but a limited dynamic range)” comparing glucose and NaCl, among others. Between the evaluated sensors, this sensor was the one presenting the highest sensitivity and the best resolution. Although, their aim was to detect much higher concentrations in a bigger dynamic range, which was not of interest to this work.

5.3.1.5 Interaction between β -Bi₂O₃ and Zn

5.3.1.5.1 Time responses using microwave and impedance measurements

The possible interaction between Zn ions and β -Bi₂O₃ based coatings was assessed by measuring the impedance parameters variation of the interaction between Zn solution at various concentrations at low-frequencies using coated Ag-IDE screen-printed on microscope slides. Likewise, the interaction between the developed f-EM sensors, based on β -Bi₂O₃ using both a ZVA 24 and an LCR bridge, was measured by time. In this way, the possibility of measuring Zn concentration variation using microwave spectroscopy, as it is strictly related to variations in impedance measurements, was evaluated. Once the sensors' output in all frequency ranges was analysed using both coated Ag electrodes and Au microwave sensors with 40 and 60 μ m of β -Bi₂O₃ based coatings, 150 Hz was selected

to determine the variation in capacitance over 30 min, with a measurement recorded every 5 s. Likewise, 2.53 GHz was selected for evaluating the variation by time using microwave measurements. The purpose of doing this was to assess changes in electrical and microwave properties as a measure of the interaction between the coated sensors with Zn solutions, and the consequent achievement of “stability”.

Results obtained with both electric and microwave measurements show how the reaction between Zn and the coating is observed to commence within 30 sec of exposure and reach an adsorption equilibrium time within 600 sec (10 minutes). Figure 5.18 shows some examples of the timeline response within 30 minutes for 60 μm of coating and Zn samples. Figure 5.18a shows the capacitance for screen-printed coatings on Ag electrodes, that have been screen-printed onto microwave slides, at 150 Hz and measured with the “crocodile clips” and the LCR bridge. The timeline response for the f-EM sensors with 60 μm of $\beta\text{-Bi}_2\text{O}_3$ based coatings is illustrated in Figure 5.18b for C measurements at 150 Hz using the LCR bridge and in Figure 5.18c for S_{11} measurements at 2.53 GHz. This shows how the C and S_{11} parameters change during the first 10 minutes and reach stability afterwards. Capacitance and S_{11} tend to increase with Zn concentration, with most of the response occurring within the first 5 minutes after application of the water sample on the sensor surface; then the signal tends to stabilise by comparison and remains stable beyond 600 seconds. This demonstrates that the interaction between the functional coating and the Zn ion reached an equilibrium at this point. Moreover, some variation detected using the uncoated sensor was probably related to the evaporation of the 400 μL volume of sample. This issue was solved as shown in the results presented in the following chapter, by immersing the sensor in water for *in situ* analysis.

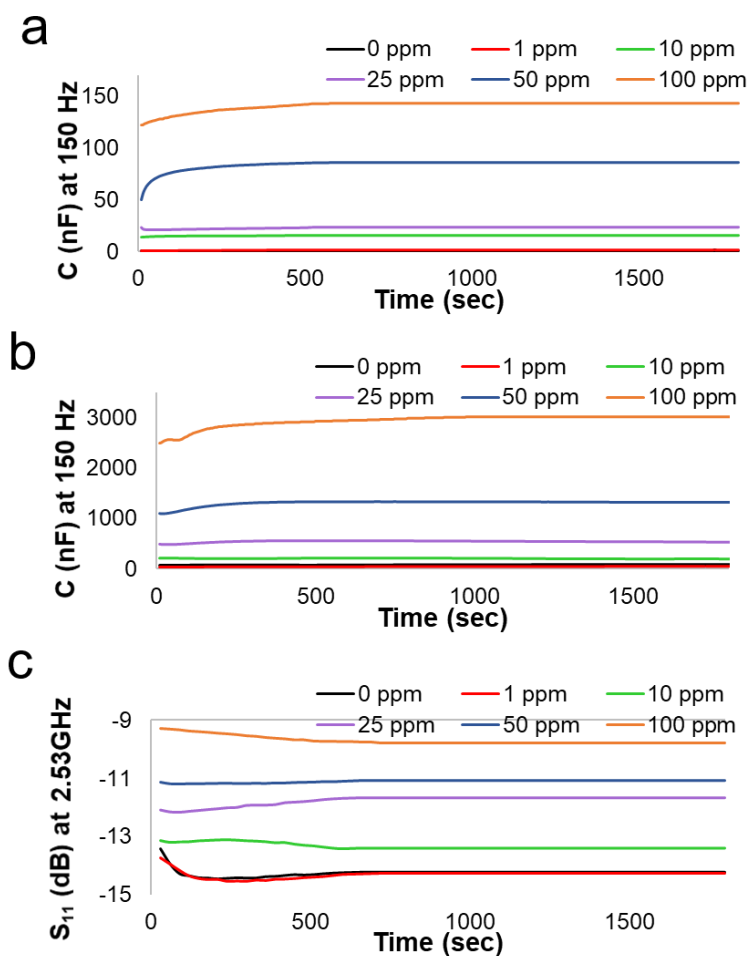


Figure 5.18 Timeline responses for 30 minutes for Zn solutions measured with a β -Bi₂O₃ based thick film (60 μ m), screen-printed onto Ag-IDE measuring C at 150 Hz (a), and screen-printed onto Au microwave sensors, measuring C at 150 Hz (b) and S₁₁ responses at 2.53 GHz (c)

5.3.1.5.2 Adsorption experiment

The adsorption of Zn onto the β -Bi₂O₃ based coatings was estimated by adding the coating material printed on a microscope slide on each Zn solution and measuring the concentration of it after 5 and 10 min using a conductivity meter ($R^2=1$ for Zn concentration 0-100 mg/L). This experiment estimates that about 4% of Zn is adsorbed on the coating after 5 minutes and 6 % after 10 min (Table 5.4). This was the time estimated of the interaction between the β -Bi₂O₃ coating and the Zn solutions to reach adsorption equilibrium, as sensor responses reached stability. Likewise, with the higher

concentrations (50 and 100 mg/l), the % of adsorption is slightly reduced presumably due to the lower pH (<2, see Table 5.2). As a matter of fact, the adsorption of cations on metal-oxide minerals in the natural environment is reduced when the pH decrease (Smith, 1999). Therefore, it is probable that the pH influences the Zn adsorption on the β -Bi₂O₃ based coating. However, the EM wave likely promotes the adsorption of Zn ions onto the sensing surface. The EM field interacts with each component of the f-EM sensor and the change in spectral response will depend on the changes in permittivity that are related to the Zn adsorption onto the coating.

Table 5.4 Estimation of the percentage of adsorption between β -Bi₂O₃ based film and Zn solutions (0-100 mg/L) after 5 and 10 minutes

Zn solutions (mg/L)	Conductivity (mS/cm) after		Concentration (mg/L) after		Adsorption (%) after	
	5 min	10 min	5 min	10 min	5 min	10 min
0	0.0021	0.0023	0	0	0	0
0.1	0.0135	0.0132	0.0957	0.9362	4.3	6.4
0.5	0.0681	0.0667	0.4479	0.4789	4.2	6.2
1	0.1261	0.1235	0.0957	0.9337	4.0	5.9
10	1.234	1.211	9.611	9.435	3.9	5.7
50	6.279	6.162	48.07	47.18	3.8	5.6
100	12.58	12.39	96.32	94.87	3.7	5.1

5.3.1.5.3 EDS and SEM analysis

The presence of Zn on the sensing layer was assessed by SEM and EDS analysis. The SEM image of the sensing surface after measurements (schematised in Figure 5.19a) is illustrated in Figure 5.19b. The elemental pattern (Figure 5.19c) and its percentage composition (Figure 5.19d), were determined with the EDS after its use, to confirm the presence of Zn ion in the sensitive layer adsorbed by the coating. This was determined after 2h of continuous measurements and 10 mg/L of Zn concentration sample, considering that the EDS used was not able to determine the presence of Zn ions after short usage and using samples with low Zn concentration, due to instrumental sensitivity limitation.

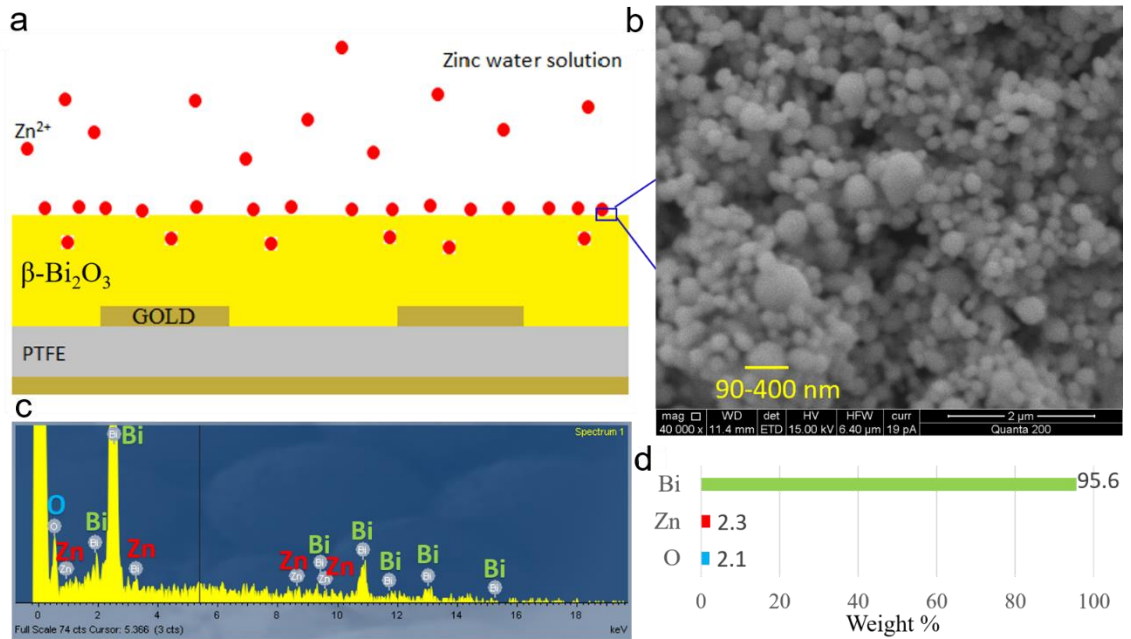


Figure 5.19 Schematisation of a partial cross-section of the f-EM sensor illustrating the sorption of Zn onto the sensing layer (a); SEM image of the coating after the sorption reaction with the Zn ions (with highlighted particle size) and its elemental spectra (c) and elemental weight % (d) of the coating after the adsorption

5.3.1.5.4 Recovery time

The sensor recovery time was evaluated using the LCR bridge and the VNA as the time needed for the response of the sensor to return to the 90 % of the original “air spectra”. The recovery time was assessed after each measurement and each f-EM sensor was rinsed in deionised water. It was recorded as being between 100-150 sec, resulting in a return to the air value respectively of 31 pF and 35 pF (Figure 5.20a) for 40 and 60 μm thickness of films with capacitance measurements. With the microwave measurements, the results are approximately the same, returning to the air spectra after 100-150 sec (Figure 5.20a and b). F-EM sensors are reusable, considering that the sensor output returned to its baseline level (air spectra) when Zn polluted water samples were removed and the sensor was rinsed and allowed to dry. This indicates that planar EM sensors are reliable and reusable, probably due to the weak solubility of metal oxides (Chu et al, 2017). In addition, it was noted that when the sensor is “dry” (unused), the reaction time is longer; when it is “wet” (previously used), it is shorter, although the final results are similar. This

is possible because the solution needs more time to saturate the voids in the film. So, when it is dry the zinc takes longer to be sorbed on the β - Bi_2O_3 tetragonal structure. Consequently, it is necessary to consider the state of the sensor when a water sample is analysed with a thick film sensor.

Part of the results discussed above have been published by Frau et al (2019a); Frau et al (2019b).

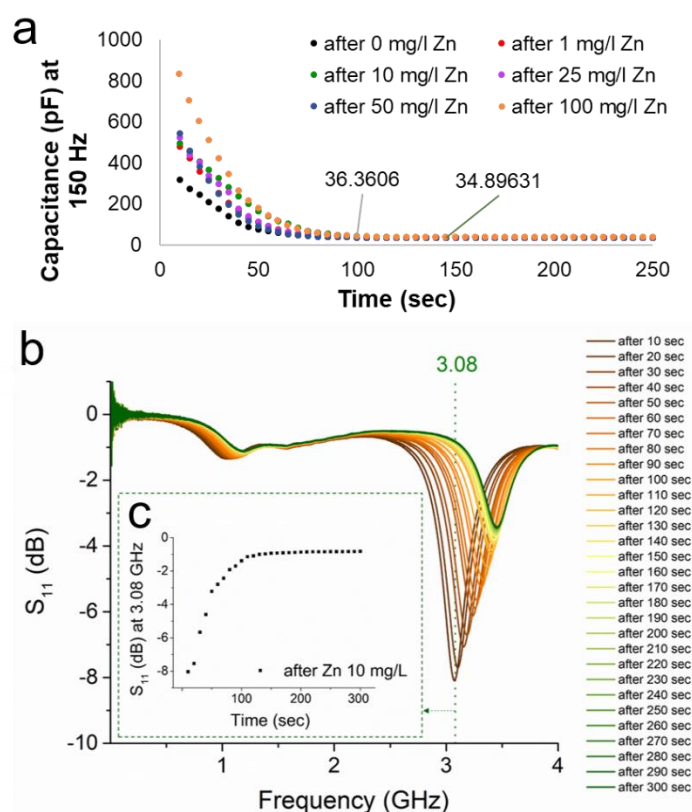


Figure 5.20 Recovery sensor time measured examples that show the spectral variation by time after the sample is taken off from the coating and allowed to dry, showing that after about 100-150 seconds the response returns to the baseline (defined as "air" spectrum) for both C (a) and S_{11} measurements (b and c)

5.4 Chelating polymers based coatings and Cu detection

As previously mentioned, chitosan and l-cysteine are abundantly used to create complexes with metal ions. Consequently, these materials were selected to be integrated onto planar sensing structures for improving the performance. Chemical-based sensors use chelating

ligands when measuring spectroscopic changes (Kim et al, 2020). Consequently, in this work the possibility of improving the selectivity and sensitivity of microwave spectroscopy toward target pollutants, specifically Cu ions, is evaluated. In this section, the focus moves onto detecting Cu, that can cause acute and chronic toxicity even at low concentrations, due to its potential for bioaccumulation and its bioavailability (Agency for Toxic Substances and Disease Registry, 2004). Environmental quality standards (EQS) for Cu in drinking water have been defined by the EU WFD (2 mg/L) and the UN Protection Agency (1.3 mg/L) (Aragay et al, 2011). Lower safe levels were established for surface water by the EU Water Framework Directive (<28 µg/L) for protecting aquatic organisms and to avoid the introduction of abnormal concentrations of Cu into the food chain. Consequently, a range of Cu solutions, at low (0, 0.1, 0.25, 0.5, 1 mg/L) and high concentrations (10, 25, 50, 100 mg/L), were prepared and tested.

Preliminary analysis, performed using various % combinations of materials, including inexpensive chelating organic polymers, of diverse metal solutions (Pb, Zn and Cu) were performed to evaluate the feasibility of using specific cheap materials for increasing the sensitivity and/or selectivity toward metals and obtain distinctive changes in electrical responses. Firstly, the possibility of developing a screen-printable paste using mixtures of chelating polymers and metal oxides, was evaluated. L-cysteine, chitosan and ruthenium oxide in powder form (Figure 5.21a) were mixed with a binder and a solvent for obtaining a screen-printable paste (L-CyChRu, 4:4:1) (Figure 5.21b), which was then screen-printed on planar sensing substrates (Figure 5.21c and d).

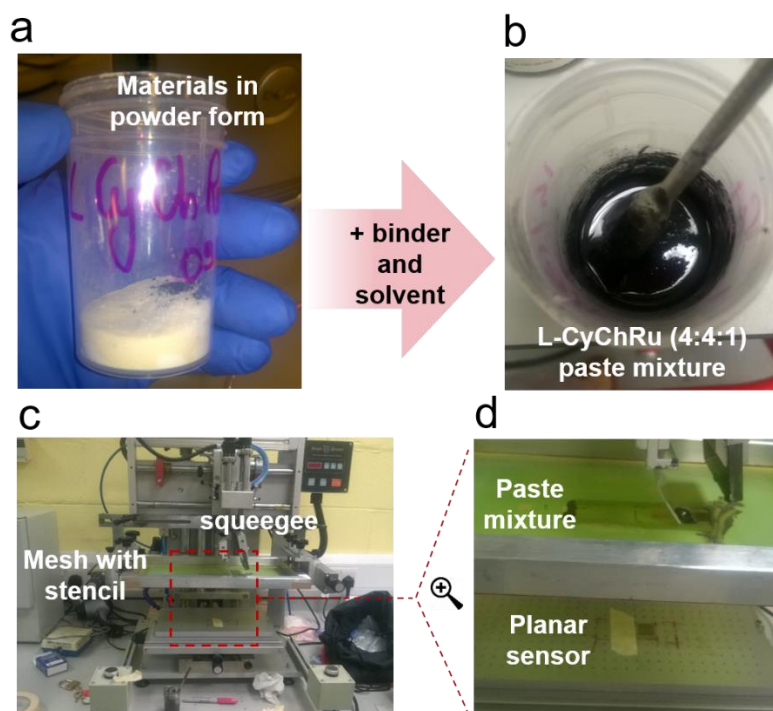


Figure 5.21 Materials in power form, namely l-cysteine, chitosan and ruthenium oxide (4:4:1) (a) were mixed with a binder and a solvent to develop a screen-printable paste (L-CyChRu) to print using a screen-printer (c) onto planar sensing substrates

Secondly, coatings based on these materials were prepared and screen-printed onto an Ag-IDE substrate for inexpensive testing. Thirdly, they were tested through connection with an LCR bridge using “crocodile clips” for measuring C and R variations at low-frequencies (30-20 kHz). Finally, specific frequencies were selected for evaluating the C variation by time. Particularly, l-cysteine and chitosan based coatings show different selectivity for these metals by measuring electrical properties, as capacitance and resistance. An example is shown in Figure 5.22, where a coating based on l-cysteine and chitosan gives a distinguishable C response at 150 Hz for Cu, and a slight variation also for Zn and Pb likewise at low concentration by time.

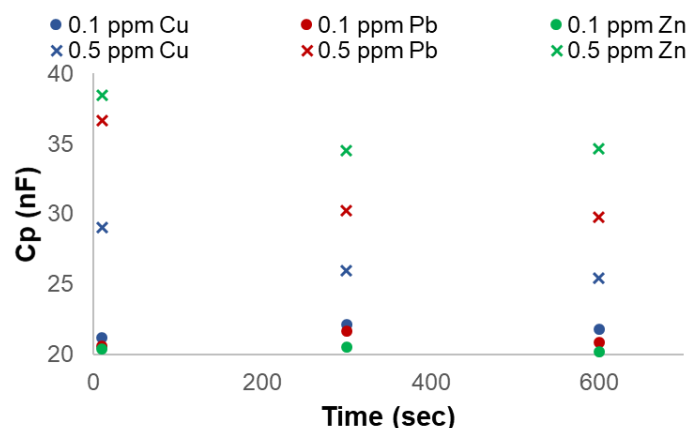


Figure 5.22 Example of C variation by time using a coating screen-printed on Ag-IDE based on a mixture of chelating polymers for selective detection of Cu, Pb and Zn

In this section, the results obtained with two series of f-EM sensors with coatings based on chelating polymers and two diverse metal oxides are illustrated and described. Specifically, i) a set of f-EM sensors was functionalised using L-cysteine, chitosan and ruthenium (VI) oxide (acronym: L-CyChRu); ii) another set using coatings based on L-cysteine, chitosan and bismuth-cobalt-zinc oxide (4:4:1) (L-CyChBCZ).

5.4.1.1 Absorbance of Cu samples

Cu samples were initially analysed optically. Absorbance measurements were performed using the aforementioned Spectrophotometer (200-1000 nm, 3.5 mL sample volume). The absorbance response for Cu water solutions was comparable with the one obtained with the Zn solution, previously described. The results in Figure 5.23a show the absorbance spectral response for Cu samples, which is comparable to the Zn solutions, with peaks at the same wavelengths (218 and 300 nm). A comparison between 10 ppm of Cu, Pb and Zn response is shown in Figure 5.23b. Also, the high linear correlation ($R^2 > 0.99$) for the same metal concentration range is the same, with higher sensitivity for low concentrations (0-1 mg/L) at 218 nm (Figure 5.23c), and lower sensitivity for high concentrations (10-100 mg/L) at 240 and 300 nm (Figure 5.23d and e).

Consequently, this method was not considered selective and appropriate for detecting potentially toxic metal ions. Although, considering the simplicity of the measurements against other more complex laboratory-based techniques (e.g. ICP-OES and ICP-MS), absorbance measurements of single metal (Pb, Cu and Zn) laboratory-prepared non-acidified standard solutions were performed for evaluating their durability and degradability after preparation and before each analysis.

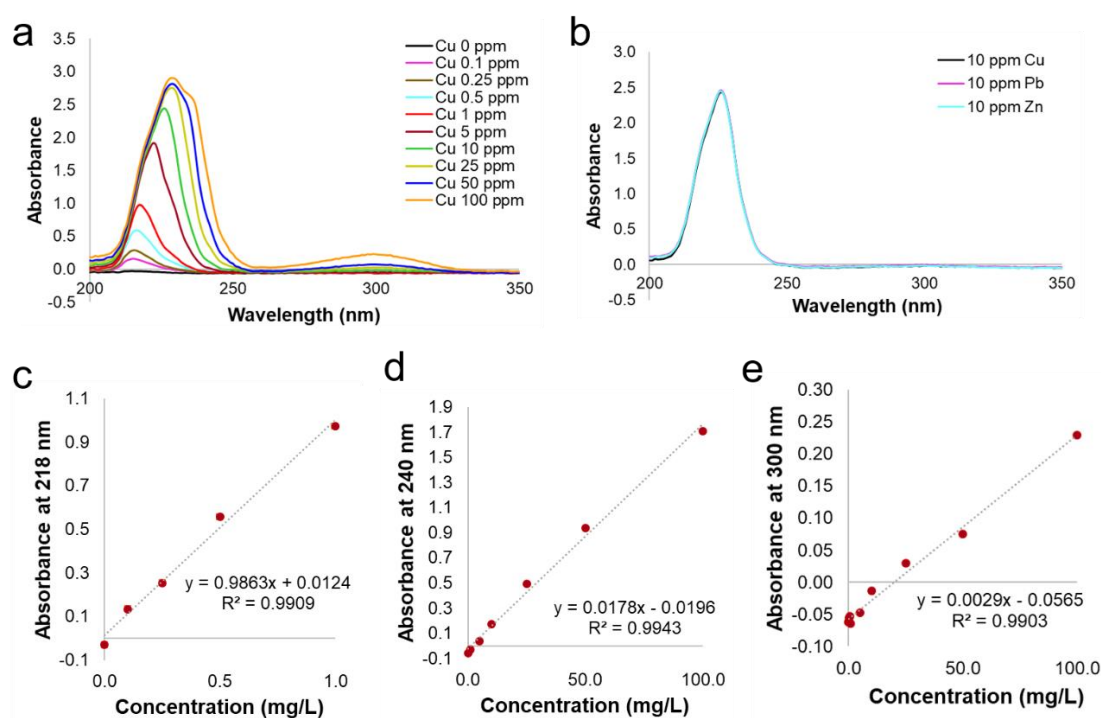


Figure 5.23 Absorbance spectra for Cu water solutions (0-100 mg/L) (a) and comparison between 10 ppm between Cu, Zn and Pb. Linear correlation at 218 nm for low Cu concentrations (0-1 mg/L) (c) and at 240 (d) and 300 nm (e) for high concentrations of Cu (1-100 mg/L)

5.4.2 L-CyChRu based coating and Cu ions

This subsection aims to evaluate the feasibility of an integrated method using microwave spectroscopy and impedance measurements using Ag-IDE and planar microwave sensors that are functionalised with thick films based on L-CyChRu (65 μm) for detecting Cu ions in laboratory-prepared water samples with higher specificity and resolutions than uncoated sensors.

5.4.2.1 Analysis, results and discussion

Copper solutions at various concentrations (0, 0.1, 0.25, 0.5, 1, 10, 25 and 50 mg/L) were prepared and tested in the laboratory using microwave and impedance measurements for evaluating the feasibility to detect changes in Cu concentrations using coatings based on chelating polymers and ruthenium oxide. Recapping from the chapter that describes the adopted methodology (Chapter 4), capacitance of Cu samples was measured using an LCR programmable bridge (Hameg 8118) and Ag-IDE screen-printed on microscope slides, covered with L-CyChRu based coatings (30 Hz–20 kHz, 400 μ L sample volume), using the “Crocodile clips” (Figures 5.23a and b). The S_{11} responses were measured using a Vector Network Analyser (Rohde & Schwarz VNA 24, (10 MHz-8 GHz) and f-EM sensors based on L-CyChRu using a small sample volume onto the sensor (Figures 5.24c and d). Both experiments require 400 μ L sample volume, placed onto the sensor using a micropipette and a specific holder. The interaction between the coating and the Cu samples was initially evaluated by time measurements at selected frequencies, with both techniques which permit a continuous measurement to monitor real-time interaction, combined with SEM and EDS analyses.

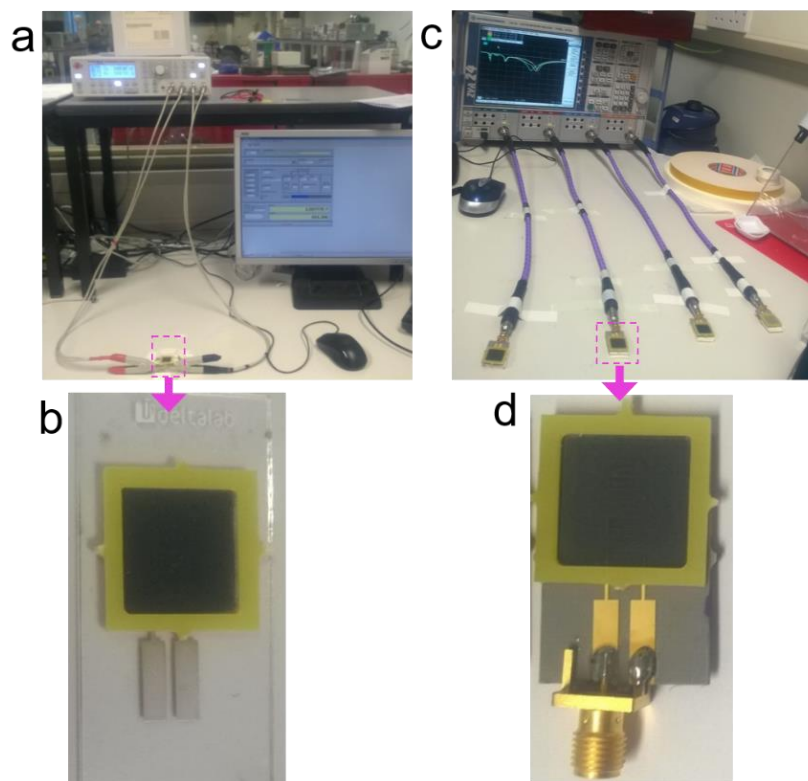


Figure 5.24 Set-up of the impedance and microwave measurements using L-CyChRu based coatings using respectively an LCR programmable bridge connected to a coated Ag-IDE screen-printed on microscope slide (a) (magnified in b) connected through crocodile clips and a ZVA 24 connected with coaxial cables to uncoated and f-EM sensors (c) (magnified in d) (Frau et al, 2018c)

5.4.2.1.1 Impedance responses

Impedance measurements performed with the coated Ag-IDE connected through “crocodile clips” to an LCR bridge were able to differentiate between Cu water solutions at low (0-5mg/L) and high concentrations (>5 mg/L), covering the dynamic range of pollution normally found in mining-impacted freshwater. Their pH and EC are illustrated in Table 5.5.

Table 5.5 pH and EC of the prepared and analysed Cu solutions

Cu solutions (mg/L)	pH	EC (mS/cm)
0	7.40	0.0016
0.1	5.68	0.0164
0.25	4.83	0.3753
0.5	4.23	0.0732
1	3.81	0.188
5	3.01	0.496
10	2.65	1.6
50	1.99	6.53

The C spectral response for all the measured Cu samples (0, 0.1, 0.25, 5, 10, 15 and 50 mg/L) is illustrated in Figure 5.25a, and the spectra for low Cu concentrations (0, 0.1, 0.25, 0.5, 1 and 5 mg/L) (in Figure 5.25b).

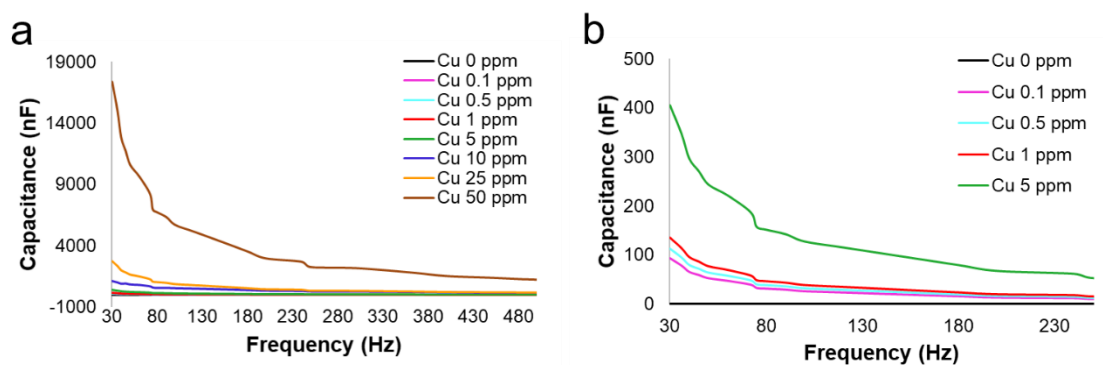


Figure 5.25 Capacitance spectra of Cu solutions (0-50 mg/L) between 30 and 500 Hz (a) and their magnification for low Cu concentrations (0-5 mg/L) at 30-250 Hz (b) using an Ag-IDE covered with an L-CyChRu based coatings

Initial time measurements of C at 150 Hz, demonstrate that the interaction between L-CyChRu coatings takes place during the first 10 minutes, reaching stability after 10-12 minutes. The measured capacitance using the coated Ag IDEs also has a high linear correlation with Cu solutions at diverse concentrations ($R^2 > 0.99$), as illustrated in Figure 5.26a by time at 30, 300 and 600 sec. Figure 5.26b shows the linear correlation curves for low concentrations of Cu samples (0-5 mg/L). Although, the sensitivity for Cu solutions considering all the concentrations analysed is higher ($\sim \Delta 76$ nF) if compared with the curve only for low Cu concentrations ($\sim \Delta 19$ nF), it is notable that with both graphs the sensitivity decreases with time. These results are an indication that the change in capacitance and EC which corresponds to the variation of Cu concentration, can reflect the variation in complex permittivity and consequently can alter the S_{11} responses at higher frequencies. Moreover, as it was described in the previous results sections, the microwave response at higher frequencies (> 100 MHz) is more specific if compared with C at lower frequencies (< 200 kHz). The microwave spectrum at high frequencies is a combination of peaks at specific frequencies (Korostynska et al, 2014a). Conversely, the

C at low frequency appears as a spectrum with a “flat” profile. This is probably because at high frequency, the EM waves have a shorter wavelength compared with low frequency which has a higher wavelength. Consequently, microwaves have the possibility to generate specific peaks in a small dynamic frequency range due to the small wavelength (cm).

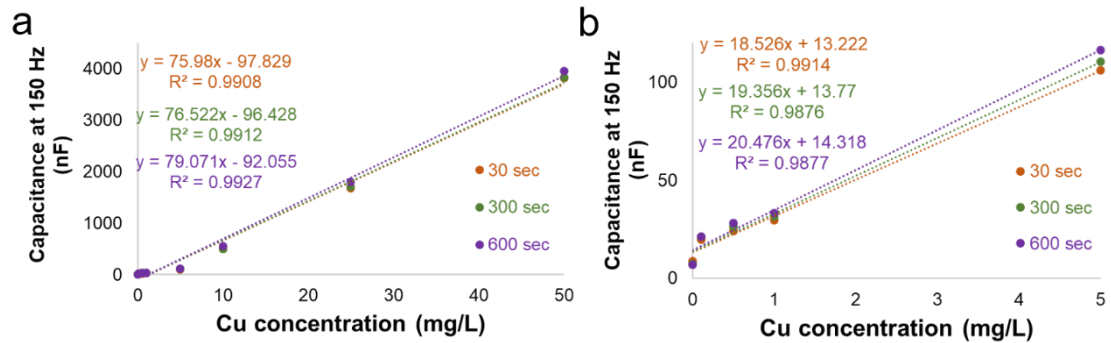


Figure 5.26 Linear correlations for C and Cu concentrations (0-50 mg/L) by time (at 30, 300 and 600 seconds) and the focus on low concentrations, 0-5 mg/L (b), at 150 Hz

5.4.2.1.2 Microwave responses

The same coatings that were screen-printed onto planar Au 8-pair IDE sensors were analysed then with the same Cu solutions. During the measurements, significant resonant peak shifts were noticed as the different concentrations of Cu samples were placed in contact with the sensor pattern, performing time measurements by extracting the data from continuous measurements every 30 seconds. The S_{11} spectral responses at 600 sec (10 min) for Cu solutions from 10 MHz to 8 GHz using uncoated and f-EM sensors based on L-CyChRu coatings are respectively illustrated in Figure 5.27a and b. A general shift toward higher frequencies with the f-EM sensor ($\Delta f_{L-CyChRu + Cu} = 100$ MHz) is notable.

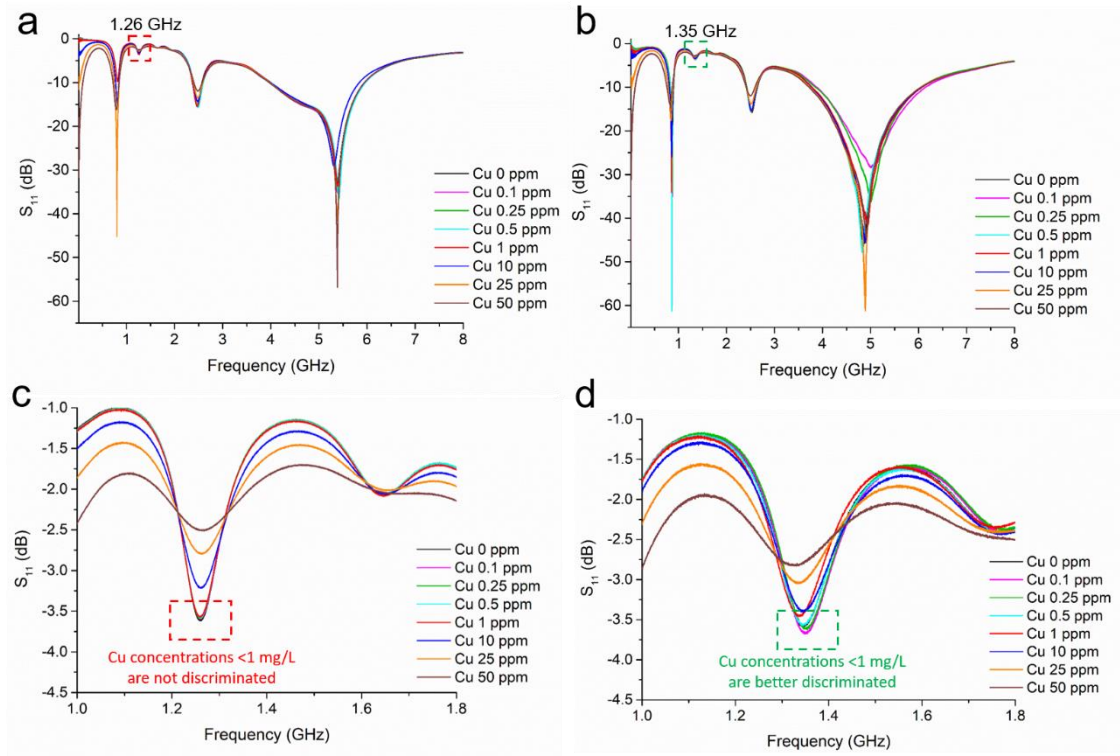


Figure 5.27 S_{11} responses between 0.01 and 8 GHz of Cu solutions (0-50 mg/L) using uncoated (a) and f-EM sensors based on L-CyChRu coatings (b), and the magnification of the peak produced respectively at 1.26 GHz and 1.37 GHz. The f-EM sensor is able to separate better low Cu concentrations (< 1 mg/L)

The effect of the L-CyChRu based thick film has been compared with uncoated sensors and showed significant differences. In the literature (Sharafadinzadeh et al, 2020), shifts toward lower frequency are determined by an increase of ϵ_r . Accordingly, it is considered that the shift toward higher frequency is determined by an increase in the dielectric constant.

The f-EM sensor enhances the sensing performance. Particularly, the peak located at 1.26 GHz with the uncoated sensor (Figure 5.27c), which shifts to 1.35 GHz with the f-EM sensor (Figure 5.27c) (which were highlighted respectively in red and green in Figures 5.27a and b) due to the coating effect presented a higher specificity for Cu concentrations < 1 mg/L. The f-EM sensor based on chelating polymers was able to detect and distinguish smaller changes of Cu concentration < 1 mg/L at 1.35 GHz with a higher linear

correlation ($R^2=0.98$) compared with the uncoated sensor ($R^2=0.94$), as illustrated in Figure 5.28a and b, by time at 30, 300 and 600 sec.

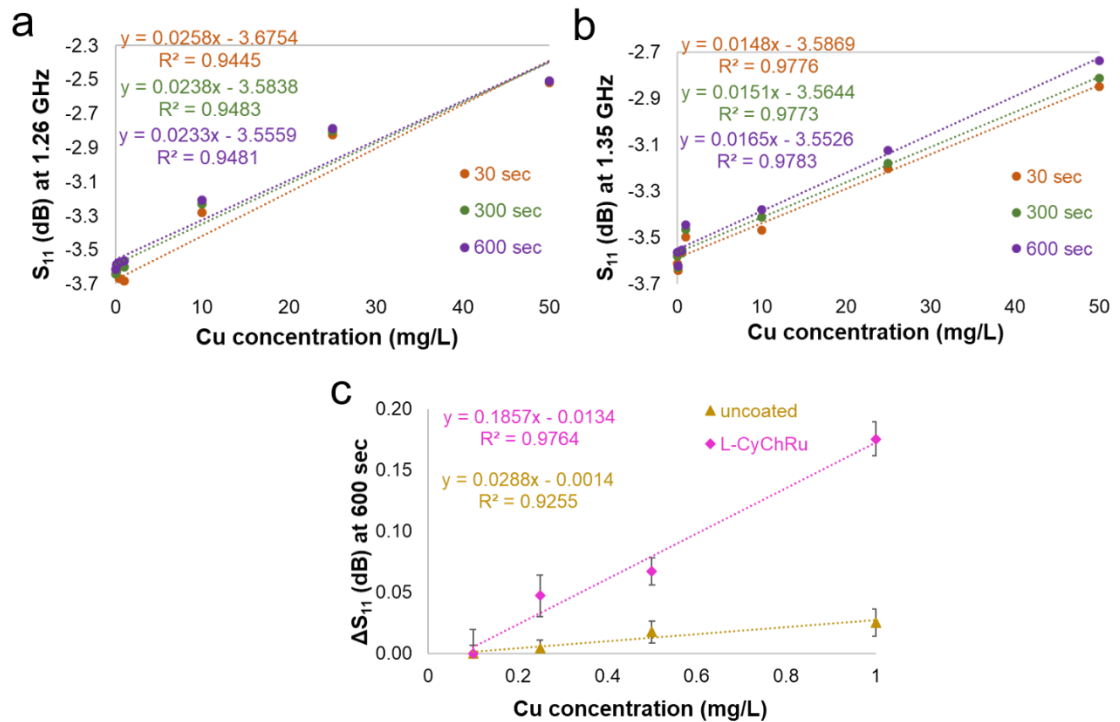


Figure 5.28 correlations by time (30, 300 and 600 sec) for the peak at 1.26 GHz using uncoated sensors (a) and at 1.35 GHz using the f-EM sensors with L-CyChRu (b). Slope, hence sensitivity comparison for Cu at low concentration (0-1 mg/L) at 600 sec (c)

Also, an increment in sensitivity for Cu concentrations < 1 mg/L, with a ΔS_{11} for every 100 μ L of 0.018 dB compared with 0.003 dB measured with the uncoated sensors, is noted. As is well known, the equations of straight lines, are in the form $y = mx + c$, where m represents the slope and c is the y-intercept. A higher slope represents a higher sensitivity. The dielectric changes are probably associated with the chelation of Cu ions on the coating and the interaction with the EM field, and it is dependent on both thickness and material properties, such as the dielectric constant and conductivity of each material which constitutes the coating, the permittivity variation of the water sample depending on the concentration, and the permittivity variation of the coating itself due to the chelation with the Cu in the water sample (Bernou et al, 2000). Consequently, the specific response at selected frequencies is given by a combination of these factors.

5.4.2.1.3 Summary of optical, impedance and microwave measurements

Summary of statistical features for Cu samples and L-CyChRu based coatings integrated onto planar IDE sensors are summarised in Table 5.6 where R^2 , CV% and sensitivity are compared for absorbance (at 217 nm), capacitance (at 150 Hz) and S_{11} measured using both uncoated (at 1.26 GHz) and f-EM sensors (at 1.35 GHz). Measurements were highly repeatable and reproducible, resulting in a CV % < 3% for all measurements.

Part of the results discussed above have been published by Frau et al (2018c).

Table 5.6 Linear correlation (R^2), CV in % and sensitivity for Cu samples (0-1 mg/L) using optical, electrical and microwave methods combined with f-EM sensors.

Measured parameter	R^2	CV %	Sensitivity ^a
Absorbance (at 217 nm)	0.98	1-2 %	0.10
C using Ag-IDE with L-CyChRu coatings (at 150 Hz) ^b	0.99	1-3%	7.91 nF
S_{11} using uncoated sensors (at 1.26 GHz) ^b	0.95	1-3%	0.003 dB
S_{11} using f-EM sensors with L-CyChRu coatings (at 1.35 GHz) ^b	0.98	2-3%	0.019 dB

^a for every 100 $\mu\text{g/L}$ change in Cu calculated for the range 0-1 mg/L; ^b at 600 sec;

5.4.3 L-CyChBCZ based coatings and Cu ions

A similar f-EM sensor was developed and tested with Cu solutions. The L-CyChBCZ based coating is formed by the two chelating polymers (l-cysteine and chitosan) and bismuth cobalt zinc (BCZ) oxide in a proportion of 4:4:1. In the L-CyChBCZ coating, the ruthenium (IV) oxide was substituted with another metal oxide, a conductive material, as a mixture of BCZ oxide ($(\text{Bi}_2\text{O}_3)_{0.07}(\text{CoO})_{0.03}(\text{ZnO})_{0.90}$) in nanopowder form ($\Phi < 100$ nm). BCZ oxide is a more conductive metal oxide if compared with the ruthenium oxide, which is a resistive oxide and is largely used for pH changes measurements in various sensing technologies (Manjakkal et al, 2016). Metal oxides have reactive sites and are able to adsorb toxic metals, their high surface area is dependent on their particles: the smaller the particle size, the higher their surface area.

This section aims to evaluate the feasibility of using f-EM sensors based on an L-CyChBCZ for Cu ions in water samples and compare the response with the previously described L-CyChRu coating.

5.4.3.1 Analysis, results and discussion

The f-EM sensor based on L-CyChBCZ coating was used for measuring Cu solutions by time using microwave measurements. This specific f-EM sensor will be described in more detail in the next chapter, where it was investigated to evaluate the feasibility of performing *in situ* measurements by applying some adaptation. Specifically:

1. The immersion of f-EM sensors directly in water for *in situ* measurements was investigated for the first time;
2. F-EM sensors based on L-CyChBCZ were tested for the first time with collected mining-impacted water samples applying the SAM for evaluating the feasibility to detect continuous changes of metal content (Cu and Zn) in collected mining-impacted water samples;
3. Spectral responses were analysed applying curve fitting functions for performing multi-peak analysis and multi-peak parameters characterisations (such as x_c , H , w , A).

5.4.3.1.1 Microwave responses

The f-EM sensor based on L-CyChBCZ oxide was able to differentiate Cu concentrations (0, 0.1, 0.25, 0.5, 1, 5, 10, 25 mg/L) in water samples. The reflection coefficient S_{11} measured using f-EM sensors based on L-CyCh-BCZ for Cu samples by time (at 1, 5 and 10 minutes) is illustrated in Figure 5.29a. The change in spectral response in the frequency range 1-3 GHz is ascribed to the interaction of the Cu ions with the coating material based

on polymers which chelate with this metal. Two resonant peaks were able to distinguish Cu ions at various concentrations (0-25 mg/L) (highlighted with a dashed square in Figure 5.29a), namely 1.4-1.5 GHz and 2.3 GHz: S_{11} and Cu content are related with a linear correlation (Figure 5.29b). The interaction between Cu and the coating produces a shift in both amplitude and frequency at the peak identified at 1.4-1.5 GHz. Considering all the analysed concentrations, a higher sensitivity was identified for the resonant peak identified at 2.3 GHz ($\Delta 0.05$ dB for every mg/L) if compared with the one produced at 1.4-1.5 GHz (0.03 dB for every mg/L). Although, the $R^2=0.94$ is slightly smaller compared to the one measured at the peak at 2.3 GHz ($R^2=0.98$), the peak identified at 1.4-1.5 GHz was able to differentiate better the Cu concentration between 0 and 1 mg/L. Specifically, if only these concentrations are considered, the sensitivity enhances to $\Delta 0.19$ dB for every mg/L, much higher than the one measured with the uncoated sensors, namely $\Delta 0.03$ dB for every mg/L.

The comparison between the spectral response measured with this coating and the previously described L-CyChRu in Figure 5.27b, indicate that the spectral response change by substituting the metal oxide as part of the coating materials (BCZ with ruthenium oxide). It is similar, but produced peak shifts to a different frequency (e.g 1.4-1.5 GHz measured with the L-CyChBCZ coating versus at 1.35 GHz measured with the L-CyChRu coating). Also, the peak located at about 800 MHz is much different from the peak produced with the L-CyChRu, with a very high reflection coefficient for 0.5 mg/L Cu (-60 dB, Figure 5.27b). Although, the improvement in sensitivity is very similar for Cu concentrations 0-1 mg/L, with about $\Delta 19$ dB for every mg/L, as was shown in Figures 5.28c and 5.29c.

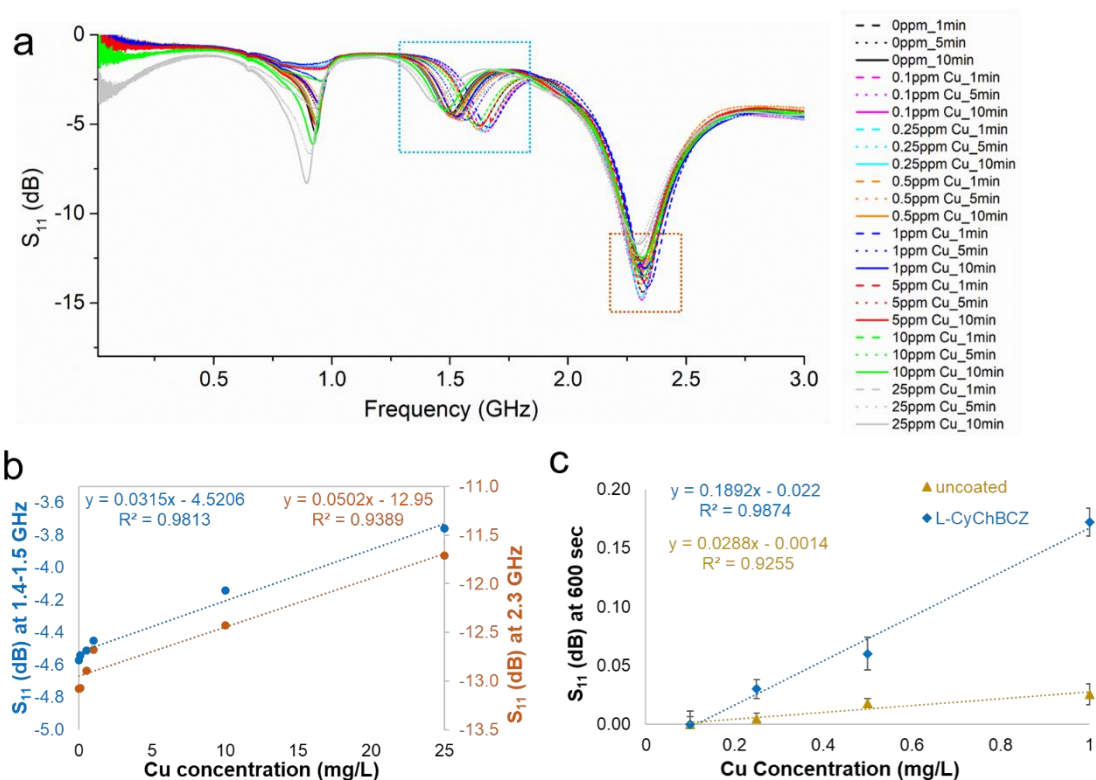


Figure 5.29 Spectral response for Cu solutions using f-EM sensor based on L-CyChBCZ extracted at 1 (dash lines), 5 (dot lines) and 10 minutes (solid lines) (a), where the highlighted areas show the best linear correlations at 1.4-1.5 GHz and 2.3 GHz (b), with an improvement in sensitivity ($\Delta 0.19\text{dB}$ for every mg/L) compared with uncoated sensors ($\Delta 0.03\text{dB}$ for every mg/L) (c) for Cu concentrations 0-1 mg/L .

Summarising, both f-EM sensors based on L-CyChRu and L-CyChBCZ based coatings were able to generate a more specific response for Cu ions at low concentrations (0-1 mg/L) and possibly to identify variations in Cu concentration in mining-impacted water. The next chapter will describe more results that were obtained by applying novel strategies for confirming this prospect.

Part of the results discussed above have been published by Frau et al (2018b).

5.4.4 Interaction of Cu with coatings based on chelating polymers

The previous two sections communicate the experimental results of using functionalised planar type microwave sensors based on chelating-polymers with metal oxide films, namely ruthenium oxide (L-CyChRu) and bismuth-cobalt-zinc oxide (L-CyChBCZ), for the real-time detection of Cu in water samples. Both f-EM sensors were able to better

detect lower Cu concentration (0-1 mg/L) than using uncoated sensors at selected frequencies of the EM spectrum (1.35-1.5 GHz), with a sensitivity improved more than 6 times higher than bare sensors. The improvement in the sensing response is given by the physical or chemical interaction between the screen-printed coatings (Chen et al, 2012). This generates a variation in electrical properties, such as capacitance and resistance, with a consequent change in the S_{11} spectral response. These changes enhance selectivity and sensitivity toward a specific target analyte enabling analytical detection and identification, due to the integration of an intermediary material which generates dielectric variations (Tanguy et al, 2020b). Very recently, the novel approach adopted and described in this dissertation was exploited by Boruah et al (2020), which functionalised six-pair Cu IDE sensors on FR4 substrates dip-coated with chitosan and glutathione for Pb ions detection at higher frequencies (9-15 GHz). They confirm the successful adaptation of this novel approach, obtaining an improvement in sensitivity and selectivity, due to the interaction between the coating material and Pb ions.

F-EM sensors based on L-CyChRu and L-CyChBCZ coatings were able to detect variations in Cu concentrations. The interaction between the chelating polymers and the metal ion under test started within 30 seconds and reach stability after approximately 10-12 minutes (600-720 sec). This was demonstrated with both coatings which presented very similar interaction and stability time, which was ascribed to the chelation with the l-cysteine and chitosan. The presence of Cu was identified on the coating using the EDS and SEM analysis, resulting in 0.6 weight % after long time measurements of 10 ppm of Cu solution using microwave spectroscopy.

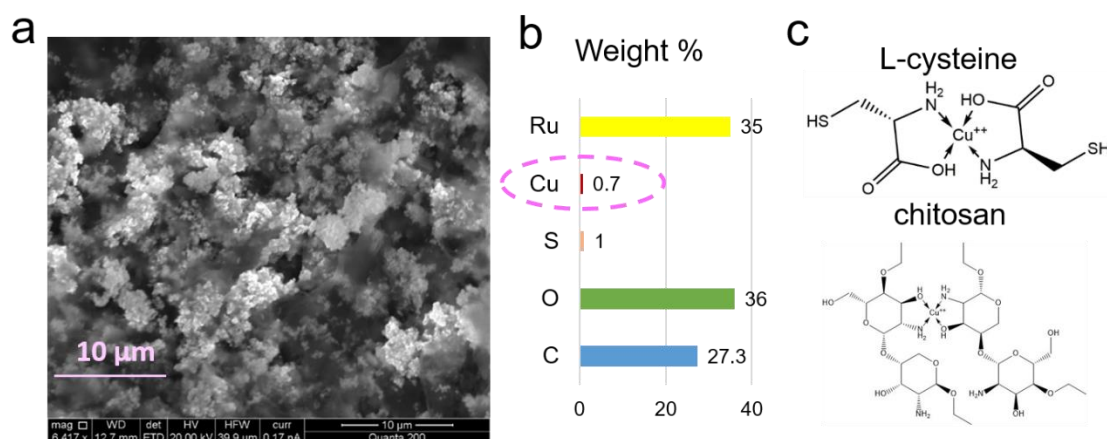


Figure 5.30 SEM image of the L-CyChRu coating (a) and its elemental composition after the interaction with Cu samples (b) and scheme of the probable chelation between Cu ions and chelating polymers (c)

Although, the available material characterisation equipment, such as the SEM and EDS, were not able to quantify low concentrations of metal in the material, due to its inadequate detection limit. Consequently, it was not possible to perform specific analyses for evaluating the percentage of Cu after interaction comparing the diverse low Cu concentration by time. More analysis using specific equipment (e.g. XPS) will be required before the mass production of the f-EM sensors based on chelating polymers mixtures.

5.4.4.1 Durability and degradability

F-EM sensors were durable and reusable. Once the readings were taken for a certain Cu concentration placed onto the f-EM sensors, they were then washed with DW and dried. The reading for “air response” and DW is again re-measured and corresponds to the same initial reading signal for both S11 and C responses. Although, the main difference between the L-CyChRu and L-CyChBCZ coating was the durability and degradability time for continuous measurements, the L-CyChRu coating had lower durability compared with the L-CyChBCZ coating. Figure 5.31 illustrates the comparison between some L-CyChRu and L-CyChBCZ coatings after 1, 24 and 72 hours, respectively shown in a, b and c and d, e and f. It is visible how the L-CyChRu starts its deterioration within 24 h.

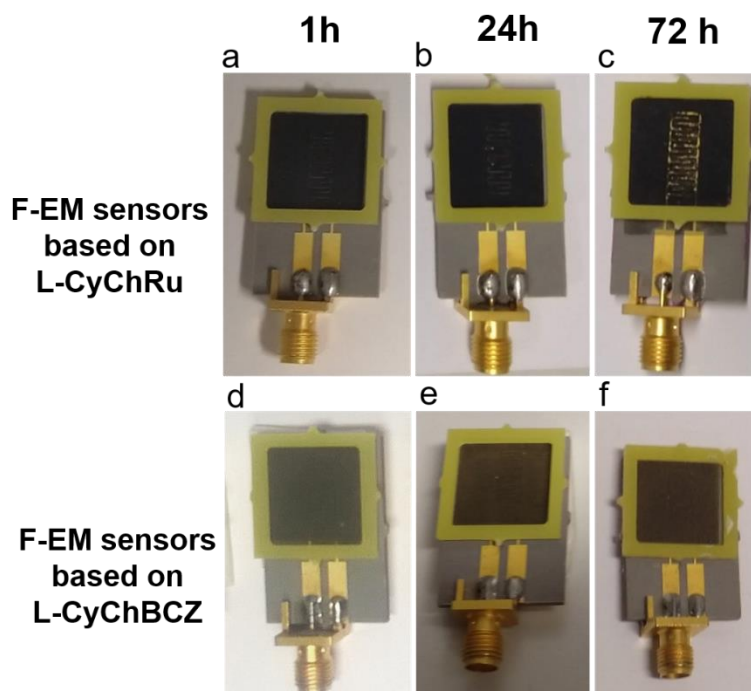


Figure 5.31 Visual comparison of durability between f-EM sensors based L-CyChRu and L-CyChBCZ, respectively after 1 h (a vs d), 24 h (b vs e) and 72 h (c and f)

The coatings based on the ruthenium oxide (as metal oxide mixed with the chelating polymers) were more degradable than the coatings based on the bismuth-cobalt-zinc oxide nanopowder (<100 nm particle size). This was probably due to the dissolubility of the ruthenium in contact with the water solutions. Moreover, it is notable as the material was mostly removed from above the IDE electrodes. Another reason could be the bigger dimension of the particles of the RuO_2 (powder and chunks), which cannot go between the IDEs (35 μm thick). Instead, nanomaterials can mix better with the other coating materials, in addition to their higher surface area (Tanguy et al, 2020b). The f-EM sensors based on L-CyChRu can be used for detecting in real-time Cu concentration in water, but they are not adaptable for long-time continuous *in situ* monitoring. Accordingly, the f-EM sensors based on L-CyChBCZ, which exhibited higher durability and lower degradability, were selected for the *in situ* measurements. Results of these experimental works are fully described in Chapter 6.

5.5 Metal oxides based coatings

The f-EM sensors that were based on metal oxide nanopowder (ITO and M10), generate a similar response to the β -Bi₂O₃ sensors, due to both material and particle size. For avoiding repetitions, and considering the evolution of strategy that is developed from the following chapter, and the insufficient improvement of selectivity, the f-EM sensors based in ITO and M10 will be described directly in Chapter 7 using the method of immersing the f-EM sensors directly in water and performing *in situ* analysis in mining-impacted water.

5.6 Summary of the main findings

5.6.1 Lacquered sensors and Pb ions

Summarising, the findings obtained using the lacquered IDE sensors compared with a resonant cavity and uncoated IDEs for detecting Pb ions are:

- The uncoated sensors present higher performance for measuring Pb concentrations (0-100 mg/L).
- These sensors are not sensitive enough to distinguish low concentrations of Pb ions, meeting the EQS.
- Lacquered sensors are advantageous for continuous monitoring, as the metal pattern is not oxidised with continuous monitoring.
- Lacquered sensors produce a modified spectrum due to the change in permittivity of the sensing system.
- Acidified water samples (1%) generate a lower sensitivity for the measurements and are not practical for *in situ* monitoring, as sample preparation is required.

5.6.2 β -Bi₂O₃ based coatings and Zn ions

The main findings obtained using functionalised sensors based on screen-printed β -Bi₂O₃ based coating for Zn detection are:

- Absorbance, impedance and the microwave sensor responses were dependent on the presence and concentration of Zn in water with $R^2=0.93-0.99$ at specific wavelengths/frequencies.
- The action of using novel F-EM sensors with β -Bi₂O₃ based coatings for analysing Zn in water was confirmed.
- The functionalised sensor with a 60 μm thick β -Bi₂O₃ based film offers improved sensitivity, compared with both the uncoated and the functionalised sensors with 40 μm thick coating, for detecting the changes of Zn concentrations in water for low pollution levels (100 and 500 $\mu\text{g/L}$).
- The time response and adsorption time between Zn ions and the sensing layer was estimated as 10 minutes.
- F-EM sensors are reusable as the recovery time was estimated to be 100-150 seconds.
- This novel sensing system could be a cost-effective and practical alternative to the current offline monitoring methods.

5.6.3 Chelating polymers based coatings and Cu detection

The main findings obtained using EM sensors based on chelating polymers (l-cysteine and chitosan) and metal oxides (ruthenium oxide and bismuth-cobalt-zinc-oxide, respectively named L-CyChRu and L-CyChBCZ) for detecting Cu ions are:

- Optical, impedance and microwave measurements were able to distinguish Cu concentration in water with a high linear correlation;

- The ability of the L-CyChRu and L-CyChBCZ coatings to detect Cu content change in water solutions was assessed;
- Both coatings were able to detect with higher sensitivity ($\Delta 19$ dB for each mg/L compared with $\Delta 0.03$ for each mg/L measured with uncoated sensors) and with higher specificity for Cu ions at lower concentrations (0-1 mg/L);
- The variation in the spectral response was associated with the overall permittivity changes of the sensing structure due to the interaction (possibly chelation) between Cu ions and the chelating polymers;
- The interaction between Cu ions and coating materials starts within 30 seconds and takes about 10-12 minutes to reach stability;
- L-CyChBCZ based coating has higher durability for continuous measurements compared with L-CyChRu based coatings;
- Consequently, the L-CyChBCZ was selected for researching novel strategies for performing *in situ* measurements;

5.7 Overall summary and implications

Microwave spectroscopy alone is not able to distinguish small changes in concentrations between similar compounds. A novel strategy for improving the performance of the EM sensors and obtaining a more specific spectral response is given by the integration of functional materials onto the sensing structure (Zarifi et al., 2018b, Chen et al., 2012). This is possible thanks to the chemical or physical interaction between the pollutant under test and the coating material, which determine a change in the overall electrical permittivity. In this chapter, the feasibility of using the novel developed f-EM sensors with screen-printed coatings based on various mixtures of materials for measuring variations in concentrations of Pb, Zn and Cu in water, was demonstrated. Also, specific

resonant peaks can be selected using a specific f-EM sensor depending on the analysis requirement for water quality control. For example, it was demonstrated that the response at frequencies around 1.3-1.7 GHz is more specific for metal concentrations <1 mg/L, conversely, a better response for higher concentrations (>1-100 mg/L) is determined at frequencies around 2.3-2.5 GHz.

These experiments and results added weight to the body of evidence supporting the notion that the integration of materials on microwave planar sensors is an attractive option for water quality analysis with minimal operational cost. Early this year, Boruah et al (2020) adopted the novel approach described in this thesis and published by Frau et al (2019a) for detecting Pb ions at low concentrations (1-80 ppb), using IDE sensors dip-coated with chitosan and glutathione. Also, Vélez et al (2019) compared the performance of various microwave sensors for solute concentration measurement in liquid solutions and described the β -Bi₂O₃ formulated in this work as the one that presented the highest sensitivity. Consequently, the novel f-EM sensors developed in this study are of global interest in the microwave research community, as they are showing important advances in facing the problem of improving sensitivity and selectivity.

Despite many recent technological advances and positive results obtained using this novel sensing system, significant work remains to be accomplished before a reliable smart sensor for water quality monitoring is achievable (Mohammadi et al, 2020a). Real mine water is more complex and characterised by high levels of dissolved metals and sulphate and, frequently, low pH. However, there are several challenges that must be overcome before this technology can ensure that measurements correctly identify distinct contaminants, despite their possible interference with each other. By analysing the response at each frequency using various f-EM sensors for different concentrations, metals, and water composition, it appears that this methodology could more accurately

characterize multi-contaminant concentrations. The following chapters are going to face other practical problems and assess the feasibility of integrating the f-EM sensors in the national monitoring system for efficiently monitoring water quality. Specifically, the next chapter describes some results analysing i) multi-element samples at low concentrations more commonly found in mining-impacted watercourses receiving mine drainage and natural dilution using the SAM and ii) adapting the f-EM sensors for direct *in situ* measurement of freshwater. Also, field trials and the combined response of using multiple f-EM sensors are described in Chapter 7.

Chapter 6 Results and discussion (phase 2): submerged f-EM sensors and mining-impacted waters

6.1 Introduction

The objective of this chapter (O2) was to research and develop f-EM sensors for directly probing more complex water samples to evaluate the feasibility of *in situ* monitoring; specifically:

- testing the adapted sensing system for *in situ* measurements (immersing the sensors in water) in the laboratory and comparing the response of various network analysers (VNAs) that are suitable for *in situ* measurements;
- testing more complex water samples, such as collected mining-impacted freshwater from polluted mining-impacted areas in the UK, which were processed with the standard addition method (SAM) for simulating a “continuous” increase in metal pollution in a collected sample.
- analysing multiple peaks and multiple peaks’ features to obtain a more detailed response.

Microwave sensors are considered good candidates for sensing devices, as they fulfil wholly the required features for continuous online monitoring (Zubiarrain-Laserna & Kruse, 2020): i) work without reference electrodes, ii) operate continuously, iii) are reagent-free and iv) have the potential to be programmed to run autonomously. Thus, the gold eight-pair IDE on PTFE substrate microwave sensor was selected for more experimental work and to demonstrate the aptitude to qualify and quantify *in situ* metal pollution in freshwater and guarantee an emergency response for unexpected changes. The integration of functional layers is a novel strategy for improving the sensing performance, although this is still at the proof of concept stage, with progressive work needed, especially for real-world applications. The successful results described in the previous chapter (Chapter 5) using mostly f-EM sensors based on β -Bi₂O₃ and chelating

polymers and metal oxides (L-CyChRu and L-CyChBCZ), were designed for small sample volumes (400 μL) placed onto the sensors. These f-EM sensors using the measurement configuration with a small sample volume onto the sensor are not practical for guaranteeing direct *in situ* field measurements, but they are very beneficial for i) quick and inexpensive laboratory analysis or ii) if just a small sample volume is available.

Consequently, in this chapter the feasibility to probe water samples directly for *in situ* monitoring of water quality is evaluated. Besides, mining-impacted waters are complex, as they are a “cocktail” of PTEs with a different dynamic depending on specific environmental conditions (e.g. flow variations) (Jarvis et al, 2019), or when in contact with materials deposited on the riverbed (Smith, 1999).

As previously noted, polluted samples were collected in four mining areas in the UK, which are briefly described in the next section.

6.1.1 Samples from mining-impacted freshwaters

In this and the following chapter, complex polluted samples are analysed, for evaluating the feasibility to use the f-EM sensors for continuous and *in situ* monitoring of the freshwater, considered as a complex chemical solution. As was described in the introduction chapter, mine waters are generally polluted by *dynamic* toxic metals. Microwave spectroscopy and f-EM sensors were considered a valuable alternative for efficiently monitoring toxic metals in water, although no researcher before this project has tested microwave sensors with mining-impacted waters.

In this work, polluted samples from mining areas were analysed for the first time using microwave spectroscopy and planar sensors. These mining-impacted areas were:

1. Wemyss Mine (Mid Wales, UK);
2. Parys Mountain mining district (Anglesey, North Wales, UK);

3. Nant y Mwyn Mine (Mid Wales, UK);
4. Leadhills Mine (Scotland, UK).

These mining areas were selected as test sites because they represent the typical toxic metal pollution range (very high, average and low) found in the UK. Specifically, Parys Mountain mining district represents an extremely polluted site, with Cu and Zn concentrations $> 20\text{mg/L}$; Wemyss and Nant y Mwyn Mines represent “averagely” polluted sites in the UK, with a Zn concentration ranging from 0.8 to 9 mg/L; and Leadhills mine is a low polluted site with metal concentrations just above the EQS, with 0.1 – 0.3 mg/L of Zn. Moreover, these sites were investigated during the same time period by other research projects granted by the Natural Environment Research Council, Natural Resources Wales and Scottish Environment Protection Agency in collaboration with the Faculty of Science at LJMU.

These are localised with yellow stars in the map (Figure 6.1) modified from the Environment Agency (2008), where non-coal and coal mines which can impact freshwater in England, Wales and Scotland are flagged respectively in blue and black. More than 465 water bodies in England and Wales are impacted by non-coal mines, which correspond to around 860 t of toxic metals released into water catchments every year (Environment Agency, 2012; Hudson et al, 2018). Initially, some freshwater samples from these areas were collected and tested in the laboratory using the sensors adapted for probing the water. *In situ* physicochemical parameters (pH, EC and T) were measured for each sample. Secondly, in the same sites, field measurements trials were performed *in situ* and continuously using the portable and practical miniVNA tiny. Results are shown respectively in this chapter (for some lab analysis) and in the next one (for *in situ* field trials).

A short overview of each polluted investigated mining site follows.

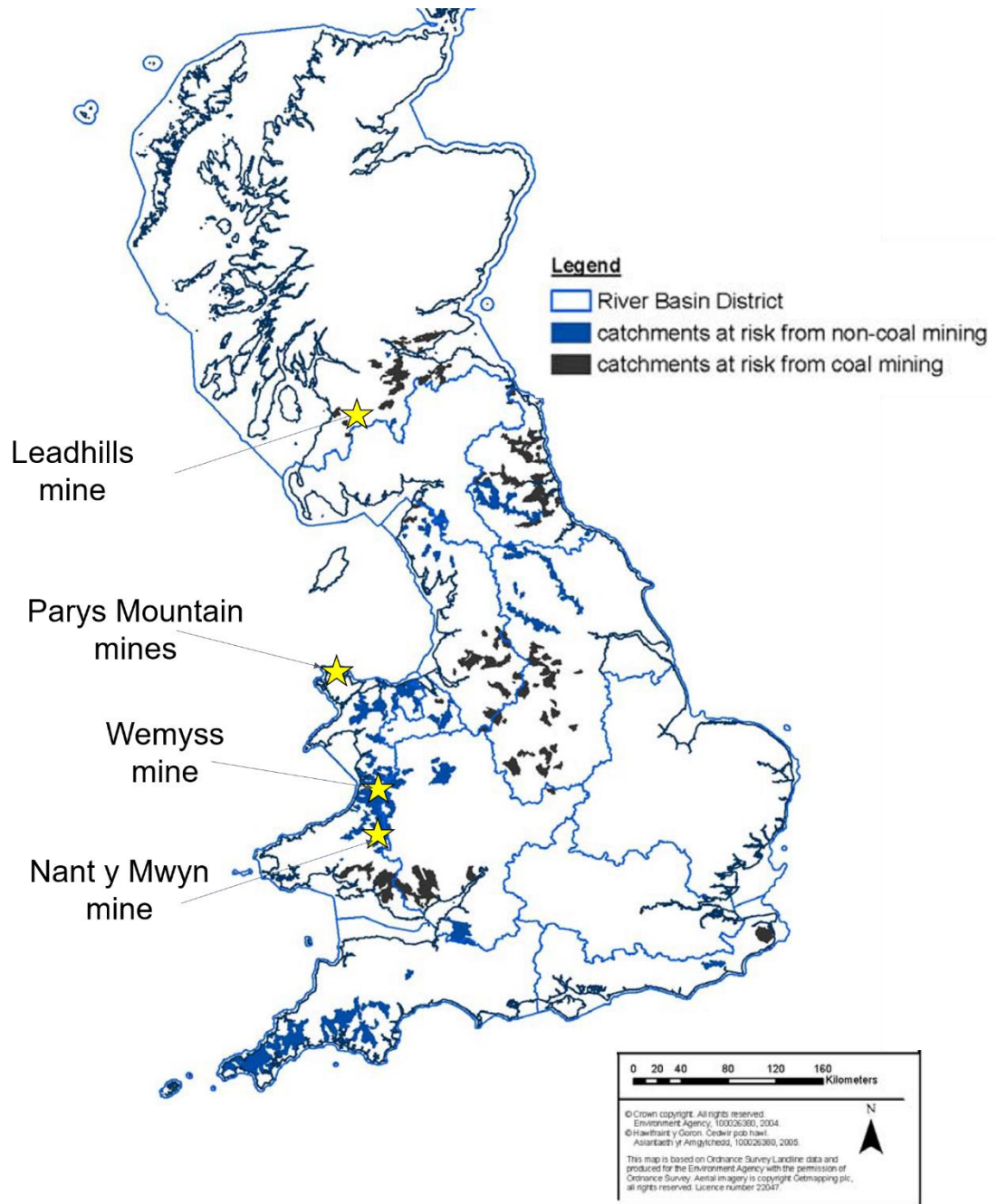


Figure 6.1 Adapted map from Environment Agency (2008) which shows catchments at risk from non-coal (in blue) and coal (in black) mines. The four mining areas, specifically Wemyss mine, Nant y Mwyn mine, Parys Mountain mine (Wales, UK) and Leadhills mine (Scotland, UK), from where mining-impacted freshwater samples were tested, are highlighted with yellow stars

6.1.1.1 Wemyss mine

Wemyss mine is located in Central Wales (UK). It was exploited for Zn and Pb until early 2000 and it is characterised by several point and diffuse sources, which contribute to the pollution of the Nant Cwmnewyddion (Figure 6.2a). One of the major point sources

polluting this stream is an adit drainage from Frongoch mine (named Frongoch adit) which emerges into this stream; diffuse sources are represented by waste heaps deposited along the stream, which differently impact the river in various weather conditions (Onnis et al, 2018). Toxic metal concentrations for Zn, Pb and Cd fail to meet the EQS established by the UK TAG of WFD. This site was classified as one of the most polluted and a priority site to remediate in the UK (Environment Agency Wales, 2002), and a clean-up feasibility contract was recently awarded to the Coal Authority (The Coal Authority, 2018).

In this area, a few freshwater samples were collected for testing the developed f-EM sensors, specifically: Frongoch Adit, Mill Race and Nant Cwmnewyddion (respective acronyms: FA, ML, and NC). Specific locations and photos can be found in Appendix 2a.

6.1.1.2 Parys Mountain mining district

Parys Mountain mining district is located in Anglesey (North Wales, UK) and is one of the most polluted mining districts in the UK with high production of AMD, due to the nature of the extracted metal sulphides (Boult et al, 1994). The Northern Afon Goch (Figure 6.2b) is the biggest contributor of Zn and Cu in the Irish Sea, in addition to Fe, Mn and Al with pH as low as 2-3. The Southern Afon Goch is 11 km long and receives drainage water from the Cu mine, which was active from the 18th century to 1911 (Dean et al, 2013). Recent studies have demonstrated a strong reduction of the contamination downstream in the Southern Afon Goch (Figure 6.2b) due to natural wetlands (Dean et al, 2013), which reduce the metal contamination and increase the pH. Natural wetlands promote naturally the reduction of contamination in water, as was demonstrated in other mining areas in Europe, such as Rio San Giorgio in Monteponi mine district (Sardinia, Italy) (De Giudici et al, 2017).

In this highly polluted area, a few samples were collected and analysed using microwave spectroscopy and f-EM sensors. Specifically, the Dyffryn Adda Adit (acronym: PM) and other two samples in the mining area (PM-1 and PM-2), and one after the wetlands (PM-w) were collected and analysed (Appendix 2b). Consequent *in situ* analyses were performed and results are described in the following chapter (Chapter 7).

6.1.1.3 Nant y Mwyn mine

Nant y Mwyn is a lead mine abandoned since 1932 and is located in Mid Wales, 10 km north of Llandovery (UK). The Nant y Bai (Figure 6.2c) is contaminated with toxic metals (Zn and Pb mostly) and fails to meet the EQS. Pollution assessment accomplished by Natural Resources Wales (2014) have evaluated run-off from spoil tips as major diffuse sources of metal load in the Nant y Bai, considering the discharge from the adit (Upper Boat Level) minimum.

Three samples were collected: two along the Nant y Bai stream (NYB-1 and NYB-2) and a right bank inflow, a run-off from tailings deposited on the riverside (NYB-R) (Appendix 2c). Also, in this mining-impacted stream, *in situ* and continuous measurements were performed using uncoated and f-EM sensors.

6.1.1.4 Leadhills mine

Leadhills (South Lanarkshire, Southern-Central Scotland) is considered the centre for lead mining in Scotland (The Coal Authority, 2011). In the area, Glengonnar Water fails to meet EQS for several metals, such as Cu, Pb and Zn; contrariwise, Wanlock Water (Figure 6.2d) was initially evaluated as in a “good status” under the WFD, but recent surveys have considered that several areas are affected by high levels of toxic metals in freshwater (Scottish Environment Protection Agency (SEPA), 2011).

In this polluted area, two samples, the Bay Mine adit (acronym: WW-A) and a sample downstream of Wanlock Water (WW-1) (Appendix 2d) were collected and analysed using microwave spectroscopy in the laboratory, and *in situ* trials were performed.

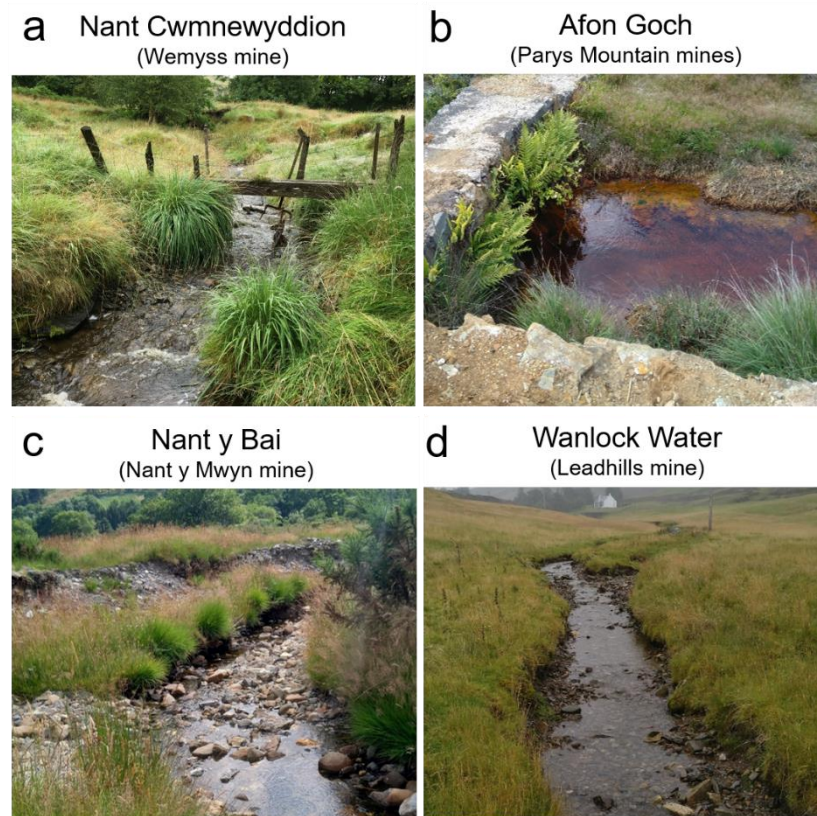


Figure 6.2 Example of polluted streams in the UK from where samples were collected and tested in the laboratory and *in situ* using microwave spectroscopy: Nant Cwmnewyddion (a), Afon Goch (b), Nant y Bai (c) (Wales) and Wanlock Water (d) (Scotland)

6.1.2 Chapter overview

This chapter describes the results for uncoated and f-EM sensors immersed directly in mining-impacted water, to which were applied the SAM for measuring continuous changes in metal concentration (Cu and Zn). Then, spectral responses were analysed using peak functions for multiple peak characterisation.

6.2 Summary of materials and methods

This section summarises the specific novel methodologies adopted in this chapter, which are schematised in Figure 6.3 and were fully described in Chapter 4. In this chapter are described results for uncoated and f-EM sensors based on L-CyChBCZ which were adapted for probing water samples (Figure 6.3-1), and measuring continuous real-time changes in Cu and Zn concentration in spiked-freshwater samples.

6.2.1 *Analysed samples and SAM*

Both laboratory-prepared and collected samples were analysed. Initially, simulated “unknown” samples with 3 (UNK3) and 0.2 (UNK0.2) mg/L of Cu and Zn respectively were prepared. Then, four polluted samples (FA, MR, NC, PM) from two mining-impacted areas in Mid (Wemyss mine) and North Wales (Parys Mountain) were collected and analysed. 40 mL of UNK3, UNK0.2 and FA were spiked with Cu and Zn using the SAM (Figure 6.3-2) by adding 1 mL of 100 mg/L Cu or Zn solution which corresponded to an increase of 1.25 mg/L in metal concentration. DW samples were also spiked likewise with Cu, Zn and Cu+Zn (1:1) solutions. Other samples (FA+0.2 mg/L of Cu and Zn) were prepared by dilution for measuring the decrease in concentration using the F-EM sensors.

6.2.2 *Measurements*

Reflection coefficient magnitude (S_{11}) was measured continuously using both ZNA 24 and the miniVNA tiny (0-3 GHz) (Figure 6.3-3); impedance measurements were measured using the LCR bridge (C and R, 30Hz – 20 kHz) and the miniVNA tiny (R, X, |Z|, 0-3 GHz). Coatings were characterised after the interaction of the sample using SEM and EDS analysis.

6.2.3 Data analysis

The S_{11} responses for sample and SAM were fitted with the Lorentzian peak fitting function and multiple peak analyses were performed (Figure 6.4-4). Once the resonant frequencies in the spectral response (between 0.01 and 3 GHz) were selected for Cu and Zn, a calibration curve was produced by using the S_{11} signal for the known quantities of the chemical of interest. R^2 , sensitivity, LOD and the Q-factor were analysed and compared for Cu and Zn concentrations using uncoated and coated sensors based on L-CyChBCZ (Figure 6.4-5).

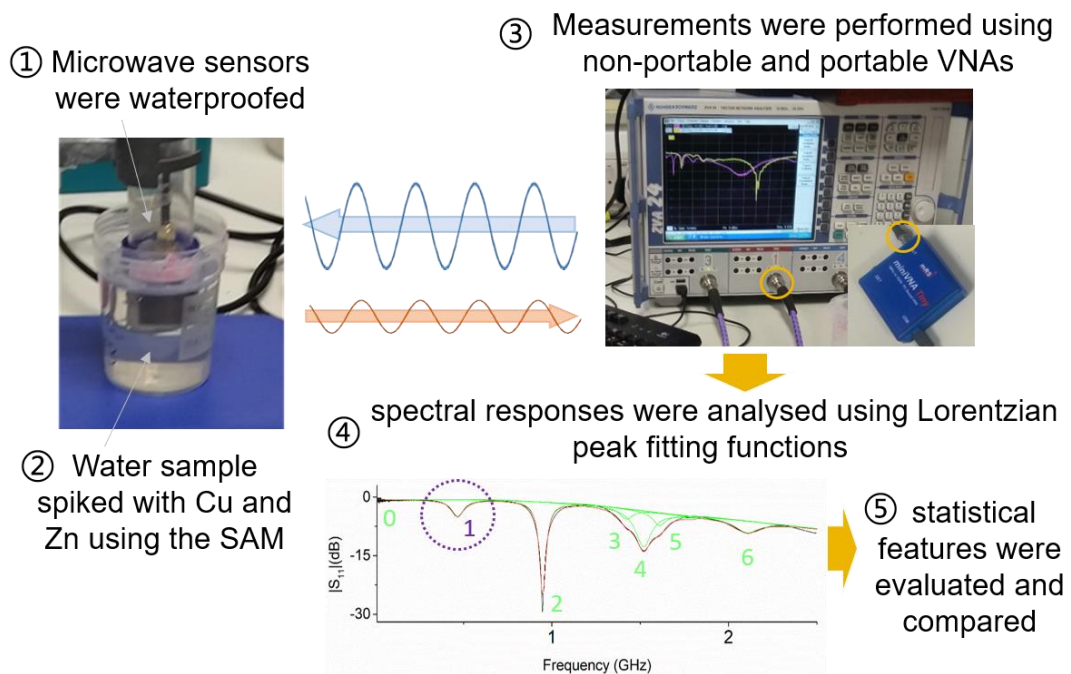


Figure 6.3 Schematisation of the approach used in this chapter: 1) sensors were adapting for directly probing the water; 2) water samples (lab-prepared and collected from impacted mining areas) were spiked with Cu and Zn solutions using the SAM; 3) measurements were performed using non-portable (ZVA 24) and portable VNAs (miniVNA tiny); 4) Spectral responses were characterised using Lorentzian peak function; 5) statistical featured were evaluated (such as R^2 , sensitivity, Q,) and compared between diverse samples

6.3 Results and discussion: submersible microwave sensors

6.3.1 400 μL method vs immersed sensors

Initial experiments demonstrated the feasibility of measuring water samples by dipping the waterproofed sensors in water samples. Figure 6.4 compares the signal response measured using the “400 μL ” method (dash line) and the submerged sensors into the water samples (solid line), using both uncoated and f-EM sensors based on L-CyChBCZ coatings. The signal response changes from using the 400 μL method described in the previous chapter, probably due to the propagation of the EM waves in a diverse volume. Similar experiments were later performed by Reyes-Vera et al (2019) for different liquids (acetone, propyl alcohol, methanol) by submerging planar sensors in the samples.

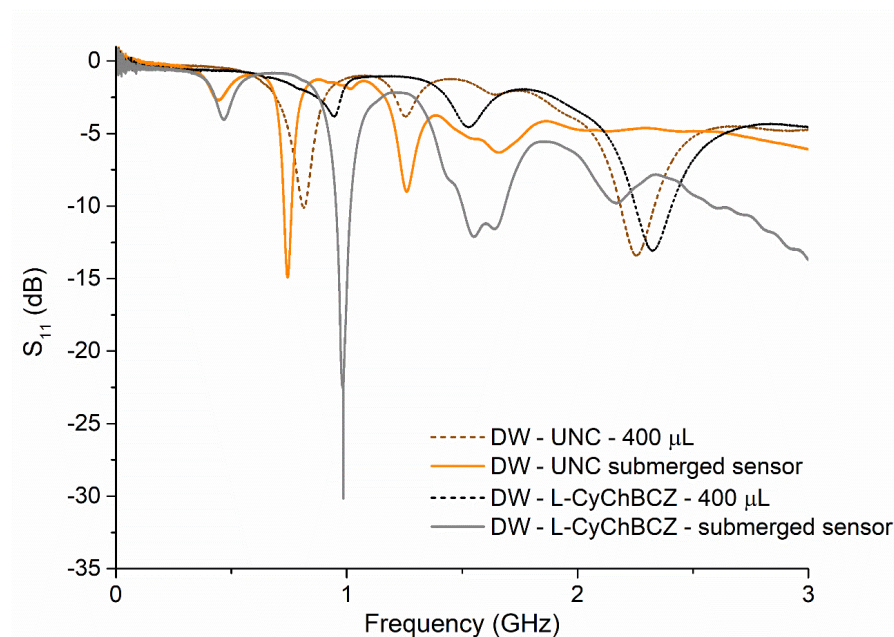


Figure 6.4 Comparison example of spectral response measured using the 400 mL sample volume onto the sensor or the submersible f-EM sensor using both uncoated and coated sensors with L-CyChBCZ based coating

6.3.2 Uncoated sensors and SAM

The uncoated sensors were immersed in the spiked-Cu and Zn samples and initially measured using the ZVA 24. The microwave response was able to determine changes of

the metal content, for both metals, with similar reflection coefficients at the same frequencies, due to the similarity of these metals. The spectral output between 0 and 2 GHz is illustrated in Figure 6.5a for the UNK3 Cu sample spiked with the Cu solution and in Figure 6.5b for UNK0.2 Zn sample spiked with the Zn solution. Three resonant peaks located at frequencies < 0.8 GHz were selected and are highlighted in both figures using dashed black lines at 0.01, 0.44 and 0.76 GHz.

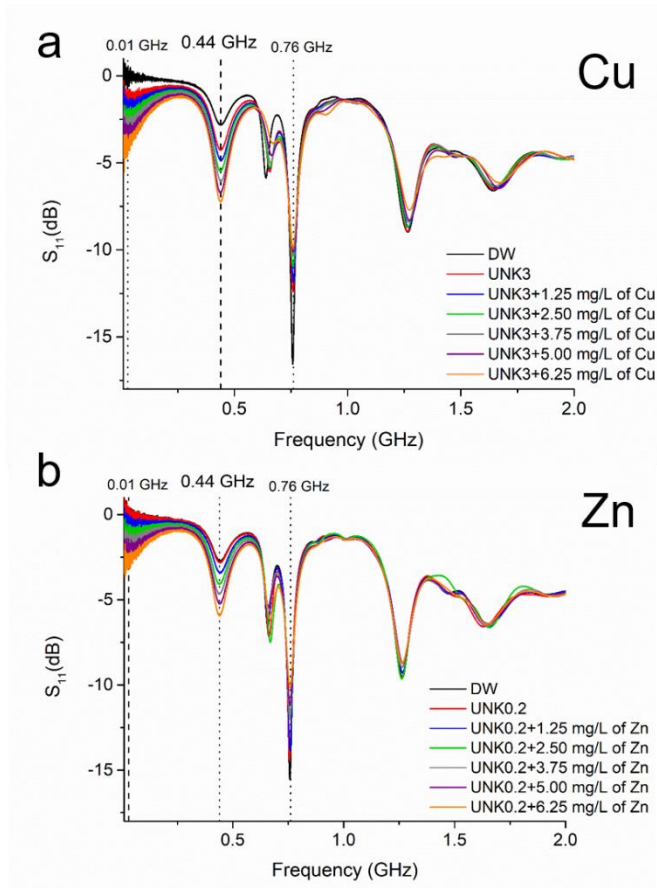


Figure 6.5 Spectral responses between 0.01 and 2 GHz for “unknown” Cu (UNK3 as 3 mg/L) solution and for “unknown” Zn (UNK0.2 as 0.2 mg/L) solutions (b) using uncoated sensors submerged in 40 mL of each water sample.

Between them, the peak located at 0.44 GHz (Figures 6.6a and b, respectively for Cu and Zn) was selected and used for quantifying the actual concentration of the samples. This peak was selected for its higher linear correlation ($R^2 > 0.99$), higher sensitivity (0.485 ± 0.003 dB for each 1 mg/L variation in Cu and Zn conc.), and low SD ($RSD < 1\%$) compared with the other two peaks. By plotting the linear correlation, the concentrations

of Cu and Zn were determined, confirming the fact that microwaves can measure the concentration of Cu and Zn continuously using the reflection coefficient, S_{11} . This value corresponds to the x-intercept of the linear correlation, resulting in 2.99 mg/L and 0.160 mg/L for UNK3 (Cu) and UNK0.2 (Zn) samples (Figure 6.6c and d respectively).

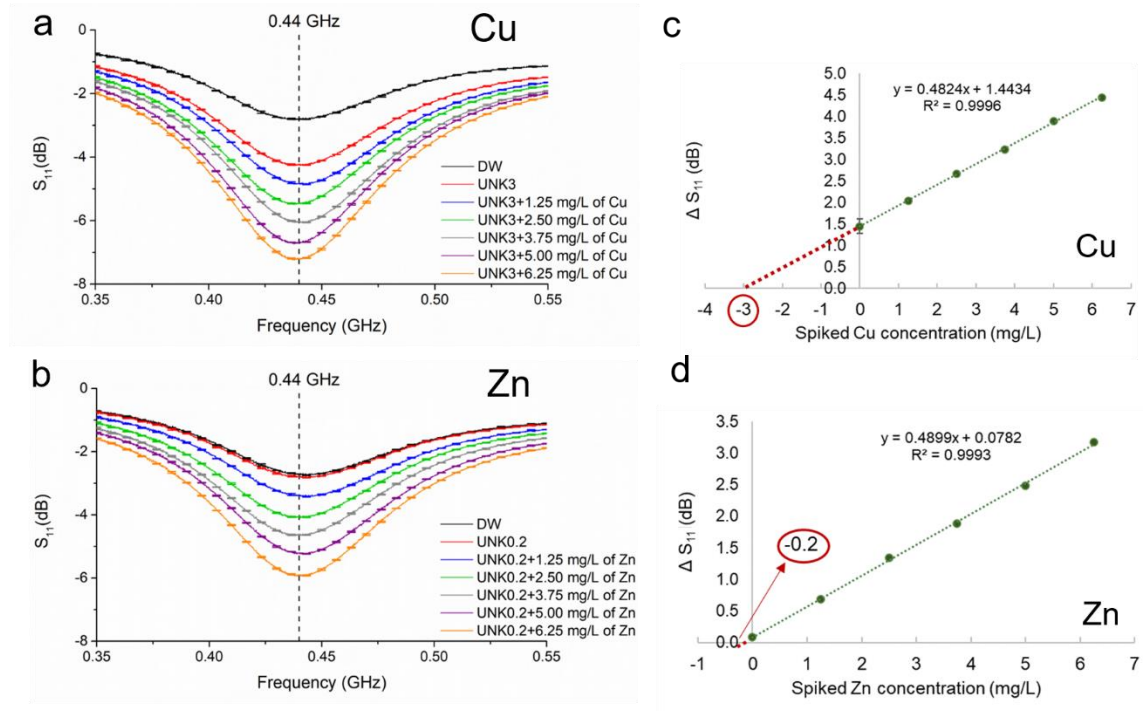


Figure 6.6 Magnification of the peak located at 440 MHz for the “unknown” Cu and Zn (UNK3 and UNK0.2) samples spiked with Cu and Zn solutions (highlighted in Figure 6.5 respectively in a and b); their calibration plots are shown in c and d respectively, where the effective concentration corresponds to the intercept of the curve.

Notably, the resonant peaks that were produced at frequencies < 0.5 GHz, have a lower dB as the metal concentration is increasing (the reflection decreases) compared to the peaks at frequencies > 0.5 GHz, where inversely a higher dB is noticed as the concentration increases (the reflection increases), both for linear and polynomial correlations. For instance, the peak located at 0.44 GHz is -4.2 dB for UNK3+1.25 mg/L of Cu and -7.2 dB for UNK3+6.25 mg/L; at 0.76 GHz the reflection coefficient is -11.9 dB for UNK3+1.25 mg/L of Cu and -9.8 dB for UNK3+6.25 mg/L.

This study demonstrates the feasibility of the microwave response to detect the increase of metal content in water and to quantify its change by probing directly the water sample

under test. However, this experiment demonstrates the necessity of finding a solution for improving the specificity, as sensitivity and selectivity for metal ions detection, considering that the calibration curve is almost identical, demonstrating the need to find novel strategies for improving the discrimination between similar pollutants, such as Cu and Zn. Although the concentration of these toxic metals was determined using a sensor submerged into water simulating the *in situ* monitoring, it is important to obtain a more selective response, considering that Zn and Cu have different toxicities in the environment.

The uncoated planar sensors used in this paper, specifically eight-pair gold IDE on PTFE substrates, can distinguish changes in the cell concentration of *Tetraselmis suecica* (Moejes et al, 2018) at 4 GHz and antibiotics at 8.7 GHz (Mason et al, 2018b). However, this sensing structure alone is not reliable for distinguishing such similar pollutants in water as Cu and Zn. Also, as it was shown in Figure 6.4, the location of the principal resonant peaks is not comparable with results of earlier experiments described in Chapter 5 for uncoated sensors, because of the different applied measurement configuration. In this chapter, sensors were submerged directly in the samples by waterproofing the SMA connectors. This is a valuable achievement, especially for i) the smaller price of the necessary electronics for developing a portable device using mini-circuit board, considering the peak locations at lower frequencies; ii) the improvement in sensitivity at low frequencies compared with the one performed by adding the sample (400 μ L) on the sensor; iii) the elimination of the peak located at 2.4-2.5 GHz, which can interfere with the wireless communication largely used at that frequency for sending data. Another advantage is the sensitivity improvement: comparing these results, the slope increases with a consequent improvement in the ability to detect lower metal concentration at lower frequencies with a lower CV. Specifically, for example, there is a

sensitivity improvement from 0.065 for each 1 mg/L variation at 2.46 GHz to 0.485 for each 1 mg/L at 0.44 GHz comparing the “Small sample volume onto sensor” method with the “Submerged sensor in water”.

6.3.3 L-CyChBCZ coatings, standard addition method and field samples

More complex solutions were spiked using the standard addition method for evaluating the feasibility of using microwave rotational spectroscopy in the real environment by spiking a freshwater sample (FA) with Cu. These solutions were analysed i) using L-CyChBCZ coatings screen-printed on silver IDE on microscope slides for low-frequency impedance analysis and ii) using uncoated and coated gold IDE sensors with L-CyChBCZ based films, by probing water samples. Then, results between non-portable and portable VNAs were compared for evaluating the feasibility to move in the field and perform *in situ* trial measurements. Spectral outputs were analysed using a Lorentzian function and Cu and Zn responses were compared. Also, time and recovery time were performed, in addition to SEM and EDS analysis. Finally, a few real samples, FA, MR, NC and PM, were analysed and compared, and possible interferences investigated.

6.3.3.1 C and R at low-frequencies

Preliminary results, as pre-characterisation of the interaction between samples and L-CyChBCZ based coatings, were attained using the LCR bridge. Changes in capacitance (C) and resistance (R) were measured to evaluate the effective changes in these properties when “real” sampled water solutions spiked with metal solutions are in contact with the L-CyChBCZ coating. Spectral responses between 30 Hz and 5 kHz are shown in Figure 6.7a (for C, nF) and Figure 6.7b (for R, k Ω). Notably, with the increment of Cu concentration in the FA sample, the C increases and the R decreases, and both decrease

at higher frequencies. Changes in impedance measurements reflect changes in permittivity, that reflects consequent changes in spectral response at specific frequencies.

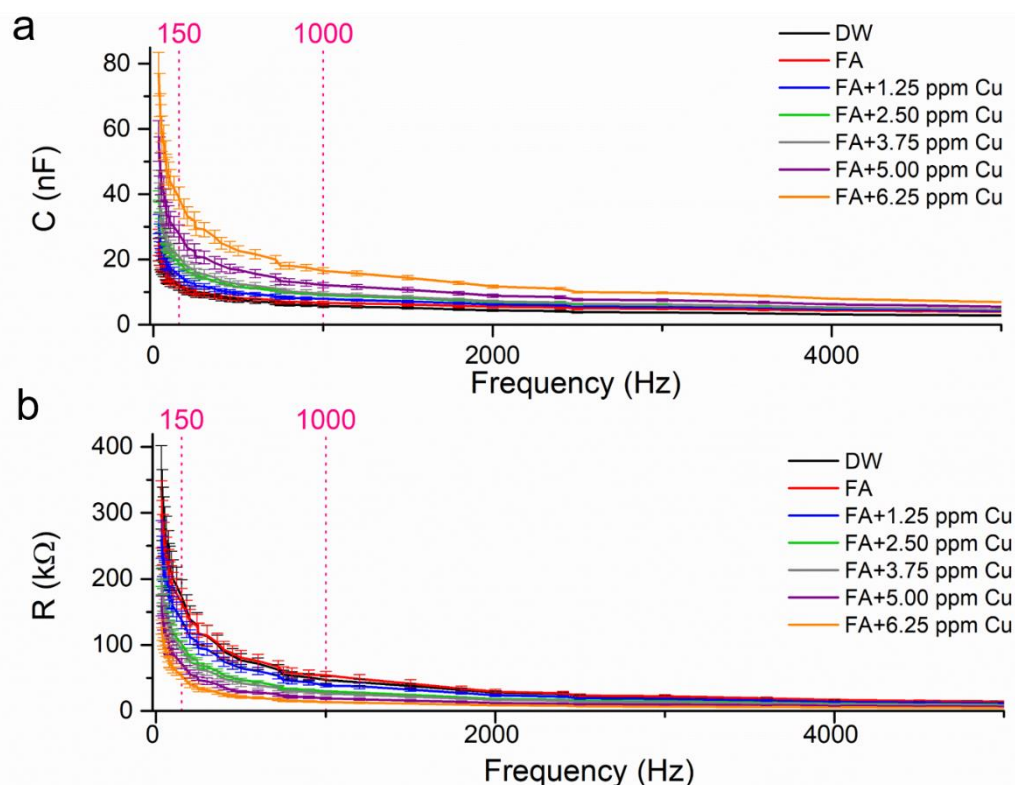


Figure 6.7 Capacitance (C) (a) and resistance (R) (b) plots measured using a LCR bridge and functionalised IDE with L-CyChBCZ based coatings for a collected polluted sample, FA, doped with the SAM

Although it was a real sample spiked with Cu solution, the sensing platform does not suffer overly from the interferences caused by the matrix, and it was able to quantify the increase of Cu content with a linear correlation. Figures 6.8 shows the correlation between the increase of Cu and the capacitance (Figures 6.8a) and resistance (Figures 6.8b), at two frequencies, namely 150 Hz and 1 kHz. Notably, the difference between FA and DW was minor, proving that the matrix does not interfere with the increase of Cu concentration and its increase in capacitance and decrease in resistance. The sensitivity for both C and R is higher at lower frequencies (150 Hz) and lower at 1 kHz, namely 4.2 nF and -21.0 kΩ compared with 1.6 nF and 6.5 kΩ for additions of Cu concentration of 1.25 mg/L. However, also the SD is proportionally higher when the sensitivity is higher.

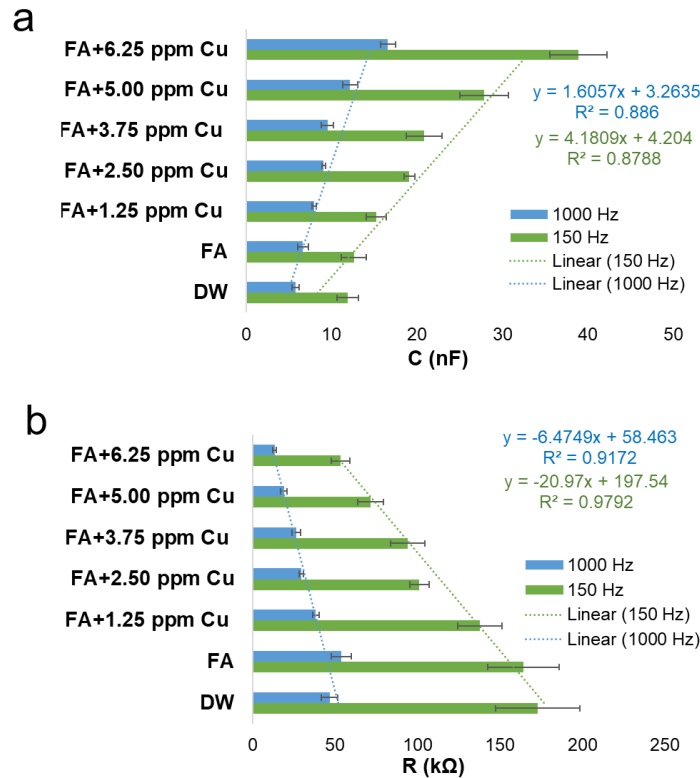


Figure 6.8 Linear correlations for capacitance (a) and resistance (b) with FA samples spiked with Cu at 1 kHz (in blu) and 150 Hz (in green)

Specifically, it jumps from an SD of 0.6-3.3 nF for C and 5.6-25 kΩ for R (higher sensitivity, low frequency, 150 Hz), to an SD of 0.2-0.8 nF for C and 1.2-6.1 kΩ for R (lower sensitivity, higher frequency, 1 kHz), probably due to the performance limitation of the LCR bridge.

Only these two parameters are not sufficient to identify selectively the Cu presence and quantify it when there are contemporary changes in other water parameters, and more specific measurements are necessary. As was shown in the previous chapter, microwave spectroscopy stands as a solution for achieving a more specific response, considering that specific resonant peaks are produced at selected frequencies depending on the chemical under test.

6.3.3.2 Uncoated and coated sensors: a comparison

FA samples (Cu-free) processed with the SAM were analysed using i) uncoated and ii) screen-printed f-EM sensors, based on L-CyChBCZ film, and the ZVA 24. Their spectra are shown in Figure 6.9a and 6.9b, respectively. The solid pink arrows in Figure 6.9b show the shift in spectral response through a higher frequency compared with Figure 6.9a; the dashed-violet-arrows show how the spectra changed due to the coating. Notably, the significant peaks that were identified at frequencies <1 GHz, which reflect the changes in the reflection coefficient magnitude using the uncoated sensors, were shifted to higher frequencies. Namely, the peaks highlighted in Figure 6.9a at 440 and 760 MHz, shifted to 470 MHz and 0.92–1.00 GHz.

Moreover, the peaks produced at frequencies between 0.92–1.00 GHz and 1.8–2.3 GHz (surrounded by the dashed violet arrows in Figure 6.9b) were characterized by a bigger change due to the microwave signal reflection, with a higher dB variation (Δ dB) for Cu concentrations. This is probably caused by i) a change in dielectric properties caused by the interaction of the Cu ions with the sensing material; ii) the thickness of the coating itself (Chen et al, 2012).

The three resonant peaks that are identified in the frequency range 0.001–1 GHz using uncoated and functionalised sensors highlighted in Figure 6.9a and Figure 6.9b with dash-vertical lines are named as peaks 0, 1 and 2.

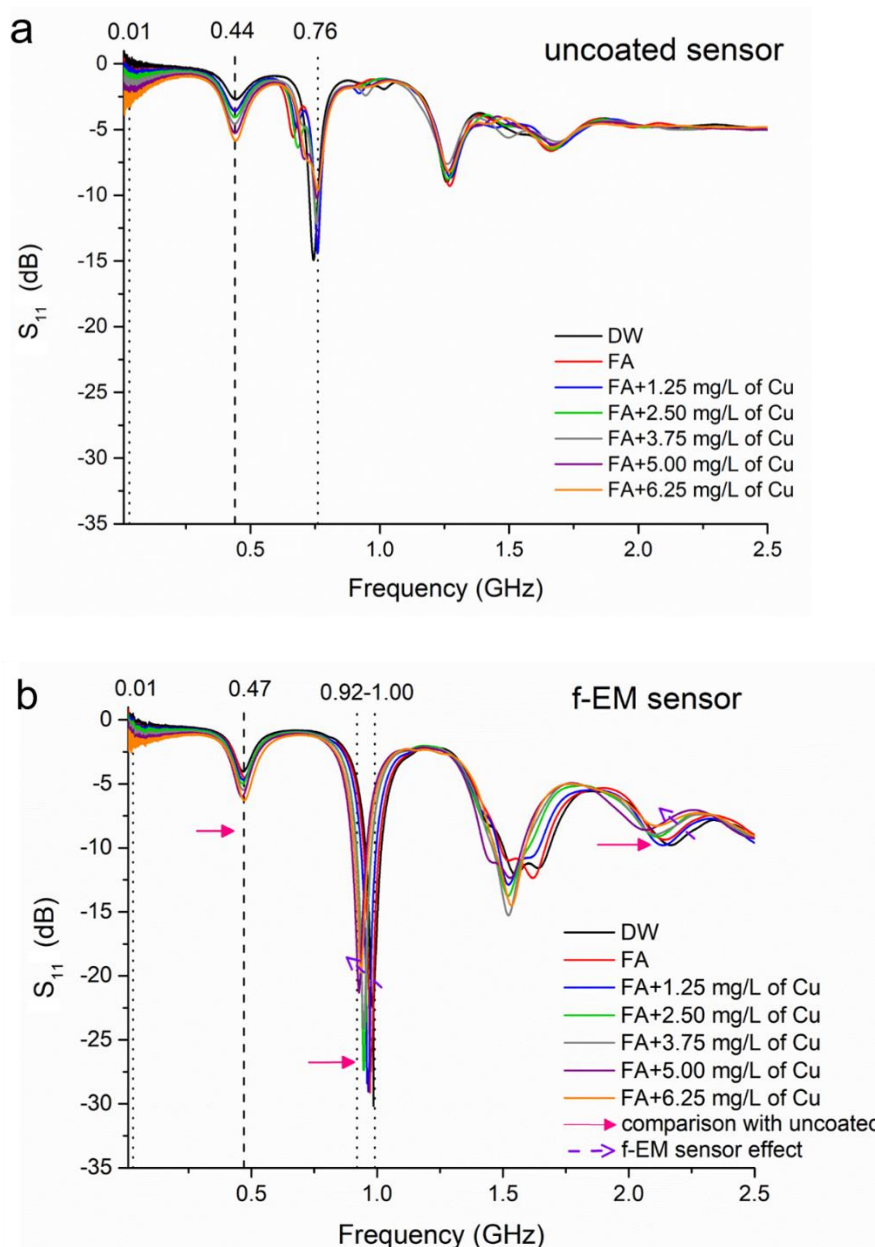


Figure 6.9 Comparison between spectral responses measured using uncoated sensors (a) and f-EM sensors with L-CyChBCZ based coating (b) for FA samples spiked with continual additions of +1.25 mg/L of Cu concentration; the solid pink arrows in b compare the sensing response with a and the dashed violet arrows show the coating effect

The comparison between the sensing performances of the uncoated and coated sensors, for Cu concentration changes in spiked mine water samples by analysing these peaks, is summarised in Table 6.1. For each sensor and peak were evaluated the R^2 , the CV, the sensitivity, the LOD and the Q-factor. The linearity of the sensing responses, sensor sensitivity and a high Q-factor are important factors for considering the sensing

efficiency, as well as its combination with shifts in resonant frequency (Benkhaoua et al, 2016). The Q-factor for peak 0 at 10 MHz cannot be evaluated, as it represented only the “extremity” of the peak.

Table 6.1 Summary of statistical information for 3 identified peaks (at frequency <1 GHz) using uncoated (UNC) and f-EM sensors based on L-CyChBCZ (f-EM) for a mine-water sample (Frongoch adit, FA) spiked with Cu using the SAM. The better performance of the f-EM sensor at peak 2 is highlighted with numbers in bold

	R²		CV (dB)		Sensitivity (ΔdB/mg/L)		LOD (mg/L)		Q-factor	
	UNC	f-EM	UNC	f-EM	UNC	f-EM	UNC	f-EM	UNC	f-EM
Peak 0	0.970	0.928	0.20	0.25	0.362	0.222	0.194	0.379	/	/
Peak 1	0.963	0.981	0.02	0.03	0.354	0.360	0.146	0.409	2.60	6.57
Peak 2	0.888	0.983	0.01	0.02	0.824	1.651	0.083	0.036	30.71	135.48

The linearity for peak 0 was higher ($R^2=0.97$) using the uncoated sensor. Also, the sensitivity (indicated by a steeper gradient) and Q-factor for both peaks 0 and 1 are higher using the uncoated sensors, with a smaller CV and LOD compared with the f-EM sensors. However, the efficacy of the f-EM sensor at peak 2 (in bold in Table 6.1) is much higher compared with the uncoated sensor, with higher linearity ($R^2=0.98$), sensitivity (1.651 dB changes for each mg/L change in Cu concentration) and Q-factor (135.5). Moreover, the low LOD (0.036 mg/L) demonstrates the prospect of detecting the Cu concentration in mine-water just above the EQS established as the “safe limit” in freshwater (28–34 μg/L). Consequently, to obtain more precise measurements, multi-peak analysis was used.

6.3.3.3 ZVA 24 vs miniVNA tiny

FA samples spiked continuously with Cu using the SAM were analysed using a portable and inexpensive VNA, specifically a miniVNA tiny, connected with a laptop and capturing data every 5 seconds, as illustrated in Figure 4.28a. Spectral responses and their SD are shown in Figure 6.10a, and the significant peaks are magnified in Figure 6.10b, c and d, which correspond to peaks 0, 1 and 2 in the previous subsection.

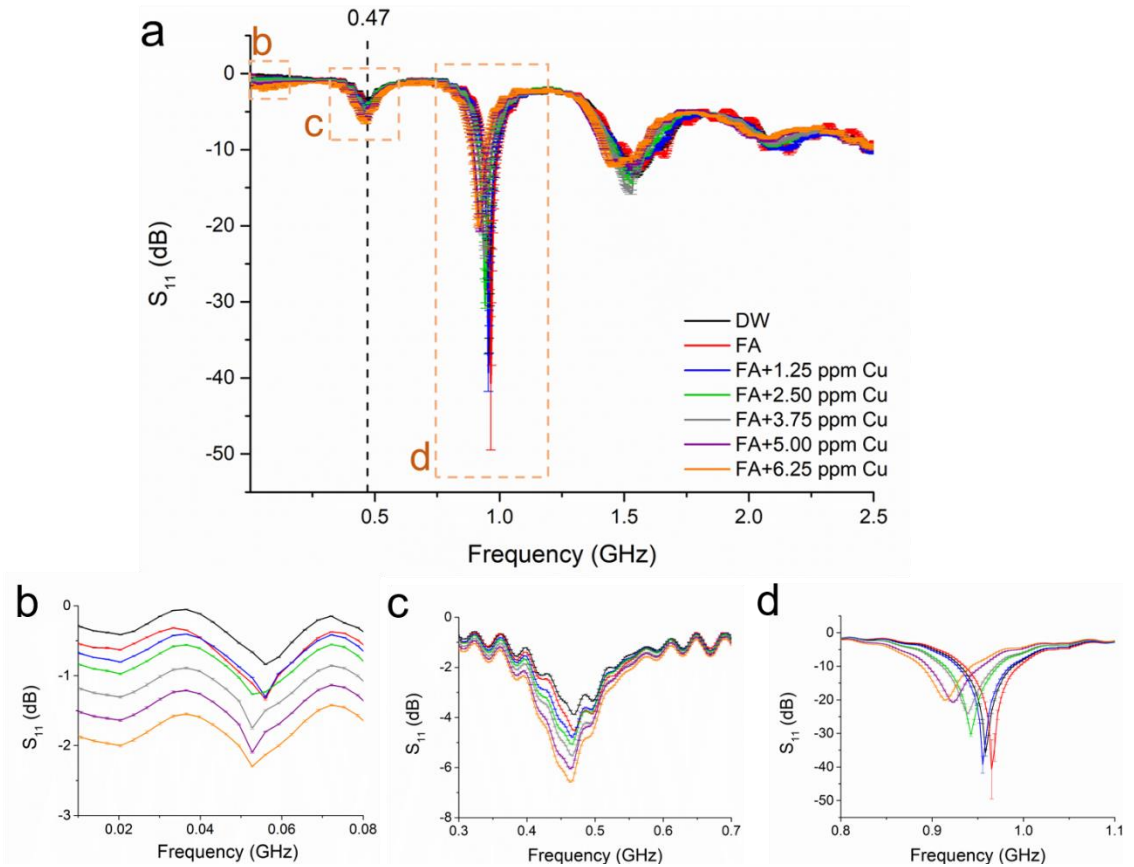


Figure 6.10 Spectral response for FA series measure with the miniVNA tiny in the frequency range 0.01-2.5 GHz (a) and its magnifications at three resonant peaks: at 0.04 GHz (b), at 0.47 GHz (c) and 0.91-0.98 GHz (d)

They reflect equivalent peak components that were identified using the non-portable and costly ZNA 24, demonstrating the ability to move in the field for performing trials of *in situ* and continuous measurements using inexpensive and practical tools. Notably, the peak 2 (Figure 6.10d) was slightly shifted to lower frequencies, from 0.92-1.00 to 0.91-0.98 GHz and manifested higher reflection coefficient for the same samples, manifesting a higher sensitivity, but a lower linear correlation with a higher error. Table 6.2 compared the sensing performances (R^2 , CV, sensitivity for every 1 mg/L changes of Cu, Q-factor and LOD) at the peaks 0, 1 and 2 between the ZVA 24 and the miniVNA tiny. The shifting of the sensor response due to the sensing coating, although reducing the R^2 , is an important characteristic that helps to improve the identification and quantification of a specific MUT, as it was assessed also by Bahoumina et al (2017) for gas sensing.

Table 6.2 Comparison of statistical features between VNAs (ZVA 24 and miniVNA tiny) using F-EM sensors based on L-CyCHBCZ coatings

	R ²		CV (dB)		Sensitivity ^a (ΔdB/mg/L)		LOD (mg/L)		Q-factor	
	ZVA 24	mini VNA	ZVA 24	mini VNA	ZVA 24	mini VNA	ZVA 24	mini VNA	ZVA 24	mini VNA
Peak 0	0.928	0.971	0.20	0.01	0.222	0.227	0.379	0.106	/	/
Peak 1	0.981	0.963	0.02	0.03	0.360	0.379	0.409	0.060	6.57	4.80
Peak 2	0.983	0.900	0.01	0.05	1.651	3.387	0.036	0.936	135.5	83.98

^aΔS₁₁ (dB) for each 1 mg/L Cu concentration change;

The results show how the performance of the cheap and portable miniVNA tiny is sufficiently comparable with the ZVA 24, demonstrating the feasibility of obtaining specific *in situ* measurements, which reflect the water chemistry, that other current methods are not able to accomplish. Also, this experiment shows that the miniVNA tiny performs better at frequencies < 0.7 GHz, with adequate performance between 0.7 and 1.2, and inferior performance above 1.5 GHz. Benkhaoua et al (2016) have recently described the successful performance of a DSS-SRR using a miniVNA tiny operating at 150 Hz in laboratory experiments for water/alcohols mixtures. This work demonstrates the successful use of a portable VNA to detect continuous variations in Cu concentration at higher frequencies using the developed f-EM sensors. The sensing can be further improved by combining the response of multiple peaks and additional f-EM sensors.

6.3.3.3.1 Impedance correspondences

Impedance parameters change, such as R, X (in series) and |Z|, which are directly correlated with variations in reflection coefficient for spiked FA sample series, were extracted with the miniVNA tiny and compared. An example of their comparisons and correspondences is illustrated in Figure 6.11 for the sample *FA+5.00 mg/L of Cu*, where the S₁₁ values are described through the primary y-axis (in black, dB) and impedance correspondences are described throughout the secondary y-axis (in red, Ω) for the frequency range 0.01-2.5 GHz.

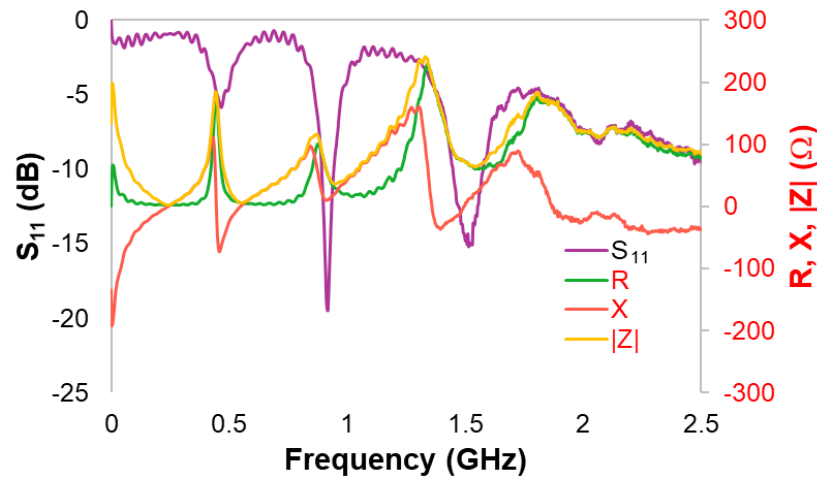


Figure 6.11 Example of S_{11} output and impedance correspondences responses (R, X, $|Z|$) for a sample (FA+5.00 mg/L of Cu) measured using the miniVNA tiny

Resistance (R), reactance (X) and impedance ($|Z|$), related by the Equation (3.7) (Yuan et al, 2018) were measured for the FA+ sample series and an f-EM sensor based on an L-CyChBCZ coating. Notably, the changes of these parameters (Figure 6.12a, b and c) reflect the changes in Cu concentration and microwave responses (S_{11}) at the same frequencies for the peaks 0, 1 and 2. Notably, the sensitivity for these parameters is higher for peaks 1 and not for peak 2 as for S_{11} measurements. Although, these data could be used in combination to ensure more precise measurements and reduce uncertainty. The linear correlations of these impedance parameters are displayed in Figures 6.12d-f, showing a particularly good correspondence with previous results for S_{11} measurements. This shows how the microwave response S_{11} matches changes in impedance parameters (Khaleghi et al, 2019). Although, measured impedance parameters at the same frequencies are not able to give more information on the behaviour generated by the interaction between the sample and the toxic metals under test with the EM waves. Consequently, considering their similarity, the focus of this dissertation complies with S_{11} changes and their characteristics.

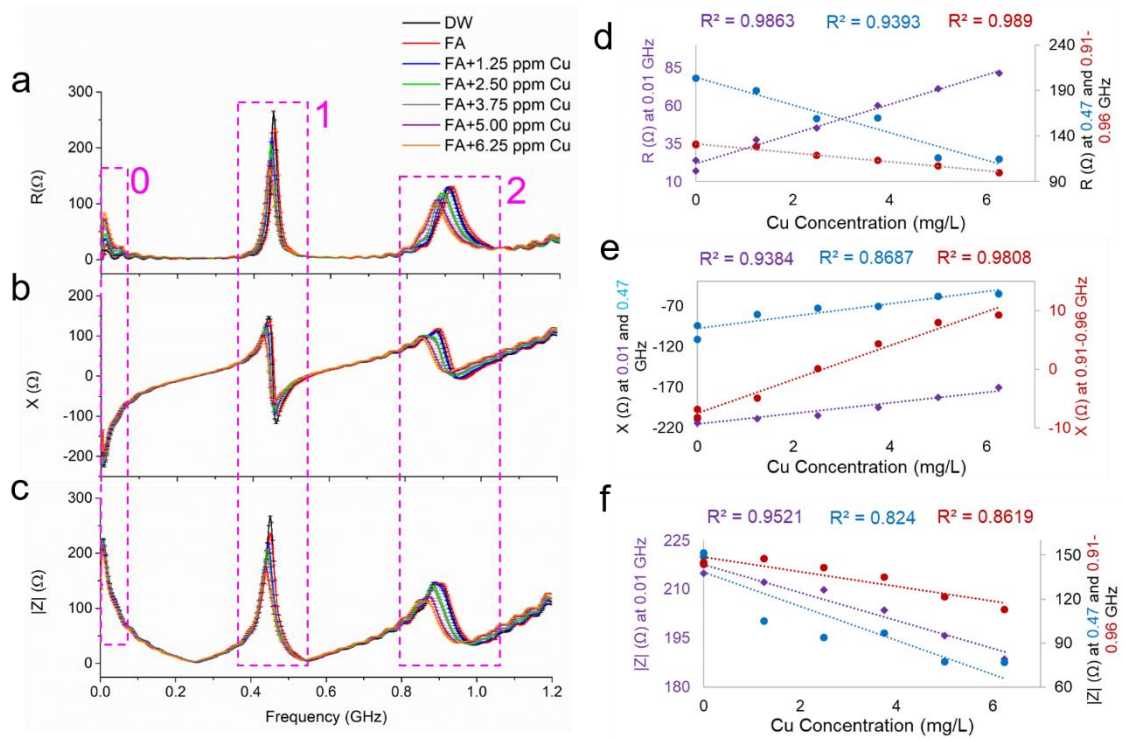


Figure 6.12 Impedance measurement, as R (a), X (b) and $|Z|$ (c), for FA+ samples series performed using the miniVNA tiny and f-EM sensors based on L-CyChBCZ coatings; their linear correlations are shown respectively in (d), (e) and (f)

6.3.3.4 Lorentzian-peak function

After analysing single peaks at specific frequencies in the EM spectrum, S_{11} spectral responses were considered in their entirety. The combined response of multiple peaks allows “pattern recognition” for a specific pollutant, with an improvement of specificity of the qualification and quantification of the severity of pollution and their variation for collected samples. To accomplish this, spectra responses were fitted using the Lorentzian function, considered the best to fit the peak produced by the interaction between samples and microwaves, as was shown in section 4.6.3. Figure 6.13 shows an example of the curve fitting outcome for each peak (green lines) and the cumulative fit peak (red line) of the S_{11} response (black line) of the sample *FA+1.25 mg/L of Cu*. The multi-peak analysis was performed, and the electromagnetic patterns were initially identified for the samples previously described in this chapter (FA+Cu series). For each sample, six distinct peaks

were identified and labelled. For consistency, these peaks follow the same denomination and location as in the previous subsections for peaks 0, 1 and 2. ΔS_{11} which is related to the small change in response at 0.01 GHz is considered “peak 0” as it is not a wide-ranging peak and it was not possible to analyse all its features. Through this novel strategy it is possible to not only identify and characterise all the peaks, including those that overlapped (e.g peaks 3, 4 and 5, highlighted in Figure 6.13) but also to investigate more parameters than just the centre of the peak (x_c) and its intensity (H), such as full width at half maximum (w) and the area of the peak (A). The fitting function converged and a chi-square tolerance value of 1×10^{-6} was obtained. Notably, the overlapped peaks between 1.25 and 1.80 GHz (pointed out with a blue dash square in Figure 6.13) encloses three distinct peaks which makes the apparent peak look irregular. Overlapping of individual peaks is common in vibrational spectroscopy such as middle-infrared and Raman frequencies (Meier, 2005). For microwave spectroscopy and f-EM planar IDE sensors this “phenomenon” mostly occurs at frequencies higher than 1 GHz.

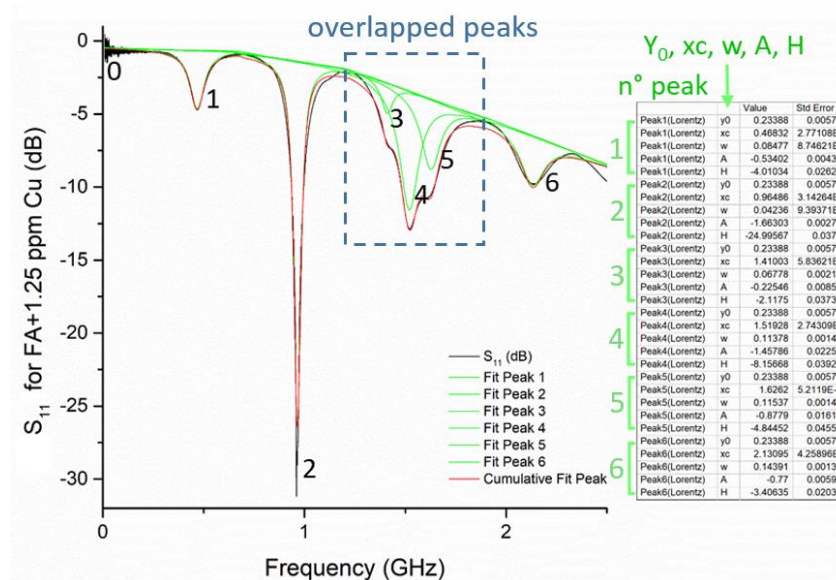


Figure 6.13 Example of the Lorentzian peak fitting function for the sample “FA+1.25 mg/L of Cu” showing an example of overlapped peaks (modified from Frau et al (2020))

The parameters obtained using the Lorentzian fitting function are plotted in the scatter graphs in Figure 6.14a-d. The most interesting data in terms of higher specificity for diverse Cu concentrations are highlighted with orange-dotted-circles. From the peak centre (x_c) graph (Figure 6.14a), it is noted that some resonant peaks (peaks 2 and 6) are shifted to lower frequencies as the Cu concentration increases. Resonant frequency shifts combined with changes in other parameters enable the identification of Cu concentration in water at specific frequencies with improved specificity. This is related to the change in permittivity, especially at low frequency, due to the small size of the sensor (Benkhaoua et al, 2016). However, this is not valid for each peak, as only the shift of x_c at peaks 2 and 6 appear to be linearly related to Cu concentrations.

FWHM, A and H present similar behaviours for the 6 peaks (Figure 6.14b, c and d). Notably, peak 5, which was part of the convoluted peak, was not distinguished for concentrations of Cu higher than +5 mg/L. Particularly, it is interesting as the values decrease for peak 1 located at 0.47 GHz when the Cu concentration increases, and increase for peak 2 (0.92–1.00 GHz). Hence, peaks 2 and 6 drift to lower frequency and decrease the S_{11} value when the Cu concentration increases. The analysis of the various parameters measured for DW (shown by grey arrows in Figure 6.14c and d), compared with the FA samples and its Cu additions, will help to identify the changes in spectral response that are related with the matrix composition.

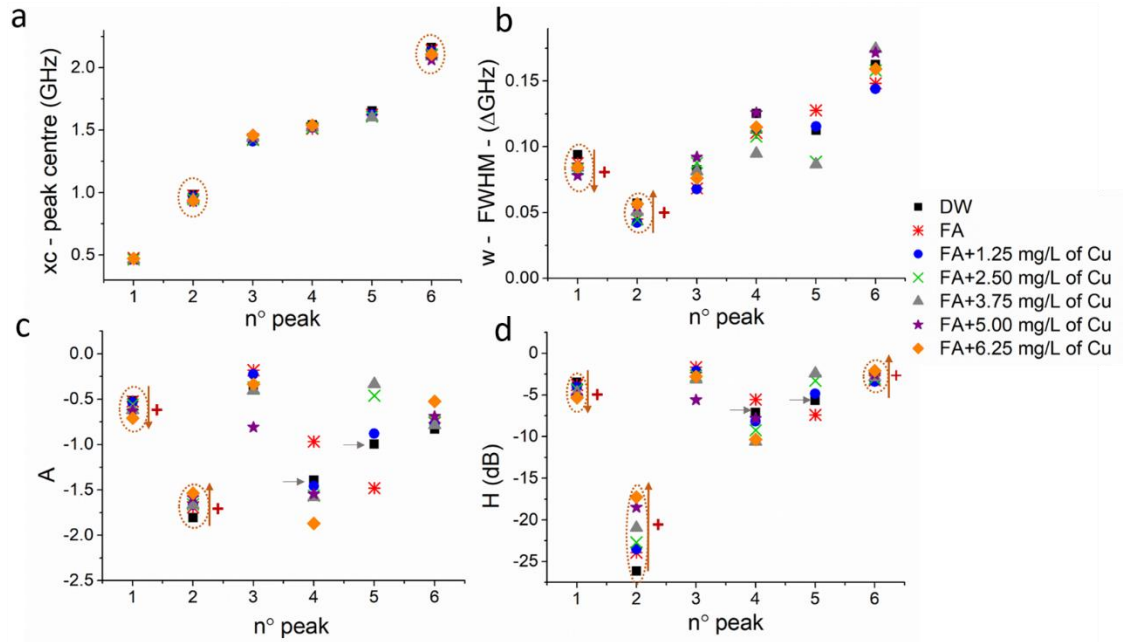


Figure 6.14 Summary of peak-parameters for FA sample spiked with the SAM, as peak centre, x_c , (a), FWHM, w , (b), area, A , (c) and height, H , (d) of the peaks determined by fitting the spectral responses with Lorentzian function with underlined points using orange-dotted-circles, orange and grey arrows (modified from Frau et al (2020))

6.3.3.5 Cu vs Zn

The comparison between the Cu and Zn response using the f-EM sensors based on an L-CyChBCZ coating and spectral analysis was performed. DW solutions spiked with Cu, Zn and both (1:1) were compared, for evaluating the inaccuracy of the sensing performance caused by the matrix of the sample and/or by the presence of other similar elements, ions or metals, which are detected at the same frequencies with the uncoated sensors and are likely to interact with the chelating polymers. The peaks were identified for all samples at similar frequencies (x_c) with some shift for the peaks that were separated in the convoluted one (peaks 3, 4 and 5). Figure 6.15a and b show selected peak-features (w and H) which compare the response for DW samples spiked with Cu, Zn, Cu+Zn and FA samples spiked with 0.2 mg/L of Cu and Zn (prepared by dilution). Peaks 1 and 2 show a good linear correlation (Figure 6.15c and d) for both Cu, Zn and Cu+Zn, with a higher R^2 ($=0.987$) for Zn at peak 1 and a higher R^2 ($=0.983$) for Cu at

peak 2. Although the S_{11} changes linearly at peaks 1 and 2, other peaks can help to differentiate between Cu and Zn. The combined peak, which includes peaks 3, 4 and 5, presents differences between the same concentrations of Cu, Zn and Cu+Zn (1:1). The divergences in other parameters (e.g w) will allow a more selective identification and quantification of the specific metal under test. For example, it is notable how the FWHM of peak 6 (Figure 6.15a) was more able to distinguish smaller concentrations of Cu, Zn and both.

The results demonstrate the capability of the proposed f-EM sensor based on L-CyChBCZ for selectivity sensing potential of increasing and decreasing of Cu and Zn in mining-impacted water. The responses for similar concentrations of these two metals show high repeatability and the potential to differentiate between these two pollutants by analysing multiple peaks which are related to changes in metal concentrations. Consequently, by combining the responses for multiple peaks and various peak parameters, the selectivity can be improved, although more data are necessary for developing mathematical functions for programmed discrimination and quantification of the toxic metals under test. The f-EM sensors based on L-CyChBCZ were able to detect changes in Cu and Zn concentration, especially in frequencies < 2.5 GHz. The detection of Cu using microwaves was also demonstrated by Puangngernmak & Chalermwisutkul (2014) using an open-ended coaxial structure, to be able to distinguish only between low (1 mg/L) and very high concentrations (100 and 1000 mg/L) and not changes in small concentration as is demonstrated in this project.

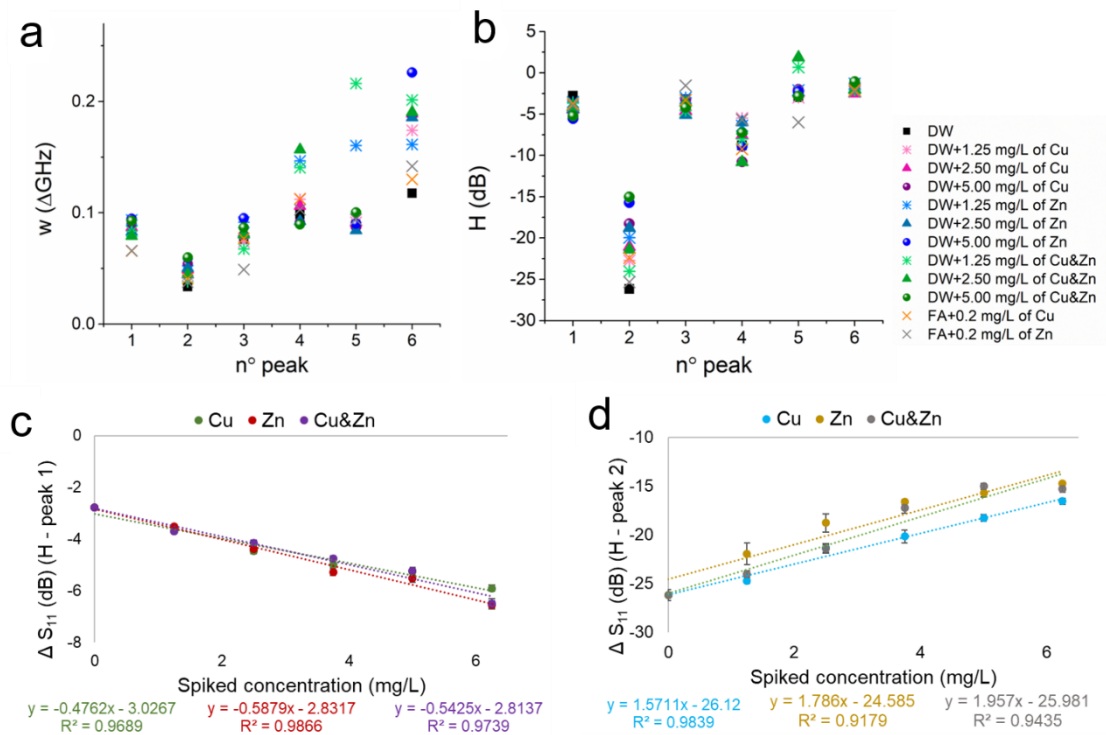


Figure 6.15 Selected peak features (w (a) and H (b)) which show the comparison between Cu and Zn solutions; linear correlations for peaks 1 and 2 and H are shown in (c) and (d) (modified from Frau et al (2020))

6.3.3.6 Time responses, SEM and EDS analysis

The interaction between Cu ions and the coating reached equilibrium after approximately 10 minutes, as shown by S_{11} in Figure 6.16a, and by C and R measurements in Figure 6.16b, using the *FA+5.00 mg/L of Cu* sample.

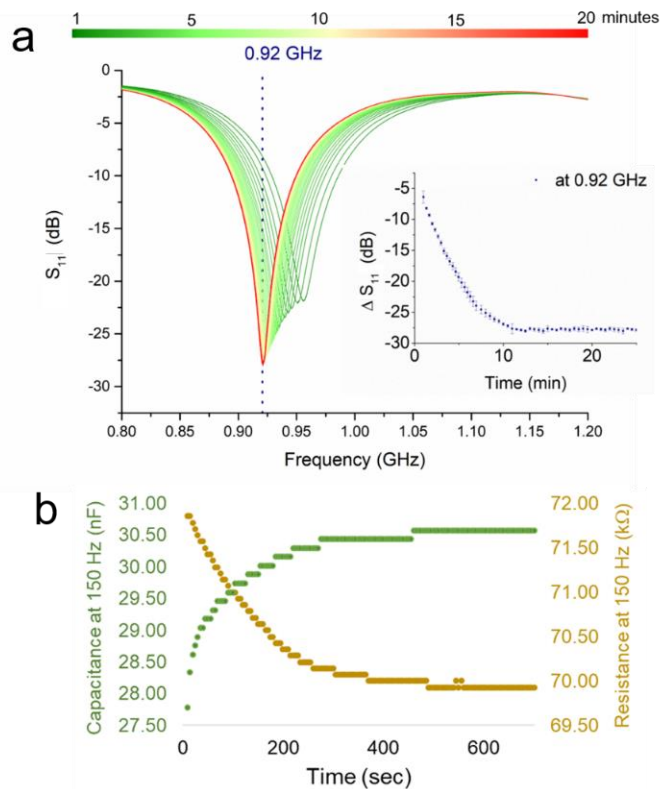


Figure 6.16 S_{11} (a), C and R (b) measurement by time demonstrating that within 10 minutes the measurements reach a stability

The presence of the copper on the sensing layer was confirmed by the SEM image (Figure 6.17a) of the coating on the f-EM sensors using EDS analysis (Figure 6.17b and c). This was expected due to the chelation with the amino and hydroxyl groups.

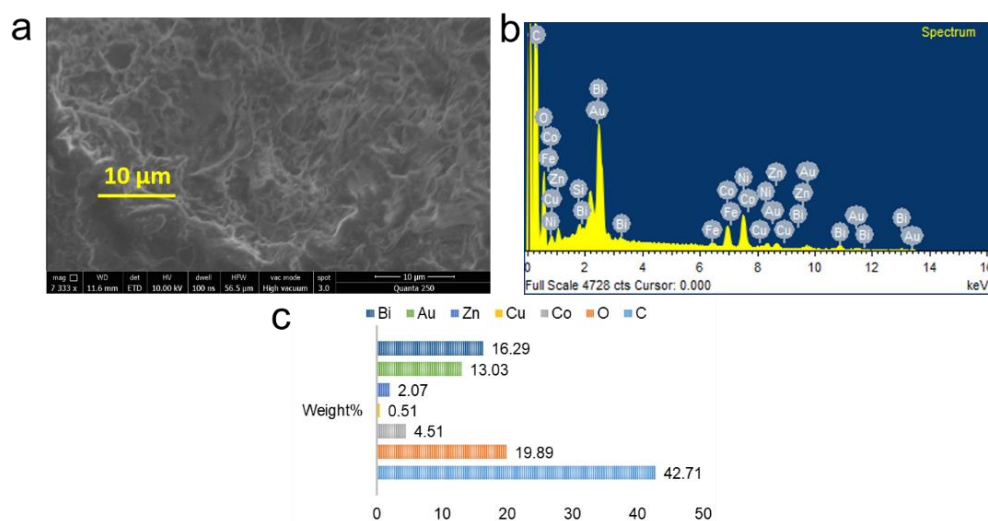


Figure 6.17 Scanning electron micrograph of the SEM image (a) and EDS analysis showing the weight percentage of the elemental composition of the L-CyChBCZ coating after the interaction with a Cu solution, on the IDE (b and c)

These changes reflect the variation in physical properties and the consequent change in complex permittivity due to the specific interaction between the Cu ions and the functional materials on the planar sensor, especially l-cysteine and chitosan that chelate with Cu ions. Consequently, the sensing performance was improved by a modification of the spectral response and the increment of specificity (Bernou et al, 2000). Notably, the EM waves interact with each part of the sensor and the sensing response will depend on the permittivity change of each component, such as the sensor itself, the coating, the coating thickness, the chelated metal ions on the coating, and the sample under test. The f-EM sensors are not only detecting the metals which are chelated on the L-CyChBCZ substrate, and which generate a variation in the spectral response, but also the overall change in the sample under test. Consequently, if there is an increase or decrease in metal concentration, the sensor would rapidly detect this change, despite the metals which chelate with the coating material.

The f-EM sensors proven in this work give the impression of being reusable and recoverable. After washing, the f-EM returns to its baseline spectrum (defined as *air spectrum*) in less than 2 minutes (Figure 6.18). However, the SEM used was not sensitive enough for quantitatively determining the Cu concentration in the coatings as a function of the concentration of the sample, or to characterise the effective interaction between the sample and the materials. The Zn was also part of the coating materials, so it was difficult to quantify. Further work will be required using more sensitive techniques, such as X-ray photoelectron spectroscopy (XPS) analysis.

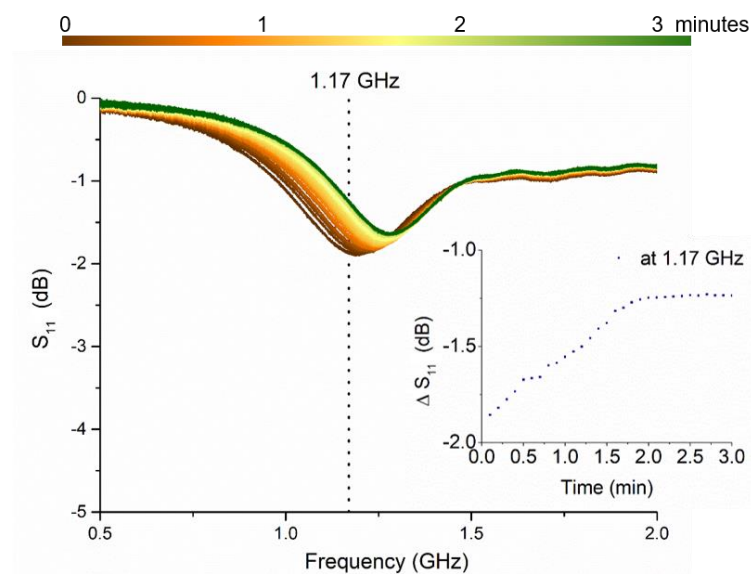


Figure 6.18 Recovery time of the sensor after being washed returning to its baseline level within 2/2.5 minutes

6.3.3.7 Feasibility of differentiating mining-water samples

A few collected samples were initially selected for testing the f-EM sensor based on L-CyChBCZ coating and evaluating the possibility of detecting both small and big differences between mining-impacted waters. Thus, three samples from the Wemyss mine area (FA, MR and NC) and a highly polluted sample from Parys Mountain mining district (PM) were selected and analysed. The metal concentrations, the pH, and the EC of these four mining-water samples were analysed using an ICP-MS and EC and pH probes respectively, and are described in Table 6.3. The samples were analysed at a constant temperature ($19.0 \pm 0.2^\circ\text{C}$) in a controlled temperature environment.

Table 6.3 Metal concentrations and physicochemical parameters for the four samples collected in two mining areas in Wales (UK).

	Cu (mg/L)	Zn (mg/L)	pH	EC ($\mu\text{S/cm}$)
FA	<0.001	9.27	6.65	175.1
MR	<0.001	5.87	5.94	89.6
NC	<0.001	2.94	7.21	118.0
PM	9.31	10.5	2.44	5,700

Their spectral responses with error bars are shown in Figure 6.19. Six peaks were identified for each sample, which corresponds with the location (xc) of the peaks identified for the laboratory prepared solutions. Some minor shifts were noticed and can likely be attributed to interference caused by the diverse water matrix or other material in the samples (e.g organic matter, other chemicals and ions). Peaks 0, 1 and 2 reflect the same general spectral behaviour identified for the previously illustrated FA sample series, with major peaks which change with sample composition that are identified at 0.01–0.05, 0.44–0.47 and 0.92–1.00 GHz. A lower S_{11} value for peaks 0 and 1 should reflect a higher Cu and Zn concentration, while for peak 2, a higher value corresponds to a higher concentration. That was perfectly reflected by the peaks located at <1 GHz for the PM samples, where the Cu contamination is a severe problem (Dean et al, 2013).

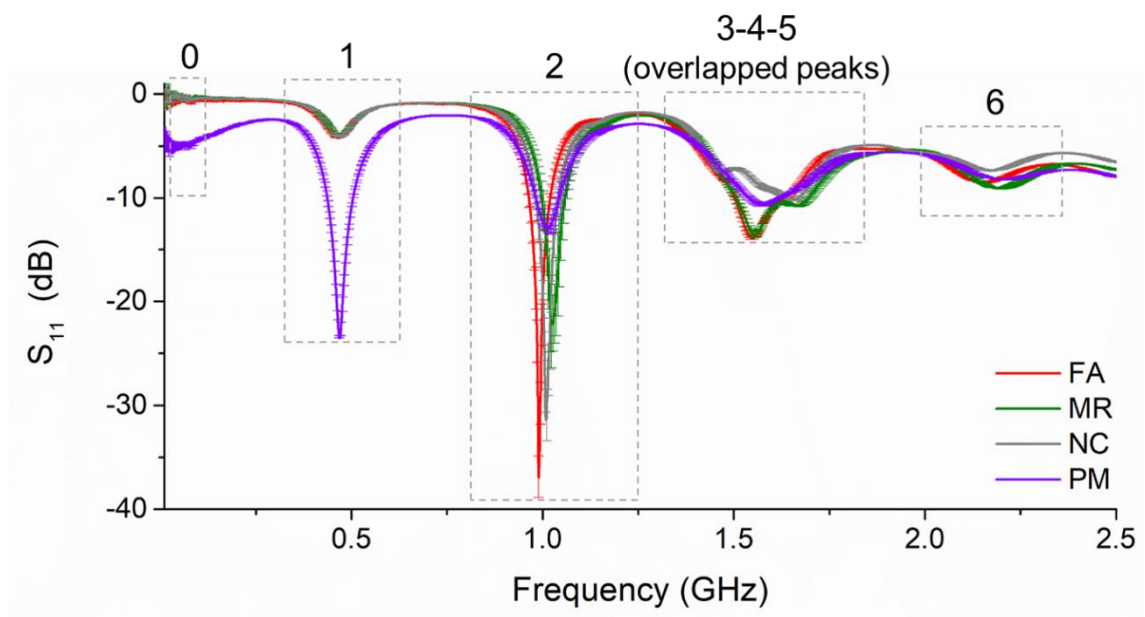


Figure 6.19 Real-mine water samples (FA, MR, NC, PM) output analysed using f-EM sensors based on L-CyChBCZ based coatings with SD

The Lorentz peak fitting function and the peak-features are shown in Figure 6.20a-f for peaks 0-6. The calibration equations obtained in section 6.3.3.5 were applied to real water samples. Results show that peaks 1 and 2 can differentiate the pollution level, discerning which sample is more or less polluted, but more data integration is necessary for a more

specific quantification and qualification of toxic metals in mining-impacted waters. Specifically, FA shows Cu concentration of 1.13 mg/L and 1.21 mg/L at peak 1 and 2, respectively. MR, 1.05 and 3.8 mg/L of Cu at peaks 1 and 2; NR 1.04 and 0.22 mg/L of Cu at same peaks; PM 34.0 and 10.2 mg/L. The concentration of Zn was quantified at peaks 1 and 2, respectively at each sample as follows: for FA was 1.2 and 1.4 mg/L; for MR 1.2 and 2.7 mg/L; for NC 1.2 and 0.6 mg/L and for PM 27.9 and 7.8 mg/L. Although the measured concentrations were not specific, the sensors were able to qualify the pollution level, as is notable comparing results with Table 6.3. This is because the linear correlation for Cu, Zn and Cu+Zn at peaks 1 and 2 is similar, thus they can interfere with each other. Even if the microwave spectrum generated by F-EM sensors which interact Cu and Zn samples is different in distinct parts of the EM spectrum, it is not sufficient to remove the interference generated by similar metals, such as Cu and Zn, completely. Consequently, integrating more parameters at different peaks (3–6) should improve selective detection.

The next chapter investigates the response of field trials and *in situ* measurements of mining-impacted water in the four mining areas previously described for assessing the feasibility to qualify and quantify differently polluted water samples from the same and diverse mining-areas in the UK.

This novel approach needs further investigation to understand the causes of every interference caused by the water matrix and other water components.

Part of the results discussed in this chapter have been published by Frau et al (2020).

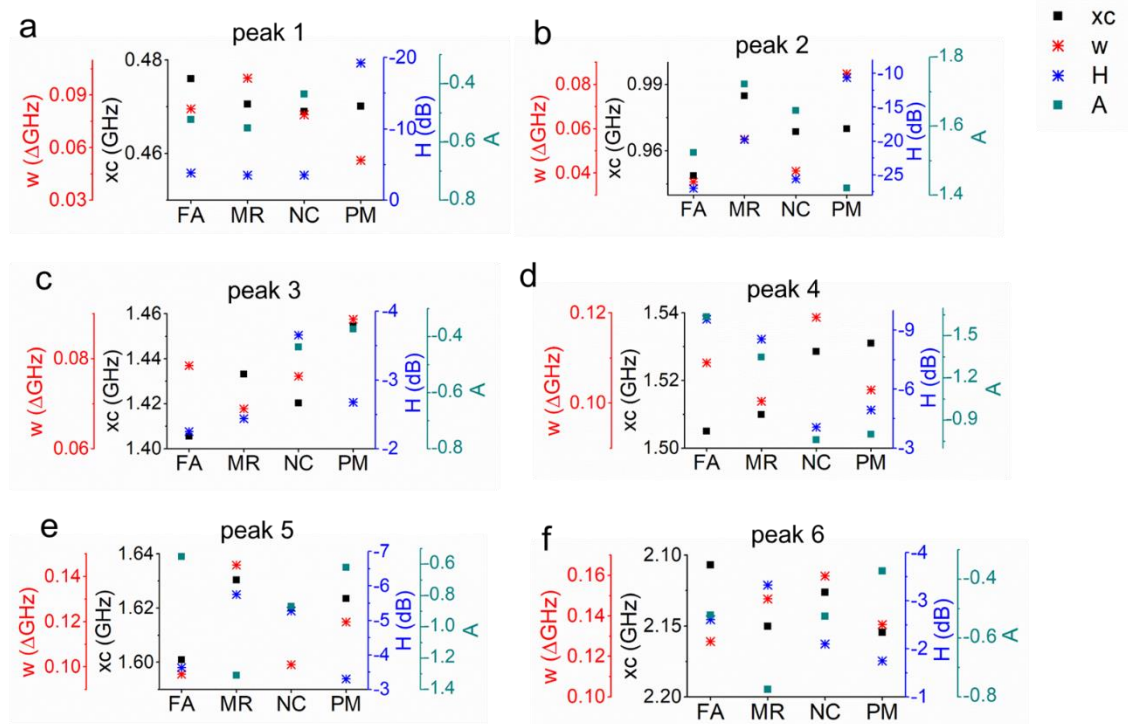


Figure 6.20 Peak properties (xc, w, H, A) comparison at peaks 1, 2, 3, 4, 5, and 6 (respectively shown in graphs a, b, c, d, e and f) which were identified for 4 collected water samples (FA, MR, NC, PM)

6.3.3.8 Interferences from other factors

Supplementary experiments were performed for evaluating how changes in other common parameters can interfere with the microwave response for selected pollutants, such as Cu and Zn. Notably, changes in pH, T, and metal species (dissolved or complexed) are strictly related to the metal concentration itself (Cidu et al, 2011). Literature suggests that changes in the microwave response can also be related to variations in other factors, such as pH, temperature, or other particles, although there is no published research which quantifies the response shift due to each of these parameters combined with the response of the selected analyte under test. For example, Abbasi et al (2020) monitored pH variation (from 7 to 11, and from 1 to 7) measuring transmission (S_{21}) and estimated frequency shifts to as the pH increase, obtaining a shift to a lower frequency when increasing the pH from 1 to 7, and a shift to higher frequencies when

increasing the pH from 7 to 11. Figure 6.21a shows some examples of variations in pH, using pH calibration solutions (4, 7 and 10) and f-EM sensors based on L-CyChBCZ coatings. It is notable how the Q-factor decreases as the pH increases.

Temperature is another factor which can affect microwave measurements and must be corrected (Ateeq et al, 2017). Figure 6.21b shows the results of an experiment where the response of a Cu&Zn solution (10 ppm, 1:1) was recorded every 30 minutes during an increase from fridge temperature (8.2°C) to lab temperature ($19.0\pm 0.2^{\circ}\text{C}$). Peak 1 shows a change in magnitude (reduced Q) while peak 2 shows a shift toward lower frequencies. The effects of T must be accounted for to achieve accurate measurements *in situ*. Wong et al (2016) described the integration of temperature compensation on microchip devices used for microwave measurements.

Other common constituents that are found in mining-impacted freshwater can interfere with the microwave signal due to the variation in concentration of one or more metals. The variation of the microwave signal due to pH and sulphate concentration, which are two factors strictly related with mining impacted water, require more investigation.

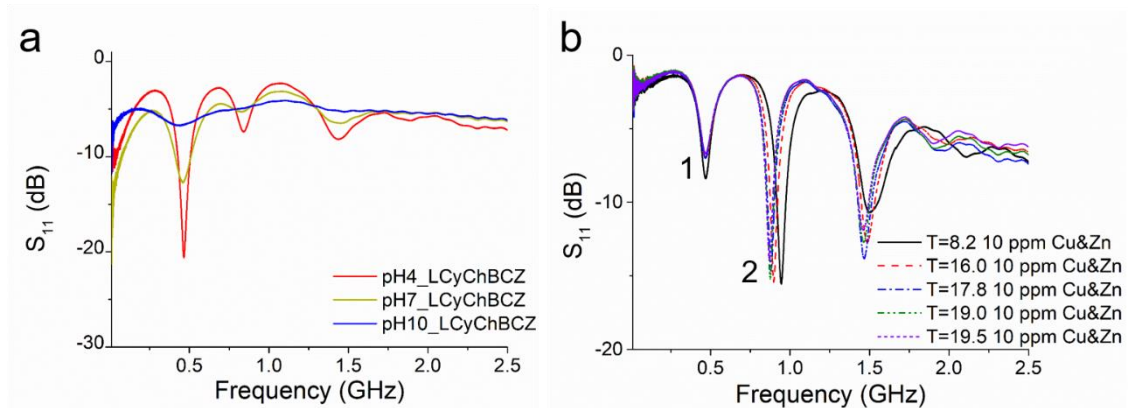


Figure 6.21 Example of spectral changes measured for the pH calibrations solution (pH= 4, 7, 10) (a) and variations in spectral responses for a 10 ppm Cu&Zn sample (1:1) due to T variation (8.2 to 19.5°C) measured every 30 minutes using a f-EM sensor based on an L-CyChBCZ coating

6.4 Summary of the main findings

The main findings obtained using uncoated and f-EM sensors based on L-CyChBCZ based coating probing water samples are:

- The signal response changes from probing the sensor in water compared with the “400 μL ” method;
- Uncoated sensors were able to quantify the unknown concentration in a sample using the SAM at 0.44 GHz with a linear $R^2 > 0.99$ and a sensitivity of 0.48 $\Delta\text{dB}/\text{mg}/\text{L}$ of Cu and Zn;
- The coated sensors based on L-CyChBCZ coating show an improvement for Cu ion detection, especially in the frequency range 0.92–1.00 GHz with an improvement in sensitivity (1.63 $\Delta\text{dB}/\text{mg}/\text{L}$), higher Q-factor (135.5) and low LOD (0.036 mg/L);
- The responses using a portable VNA (miniVNA tiny) was successfully compared, assessing the feasibility to perform in situ trials;

6.5 Overall summary and implications

This chapter demonstrates the feasibility of detecting metal pollution by immersing the modified sensing structure in complex water samples, using both uncoated and coated sensors using L-CyChBCZ. The ability to detect and differentiate water samples polluted by Cu and Zn was assessed.

The polluted mining-impacted areas, from which water was tested during this research, are briefly described. The continuous increase (and decrease) of Cu and Zn were evaluated using the SAM, which consists of spiking water samples with known metal concentrations and quantifying the increase of metal concentration despite the interferences that can be caused by the matrix or other chemicals or particles in the water.

The coated sensors based on L-CyChBCZ thick films show an improvement for Cu ion detection, demonstrating the feasibility to detect Cu concentration just above the environmental quality standards for freshwater (28–34 $\mu\text{g/L}$). Responses for Cu and Zn were then compared by analysing microwave spectral responses using a Lorentzian peak fitting function and investigating multi-peaks (peaks 0-6) and multi-peak' parameters (x_c , w , H , A) for specific discrimination between these two similar toxic metals. It is useful to compare additional parameters for determining the selectivity, as demonstrated by Harnsoongnoen et al (2019) for distinguishing between nitrates and phosphates. Lastly, four collected polluted samples (FA, MR, NC and PM) from two mining areas in the UK (Wemyss mine and Parys Mountain mining district) were measured and compared, demonstrating the suitability to differentiate polluted samples from the same or different areas. The analyses of collected water samples in a polluted mining area have demonstrated the feasibility of using this method for obtaining a different response using more complex waters with different chemical composition.

The demanding task to obtain both high sensitivity and selectivity between very similar pollutants is challenging using microwave spectroscopy and f-EM sensors. Another novel approach has been integrated during this project and is described in the following Chapter: combining the response of various f-EM sensors for obtaining a more specific response for mining-impacted water samples, as was recently experimented by Zhao et al (2020) for guaranteeing water quality, with the difference that sensors covering various frequency ranges were complemented. Every targeted experiment and achievement opens research to face novel limitations for the development of a reliable sensing platform.

In the following chapter, results are described for the produced f-EM sensors for monitoring mining-impacted water samples. The combined response of multiple f-EM sensors (named as f-EM sensor array or electronic tongue) is investigated and compared

for guaranteeing a more specific characterisation of polluted waters. Then, the responses of some experimental field trial and *in situ* measurements in the four mining areas are illustrated and discussed.

Chapter 7 Results and discussion (phase 3): *in situ* field trials and multiple f-EM sensors

7.1 Introduction

The objective (O3) of this final *Results and Discussion* chapter is to evaluate the combined response of using multiple f-EM sensors, defined as an *f-EM sensor array* (or electronic tongue), for measuring complex water samples and to perform *in situ* trial measurements.

Water samples from 4 mining areas, Wemyss mine, Parys mountain mining district, Nant y Mwyn mine and Leadhills mine in the UK were tested *in situ*, providing evidence for the feasibility of using microwave spectroscopy and f-EM sensors for characterising and differentiating polluted water samples. Moreover, the action of measuring continuous changes in water parameters *in situ* and the return to the baseline spectrum was tested with a tracer (NaCl) slug injection.

7.2 Brief recapping of materials and methods

In this final results and discussion chapter, the use of multiple f-EM sensors emerged, as an approach to fully characterise toxic metals in a water sample. Various water samples with different chemistry from four mining areas in the UK were analysed using microwave spectroscopy and ICP-MS (or ICP-OES). Then, some *in situ* measurements were performed in the same sample sites. Sample locations are shown in aerial images and photos representing both sites and *in situ* set-up measurements in Appendixes 2a, b, c and d, respectively for Wemyss mine, Parys Mountain mining district, Nant y Mwyn mine and Leadhills mine.

7.2.1 f-EM sensor array

The idea of combining the sensing response of all the developed f-EM sensors as an f-EM sensor array is an attractive approach to identify the concentrations of different toxic metals simultaneously (refer to Appendix 1 for the progression of this idea). Other researchers (Macias et al, 2019; Vlasov et al, 2002) have defined the combined response of multiple sensors as an *electronic tongue*, due to the contact between the sensing structure and the sample under test. The use of a sensor array has been proved to guarantee more information and reliability compared with a single sensing structure. Potentiometric and colorimetric techniques (Huang et al, 2019; Savosina et al, 2020) make use of a sensor array for obtaining a more specific response for a target analyte.

Recently, some researchers have experimented with the application of a microwave sensor array. For example, Zhang et al (2019) integrated elements, which operate at different frequencies between 1 and 10 GHz, into a microwave array for collecting more information on various water samples. Then, Harrison et al (2020) combined machine learning to the sensor array for obtaining a more specific response for diverse cardboard, wood and plastic samples.

In this work, the same principle was applied but it combined the responses of f-EM sensors with different coatings. The f-EM sensors were tested in the field and real-time *in situ* measurements were performed.

7.2.2 In situ trial measurements

After having evaluated the feasibility of detecting and distinguishing different water samples from the same and different mining areas, f-EM sensors were tested in the field using the portable and practical miniVNA tiny, connected to a smartphone or a laptop. Regular and continuous measurements were performed in the 4 mining areas. Appendix 2

shows examples of *in situ* measurements performed using both a smartphone and a laptop as the output device: MR and NC sites (Appendix 2a.b and 2a.d) in Wemyss mine area; PM-1, PM-2 and PM sites in Parys Mountain mining district area (Appendix 2b.b, 2b.c and 2d.d); NYB-1 and NYB sites in Nant y Mwyn mine (Appendix 2c.b and 2c.d); and WW-A in Leadhills mine (Appendix 2c.d). Physicochemical parameters (EC, pH and T) were measured in the field and results are shown in Appendix 3. Metal concentrations (Zn, Cu, Pb, Cd, Fe and Mn) were measured using ICP-MS and/or ICP-OES and results are shown in Appendix 4. Also, for *in situ* measurement, the stability of the sensing response due to the river flow and the feasibility of performing continuous monitoring were evaluated. Then, the S_{11} spectral responses of various samples between the same and diverse mining areas were analysed using Lorentzian peak functions and compared, indicating the feasibility of qualifying and quantifying the severity of the metal contamination in each selected site. Moreover, the ability to detect an “unexpected” change in water composition and the return to the baseline spectrum with a slug injection of sodium chloride (NaCl) as a tracer during sampling campaigns in Wemyss and Nant y Mwyn mines, was evaluated.

7.3 Results and discussion: characterise polluted waters using multiple f-EM sensors

This chapter describes and discusses the results and the feasibility of using f-EM sensors for quantifying polluted samples from the same and different mining areas, using combined responses of the sensors. In the previous chapter, the possibility of quantifying the increase in metal Cu and Zn content using the SAM, and distinguishing polluted samples (FA, MR, NC and PM), using f-EM sensors based on L-CyChBCZ coatings, was evaluated. Consequently, the f-EM sensor array idea was developed and studied.

7.3.1 F-EM sensors: general laboratory comparisons

The microwave sensing response using multiple f-EM sensors for metal content qualification and quantification was studied. Initially, the output responses for the DW, FA and FA+5.00 ppm of Cu samples, were compared. The FA sample is Cu-free with a concentration of Zn of 9.3 mg/L, Pb 0.23 mg/L, and Cd Fe and Mn <10 µg/L (Appendix 4). This simple experiment is used for evaluating the change in response due to the increase in Cu and its difference from a DW sample using all sensors (after 10 min). Figure 7.1a illustrates the sensing response between 0.01 and 2.5 GHz for the samples DW (dotted lines), FA (dashed lines) and FA+5.00 ppm of Cu (solid lines) using uncoated (UNC) sensors (black lines) and f-EM sensors based on L-CyChBCZ (gold lines), β -Bi₂O₃ (yellow lines), lacquer (grey lines), and ITO (cyan lines) coatings. For explicitness, the sensing output colour resembles the coating colour when it is possible.

It is clear that every sensor can detect variations in metal content or distinguish between freshwater and DW. Then, the location of the resonant peaks for each microwave sensors was analysed. For simplicity, the spectral responses for the sample FA+5.00 ppm of Cu using the five sensors are compared. Figure 7.1b shows the locations of peaks 0 (p0) and 1 (p1) for all sensors. It is clear how the lacquered sensor has a lower S_{11} (-26.7 dB) for peak 1 at higher frequencies (0.57 GHz). Notably, the change in resonant behaviour between 0.61-0.62 GHz, as lower S_{11} for peaks 0 and 1 reflects higher Cu and Zn concentrations, while for peak 2 a higher S_{11} corresponds to a higher concentration, described in the previous chapter for uncoated sensors and L-CyChBCZ based coating, it was not noticed for the other three sensors between 0.61-0.64 GHz (Figure 7.1c and d). β -Bi₂O₃ and ITO based coatings present a similar behaviour for all identified peaks, with a slight shift to higher frequencies for the ITO based f-EM sensor due to its higher conductivity and thickness (~80 µm) (Figure 7.1d).

This preliminary experiment demonstrates that each sensor can give a specific and different response for variations in water composition due to the increase in metal content (FA vs FA+5.00 ppm of Cu) and between water matrix (DW vs FA). Consequently, the idea of using an f-EM sensor array to characterise contaminated water samples from mining areas was appraised. Calibration curves for metal content variation, as described in the previous chapter for L-CyChBCZ, were developed for Cu and Zn with every f-EM sensor configured for immersion in water. Linear calibration curves were evaluated at peaks 1 and 2 between 0 and 10 mg/L for fitting the response of the analysed polluted samples. Their physicochemical parameters (EC, pH and T) measured in both the field and the lab are described in Appendix 3; their Zn, Cu, Pb, Cd, Fe and Mn concentrations (in $\mu\text{g/L}$) are illustrated in Appendix 4. Specific calibration curves were selected depending on the metal concentration analysed. For example, samples collected in Parys Mountain mining district (PM, PM-1 and PM-2) have Cu and Zn concentrations between 7 and 25 mg/L. Moreover, it was investigated for both f-EM sensors and UNC sensors based on L-CyChBCZ coatings at which concentration the S_{11} was similar at peak 1 and 2, considering these peaks present an inverse behaviour: lower and higher S_{11} respectively at peak 1 and 2 for higher concentrations.

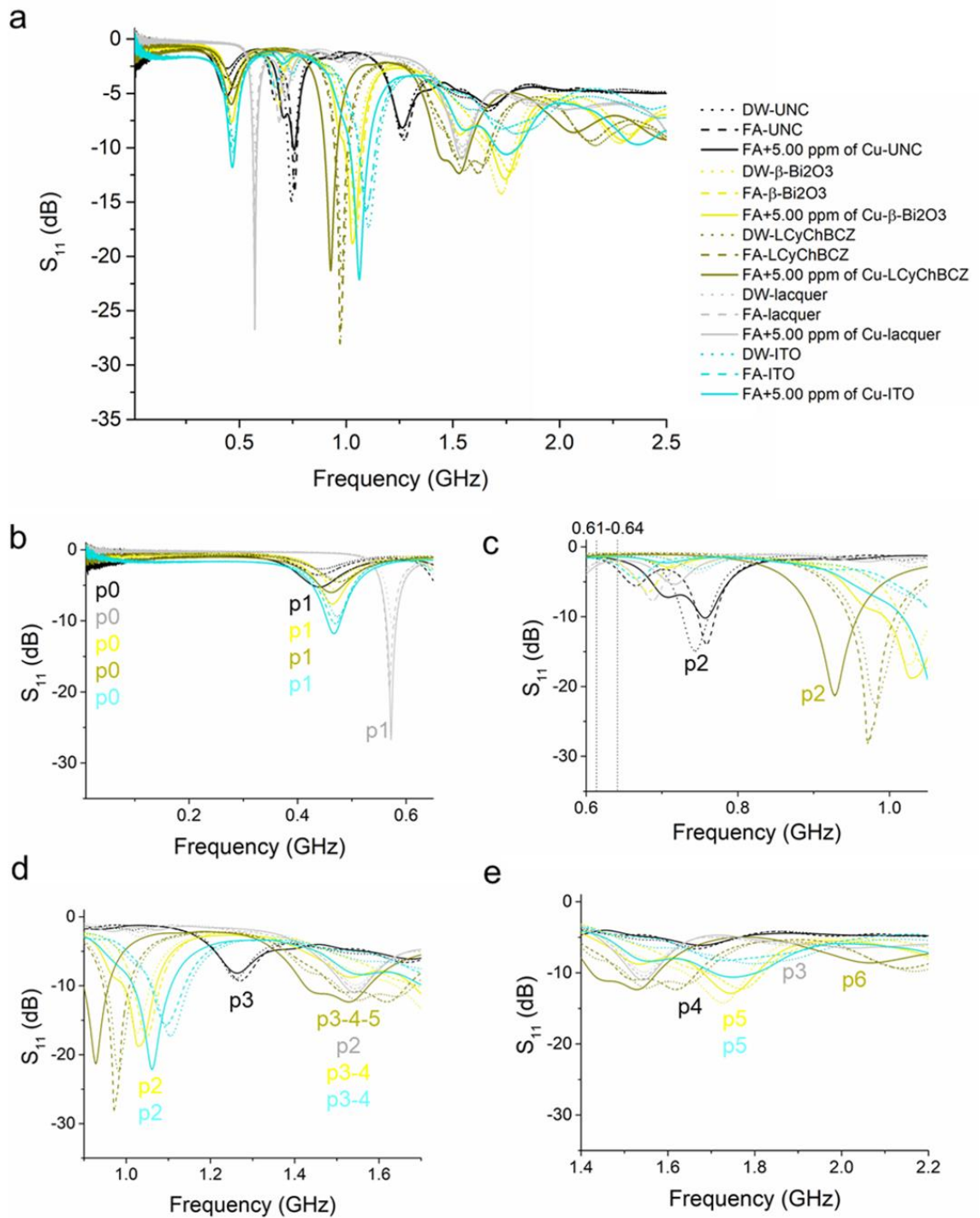


Figure 7.1 Comparison between sensing responses using multiple microwave sensors (uncoated (UNC), f-EM sensors based on β - Bi_2O_3 , L-CyChBCZ, lacquer, ITO coatings) for DW (dotted line), FA (dashed line) and FA+5ppm of Cu (solid line) samples (a). Magnification of selected frequency range and peaks (p) number identification: 0.01 to 0.65 GHz (b); 0.6 to 1.05 GHz (c); 0.9 to 1.7 GHz; and 1.4 to 2.2 GHz. For straightforwardness, curves have the same colour as the represented coated sensor

For example, Figure 7.2 illustrates that for the L-CyChBCZ (solid lines) based f-EM sensor a similar response at peaks 1 and 2 is individuated by detecting ≈ 15 ppm of Cu;

for the UNC sensors a similar S_{11} was assessed for ≈ 12 mg/L of Cu (Figure 7.2). Also, this graph shows how the sensors were able to distinguish between DW and tap water (TW).

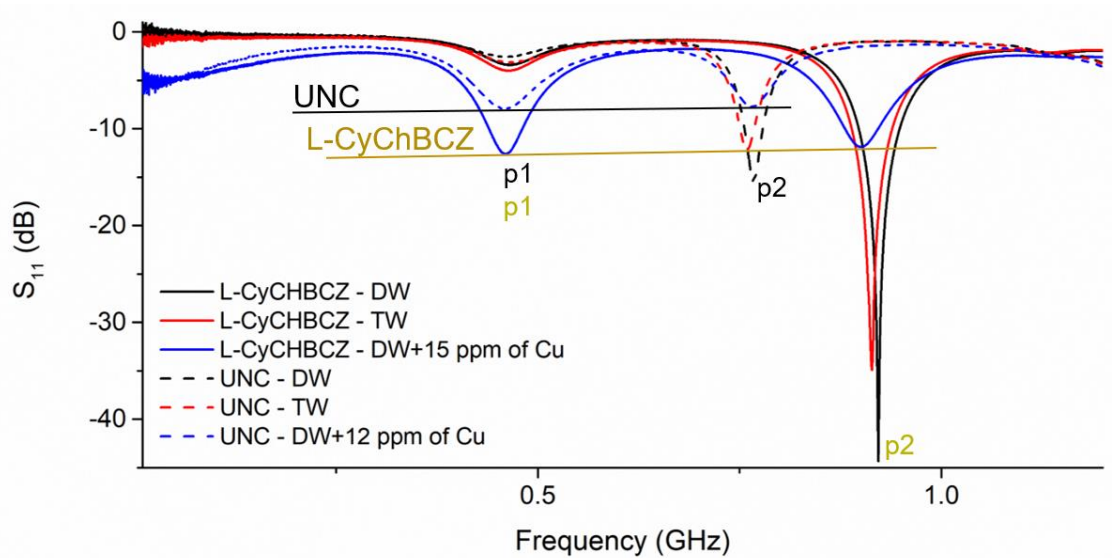


Figure 7.2 Comparison between L-CyChBCZ (solid line) and UNC (dashed line) sensors focusing on describing when the reflection coefficient S_{11} is similar at peaks 1 and 2; and comparison between DW and tap water (TW)

For the development of a novel analytical sensing device, it is necessary to *train* the machine by analysing the sensing response. Mass spectroscopy, a well-developed analytical technique, knows which selected wavelengths have to detect specific metals, due to their mass. Microwave spectroscopy works with the permittivity and conductivity variation of materials, and works with less energy and at lower frequencies. So, it needs less power and results are less selective. Consequently, more and other/ novel strategies have to be applied for obtaining a specific response for a contaminant under test.

7.3.2 *In situ analysis of polluted freshwater*

In situ trial measurements were performed using various f-EM sensors and the inexpensive, portable and practical miniVNA tiny. Physicochemical parameters, that are EC, pH and T, were measured *in situ*, and samples were collected for comparing and

performing measurements in the laboratory using the ZVA 24 which provided a higher data resolution. When microwave lab-measurements were performed, EC, pH and T were re-measured, for having the correspondence of these physicochemical values at a constant temperature ($19.0\pm 0.2^{\circ}\text{C}$). Sample concentrations were measured using an ICP-MS. For instance, only PM samples collected at Parys mountain were extremely highly polluted and were measured also with the ICP-OES.

7.3.2.1 Wemyss mine

The first *in situ* measurements were performed in Wemyss mine area in July 2018 during low flow condition (Byrne et al. 2020, submitted). Both rapid and continuous measurements were performed. Then, three samples were collected for laboratory analysis and testing the f-EM sensors with polluted freshwater. In the previous chapter, results for the FA sample processed with the SAM and comparison with MR and NC samples using uncoated and f-EM sensors based on L-CyChBCZ coatings were extensively investigated.

Considering it was the first time that submersible sensors were developed and tested, only a few sensors (which were developed before July 2018) were tested *in situ*, such as the lacquered, $\beta\text{-Bi}_2\text{O}_3$ and ITO based sensors, which offer both sensor protection and high response stability and repeatability.

In general, the investigated sites had an EC between 89-210 $\mu\text{S}/\text{cm}$ and a pH between 5.9 and 6.6 (Appendix 3). The most polluted sample was FA, followed by MR and NC. All samples were $\text{Cu} < 0.0025 \mu\text{g}/\text{L}$, with Zn concentration between 2.9 and 9.2 mg/L . 200 $\mu\text{g}/\text{L}$ of Pb were detected at FA and 2.4 mg/L at MR (Appendix 4).

7.3.2.1.1 First in situ trial measurement at Wemyss mine

The response of the first *in situ* trial measurements with SD (which illustrate the variability of the sensing response) is shown in Figure 7.3. Specifically, the comparison between the same sample (FA) and various sensors (ITO, lacquered and β -Bi₂O₃ based f-EM sensors) is illustrated in Figure 7.3a and b; then, a comparison using the same sensor (ITO) for diverse samples in the same mining area, so with similar matrix and chemical composition, is shown in Figure 7.3c and d. It is observable how i) diverse sensors can guarantee a singular response for the same sample and ii) the same f-EM sensor can guarantee a diverse response for diverse but similar samples collected in the same mining area. The microwave response using the miniVNA tiny produces stable results until 1.3 GHz. Between 1.3 and 2.5 GHz the response is a bit noisy, although the differentiation between samples using the same sensor or between different sensors analysing the same sample is clear.

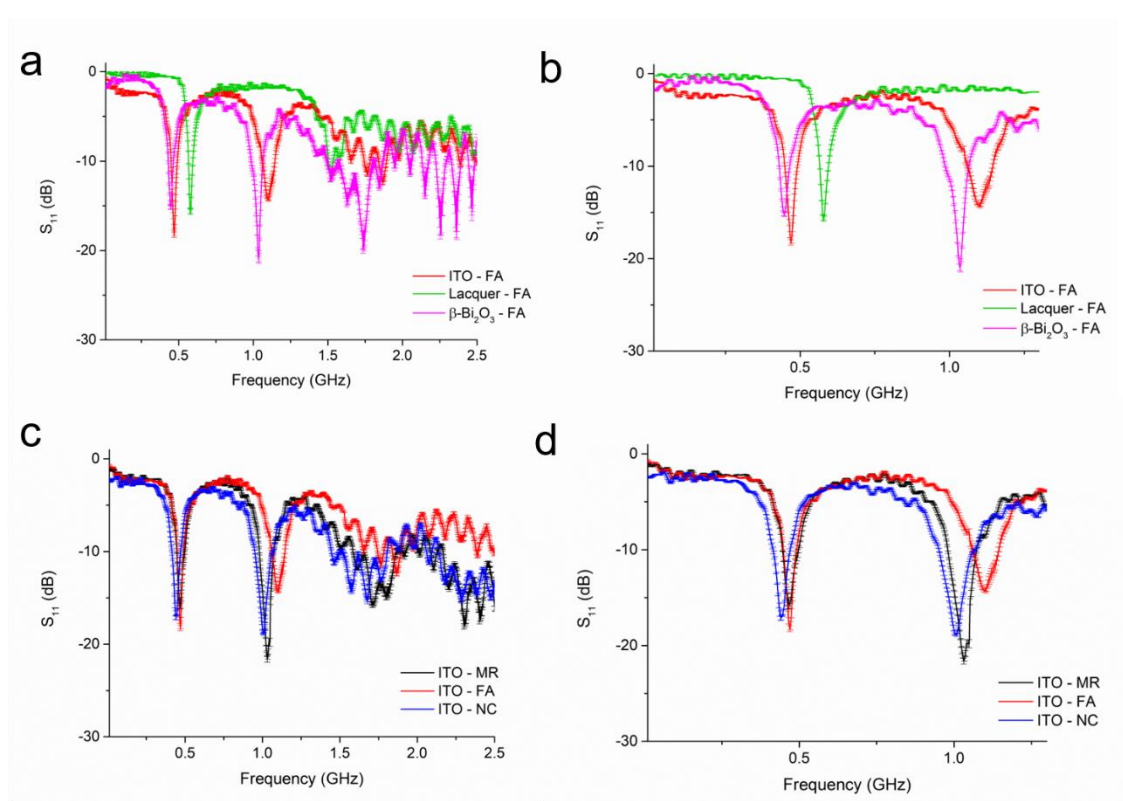


Figure 7.3 Example of *in situ* trials performed in Wemyss mine areas for FA sample using three f-EM sensors based on ITO, lacquered and β -Bi₂O₃ (a and b) and for diverse samples (MR, FA and NC) using the same sensor (ITO)

7.3.2.2 Parys Mountain mining district

The water chemistry of the samples from Parys Mountain varies highly from the other three sites in the UK as it is severely polluted. Two samples (PM-1 and PM-2) were selected in the mining district for *in situ* analysis using various f-EM sensors. They were collected and analysed in the lab using the f-EM sensor array; also the adit (PM), which emerges into the Northern Afon Goch, and a sample after the wetland with reduced contamination (PM-W) were collected and analysed in the lab using the ZVA 24. Sample location, measurement set-up and their aspect are illustrated in Appendix 2b.a-e. Samples EC ranged from 1,634 to 7,570 μ S/cm and a pH range between 1.8 and 2.78, which suggests that these samples are extremely polluted; different chemistry was reported for

the sample collected after the wetland (Dean et al, 2013; Marsay, 2018), which is reported to have a reduced metal level with a measured EC of 249 $\mu\text{S}/\text{cm}$ and a pH of 5.9.

Their metal concentration is reported in Appendix 4, which suggest that the PM-2 was the most polluted sample collected in the area followed by PM and PM-1, and PM-W with reduced pollution due to the wetlands. Specifically, PM-2 (Appendix 2b.c) has a concentration of 13.5 mg/L of Zn and 25.0 mg/L of Cu. PM (adit) and PM-1 have Zn and Cu concentrations respectively of 10.6 and 9.7 mg/L and 12.5 and 7.0 mg/L. PM-W has reduced contamination, with Zn and Cu concentration of 1.1 and 1.2 mg/L respectively. Also, Pb, Cd, Fe and Mn have high concentrations ($\gg\text{EQS}$) for all measured samples. The Fe concentration result was extremely high (>500 mg/L) for PM-2, but it is not considered a reliable value as it was above the calibration curve measured with the ICP-OES.

7.3.2.2.1 In situ trial at Parys Mountain mining district

Parys Mountain mining-water was firstly assessed *in situ* during July 2018 using a lacquered sensor, but the resulting response was unpredicted and considered unsuccessful. An example of the unusual sensing response is shown in Figure 7.4, where the spectrum manifested a distinct shape.

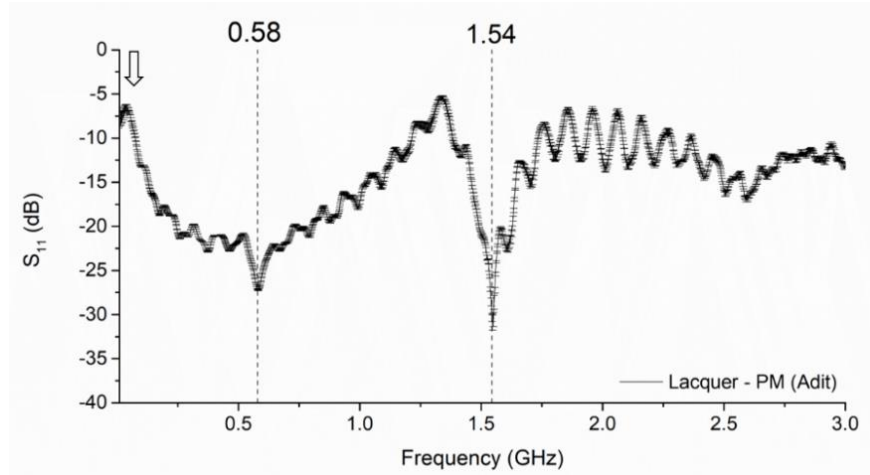


Figure 7.4 Example of *in situ* measurement for the PM (adit) sample using a lacquered sensor

The spectrum shifted to lower dB, and peak 1 (0.58 GHz) displayed a “convex shape”, although the location of the resonant peaks was at the same frequency as that of the other *in situ* mining-impacted analysed water. This was probably due to the extreme contamination in the sample, its extremely low pH (2.44) and very high EC (3,200 $\mu\text{S}/\text{cm}$). This sample was analysed and compared with others in a laboratory, as described in the previous chapter, demonstrating that the problem was caused by some other factor, such as a short circuit or water infiltration in the connector.

After more laboratory testing and sensor development, another trial was then performed in November 2019 using a combination of various f-EM sensors and testing the f-EM sensor array concept *in situ* and continuously at PM-1 and PM-2 sites. The temperature (10.2-10.8 °C) was much lower than the subsequent laboratory analysis (19.0 \pm 0.2°C), which can influence the measurements. In Figure 7.5 are shown the mean of continuous measurements that were performed at PM-1 (solid lines) and PM-2 (dashed lines) using uncoated (black lines) and f-EM sensors based on $\beta\text{-Bi}_2\text{O}_3$ (yellow lines), ITO (cyan lines) and L-CyChBCZ (gold lines). It is visible how each sensor was able to differentiate between these two differently polluted water samples.

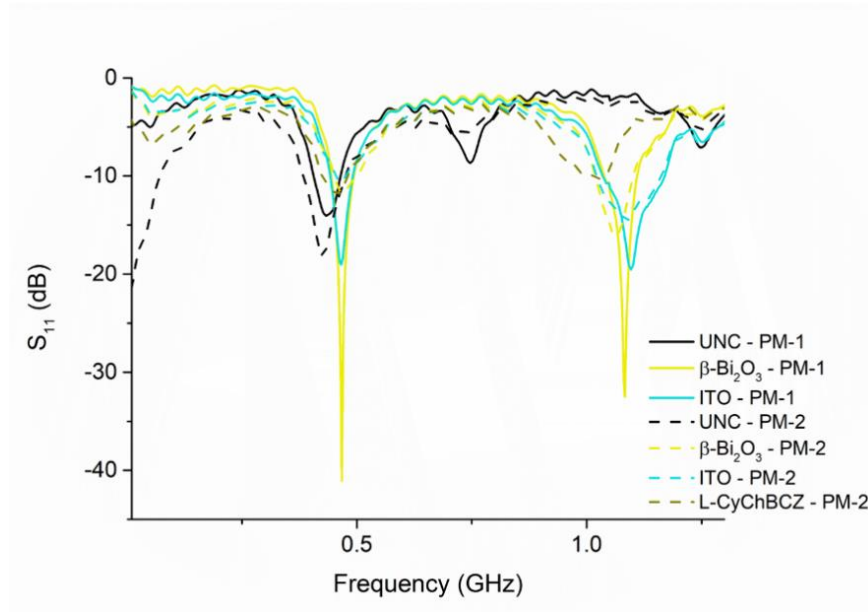


Figure 7.5 *In situ* measurements at Parys Mountain mining district in Nov 2019 using a combination of f-EM sensors at PM-1 and PM-2 sites, two highly polluted water samples located in the mining area

This demonstrates the feasibility of using a combination of various f-EM sensors to give a more specific response about water quality. Specifically, the concept of using a combination of f-EM sensors was tested *in situ*. Considering that this sensing system is novel, it is necessary to study the sensing response in different conditions for understanding the variations in the sensing response. Figure 7.6a and b show the S_{11} average responses with the SD, showing the repeatability and reproducibility of the measurements. The comparison between each sensor and the two samples is illustrated in Figures 7.6c, d and e, and reflect the sensor's responses presented in the previous chapters. Specifically, uncoated sensors presented a lower dB at 0.01 and 0.42 GHz and a higher dB at 0.76 GHz when the concentration is higher (Figure 7.6c); inversely, sensors based on metal oxides (β - Bi_2O_3 and ITO) produce a lower dB at 0.05 GHz and higher at 0.47 and 1.06-1.10 GHz (Figure 7.6d and e).

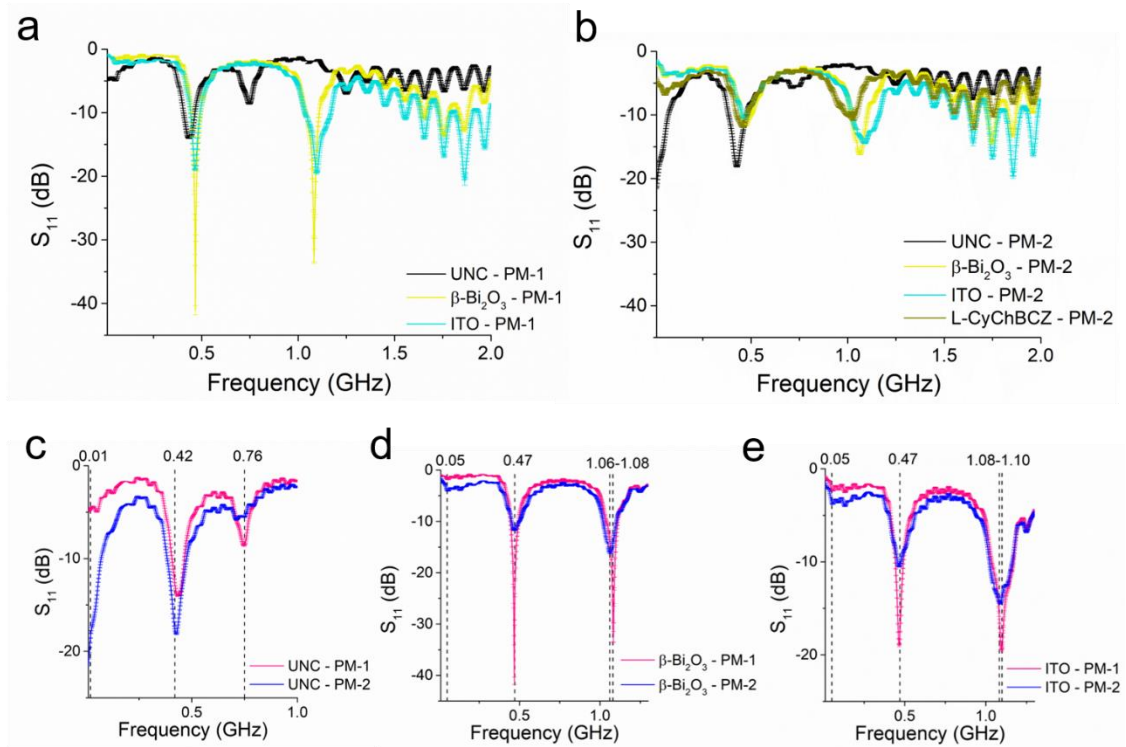


Figure 7.6 Comparison between PM-1 (a) and PM-2 (b) samples analysed *in situ* using an f-EM sensor array with mean and SD from 0.01 and 2 GHz; each sensor, UNC (c), β -Bi₂O₃ (d) and ITO (e) was able to distinguish between these two samples at three frequencies

Between them, the β -Bi₂O₃ based f-EM sensor produces a lower dB as S_{11} for lower concentration if compared with the ITO sensor, and a similar S_{11} for the higher concentration.

For instance, analysing correspondent collected samples in the lab, interferences were noticed, probably caused by organic matter or other chemical substances in the waters. More comparisons between diverse concentrations, water chemistry and sensors are illustrated at the end of the punctual description of the *in situ* trial in each area.

7.3.2.3 Nant y Mwyn mine

The water samples from Nant y Mwyn mine were generally “less polluted” than the samples from the two previously described sites (Wemyss and Parys Mountains mines). NYB-1 and NYB-2 sites (Appendix 2c.c and 2c.d) were selected to accomplish *in situ*

measurements, using various f-EM sensors and EC, pH and T probes. Also, at NYB-2 site a trial was performed using an f-EM sensor array, by probing various f-EM sensors *in situ* consecutively using the miniVNA tiny and a smartphone as the output device (Figure 7.7a-e). Samples were collected and analysed then in the lab using both an ICP-MS and a ZVA 24. In addition, another sample, NYB-R, was taken from a right bank inflow, which is a runoff from a tailings deposit next to the Nant y Bai (Appendix 2c.b). Samples EC ranged from 76.1 to 109.3 $\mu\text{S}/\text{cm}$, with circumneutral pH (6.6). At first instance, the NYB-R looks like the most polluted sample, followed by NYB-1 and NYB-2. Laboratory standard analysis confirmed this pattern for the toxic metal concentrations analysis (Appendix 4), especially for Zn and Pb, the highly concentrated samples, in line with the fact that the mine exploited these metals. Specifically, NYB-R suffers from 1.7 mg/L of Zn and 1.9 mg/L of Pb, followed by NYB-1, with 0.951 mg/L of Zn and 0.417 mg/L of Pb, and by NYB-2 with 0.754 mg/L of Zn and 0.331 mg/L of Pb.

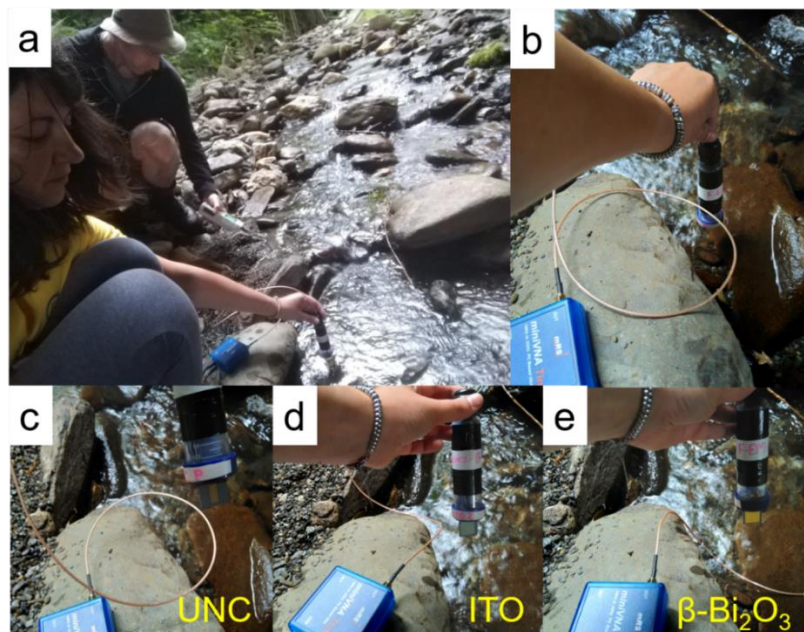


Figure 7.7 Example of *in situ* measurements probing the sensors directly in water (a and b) using various f-EM sensors, such as uncoated (c) and based on ITO (d) and $\beta\text{-Bi}_2\text{O}_3$ (e) for assessing the f-EM sensor array principle in the real environment

7.3.2.3.1 *In situ* measurements using multiple f-EM sensors

The *in situ* trial at Nant y Mwyn mining area, with immersion of the sensing structure in the Nant Y Bai at two sites (NYB-1 and NYB-2), was performed in July 2019. The temperature at NYB-2 during the measurements (18.7°C) was similar to the consequent lab measurements (19.2°C); contrariwise, at NYB-1 the T during the *in situ* measurement was lower (14.7°C), with a consequent possible interference on the measurements. NYB-1 and NYB-2 have similar water chemistry, considering that they are two samples in two different sites of the same stream, and a similar level of pollution, with NYB-1 slightly more contaminated than NYB-2. Although, mining-impacted areas are complex, evaluating the variation in contamination between different sites is relevant for applying efficient remediation strategies.

Figure 7.8 shows the *in situ* response at the two sites, NYB-1 (solid lines) and NYB-2 (dashed lines) using two f-EM sensors: one based on β -Bi₂O₃ (orange lines) and one based on L-CyChBCZ (gold lines). Both sensors were able to distinguish the two diverse (but similar) contaminated samples in Mid Wales. As described in the previous chapters, changes in dB at 0.01 GHz (peak 0) are not manifested for low metal concentrations (Figure 7.8 and 7.9a and b). Thus, the f-EM sensors do not resonate at this frequency considering the low metal concentration, as it is < 1 mg/L for all toxic metals and both samples.

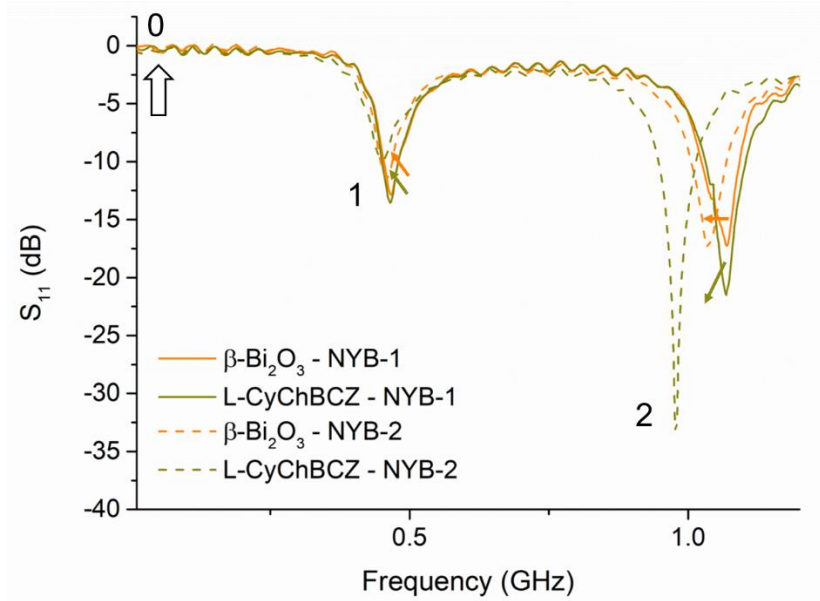


Figure 7.8 Spectral response for the NYB-1 (solid line) and NYB-2 (dashed line) measurement water sites using a f-EM sensor based on β - Bi_2O_3 coating (orange) and a f-EM sensor based on an L-CyChBCZ coating (gold). The respective arrows show the spectral change from higher to lower polluted sample (NYB-1 is more polluted than NYB-2)

As expected, both sensors exhibit a higher dB for the less polluted samples at peak 1. A more clear comparison between each of the sensors and the sample is shown in Figure 7.9a for the f-EM sensor based on β - Bi_2O_3 , and in Figure 7.9b for the f-EM sensor based on L-CyChBCZ. The β - Bi_2O_3 was able to distinguish between the two samples at both peaks, at 0.47 and 1.03-1.07 GHz). Although, a change in resonant frequency with the same amplitude (~ -18 dB), but at a diverse resonant frequency, is manifested at peak 2, between 1.03 and 1.07 GHz.

If the response between these two samples and the f-EM sensors based on β - Bi_2O_3 is compared with the two highly polluted PM sites, especially with PM-1, it is important to consider the spectral response in its entirety. The main difference is notable at peak 0. In point of fact, between the NYB-1 and PM-2, which have different water chemistry, the main difference is given by the amplitude shift (-4 dB) for PM-2 at 50 MHz.

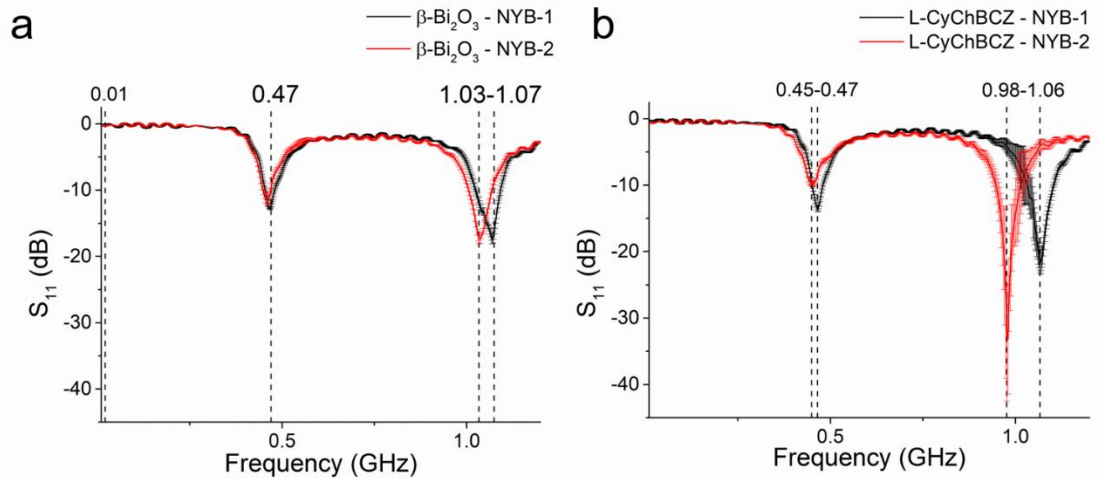


Figure 7.9 Comparisons between NYB-1 (black) and NYB-2 (red) *in situ* measurements with SD using the f-EM sensor based on $\beta\text{-Bi}_2\text{O}_3$ (a) and L-CyChBCZ (b)

Consequently, in this work, the necessity to consider all the resonant peaks in the spectral response for characterising complex water samples, and not only the specific magnitude as S_{11} at a selected frequency, has been demonstrated.

The f-EM sensor based on the L-CyChBCZ coating (Figure 7.9b) was able to distinguish with higher amplitude (higher dB), manifesting also a frequency shift, between the two NYB samples, at both peaks 1 and 2, respectively at 0.45-0.47 GHz and 0.98-1.06 GHz. These *in situ* trials demonstrated the benefit of combining diverse f-EM sensors for obtaining a more specific response between differently polluted mining-impacted water samples. For this reason, NYB-2 was selected as a water site for *in situ* continuous testing of the f-EM sensor array. The combined S_{11} responses and their SD of this field measurement are illustrated in Figure 7.10 in the frequency range 0.01-2.5 GHz. For straightforwardness, also in this instance, colours in the graph correspond to “coatings colour” (except for M10). It is observable how all sensors, except the lacquered one, resonate for peak 1 at about 0.44-0.47 GHz. Peak 2 is produced between 0.66 and 1.29 GHz, showing differentiation of frequency detection with all f-EM sensors.

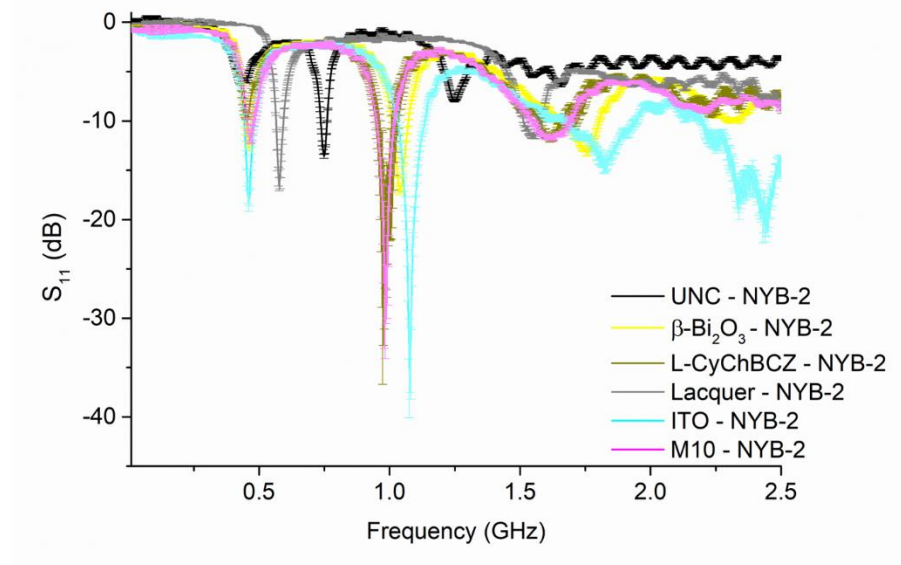


Figure 7.10 Reflection coefficient spectral response and SD using various f-EM sensors (as f-EM sensor array) for *in situ* measurements of the sample NYB-2 using a miniVNA tiny

For a detailed and punctual description of the spectral responses, they were fitted using the Lorentzian function. For every f-EM sensor, 1 to 6 resonant peaks were identified, with the purpose i) to characterise the spectral response in its entirety using multiple peaks and ii) to analyse various peak properties, including the centre of the peak (x_c), its intensity (H), its full width at half maximum (w) and the area of the peak (A) (Figure 7.11a-d). The combination of the response from diverse sensors as an array, offers dimensions to observation, helping to evaluate more parameters and improving the estimation performance. In addition, the combination of more peak parameters for every sensor can help to classify with higher precision the quality of the water under test. Specifically, the x_c (Figure 7.11a) illustrates the resonant frequency of each of the 6 peaks, which is more marked at peak 2, with a shift for the lacquered coating at peak 1. w and A (Figures 7.11b and c), which are not commonly analysed for microwave measurements, do not follow the same pattern of the other most common measurements, x_c and H (Figures 7.11a and d, which represent the resonant frequency and the

amplitude), suggesting that they can offer more details and the ability to quantify water quality with higher precision.

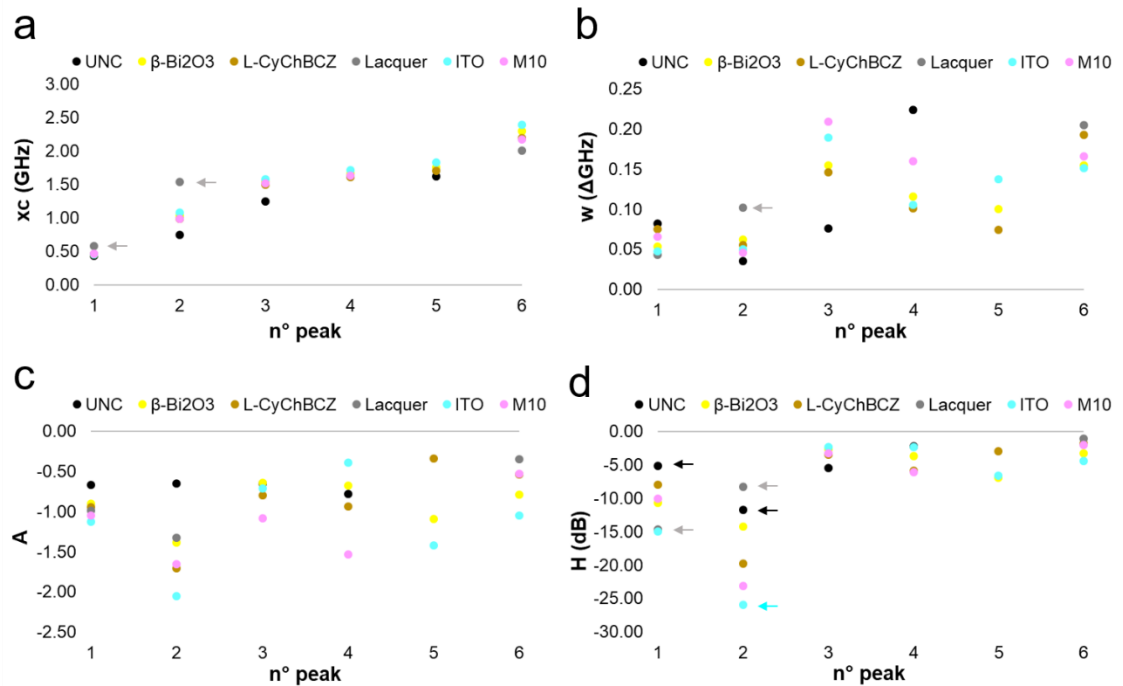


Figure 7.11 Peak parameters, xc (a), w (b), A (c) and H (d) analysed using a Lorentzian peak fitting function of the S_{11} responses of *in situ* measurement of the NYB-2 site using a miniVNA tiny. As the previous graph, colours in the graph corresponds to “coatings colour” (except for M10)

The H varies for all sensors, and it is notable how the uncoated and lacquered sensors have a much lower dB than the f-EM sensors based on both metal oxide based and chelating polymer mixtures. The combination between the various sensors’ response, multiple peaks and multiple peak’ parameters can offer an advanced understanding of the sample. More comparisons between sensors and water samples are described in the following section.

7.3.2.4 Leadhills mine

Water in Leadhills mine area was measured *in situ* using a lacquered sensor (WW-A) and on-site using an uncoated sensor, and f-EM sensors based on β -Bi₂O₃ and L-CyChBCZ in September 2019. This area suffers mostly from Zn contamination (109-273 μ g/L) and

circumneutral pH (7.4-7.5) (Appendix 3 and 4). Results are illustrated in Figure 7.12 and follow the same pattern of the previously described *in situ* measurements and are compared successively.

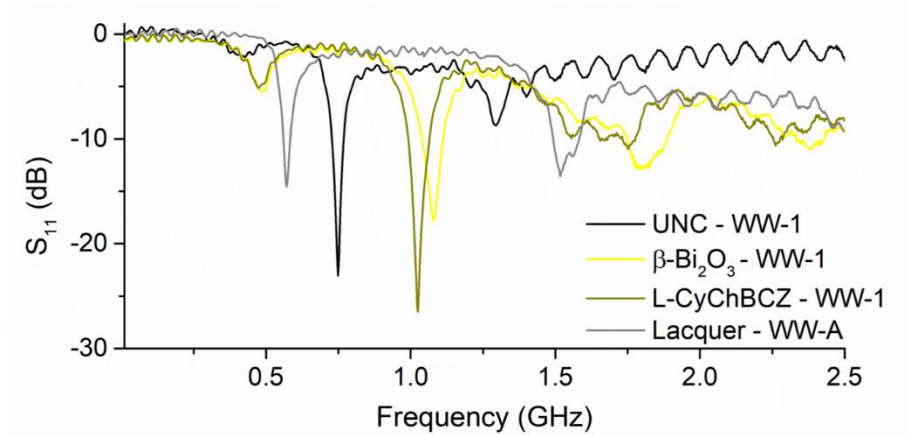


Figure 7.12 *In situ* response for WW-1 and WW-A using various sensors

7.3.2.5 Other *in situ* trial measurements

The described results have demonstrated the feasibility to detect and distinguish between contaminated waters from mining areas using various microwave sensors, both uncoated and functionalised, assessing the possibility to detect unexpected variation in water quality in real-time and at low cost. Considering the infeasibility to measure *in situ* “unexpected” increases of toxic metal contamination in water and the return to the baseline spectrum when the concentration decreases using microwave sensors, this was experimented using a slug salt injection.

7.3.2.5.1 Results from a slug injection trial

After having evaluated the feasibility to detect changes in “salt”, such as NaCl and NaBr, using planar microwave IDE sensors in laboratory analysis with non-portable and portable VNAs, and sensors probing the water, a field trial was performed in the Nant

Cwmnewyddion (Wemyss mine) for measuring the “unexpected” variation of a water parameter and the return to the baseline spectrum.

For this experiment, performed in July 2018, 250 g of NaCl was dissolved in 10 L of river water ($T= 20^{\circ}\text{C}$). Its EC measured in the bucket was 36.6 mS/cm. This solution was “gulp” injected in the river and *in situ* measurements were performed ~100 m downstream (as was illustrated in Figure 4.30) using i) a conductivity meter and ii) a lacquered sensor connected to a mini VNA tiny and using a laptop as the output device. Measurements were performed every 5 seconds with both sensing devices for 27 minutes. The selected part of the spectral responses, between 0.45 and 0.70 GHz is illustrated in Figure 7.13a, which comprises of 325 S_{11} measurements (every 5 sec for 1,650 sec); 0.565 GHz is the frequency that has been selected as able to monitor continuously the variation of “salt in water”. The S_{11} response by time at 565 MHz is plotted in Figure 7.13b. The back dots in the graph are some selected instants where data are compared with EC and NaCl in Table 7.1. The NaCl concentration was measured successively using correspondence measurement between EC and g/L of salt in the lab with calibration curves developed on the same water samples. The variation of the salt concentration matches with both EC and S_{11} parameter, which is in line with the increase and decrease of the salt concentration at each instant. The S_{11} increases with the increase in EC and salt concentration.

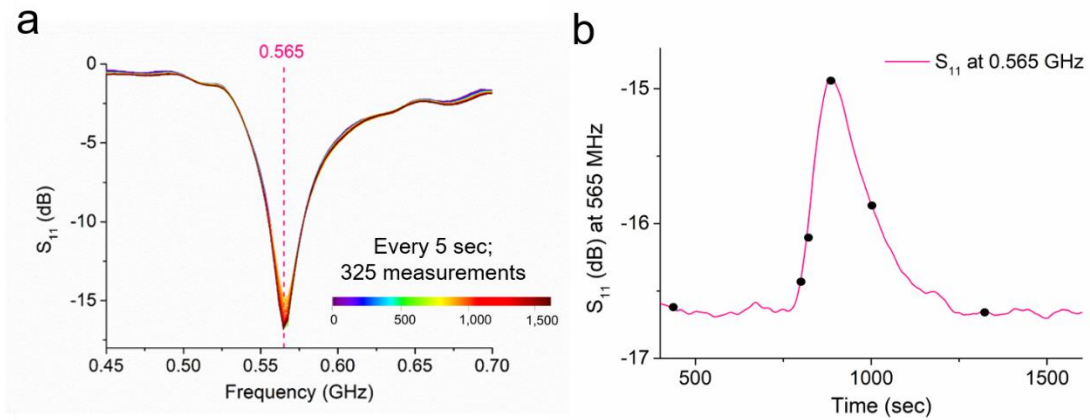


Figure 7.13 Results from an experimental trial of a slug injection of NaCl using a lacquered sensors probing the Nant Cwmnewyddion water measured every 5 seconds for 1,625 sec (27 minutes), demonstrating the feasibility of measuring *in situ* and in real-time the variation in a water parameter (a); the variation in the S_{11} response at 0.565 GHz by time and its return to the baseline once the concentration decrease (b)

This experiment has demonstrated the feasibility to measure the “unexpected” variation of a water parameter and its return to the baseline spectrum using microwave technology and planar sensors. The development of a sensing platform that is able to detect both NaCl and toxic metals variations in complex catchments can provide strong support for researchers that work on fully characterising polluted areas and set priorities for remediation actions (Mayes et al, 2009). Using microwave measurement for real-time variations in both flow and metals could help to successfully manage polluted areas, in the UK and worldwide.

Table 7.1 Variation of EC and S_{11} signal by time due to change in salt *in situ* and in real-time and the return to the baseline spectrum. NaCl was successively measured by applying conversion equations.

Time (sec)		EC ($\mu\text{S}/\text{cm}$)	S_{11} at 565 MHz (dB)	NaCl (mg/L)
0	baseline	113.6	-16.60	0
780	salt detected	124.2	-16.43	0.004
820	salt increasing	235	-16.08	0.005
880	peak of salt	379	-14.93	0.131
995	decrease of salt	226	-15.86	0.056
1,320	return to the baseline	110.0	-16.65	0

7.3.3 Comparisons between mining-impacted water

Multiple f-EM sensors were able to measure and distinguish between waters in various mining areas around the UK, *in situ* and in real-time. Despite this, considering the complexity of the analysed mining-impacted water samples, which contained a mixture of various metal concentrations, such as Zn, Cu, and Pb and the variation in other water parameters, there was not an identical correspondence between sensor output from the laboratory and the *in situ* measurements. Consequently, there was not the possibility to fit data in the previous calibration curves, although the samples follow the same trend. Consequently, an inverse relationship between pollution level and quantification was performed, by comparing the microwave response using multiple f-EM sensors and their combined response for samples from different mining areas.

Summarising, generalised “contamination” level of each polluted water sample from the four surveyed mining areas (Appendices 3 and 4) can be represented as follows:

- **Wemyss mine:** FA > MR > NC
- **Parys Mountain mining district:** PM-2 > PM-1 > PM > PM-W
- **Nant y Mwyn mine:** NYB-R > NYB-1 > NYB-2
- **Leadhills mine:** WW-1 > WW-A

The contamination level by area instead can be generalised, from most to least polluted as:

- Parys Mountain > Wemyss > Nant y Mwyn > Leadhills.

Mining-impacted waters that were previously measured *in situ*, have been collected and analysed in the laboratory using all the developed f-EM sensors, for performing comparisons by reducing possible errors, given by temperature and sample volume, for example. Also, the ZVA24 is able to give a more detailed response than the cheap and portable miniVNA tiny.

7.3.3.1 *In situ* measurements comparisons: an overview

In situ microwave measurements performed with various f-EM sensors are compared for evaluating the possibility of differentiating between contaminated samples and consequently for prioritising remediation actions. For this purpose, spectral responses were fitted using the Lorentzian peak function.

7.3.3.1.1 Uncoated sensors

Uncoated sensors were able to qualify and differentiate mining-impacted waters *in situ*. As previously assessed, the uncoated sensors at 10 MHz (peak 0) is able to detect high metal concentrations (Figure 7.14).

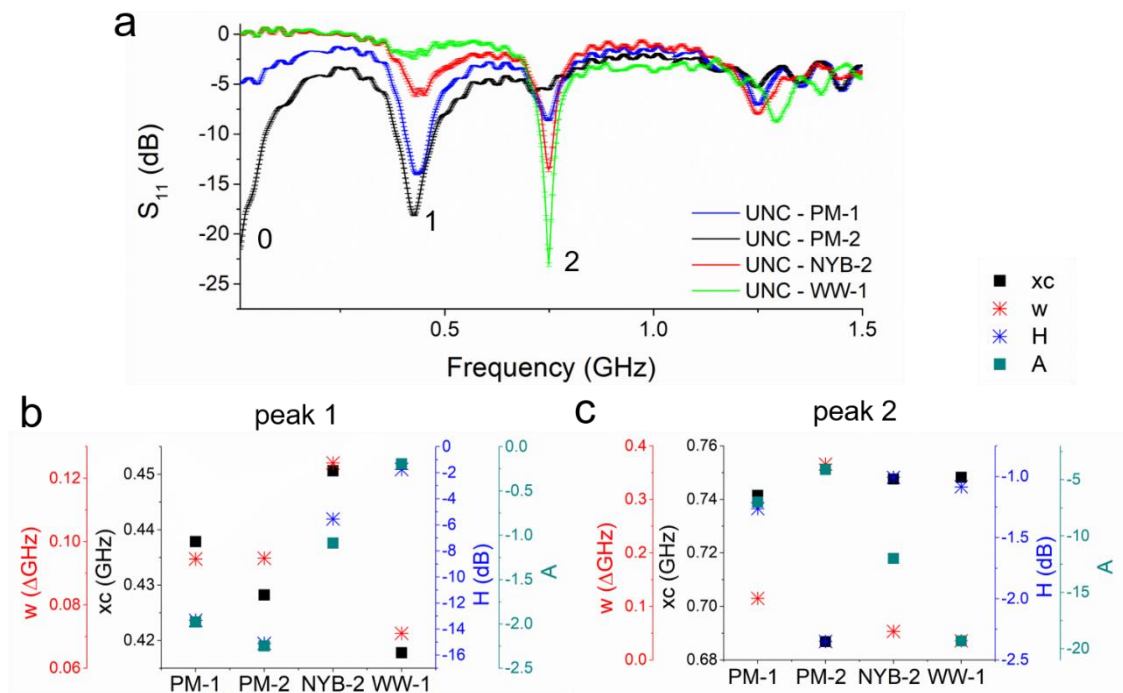


Figure 7.14 *In situ* comparisons between different areas using uncoated sensors probing the water (a) and their peak parameters comparisons at peak 1 (b) and 2 (c)

The sensor resonates at this frequency only for the samples analysed at Parys Mountain mining district, which suffers from severe contamination, with PM-1 with 12.5 mg/L of Zn and 13.5 mg/L and PM-2 with 7.0 and 25.0 mg/L of Zn and Cu, respectively. Also,

both have a high concentration of Pb, Cu, Fe and Mn. The responses for peaks 1 and 2, reflect the principle previously assessed: lower dB at peak 1, corresponds to the higher concentration; lower dB at peak 1 corresponds to lower concentration. The results shown in these graphs follow the contamination level in the samples: PM-2 > PM-1 > NYB-1 and WW-1. Peak parameters at these two peaks (respectively in Figure 7.14b and c) follow this pattern for the uncoated sensors.

7.3.3.1.2 F-EM sensors based on β -Bi₂O₃ coatings

The f-EM sensors based on β -Bi₂O₃ coatings were able to measure *in situ* mining-impacted water. This sensor resonates at peak 0 only for extremely high concentrations (PM-2) (Figure 7.15a). At peaks 1 and 2, which slightly shift depending on the sample analysed (Figure 7.15a and b), the integration of more peaks and their parameters (Figure 7.15c and d) can help to characterise more specifically the water under test. Although, some analysed samples (as PM-1) give an unexpected response if compared with the other samples and their concentrations, with higher amplitude (H), it is not the most polluted sample as expected. The cause of this can be the high presence of particulate and iron oxide in the water (Appendix 2b). Although, for PM-2 the spectral response shift to lower dB, shows the importance of analysing more parameters and not only a singular peak, which can be deceptive. Also, NYB-1 and NYB-2 samples, show a different resonance at both peaks, with a different H at peak 1 and a similar H at peak 2 at a diverse xc. In agreement, the WW-1 sample, being less polluted, presents a higher dB at peak 1, but a similar dB at peak 2 with other samples but a diverse frequency, allowing more specific classification of the sample.

This sensor offers the opportunity to differentiate between different samples by combining the response at various frequencies and using multiple peaks features.

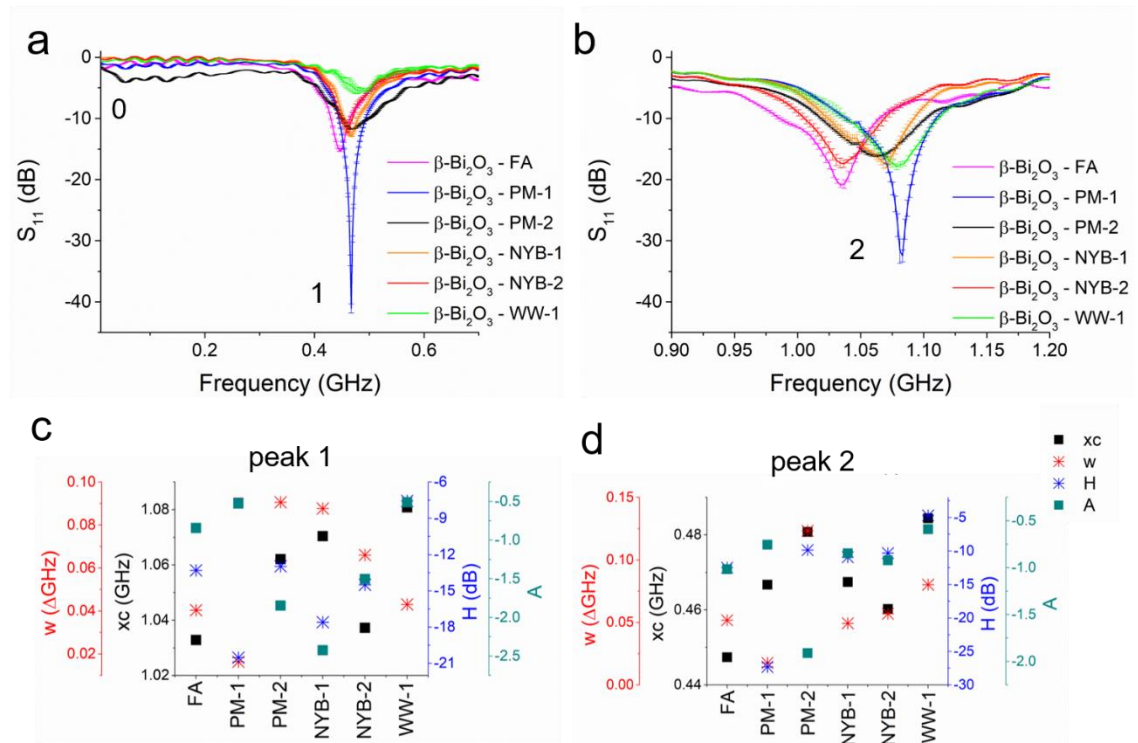


Figure 7.15 *In situ* measurements comparison using f-EM sensors based on β - Bi_2O_3 coatings in various sites (a and b) and their peaks parameters comparisons at peak 1 (c) and 2 (d)

7.3.3.1.3 F-EM sensors based on L-CyChBCZ coatings

The L-CyChBCZ based f-EM sensors were demonstrated as being able to distinguish between low concentrations of Cu and Zn. Though, for complex water, it is more challenging to quantify specifically the metal concentration in mining-impacted water (as was described in Chapter 6).

This sensor is able to distinguish *in situ* between high and low polluted water (Figure 7.16a and b). As the β - Bi_2O_3 coating, spectral response for extremely polluted water (PM-2) shift at lower dB; lower sample concentrations are better described and peak 1 shows a linear pattern for WW-1, NYB-2 and NYB-1, from higher to lower dB with increasing contamination, as expected from previous experiments. At peak 2, more defined peaks with a lower dB can be distinguished for lower concentrations, with both shift in frequency and amplitude, demonstrating that this sensor can be more useful for

distinguishing lower contaminated samples, as those analysed in Nant y Mwyn and the one from Leadhills mines. The integration of the other peaks' parameters can give a more detailed description of the peaks, helping to characterise differently polluted waters. For example, the WW-1 samples, being less polluted, present a lower w at both peaks compared with the other samples.

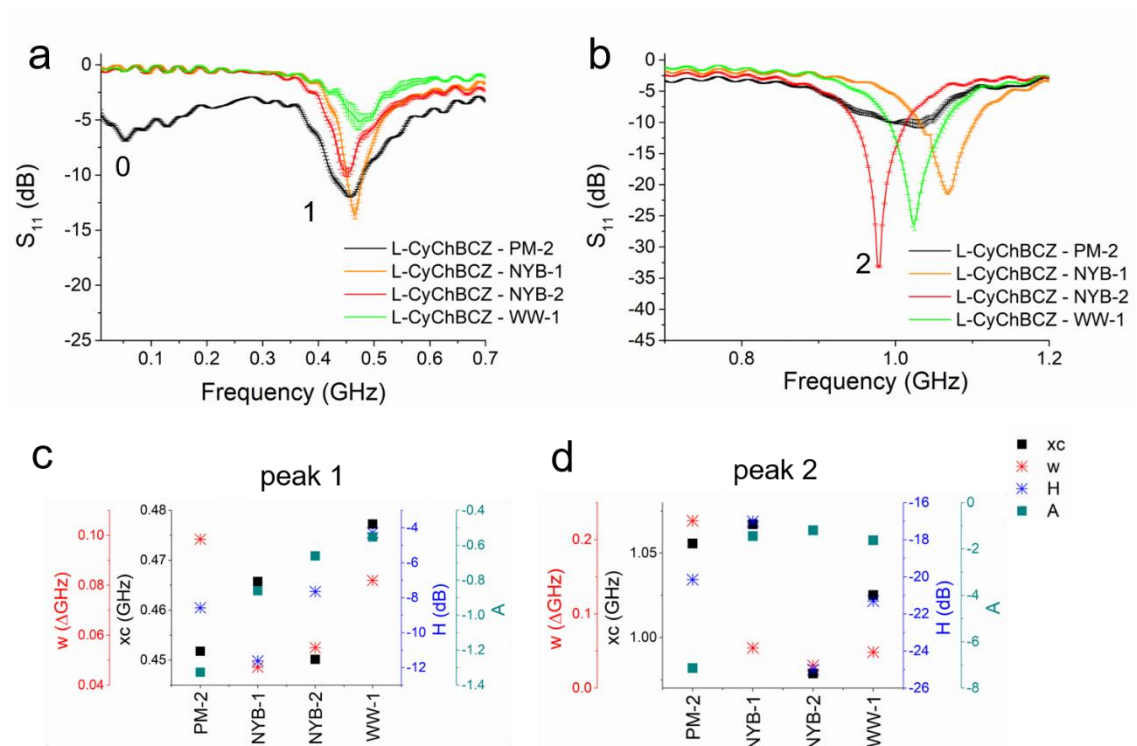


Figure 7.16 *In situ* analysis comparisons using f-EM sensors based on L-CyChBCZ coatings (a and b) and their peaks parameters (c and d)

7.3.3.1.4 Lacquered sensors

The lacquered sensor was poor at differentiating between samples compared with the other sensors (Figure 7.17a). The differentiation between contaminated samples from diverse mining areas is minimum at peak 1, and unclear at peak 2, although this sensor is protected with a coating which can be advantageous for monitoring unexpected variation in a water parameter, as demonstrated by the slug injection of salt.

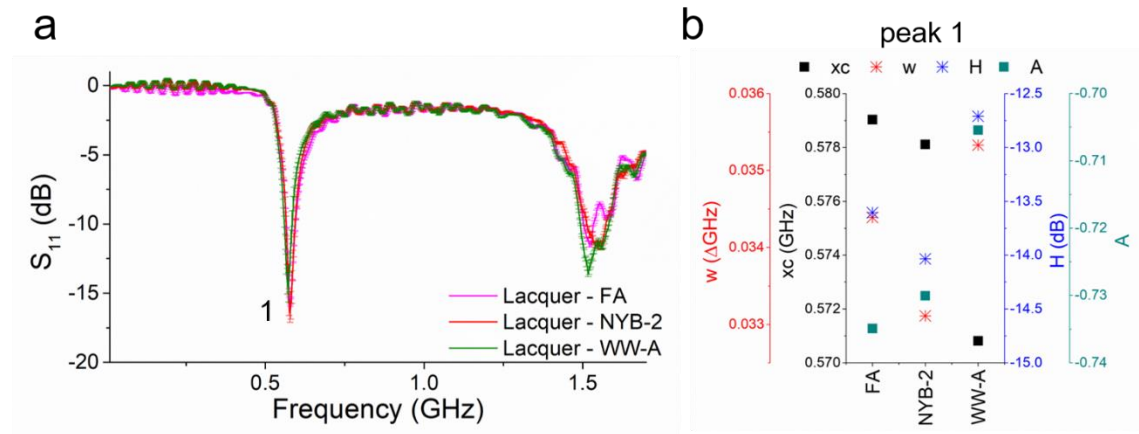


Figure 7.17 *In situ* analysis using a lacquered sensor (a) and the description of the peak 1 (b)

7.3.3.1.5 F-EM sensors based on ITO coatings

The ITO based sensor should replicate a similar output of the β -Bi₂O₃ sensors. The sensing output produced for the PM-2 sample follows a similar behaviour if compared to the one produced by the other f-EM sensors. Consequently, high concentrations are well detected with all sensors. For low concentrations and multiple metals, the situation is a bit different. As shown in Figure 7.18 a and b, this sensor was able to measure all mining-impacted water, producing a specific and different peak with different features at peak 1 and 2 (Figure 7.18c and d). Specific parameters are identified for various samples from different mining areas, giving more data for describing different samples, as the amplitude alone is not sufficient for specifically quantifying each metal in the water. Although, the combination of the response of multiple f-EM sensors, as the f-EM sensor array, can guarantee a tool for classifying and prioritising polluted water in mining areas, *in situ* and in real-time.

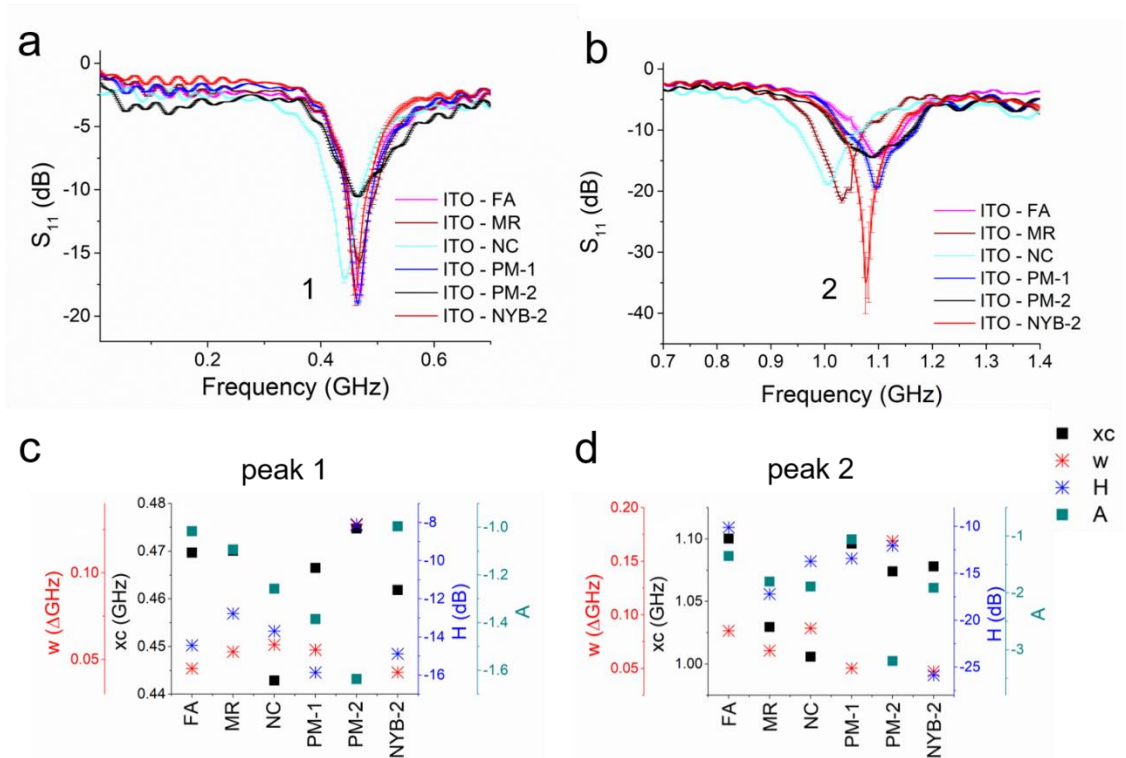


Figure 7.18 Sensing output of the f-EM sensor based on ITO for *in situ* measurements (a and b) and peaks features comparisons (c and d)

7.3.3.2 Laboratory comparisons

The mining-impacted waters that were analysed *in situ* using f-EM sensors (summarised in Appendices 3 and 4) and the miniVNA tiny were then analysed in the laboratory using the ZVA 24, at constant temperature ($19.0 \pm 0.2^\circ\text{C}$). Results are illustrated in Appendix 5a (for Parys Mountain mining-water samples) and 5b (for the other three mining sites), using the developed sensors: uncoated, and f-EM sensors based on $\beta\text{-Bi}_2\text{O}_3$, L-CyChBCZ, lacquered, ITO and M10 (respectively in a-f). Some variation in the spectral response was assessed, probably caused by 1) the variation in T; 2) the imprecise response given by the miniVNA tiny; 3) other particles in the water; 4) variation in the water volume.

7.3.3.3 Summary of *in situ* measurements

In this work, *in situ* microwave measurements were performed for the first time in freshwater in mining-impacted catchments. Although the response of quantifying the single metal concentration in complex water by directly probing water, was imprecise:

- Each f-EM sensor was able to differentiate between the contamination severity in various polluted sites around the UK, offering the feasibility of prioritising specific sources that pose a risk to the environment.
- The combined response of various f-EM sensors and the multiple peak analysis can offer a more specific characterisation of water resources, *in situ* and in real-time.

Array-based sensing platforms have arisen as promising alternatives due to their simple fabrication, adaptability, flexibility and analysis (Huang et al, 2019). This is due to the use of a series of cross-reactive sensors, and each one gives a specific response for the analysed sample. Subsequently, the combined response can offer a more specific description of the sample under test. This novel successful approach based on the integration of functional material onto planar sensors will help to characterise with higher specificity different impacted waters, more accurately than using a single and simple microwave structure.

This work offers the basis for the further development of specific f-EM sensors which can classify and compare *in situ* and real-time polluted mining-impacted water. The sensing platform can then be coupled with appropriate wireless hardware, enabling remote operation in mining-affected rivers for true online monitoring (Tanguy et al, 2020b).

7.4 Discussion of overall results and implications

The results described in the three *Results and discussion chapters* (5, 6 and 7) show the ability and limitations of using microwave spectroscopy and f-EM sensors for water quality testing. The use of sensor arrays (or electronic tongue) for toxic metal analysis has been demonstrated to be an interesting alternative to address the challenge of simple operation, low-cost, fast response and adaptation for *in situ* analysis (Shimizu et al, 2019). This research leads the way towards the advent of a new generation of water quality sensors, which can be i) compact, ii) cost-effective for mass-production, iii) distributed over vast and remote polluted bodies of water; iv) passive to reduce maintenance cost; v) flexible to be adapted for modification on a particular purpose for a specific pollutant, increasing selectivity and sensitivity.

In this work, progresses in microwave spectroscopy for liquid sensing are described using a novel approach based on planar microwave sensors, material integration, adaptation for probing water and spectral response analysis for monitoring toxic metals. This is a fast-evolving field which is expected to grow exponentially due to constant advances in sensors and materials fabrication, and signal analysis (Yaroshenko et al, 2020). As with microwave gas sensing (Li et al, 2019), important features such as selectivity, sensitivity and long term stability are not yet satisfactorily reported for water quality contaminants in collected water samples. Mostly, researchers worldwide have demonstrated the differentiation between laboratory prepared liquid samples (mostly % mixtures water/alcohol) due to permittivity variations and consequent frequency shift, combining simulations and experiments at room temperature, obtaining selectivity in separated samples (Mohammadi et al, 2020b; Salim et al, 2018; Tanguy et al, 2020a), as initially experimented in this work. The development of chemical sensors based on metal oxides has also been proved to change the sensitivity and selectivity for detection in the liquid

phase (Devi et al, 2020), and be integrated on novel real-time technologies, as microwave sensing. Water quality sensors are required to operate without a reference electrode and work completely in the solid-state for being good candidates for continuous monitoring (Zubiarrain-Laserna & Kruse, 2020)

Data analysis is another relevant factor for assessing selectivity and sensitivity using microwave sensing. Multiple peaks analysis and multiple peaks' parameters in the microwave response at selected frequency ranges, as experimented for the first time in this work, has been shown to be advantageous for evaluating the specificity of the response for a particular sample under test, *in situ* and in real-time. A similar approach was used by Kovacs et al (2016) using near-infrared spectroscopy which analysed water spectral patterns as biomarkers of water quality to provide quick information about qualitative changes in water. Other researchers, have used PCA for classifying hazardous materials in liquid (Ozturk, 2019) and discriminated between organic and inorganic materials (Harnsoongnoen et al, 2018). In the future, it would be interesting to integrate PCA with the f-EM sensors.

Recently, Vélez et al (2019) evaluated one of the f-EM sensors developed in this work, based on β -Bi₂O₃ and published by Frau et al (2019a), as the sensor that shows the highest sensitivity and resolution, compared to other microfluidic sensors. This is probably due i) to the direct contact between the sample and the coating, and the vicinity of the EM waves, and ii) the interaction between the Zn ions and the coating material, which changes the total permittivity of the structure. The integration of a microfluidic channel reduces the sensitivity of the liquid under test. The successful action of directly probing a microwave sensor in water and the use of a cheap and portable VNA, as demonstrated in this work, was also assessed by Reyes-Vera et al (2019).

This research has contributed novel results for accomplishing innovative devices based on microwave spectroscopy, for *in situ* and real-time monitoring of water resources. F-EM sensors can be used in the real environment and can offer a low-cost solution to monitor specific changes in water quality.

7.4.1 Future strategies for effective applicability

This novel methodology offers the potential to reduce analytical costs by combining wireless sensing systems to provide continuous, *in situ* remote monitoring, thus facilitating the targeted treatment of mining-affected waters. The f-EM sensors can be connected using a microcontroller-based system for measuring S_{11} and analysing the data. Then, results can be integrated with “risk-ranking”, for ranking mining-impacted freshwater that threatens the environment (Donnachie et al, 2014).

The functionalised microwave sensors presented in this work can be the prototype for a smaller, portable, online system capable of monitoring pollution in mining areas. This sensing technology could provide continuous verification of water quality and safety, and provide immediate warning of contamination variations or water quality guideline threshold breaches. It could also offer the ability for *in situ*, real-time monitoring and reporting of water quality over large, remote geographical areas.

Moreover, a dense wireless system of sensors can be deployed in mining-impacted catchments offering the potential to reduce these costs considerably, as well as provide more useful, continuous monitoring capabilities by giving an accurate idea of the changes in water quality in real-time. Developed sensors can provide early warning of contamination variations during storm events and track pollutants’ movements through the system. In this way, the major source of contaminants and how metals behave and react alongside a river can be understood in real time, *in situ* and at low cost.

7.5 Overall summary and implications

This work demonstrates the ability to use microwave planar sensors integrated with functional materials for *in situ* monitoring of water quality in mining-impacted water. The S_{11} response of various f-EM sensors (as an f-EM sensor array) was evaluated for obtaining a more specific response of water samples under test, by analysing differences in resonant peaks between different sensors and their amplitude.

F-EM sensors were tested *in situ*, by probing the sensing device directly in the water, using a portable VNA and a laptop or a smartphone as the output devices. Four mining areas were selected for the field testing: Paris Mountain (extremely polluted), Wemyss, Nant y Mwyn and Leadhills mines. Each sensor was able to give a specific response dependent on the water composition. Spectral responses were analysed using Lorentzian peak functions for multiple peak analysis and multiple peaks parameters (x_c , w , H , A) for better differentiation between samples from the same and different areas.

The potential of using microwave spectroscopy and various f-EM sensors for classifying and prioritising polluted water was assessed, *in situ* and in real-time.

Chapter 8 Conclusions

This work describes a novel strategy that has been researched, developed and tested to meet the challenge of detecting real-time variations of toxic metals contamination in mining-impacted waters, at low-cost and *in situ*. Currently, no method can guarantee continuous monitoring of water resources and evaluate real-time changes in water quality. Microwave spectroscopy is a low-cost sensing technology which allows a real-time and inexpensive response as soon as a material is in contact with the EM waves through a sensing structure.

In this work, novel f-EM sensors were researched, formulated, developed, by integrating screen-printed thick films (coatings), based on mixtures of metal oxides and chelating polymers, onto already developed planar microwave sensors, with the aim to monitor toxic metals in mining-impacted water at low-cost.

The first objective (O1) was accomplished in Chapter 5, which describes the improved performance of the developed f-EM sensors for measuring a small volume (400 μ L) of laboratory-prepared solutions of Pb, Zn and Cu on the sensing structure. F-EM sensors based on β -Bi₂O₃ and L-CyChBCZ provided improved sensitivity, especially for detecting low concentrations of Zn and Cu, respectively, thanks to the interaction between the coating materials and the metals under test, and the consequent change in the microwave response at specific frequencies.

The second objective (O2) was achieved in Chapter 6, which describes the successful action of the adapted sensing structure for directly probing complex water samples (40 mL) for measuring changes in Cu and Zn concentration. The f-EM sensors based on L-CyChBCZ coating was able to measure changes in concentration of a collected mining-impacted water sample (Frongoch adit) that was spiked using the standard addition method, reaching a higher sensitivity and selectivity compared with the uncoated sensor.

Also, the f-EM sensor based on an L-CyChBCZ coating was able to distinguish between collected polluted samples, although the desired selectivity and sensitivity was not achieved in complex mining-impacted waters with different concentrations of various toxic metals.

The third objective (O3) was attained in Chapter 7, which describes the microwave response of various f-EM sensors for *in situ* measurements using a portable VNA (a mini VNA tiny) in four mining-impacted catchments in the UK: Parys Mountain mining district, Wemyss mine, Nant y Mwyn mine and Leadhills mine. F-EM sensors were able to differentiate between polluted samples, from the same and different mining areas. The response of multiple f-EM sensors (as an f-EM sensor array) is beneficial for a more specific characterisation, qualification and prioritisation of polluted water. Although, more research is necessary for achieving a higher selectivity in complex water samples.

Summarising, this work has demonstrated for the first time:

- The feasibility of using microwave spectroscopy for characterising different toxic metal concentrations in mining-impacted water;
- The feasibility of using planar IDE sensors functionalised with thick films (f-EM sensors) for a more specific qualification and quantification of toxic metals in water;
- The practicability of characterising *in situ* different polluted water, in the same or diverse mining areas using multiple developed f-EM sensors (as f-EM sensors array);
- A novel approach for data analysis, using both multiple peaks analysis and multiple peaks' parameters.

In conclusion, microwave spectroscopy and f-EM sensors can help to monitor, identify, characterise and prioritise freshwater quality.

8.1 Limitations of the research

More work is needed to ensure that f-EM sensors are robust and reliable enough to be adopted for effective *in situ* monitoring and for being integrated in the national monitoring water system. This requires novel strategies to uniquely identify and quantify toxic metals in complex water, and sensing materials able to introduce the desired impedance change when under the influence of the target stimulus (Mc Gee et al, 2019).

The f-EM sensors are able to detect with higher sensitivity and selectivity toxic metals in water compared with the uncoated sensors. Although, the interaction time and the saturation of the coatings are a limitation for continuous monitoring, which can be performed by the uncoated sensors. Consequently, the uncoated sensors can be integrated in the national monitoring system, and the f-EM sensors can be used for measuring more specifically *in situ* the water contamination at selected water point.

8.2 Recommendations for future research

More research and data are necessary for the successful deployment of the f-EM sensor array *in situ*, and for evaluating the causes of each interference and the durability of the coatings in the real environment. More experiments and data are also necessary for integrated peak features on the correlation between metal ions and the reflection coefficient.

The interaction between coatings and metals requires further investigation, using more sensitive instrumentation such as XPS. The durability and degradability of the coatings in the real world also requires further research.

8.2.1 Study of interferences

Additional work is required to evaluate and correlate changes with the water composition to further understand the effect of real water samples on the coating and its interaction with toxic metals. Particularly, it will be necessary i) to evaluate the different microwave responses for free and complexed metals, ii) to qualify and quantify the interference in the spectral response due to other inorganic and/or organic material in water, and iii) to measure and correct changes caused by temperature variations. For example, it is particularly important to investigate the response for iron, and evaluate the difference between +2 or +3 form.

Possible interferences need to be studied due to the common constituents of mining-impacted waters. These include the comparison of the sensing response with other metals, low pH, and sulphate concentration. Also, the variation of the sensing response has to be investigated by adding singularly various metals or other element/ions, one by one, for measuring variation of the sensing response caused by each factor.

References

- Abbasi, Z., Niazi, H., Abdolrazzagli, M., Chen, W. & Daneshmand, M. (2020) Monitoring pH Level Using High-Resolution Microwave Sensor for Mitigation of Stress Corrosion in Steel Pipelines. *IEEE Sensors Journal*, 20(13), 7033-7043.
- Abrahamyan, T., Khachatryan, R., Hambaryan, D., Hovhannisyan, B., Minasyan, B., Odabashyan, L. & Babajanyan, A. (2019) Investigation of Ag Nanoparticles/Water Solutions by Microwave Stripline Sensor. *Journal of Contemporary Physics (Armenian Academy of Sciences)*, 54(2), 196-202.
- Adhikari, K. K., Wang, C., Qiang, T. & Wu, Q. (2019) Polyimide-derived laser-induced porous graphene-incorporated microwave resonator for high-performance humidity sensing. *Applied Physics Express*, 12(10), 106501.
- Afsarimanesh, N., Mukhopadhyay, S. C. & Kruger, M. (2018) Performance Assessment of Interdigital Sensor for Varied Coating Thicknesses to Detect CTX-I. *IEEE Sensors Journal*, 18(10), 3924-3931.
- Agency for Toxic Substances and Disease Registry (2004) *Toxicological profile for Copper*, [eBook]. Atlanta, GA: U.S. Department of Health and Human Services, Public Health Service.
- Agency for Toxic Substances and Disease Registry (2017) *ATSDR's Substance Priority List*.
- Al-Kizwini, M. A., Wylie, S. R., Al-Khafaji, D. A. & Al-Shamma'a, A. I. (2013) The monitoring of the two phase flow-annular flow type regime using microwave sensor technique. *Measurement*, 46(1), 45-51.
- Alderton, D. H. M., Serafimovski, T., Mullen, B., Fairall, K. & James, S. (2005) The Chemistry of Waters Associated with Metal Mining in Macedonia. *Mine Water and the Environment*, 24(3), 139-149.
- Ali, H., Khan, E. & Ilahi, I. (2019) Environmental Chemistry and Ecotoxicology of Hazardous Heavy Metals: Environmental Persistence, Toxicity, and Bioaccumulation. *Journal of Chemistry*, 2019, 6730305.
- Altenburger, R., Ait-Aissa, S., Antczak, P., Backhaus, T., Barceló, D., Seiler, T.-B. & et al. (2015) Future water quality monitoring — Adapting tools to deal with mixtures of pollutants in water resource management. *Science of The Total Environment*, 512, 540-551.
- Amirian, M., Karimi, G., Wiltshire, B. D. & Zarifi, M. H. (2019) Differential Narrow Bandpass Microstrip Filter Design for Material and Liquid Purity Interrogation. *IEEE Sensors Journal*, 10.1109/JSEN.2019.2932693, 1-1.

- Andria, G., Attivissimo, F., Di Nisio, A., Trotta, A., Camporeale, S. M. & Pappalardi, P. (2019) Design of a microwave sensor for measurement of water in fuel contamination. *Measurement*, 136, 74-81.
- Aragay, G. & Merkoçi, A. (2012) Nanomaterials application in electrochemical detection of heavy metals. *Electrochimica Acta*, 84, 49-61.
- Aragay, G., Pons, J. & Merkoçi, A. (2011) Recent trends in macro-, micro-, and nanomaterial-based tools and strategies for heavy-metal detection. *Chemical Reviews*, 111(5), 3433-3458.
- Ardau, C., Podda, F., Da Pelo, S. & Frau, F. (2013) Stream water chemistry in the arsenic-contaminated Baccu Locci mine watershed (Sardinia, Italy) after remediation. *Environmental Science and Pollution Research*, 20(11), 7550-7559.
- Ateeq, M., Shaw, A., Garrett, R. & Dickson, P. (2017) A Proof of Concept Study on Utilising a Non-invasive Microwave Analysis Technique to Characterise Silver Based Materials in Aqueous Solution. *Sensing and Imaging*, 18(1), 13.
- Awual, M. R. (2019) A facile composite material for enhanced cadmium(II) ion capturing from wastewater. *Journal of Environmental Chemical Engineering*, 7(5), 103378.
- Azmi, A., Azman, A. A., Kaman, K. K., Ibrahim, S., Mukhopadhyay, S. C., Nawawi, S. W. & Yunus, M. A. M. (2017) Performance of Coating Materials on Planar Electromagnetic Sensing Array to Detect Water Contamination. *IEEE Sensors Journal*, 17(16), 5244-5251.
- Bader, M. (1980) A systematic approach to standard addition methods in instrumental analysis. *Journal of Chemical Education*, 57(10), 703.
- Bahoumina, P., Hallil, H., Lachaud, J. L., Abdelghani, A., Frigui, K., Bila, S., Baillargeat, D., Ravichandran, A., Coquet, P., Paragua, C., Pichonat, E., Happy, H., Rebière, D. & Dejous, C. (2017) Microwave flexible gas sensor based on polymer multi wall carbon nanotubes sensitive layer. *Sensors and Actuators B: Chemical*, 249, 708-714.
- Bansod, B., Kumar, T., Thakur, R., Rana, S. & Singh, I. (2017) A review on various electrochemical techniques for heavy metal ions detection with different sensing platforms. *Biosensors and Bioelectronics*, 94, 443-455.
- Barton, J., García, M. B. G., Santos, D. H., Fanjul-Bolado, P., Ribotti, A., McCaul, M., Diamond, D. & Magni, P. (2016) Screen-printed electrodes for environmental monitoring of heavy metal ions: a review. *Microchimica Acta*, 183(2), 503-517.
- Benkhaoua, L., Benhabiles, M. T., Mouissat, S. & Riabi, M. L. (2016) Miniaturized Quasi-Lumped Resonator for Dielectric Characterization of Liquid Mixtures. *IEEE Sensors Journal*, 16(6), 1603-1610.

- Bernou, C., Rebière, D. & Pistré, J. (2000) Microwave sensors: a new sensing principle. Application to humidity detection. *Sensors and Actuators B: Chemical*, 68(1), 88-93.
- Bhatia, M., Satish Babu, R., Sonawane, S. H., Gogate, P. R., Girdhar, A., Reddy, E. R. & Pola, M. (2017) Application of nanoadsorbents for removal of lead from water. *International Journal of Environmental Science and Technology*, 14(5), 1135-1154.
- Boruah, B. S., Gogoi, D. j. & Biswas, R. (2020) Bio-Inspired Finger like Cu-Electrodes as an Effective Sensing Tool for Heavy Metal Ion in Aqueous Solution. *Journal of The Electrochemical Society*, 167(2), 027526.
- Boult, S., Collins, D. N., White, K. N. & Curtis, C. D. (1994) Metal transport in a stream polluted by acid mine drainage—The Afon Goch, Anglesey, UK. *Environmental Pollution*, 84(3), 279-284.
- Bozau, E., Licha, T. & Ließmann, W. (2017) Hydrogeochemical characteristics of mine water in the Harz Mountains, Germany. *Geochemistry*, 77(4), 614-624.
- Brack, W., Dulio, V., Ågerstrand, M., Allan, I., Altenburger, R., Brinkmann, M., ... & Vrana, B. (2017) Towards the review of the European Union Water Framework management of chemical contamination in European surface water resources. *Science of The Total Environment*, 576, 720-737.
- Bruce, G. R. & Gill, P. S. (1999) Estimates of Precision in a Standard Additions Analysis. *Journal of Chemical Education*, 76(6), 805.
- Buchner, R., Barthel, J. & Stauber, J. (1999) The dielectric relaxation of water between 0°C and 35°C. *Chemical Physics Letters*, 306(1), 57-63.
- Byrne, P., Reid, I. & Wood, P. J. (2013) Stormflow hydrochemistry of a river draining an abandoned metal mine: the Afon Twymyn, central Wales. *Environmental Monitoring and Assessment*, 185(3), 2817-2832.
- Byrne, P., Wood, P. J. & Reid, I. (2012) The Impairment of River Systems by Metal Mine Contamination: A Review Including Remediation Options. *Critical Reviews in Environmental Science and Technology*, 42(19), 2017-2077.
- Cases-Utrera, J., Escudé-Pujol, R., Ibáñez-Otazua, N. & Javier del Campo, F. (2015) Development of an Automated Heavy Metal Analyser. *Electroanalysis*, 27(4), 929-937.
- Cashman, S., Korostynska, O., Shaw, A., Lisboa, P. & Conroy, L. (2017) Detecting the presence and concentration of nitrate in water using microwave spectroscopy. *IEEE Sensors Journal*, 17(13), 4092-4099.
- Castillo, E. S. R., Fernandez, E., Aranibar, P. C. & Vargas, D. S. (2018) Metamaterial Inspired Multiband Planar Array to Detect Glyphosate in Water by Real-Time

Electromagnetic Wave Sensor, *2018 IEEE MTT-S Latin America Microwave Conference (LAMC 2018)*. 12-14 Dec. 2018.

Chapin, T. P. (2015) High-frequency, long-duration water sampling in acid mine drainage studies: A short review of current methods and recent advances in automated water samplers. *Applied Geochemistry*, 59, 118-124.

Chatterjee, P. K. & SenGupta, A. K. (2011) Toxic Metal Sensing through Novel Use of Hybrid Inorganic and Polymeric Ion-Exchangers. *Solvent Extraction and Ion Exchange*, 29(3), 398-420.

Chen, T., Li, S. & Sun, H. (2012) Metamaterials Application in Sensing. *Sensors*, 12(3), 2742.

Chu, Z., Peng, J. & Jin, W. (2017) Advanced nanomaterial inks for screen-printed chemical sensors. *Sensors and Actuators B: Chemical*, 243, 919-926.

Chuma, E. L., Iano, Y., Fontgalland, G. & Roger, L. L. B. (2018) Microwave Sensor for Liquid Dielectric Characterization Based on Metamaterial Complementary Split Ring Resonator. *IEEE Sensors Journal*, 18(24), 9978-9983.

Cidu, R. (1996) COMPARISON OF ICP-MS AND ICP-OES IN THE DETERMINATION OF TRACE ELEMENTS IN WATER. *Atomic Spectroscopy*, 17(4), 155-162.

Cidu, R., Frau, F. & Da Pelo, S. (2011) Drainage at Abandoned Mine Sites: Natural Attenuation of Contaminants in Different Seasons. *Mine Water and the Environment*, 30(2), 113-126.

Cui, L., Wu, J. & Ju, H. (2015) Electrochemical sensing of heavy metal ions with inorganic, organic and bio-materials. *Biosensors and Bioelectronics*, 63, 276-286.

Da Pelo, S., Musu, E., Cidu, R., Frau, F. & Lattanzi, P. (2009) Release of toxic elements from rocks and mine wastes at the Furtei gold mine (Sardinia, Italy). *Journal of Geochemical Exploration*, 100(2), 142-152.

Dada, A. O., Olalekan, A., Olatunya, A. & Dada, D. O. (2012) Langmuir, Freundlich, Temkin and Dubinin-Radushkevich isotherms studies of equilibrium sorption of Zn²⁺ unto phosphoric acid modified rice husk. *IOSR Journal of Applied Chemistry* 3(1), 38-45.

De Giudici, G., Medas, D., Cidu, R., Lattanzi, P., Rigonat, N., Frau, I., Podda, F., Marras, P. A., Dore, E., Frau, F., Rimondi, V., Runkel, R. L., Wanty, R. B. & Kimball, B. (2019) Assessment of origin and fate of contaminants along mining-affected Rio Montevecchio (SW Sardinia, Italy): A hydrologic-tracer and environmental mineralogy study. *Applied Geochemistry*, 109, 104420.

De Giudici, G., Pusceddu, C., Medas, D., Meneghini, C., Gianoncelli, A., Rimondi, V., Podda, F., Cidu, R., Lattanzi, P., Wanty, R. B. & Kimball, B. A. (2017) The role of natural biogeochemical barriers in limiting metal loading to a stream affected by mine drainage. *Applied Geochemistry*, 76, 124-135.

Dean, A. P., Lynch, S., Rowland, P., Toft, B. D., Pittman, J. K. & White, K. N. (2013) Natural wetlands are efficient at providing long-term metal remediation of freshwater systems polluted by acid mine drainage. *Environmental Science and Technology*, 47(21), 12029-12036.

Department for Environment Food & Rural Affairs (2014) *Water Framework Directive implementation in England and Wales: new and updated standards to protect the water environment* London, TSO: Available online: https://assets.publishing.service.gov.uk/government/uploads/system/uploads/attachment_data/file/307788/river-basin-planning-standards.pdf.

Devi, K. S. S., Anantharamkrishnan, A., Krishnan, U. M. & Yakhmi, J. (2020) Chemical Sensors Based on Metal Oxides, in Heidari, H. H. a. H. (ed), *Smart Sensors for Environmental and Medical Applications*, 103-127.

Donnachie, R. L., Johnson, A. C., Moeckel, C., Pereira, M. G. & Sumpter, J. P. (2014) Using risk-ranking of metals to identify which poses the greatest threat to freshwater organisms in the UK. *Environmental Pollution*, 194, 17-23.

Duffus, J. (2002) Heavy metals” a meaningless term? (IUPAC Technical Report). *Pure and Applied Chemistry*, 74, 793-807.

Ebrahimi, A., Withayachumnankul, W., Al-Sarawi, S. & Abbott, D. (2014) High-Sensitivity Metamaterial-Inspired Sensor for Microfluidic Dielectric Characterization. *IEEE Sensors Journal*, 14(5), 1345-1351.

Eddaif, L., Shaban, A. & Telegdi, J. (2019) Sensitive detection of heavy metals ions based on the calixarene derivatives-modified piezoelectric resonators: a review. *International Journal of Environmental Analytical Chemistry*, 99(9), 824-853.

Eltzov, E., Yehuda, A. & Marks, R. S. (2015) Creation of a new portable biosensor for water toxicity determination. *Sensors and Actuators B: Chemical*, 221, 1044-1054.

Environment Agency (2008) *Abandoned mines and the water environment*. Bristol: Environment Agency. Available online: https://assets.publishing.service.gov.uk/government/uploads/system/uploads/attachment_data/file/291482/LIT_8879_df7d5c.pdf.

Environment Agency (2011) *H1 Annex D-Basic Surface water discharges*. Bristol: Environment Agency. Available online: [http://www.fwr.org/WQreg/Appendices/horizontal_Guidance_H1_Annex_D_Surface_Water_Basic_geho0810bsxl-e-e\(1\).pdf](http://www.fwr.org/WQreg/Appendices/horizontal_Guidance_H1_Annex_D_Surface_Water_Basic_geho0810bsxl-e-e(1).pdf).

Environment Agency (2012) *Prioritisation of abandoned noncoal mine impacts on the environment: (SC030136/R2) The national picture*. Environment Agency, Bristol: Available online: https://assets.publishing.service.gov.uk/government/uploads/system/uploads/attachment_data/file/290866/scho1111bubx-e-e.pdf.

Environment Agency Wales (2002) *Metal Mine - Strategy for Wales*. Available online: <https://naturalresources.wales/media/680181/metal-mines-strategy-for-wales-2.pdf>.

PROGRAMME OF ACTION OF THE EUROPEAN COMMUNITIES ON THE ENVIRONMENT (1973), Chapter European Union: <https://eur-lex.europa.eu/legal-content/EN/TXT/HTML/?uri=CELEX:41973X1220&rid=1>.

European Parliamentary Research Service (EPRS) (2018) *Environment action programme. Living well, within the limits of our planet*. Available online: [http://www.europarl.europa.eu/RegData/etudes/BRIE/2018/630336/EPRS_BRI\(2018\)630336_EN.pdf](http://www.europarl.europa.eu/RegData/etudes/BRIE/2018/630336/EPRS_BRI(2018)630336_EN.pdf).

Fernández, B., Lobo, L. & Pereiro, R. (2019) Atomic Absorption Spectrometry | Fundamentals, Instrumentation and Capabilities, in Worsfold, P., Poole, C., Townshend, A. & Miró, M. (eds), *Encyclopedia of Analytical Science (Third Edition)*. Oxford: Academic Press, 137-143.

Ferrari, V. & Prudenziati, M. (2012) 8 - Printed thick-film capacitive sensors, *Printed Films* Woodhead Publishing, 193-220.

Frau, I., Korostynska, O., Byrne, P. & Mason, A. (2017) Feasibility of in-situ quality assessment of zinc contamination in water, *2017 IEEE First Ukraine Conference on Electrical and Computer Engineering (UKRCON)*. 29 May-2 June 2017.

Frau, I., Korostynska, O., Mason, A. & Byrne, P. (2018a) Comparison of Electromagnetic Wave Sensors with Optical and Low-frequency Spectroscopy Methods for Real-time Monitoring of Lead Concentrations in Mine Water. *Mine Water and the Environment*, 37(3), 617-624.

Frau, I., Wylie, S., Byrne, P., Cullen, J., Korostynska, O. & Mason, A. (2018b) Continuous Detection of Copper and Bromide in Polluted Water using f-EM Sensors, *2018 12th International Conference on Sensing Technology (ICST)*. 4-6 Dec. 2018.

Frau, I., Wylie, S., Byrne, P., Cullen, J., Korostynska, O. & Mason, A. (2018c) Screen-Printed f-EM Sensors Based on Two Chelating-Polymers and a Metal Oxide for the Continuous Detection of Cu Ions in Surface Water. *Proceedings*, 2(13), 828.

Frau, I., Wylie, S., Byrne, P., Cullen, J., Korostynska, O. & Mason, A. (2019a) Detection of Zn in water using novel functionalised planar microwave sensors. *Materials Science and Engineering: B*, 247, 114382.

- Frau, I., Wylie, S., Cullen, J., Korostynska, O., Byrne, P. & Mason, A. (2019b) Microwaves and Functional Materials: A Novel Method to Continuously Detect Metal Ions in Water, in Mukhopadhyay, S. C., Jayasundera, K. P. & Postolache, O. A. (eds), *Modern Sensing Technologies*. Cham: Springer International Publishing, 179-201.
- Frau, I., Wylie, S. R., Byrne, P., Cullen, J. D., Korostynska, O. & Mason, A. (2020) Functionalised microwave sensors for real-time monitoring of copper and zinc concentration in mining-impacted water. *International Journal of Environmental Science and Technology*, 17(4), 1861-1876.
- Gao, Y. & Bradshaw, A. D. (1995) The containment of toxic wastes: II. Metal movement in leachate and drainage at Parc lead-zinc mine, North Wales. *Environmental Pollution*, 90(3), 379-382.
- Gennarelli, G. & Soldovieri, F. (2013) A non-specific microwave sensor for water quality monitoring. *International Water Technology Journal*, 3(2), 70-77.
- Gogoi, H., Leiviskä, T., Heiderscheidt, E., Postila, H. & Tanskanen, J. (2018) Removal of metals from industrial wastewater and urban runoff by mineral and bio-based sorbents. *Journal of Environmental Management*, 209, 316-327.
- Gozzard, E., Mayes, W. M., Potter, H. A. B. & Jarvis, A. P. (2011) Seasonal and spatial variation of diffuse (non-point) source zinc pollution in a historically metal mined river catchment, UK. *Environmental Pollution*, 159(10), 3113-3122.
- Graunke, T., Schmitt, K., Busch, S., Raible, S. & Wöllenstein, J. (2018) Towards an Empirical Model for the Prediction of the Selectivity of Polymer Membranes. *Proceedings*, 2(13), 979.
- Greene, J., Abdullah, B., Cullen, J., Korostynska, O., Louis, J. & Mason, A. (2019) Non-invasive Monitoring of Glycogen in Real-Time Using an Electromagnetic Sensor, in Mukhopadhyay, S. C., Jayasundera, K. P. & Postolache, O. A. (eds), *Modern Sensing Technologies*. Cham: Springer International Publishing, 1-15.
- Guang, S. X. & Kim, S. (2008) Formation of some cysteine-containing peptide monolayers on Au electrodes and their applications for metal ion sensing and electrocatalytic reactions. *Bulletin of the Korean Chemical Society*, 29(7), 1301-1302.
- Gumpu, M. B., Sethuraman, S., Krishnan, U. M. & Rayappan, J. B. B. (2015) A review on detection of heavy metal ions in water – An electrochemical approach. *Sensors and Actuators B: Chemical*, 213, 515-533.
- Guo, Z., Niu, Q., Li, T., Sun, T. & Chi, H. (2019) A fast, highly selective and sensitive colorimetric and fluorescent sensor for Cu²⁺ and its application in real water and food samples. *Spectrochimica Acta Part A: Molecular and Biomolecular Spectroscopy*, 213, 97-103.

- Halkare, P., Punjabi, N., Wangchuk, J., Nair, A., Kondabagil, K. & Mukherji, S. (2019) Bacteria functionalized gold nanoparticle matrix based fiber-optic sensor for monitoring heavy metal pollution in water. *Sensors and Actuators B: Chemical*, 281, 643-651.
- Harnsoongnoen, S., Wanthong, A., Charoen-In, U. & Siritaratiwat, A. (2018) Planar microwave sensor for detection and discrimination of aqueous organic and inorganic solutions. *Sensors and Actuators B: Chemical*, 271, 300-305.
- Harnsoongnoen, S., Wanthong, A., Charoen-In, U. & Siritaratiwat, A. (2019) Microwave Sensor for Nitrate and Phosphate Concentration Sensing. *IEEE Sensors Journal*, 19(8), 2950-2955.
- Harris, D. C. (2007) *Quantitative Chemical Analysis*, Seventh Edition edition. New York: W.H. Freeman.
- Harrison, L., Ravan, M., Tandel, D., Zhang, K., Patel, T. & K Amineh, R. (2020) Material Identification Using a Microwave Sensor Array and Machine Learning, 9, 288-299.
- Hassanein, A., Salahuddin, N., Matsuda, A., Kawamura, G. & Elfiky, M. (2017) Fabrication of biosensor based on Chitosan-ZnO/Polypyrrole nanocomposite modified carbon paste electrode for electroanalytical application. *Materials Science and Engineering: C*, 80(Supplement C), 494-501.
- Heifetz, A., Bakhtiari, S., Juan, L., Aranson, I. S., Vinokur, V. M. & Bentivegna, A. F. (2017) Development of microwave and impedance spectroscopy methods for in-situ nondestructive evaluation of alkali silica reaction in concrete, *43rd Annual Review of Progress in Quantitative Nondestructive Evaluation, 17-22 July 2016*. USA: AIP - American Institute of Physics.
- Holmes, J., Pathirathna, P. & Hashemi, P. (2019) Novel Frontiers in Voltammetric Trace Metal Analysis: Towards Real Time, On-Site, In Situ Measurements. *TrAC Trends in Analytical Chemistry*, 111, 206-219.
- Hrubesh, L. W. (1973) MICROWAVE ROTATIONAL SPECTROSCOPY: A TECHNIQUE FOR SPECIFIC POLLUTANT MONITORING. *Radio Science*, 8(3), 167-175.
- Huang, Y., Cheng, P. & Tan, C. (2019) Visual artificial tongue for identification of various metal ions in mixtures and real water samples: a colorimetric sensor array using off-the-shelf dyes. *RSC Advances*, 9(47), 27583-27587.
- Hudson-Edwards, K. (2016) Tackling mine wastes. *Science*, 352(6283), 288-290.
- Hudson-Edwards, K. A., Schell, C. & Macklin, M. G. (1999) Mineralogy and geochemistry of alluvium contaminated by metal mining in the Rio Tinto area, southwest Spain. *Applied Geochemistry*, 14(8), 1015-1030.

- Hudson, E., Kulesa, B., Edwards, P., Williams, T. & Walsh, R. (2018) Integrated Hydrological and Geophysical Characterisation of Surface and Subsurface Water Contamination at Abandoned Metal Mines. *Water, Air, & Soil Pollution*, 229(8), 256.
- Hwang, G. H., Han, W. K., Park, J. S. & Kang, S. G. (2008) An electrochemical sensor based on the reduction of screen-printed bismuth oxide for the determination of trace lead and cadmium. *Sensors and Actuators, B: Chemical*, 135(1), 309-316.
- Igreja, R. & Dias, C. J. (2006) Dielectric response of interdigital chemocapacitors: The role of the sensitive layer thickness. *Sensors and Actuators B: Chemical*, 115(1), 69-78.
- Iqbal, J., Yiping, D. U., Howari, F., Bataineh, M., Muhammad, N. & Rahim, A. (2017) Simultaneous Enrichment and On-line Detection of Low-Concentration Copper, Cobalt, and Nickel Ions in Water by Near-Infrared Diffuse Reflectance Spectroscopy Combined with Chemometrics. *Journal of AOAC International*, 100(2), 560-565.
- Islam, T. & Mukhopadhyay, S. C. (2017) Wearable sensors for physiological parameters measurement: physics, characteristics, design and applications, *Wearable Sensors*[eBook].IOP Publishing, 1-1-1-31.
- Ismail, A., Kawde, A., Muraza, O., Sanhoob, M. A., Aziz, M. A. & Al-Betar, A. R. (2019) Modified Lanthanum–Zeolite for Sensitive Electrochemical Detection of Heavy Metal Ions. *Arabian Journal for Science and Engineering*, 44(1), 217-226.
- Jarvis, A. P., Davis, J. E., Orme, P. H. A., Potter, H. A. B. & Gandy, C. J. (2019) Predicting the Benefits of Mine Water Treatment under Varying Hydrological Conditions using a Synoptic Mass Balance Approach. *Environ Sci Technol*, 53(2), 702-709.
- Jiao, Z., Zhang, P., Chen, H., Li, C., Chen, L., Fan, H. & Cheng, F. (2019) Differentiation of heavy metal ions by fluorescent quantum dot sensor array in complicated samples. *Sensors and Actuators B: Chemical*, 295, 110-116.
- Jilani, M. T., Rehman, M. Z. u., Khan, A. M., Khan, M. T. & Ali, S. M. (2012) A Brief Review of Measuring Techniques for Characterization of Dielectric Materials. *International Journal of Information Technology and Electrical Engineering*, 1(1).
- Johnson, D. B. (2003) Chemical and Microbiological Characteristics of Mineral Spoils and Drainage Waters at Abandoned Coal and Metal Mines. *Water, Air and Soil Pollution: Focus*, 3(1), 47-66.
- Kadara, R. O., Jenkinson, N. & Banks, C. E. (2009) Disposable Bismuth Oxide Screen Printed Electrodes for the High Throughput Screening of Heavy Metals. *Electroanalysis*, 21(22), 2410-2414.
- Kapilevich, B. & Litvak, B. (2007) Microwave sensor for accurate measurements of water solution concentrations, *2007 Asia-Pacific Microwave Conference*. 11-14 Dec. 2007.

- Khaleghi, S. S. M., Moradi, G., Shirazi, R. S. & Jafargholi, A. (2019) Microstrip Line Impedance Matching Using ENZ Metamaterials, Design, and Application. *IEEE Transactions on Antennas and Propagation*, 67(4), 2243-2251.
- Kilpijärvi, J., Halonen, N., Juuti, J. & Hannu, J. (2019) Microfluidic Microwave Sensor for Detecting Saline in Biological Range. *Sensors*, 19(4), 819.
- Kim, H., Jang, G. & Yoon, Y. (2020) Specific heavy metal/metalloid sensors: current state and perspectives. *Applied Microbiology and Biotechnology*, 104, 907–914.
- Kohl, M., Veltl, G. & Busse, M. (2014) Printed Sensors Produced via Thick-film Technology for the Use in Monitoring Applications. *Procedia Technology*, 15, 107-113.
- Koneswaran, M. & Narayanaswamy, R. (2009) l-Cysteine-capped ZnS quantum dots based fluorescence sensor for Cu²⁺ ion. *Sensors and Actuators B: Chemical*, 139(1), 104-109.
- Kopitzke, S. & Geissinger, P. (2014) An Optical Fiber-Based Sensor Array for the Monitoring of Zinc and Copper Ions in Aqueous Environments. *Sensors*, 14(2), 3077-94.
- Korostynska, O., Mason, A. & Al-Shamma'a, A. I. (2012) Proof-of-concept microwave sensor on flexible substrate for real-time water composition analysis, *2012 Sixth International Conference on Sensing Technology (ICST 2012), 18-21 Dec. 2012*. Piscataway, NJ, USA: IEEE.
- Korostynska, O., Mason, A. & Al-Shamma'a, A. I. (2013a) Flexible microwave sensors for real-time analysis of water contaminants. *Journal of Electromagnetic Waves and Applications*, 27(16), 2075-2089.
- Korostynska, O., Mason, A. & Al-Shamma'a, A. I. (2013b) Monitoring pollutants in wastewater: traditional lab based versus modern real-time approaches, in Mukhopadhyay, S. C. & Mason, A. (eds), *Smart Sensors for Real-Time Water Quality Monitoring*. Berlin, Heidelberg: Springer Berlin Heidelberg, 1-24.
- Korostynska, O., Mason, A. & Byrne, P. (2016) The use of electromagnetic sensors to determine heavy metal content in mine waters, *16th International Multidisciplinary Scientific GeoConference SGEM 2016*. June 28 - July 6, 2016. Libadmin2016, 765-772 pp.
- Korostynska, O., Mason, A., Ortoneda-Pedrola, M. & Al-Shamma'a, A. (2014a) Electromagnetic wave sensing of NO₃ and COD concentrations for real-time environmental and industrial monitoring. *Sensors and Actuators B: Chemical*, 198, 49-54.
- Korostynska, O., Ortoneda-Pedrola, M., Mason, A. & Al-Shamma'a, A. I. (2014b) Flexible electromagnetic wave sensor operating at GHz frequencies for instantaneous

concentration measurements of NaCl, KCl, MnCl₂ and CuCl solutions. *Measurement Science and Technology*, 25(6), 065105 (6 pp.).

Kot, P., Muradov, M., Rycroft, S., Pedrola, M. O., Shaw, A., Hemingway, J., Deb, R. & Coleman, M. (2018) Identification of Optimal Frequencies to Determine Alpha-Cypermethrin Using Machine Learning Feature Selection Techniques, *2018 IEEE Congress on Evolutionary Computation (CEC)*. 8-13 July 2018.

Kot, P., Shaw, A., Riley, M., Ali, A. S. & Cotgrave, A. (2017) The Feasibility of Using Electromagnetic Waves in Determining Membrane Failure Through Concrete. *International Journal of Civil Engineering*, 15(2), 355-362.

Kovacs, Z., Bázár, G., Oshima, M., Shigeoka, S., Tanaka, M., Furukawa, A., Nagai, A., Osawa, M., Itakura, Y. & Tsenkova, R. (2016) Water spectral pattern as holistic marker for water quality monitoring. *Talanta*, 147, 598-608.

Laverghetta, T. (2005) *Microwaves and Wireless Simplified*, <http://ebookcentral.proquest.com/lib/ljmu-trial/detail.action?docID=231642>. Norwood, UNITED STATES: Artech House.

Leng, T., Pan, K., Zhang, Y., Li, J., Afroj, S., Novoselov, K. S. & Hu, Z. (2019) Screen-Printed Graphite Nanoplate Conductive Ink for Machine Learning Enabled Wireless Radio-Frequency-Identification Sensors. *ACS Applied Nano Materials*, 10.1021/acsanm.9b01034.

Li, F., Zheng, Y., Hua, C. & Jian, J. (2019) Gas Sensing by Microwave Transduction: Review of Progress and Challenges. *Frontiers in Materials*, 6(101).

Li, S., Zhang, C., Wang, S., Liu, Q., Feng, H., Ma, X. & Guo, J. (2018) Electrochemical microfluidics techniques for heavy metal ion detection. *Analyst*, 143(18), 4230-4246.

Liu, H., Wang, Q., Sheng, W., Wang, X., Zhang, K., Du, L. & Zhou, J. (2019) Humidity Sensors with Shielding Electrode Under Interdigitated Electrode. *Sensors*, 19(3), 659.

Long, F., Zhu, A., Shi, H., Wang, H. & Liu, J. (2013) Rapid on-site/in-situ detection of heavy metal ions in environmental water using a structure-switching DNA optical biosensor. *Scientific Reports*, 3, 2308.

Lu, Y., Liang, X., Niyungeko, C., Zhou, J., Xu, J. & Tian, G. (2018) A review of the identification and detection of heavy metal ions in the environment by voltammetry. *Talanta*, 178, 324-338.

Lu, Y., Liu, J., Li, J., Brueshoff, P. J., Pavot, C. M. B. & Brown, A. K. (2003) New highly sensitive and selective catalytic DNA biosensors for metal ions. *Biosensors and Bioelectronics*, 18(5-6), 529-540.

- Lukyanenko, K. A., Denisov, I. A., Sorokin, V. V., Yakimov, A. S., Esimbekova, E. N. & Belobrov, P. I. (2019) Handheld Enzymatic Luminescent Biosensor for Rapid Detection of Heavy Metals in Water Samples. *Chemosensors*, 7(1), 16.
- Macias, G., Sperling, J. R., Peveler, W. J., Burley, G. A., Neale, S. L. & Clark, A. W. (2019) Whisky tasting using a bimetallic nanoplasmonic tongue. *Nanoscale*, 11(32), 15216-15223.
- Mamishiev, A. V., Sundara-Rajan, K., Fumin, Y., Yanqing, D. & Zahn, M. (2004) Interdigital sensors and transducers. *Proceedings of the IEEE*, 92(5), 808-845.
- Manjakkal, L., Synkiewicz, B., Zaraska, K., Cvejic, K., Kulawik, J. & Szwagierczak, D. (2016) Development and characterization of miniaturized LTCC pH sensors with RuO₂ based sensing electrodes. *Sensors and Actuators, B: Chemical*, 223, 641-649.
- Marsay, N. (2018) Is the Remediation at Parys Mountain Successfully Reducing Acid Mine Drainage? *Journal of Environmental Protection*, 9, 540-553.
- Mason, A., Abdullah, B., Muradov, M., Korostynska, O., Al-Shammaa, A., Bjarnadottir, S. G., Lunde, K. & Alvseike, O. (2016) Theoretical basis and application for measuring pork loin drip loss using microwave spectroscopy. *Sensors*, 16(2), 182 (13 pp.).
- Mason, A., Korostynska, O., Louis, J., Cordova-Lopez, L. E., Abdullah, B., Greene, J., Connell, R. & Hopkins, J. (2018a) Non-Invasive In-situ Measurement of Blood Lactate using Microwave Sensors. *IEEE Trans Biomed Eng*, 65(3), 698 - 705.
- Mason, A., Soprani, M., Korostynska, O., Amirthalingam, A., Cullen, J., Muradov, M., Carmona, E. N., Sberveglieri, G., Sberveglieri, V. & Al-Shamma'a, A. (2018b) Real-time microwave, dielectric, and optical sensing of lincomycin and tylosin antibiotics in water: Sensor fusion for environmental safety. *Journal of Sensors*, 2018, 7976105.
- Mayes, W. M., Johnston, D., Potter, H. A. B. & Jarvis, A. P. (2009) A national strategy for identification, prioritisation and management of pollution from abandoned non-coal mine sites in England and Wales. I. *Science of The Total Environment*, 407(21), 5435-5447.
- Mayes, W. M., Potter, H. A. B. & Jarvis, A. P. (2010) Inventory of aquatic contaminant flux arising from historical metal mining in England and Wales. *Science of The Total Environment*, 408(17), 3576-3583.
- Mayes, W. M., Potter, H. A. B. & Jarvis, A. P. (2013) Riverine flux of metals from historically mined orefields in England and Wales. *Water, Air, & Soil Pollution*, 224(2), 1425 (14 pp.).
- Medas, D., Cidu, R., Lattanzi, P., Podda, F., Wanty, R. B. & De Giudici, G. (2012) Hydrozincite seasonal precipitation at Naracauli (Sardinia – Italy): Hydrochemical

factors and morphological features of the biomineralization process. *Applied Geochemistry*, 27(9), 1814-1820.

Meier, R. J. (2005) On art and science in curve-fitting vibrational spectra. *Vibrational Spectroscopy*, 39(2), 266-269.

Modern Water (2012) *PDV6000 plus - portable trace metals analyser: Operation manual* Available online: [Accessed].

Moejes, K., Sherif, R., Dürr, S., Conlan, S., Mason, A. & Korostynska, O. (2018) Real-Time Monitoring of *Tetraselmis suecica* in A Saline Environment as Means of Early Water Pollution Detection. *Toxics*, 6(4), 57.

Mohammadi, S., Nadaraja, A. V., Roberts, D. J. & Zarifi, M. H. (2020a) Real-time and hazard-free water quality monitoring based on microwave planar resonator sensor. *Sensors and Actuators A: Physical*, 303, 111663.

Mohammadi, S., Wiltshire, B., Chajer Jain, M., V. N, A., Golovin, K., Roberts, D. & Zarifi, M. H. (2020b) Gold Coplanar Waveguide Resonator Integrated with a Microfluidic Channel for Aqueous Dielectric Detection. *IEEE Sensors Journal*.

Moore, D. (2004) Introduction to salt dilution gauging for streamflow measurement: Part 1. *Streamline: Watershed Management Bulletin Winter 2003/04*, 7(4), 20-23.

Morton, J., Havens, N., Mugweru, A. & Wanekaya, A. K. (2009) Detection of Trace Heavy Metal Ions Using Carbon Nanotube- Modified Electrodes. *Electroanalysis*, 21(14), 1597-1603.

Mukhopadhyay, S. C. & Mason, A. (2015) *Smart sensors for real-time water quality monitoring*, SSMI, 4 Heidelberg: Springer.

Munim, S. A., Saddique, M. T., Raza, Z. A. & Majeed, M. I. (2020) Fabrication of cellulose-mediated chitosan adsorbent beads and their surface chemical characterization. *Polymer Bulletin*, 77(1), 183-196.

Nag, A., Alahi, M. E. E., Feng, S. & Mukhopadhyay, S. C. (2019a) IoT-based sensing system for phosphate detection using Graphite/PDMS sensors. *Sensors and Actuators A: Physical*, 286, 43-50.

Nag, A., Mukhopadhyay, S. C. & Kosel, J. (2019b) *Printed Flexible Sensors: Fabrication, Characterization and Implementation*, SSMI, 33 Springer, Cham.

Nag, A., Zia, A. I., Babu, A. & Mukhopadhyay, S. C. (2015) Printed electronics: present and future opportunities, *2015 9th International Conference on Sensing Technology (ICST)*, 8-10 Dec. 2015. Piscataway, NJ, USA: IEEE.

- Natural Resources Wales (2014) *Abandoned Mine Case Study: Nant y Mwyn Lead Mine*. Natural Resources Wales. Available online: https://naturalresources.wales/media/679805/nant-y-mwyn-mine-case-study_2014_05.pdf.
- Nie, Z., Nijhuis, C. A., Gong, J., Chen, X., Kumachev, A., Martinez, A. W., Narovlyansky, M. & Whitesides, G. M. (2010) Electrochemical sensing in paper-based microfluidic devices. *Lab on a Chip*, 10(4), 477-483.
- Niu, Y., Hu, W., Guo, M., Wang, Y., Jia, J. & Hu, Z. (2019) Preparation of cotton-based fibrous adsorbents for the removal of heavy metal ions. *Carbohydrate Polymers*, 225, 115218.
- Nordstrom, D. K. (2009) Acid rock drainage and climate change. *Journal of Geochemical Exploration*, 100(2), 97-104.
- Nyfors, E. (2000) Industrial Microwave Sensors—A Review. *Subsurface Sensing Technologies and Applications*, 1(1), 23-43.
- O'Flynn, B., Regan, F., Lawlor, A., Wallace, J., Torres, J. & O'Mathuna, C. (2010) Experiences and recommendations in deploying a real-time, water quality monitoring system. *Measurement Science and Technology*, 21(12), 4004-4014.
- Oehme, I. & Wolfbeis, O. S. (1997) Optical sensors for determination of heavy metal ions. *Microchimica Acta*, 126(3), 177-192.
- Onnis, P., Byrne, P., Hudson-Edwards, K. A., Stott, T. & Hunt, C. (2018) Source Apportionment of Trace Metals Over a Range of Stream Flows Using a Multi-method Tracer Approach, *11th ICARD / IMWA / MWD Conference – “Risk to Opportunity”*. Pretoria, South Africa (Tshwane University of Technology)
- Oon, C. S., Ateeq, M., Shaw, A., Wylie, S., Al-Shamma'a, A. & Kazi, S. N. (2016) Detection of the gas-liquid two-phase flow regimes using non-intrusive microwave cylindrical cavity sensor. *Journal of Electromagnetic Waves and Applications*, 30(17), 2241-2255.
- Ozturk, T. (2019) Classification of measured unsafe liquids using microwave spectroscopy system by multivariate data analysis techniques. *Journal of Hazardous Materials*, 363, 309-315.
- Parat, C. & Pinheiro, J. P. (2015) ISIDORE, a probe for in situ trace metal speciation based on Donnan membrane technique with related electrochemical detection part 1: Equilibrium measurements. *Analytica Chimica Acta*, 896, 1-10.
- Patil, S. & Puri, V. (2010) Effect of bismuth oxide thick film overlay on microstrip patch antenna. *Microelectronics International*, 27(2), 79-83.

- Pearson, D., Weindorf, D. C., Chakraborty, S., Li, B., Koch, J., Van Deventer, P., de Wet, J. & Kusi, N. Y. (2018) Analysis of metal-laden water via portable X-ray fluorescence spectrometry. *Journal of Hydrology*, 561, 267-276.
- Perkins, W. T., Bird, G., Jacobs, S. R. & Devoy, C. (2016) Field-scale study of the influence of differing remediation strategies on trace metal geochemistry in metal mine tailings from the Irish Midlands. *Environmental Science and Pollution Research*, 23(6), 5592-5608.
- Priya, T., Dhanalakshmi, N., Thennarasu, S. & Thinakaran, N. (2017) A novel voltammetric sensor for the simultaneous detection of Cd 2+ and Pb 2+ using graphene oxide/ κ -carrageenan/L-cysteine nanocomposite, 182, 199-206.
- Prudenziati, M. & Hormadaly, J. (2012) 1 - Technologies for printed films, in Prudenziati, M. & Hormadaly, J. (eds), *Printed Films* Woodhead Publishing, 3-29.
- Puangngernmak, N. & Chalermwisutkul, S. (2014) Characterization of Heavy Metal Contaminated Wastewater using a Coaxial Sensor and Electromagnetic Wave Reflection Technique. *Applied Mechanics and Materials*, 548-549, 678-82.
- Pujol, L., Evrard, D., Groenen-Serrano, K., Freyssinier, M., Ruffien-Cizsak, A. & Gros, P. (2014) Electrochemical sensors and devices for heavy metals assay in water: the French groups' contribution. *Front Chem*, 2, 19.
- Radovanović, M., Vasiljević, D., Krstić, D., Antić, I., Korzhyk, O., Stojanović, G. & Škrbić, B. D. (2019) Flexible sensors platform for determination of cadmium concentration in soil samples. *Computers and Electronics in Agriculture*, 166, 105001.
- Rahman, M. M., Alam, M. M. & Asiri, A. M. (2018) Sensitive 1,2-dichlorobenzene chemi-sensor development based on solvothermally prepared FeO/CdO nanocubes for environmental safety. *Journal of Industrial and Engineering Chemistry*, 62, 392-400.
- Rahman, N. A., Zakaria, Z., Rahim, R. A., Dasril, Y. & Mohd Bahar, A. A. (2017) Planar Microwave Sensors for Accurate Measurement of Material Characterization: A Review. *TELKOMNIKA*, 15(3), 1108-1118.
- Reimhult, E. & Höök, F. (2015) Design of Surface Modifications for Nanoscale Sensor Applications. *Sensors (Basel, Switzerland)*, 15(1), 1635-1675.
- Reyes-Vera, E., Acevedo-Osorio, G., Arias-Correa, M. & Senior, D. E. (2019) A Submersible Printed Sensor Based on a Monopole-Coupled Split Ring Resonator for Permittivity Characterization. *Sensors*, 19(8), 1936.
- Salim, A. & Lim, S. (2018) Review of Recent Metamaterial Microfluidic Sensors. *Sensors*, 18(1), 232.

- Salim, A., Memon, M. & Lim, S. (2018) Simultaneous Detection of Two Chemicals Using a TE₂₀-Mode Substrate-Integrated Waveguide Resonator. *Sensors*, 18(3), 811.
- Savosina, J., Agafonova-Moroz, M., Yaroshenko, I., Ashina, J., Babain, V., Lumpov, A., Legin, A. & Kirsanov, D. (2020) Plutonium (IV) Quantification in Technologically Relevant Media Using Potentiometric Sensor Array. *Sensors*, 20(6), 1604.
- Scottish Environment Protection Agency (SEPA) (2011) *Review of metal concentrations data held for Glengonnar Water and Wanlock Water, South Central Scotland*. Available online: https://www.sepa.org.uk/media/163236/metals_glengonnar_wanlock_waters_review.pdf.
- Sen Gupta, S. & Bhattacharyya, K. G. (2011) Kinetics of adsorption of metal ions on inorganic materials: A review. *Advances in Colloid and Interface Science*, 162(1-2), 39-58.
- Serrano, N., Alberich, A., Díaz-Cruz, J. M., Ariño, C. & Esteban, M. (2013) Coating methods, modifiers and applications of bismuth screen-printed electrodes. *TrAC Trends in Analytical Chemistry*, 46, 15-29.
- Sharafadinzadeh, N., Abdolrazzahi, M. & Daneshmand, M. (2020) Investigation on planar microwave sensors with enhanced sensitivity from microfluidic integration. *Sensors and Actuators, A: Physical*, 301.
- Shimizu, F., Braunger, M. & Riul Jr, A. (2019) Heavy Metal/Toxins Detection Using Electronic Tongues. *Chemosensors*, 7, 36.
- Smith, K. S. (1999) *Metal sorption on mineral surfaces: an overview with examples relating to mineral deposits, Volume 6A; Reviews in Economic Geology, Society of Economic Geologists*.
- Švancara, I., Prior, C., Hočevar, S. B. & Wang, J. (2010) A Decade with Bismuth-Based Electrodes in Electroanalysis. *Electroanalysis*, 22(13), 1405-1420.
- Takaluoma, E., Pikkarainen, T. & Kemppainen, K. (2018) Adsorption And Desorption Of Metals Onto Reusable Adsorbent, *11th ICARD / IMWA / WISA MWD 2018 Conference – Risk to Opportunity*. Pretoria, South Africa (Tshwane University of Technology)
- Tang, X., Wang, P.-Y. & Buchter, G. (2018) Ion-Selective Electrodes for Detection of Lead (II) in Drinking Water: A Mini-Review. *Environments*, 5(9), 95.
- Tanguy, N., Wiltshire, B., Arjmand, M., Zarifi, M. H. & Yan, N. (2020a) Highly Sensitive and Contactless Ammonia Detection Based on Nanocomposites of Phosphate Functionalized Reduced Graphene Oxide/Polyaniline Immobilized on Microstrip Resonators. *ACS Applied Materials & Interfaces*, 10.1021/acsami.9b21063.

- Tanguy, N., Wiltshire, B., Arjmand, M., Zarifi, M. H. & Yan, N. (2020b) Highly Sensitive and Contactless Ammonia Detection Based on Nanocomposites of Phosphate Functionalized Reduced Graphene Oxide/Polyaniline Immobilized on Microstrip Resonators. *ACS Applied Materials & Interfaces*, 12(8), 9746–9754.
- Tchounwou, P. B., Yedjou, C. G., Patlolla, A. K. & Sutton, D. J. (2012) Heavy Metals Toxicity and the Environment. *EXS*, 101, 133-164.
- Teka, S., Gaied, A., Jaballah, N., Xiaonan, S. & Majdoub, M. (2016) Thin sensing layer based on semi-conducting β -cyclodextrin rotaxane for toxic metals detection. *Materials Research Bulletin*, 74, 248-257.
- Teng, K. H., Shaw, A., Ateeq, M., Al-Shamma'a, A., Wylie, S., Kazi, S. N., Chew, B. T. & Kot, P. (2017) Design and implementation of a non-invasive real-time microwave sensor for assessing water hardness in heat exchangers. *Journal of Electromagnetic Waves and Applications*, 32(7), 797-811.
- Tesarova, E., Baldrianova, L., Hocevar, S. B., Svancara, I., Vytras, K. & Ogorevc, B. (2009) Anodic stripping voltammetric measurement of trace heavy metals at antimony film carbon paste electrode. *Electrochimica Acta*, 54(5), 1506-1510.
- The Coal Authority (2011) *The impacts of mining on the Glengonnar Water, Leadhills, South Lanarkshire*. Available online: https://www.sepa.org.uk/media/218985/impacts_mining_glengonnar_water.pdf
- The Coal Authority (2018) *Coal Authority wins Welsh contract* Coal Authority press office. Available at: <https://www.gov.uk/government/news/coal-authority-wins-welsh-contract>, 20 November 2018.
- Todoli, J.-L. & Mermet, J.-M. (2008a) 1 - Introduction, in Todoli, J.-L. & Mermet, J.-M. (eds), *Liquid Sample Introduction in ICP Spectrometry*. Amsterdam: Elsevier, 1-2.
- Todoli, J.-L. & Mermet, J.-M. (2008b) 2 - Specifications of a Sample Introduction System to be Used with an ICP, in Todoli, J.-L. & Mermet, J.-M. (eds), *Liquid Sample Introduction in ICP Spectrometry*. Amsterdam: Elsevier, 3-15.
- UK Technical Advisory Group on the Water Framework Directive (2008) *UK environmental standards and conditions (phase 1 - SRI-2006)*. Available online: https://www.wfduk.org/sites/default/files/Media/Environmental%20standards/Environmental%20standards%20phase%201_Finalv2_010408.pdf.
- United States Environmental Protection Agency (1986) *Quality criteria for water*, 440. Washington, DC 20460: EPA.
- Varun, S. & Daniel, S. C. G. K. (2018) Emerging Nanosensing Strategies for Heavy Metal Detection, in Hussain, A. K. M. a. C. M. (ed), *Nanotechnology for Sustainable Water Resources*, 200-224.

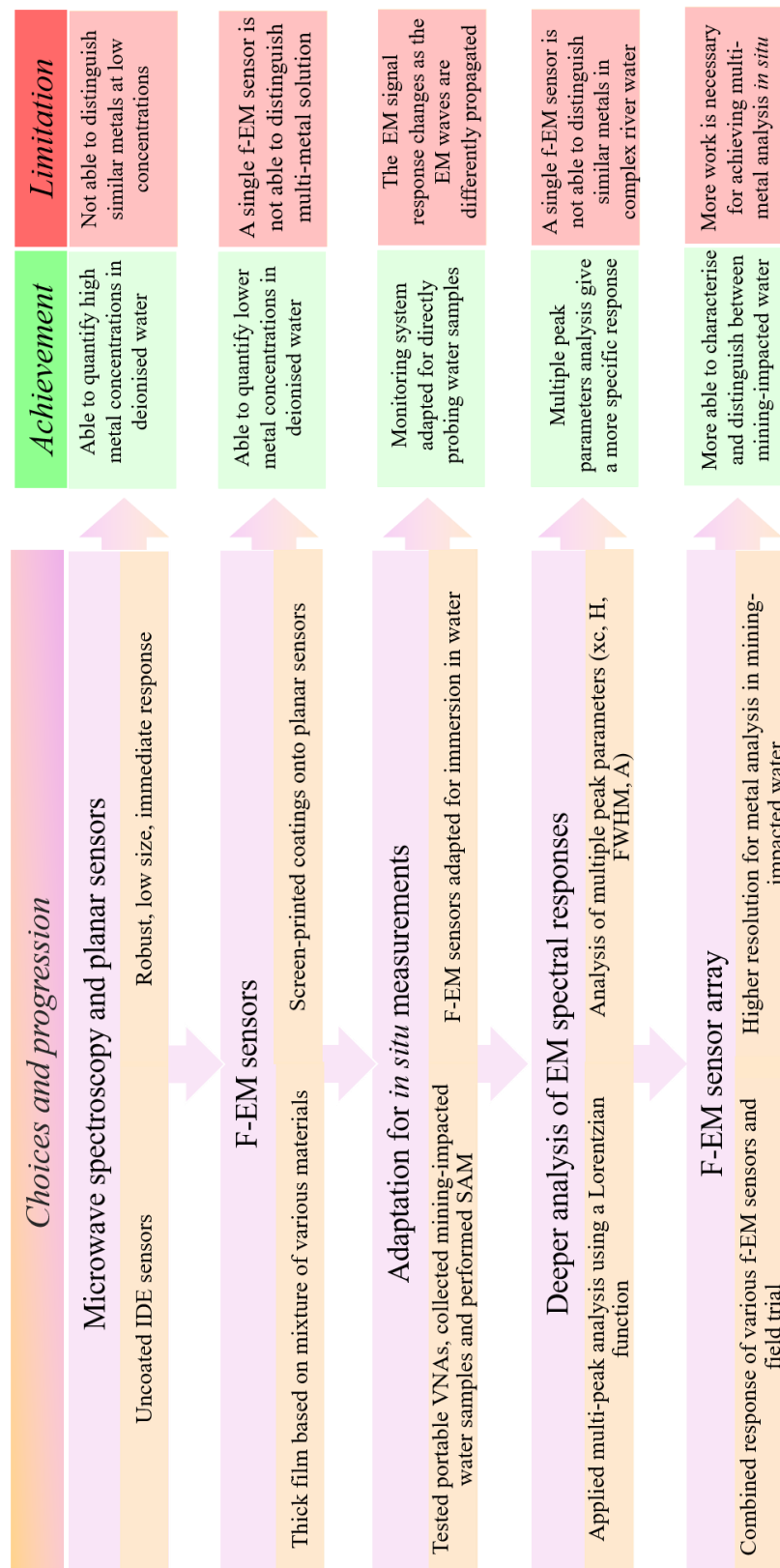
- Vélez, P., Muñoz-Enano, J., Gil, M., Mata-Contreras, J. & Martín, F. (2019) Differential Microfluidic Sensors Based on Dumbbell-Shaped Defect Ground Structures in Microstrip Technology: Analysis, Optimization, and Applications. *Sensors*, 19(14), 3189.
- Verma, R. & Gupta, B. D. (2015) Detection of heavy metal ions in contaminated water by surface plasmon resonance based optical fibre sensor using conducting polymer and chitosan. *Food Chemistry*, 166, 568-575.
- Vlasov, Y., Legin, A. & Rudnitskaya, A. (2002) Electronic tongues and their analytical application. *Analytical and Bioanalytical Chemistry*, 373(3), 136-146.
- Wanekaya, A. K. (2011) Applications of nanoscale carbon-based materials in heavy metal sensing and detection. *Analyst*, 136(21), 4383-4391.
- Wang, L. (2018) Microwave sensors for breast cancer detection. *Sensors (Switzerland)*, 18(2).
- Wang, X., Wang, Y., Leung, H., Mukhopadhyay, S. C., Tian, M. & Zhou, J. (2015) Mechanism and Experiment of Planar Electrode Sensors in Water Pollutant Measurement. *IEEE Transactions on Instrumentation and Measurement*, 64(2), 516-23.
- Wei, Z., Huang, J., Li, J., Xu, G., Ju, Z., Liu, X. & Ni, X. (2018) A High-Sensitivity Microfluidic Sensor Based on a Substrate Integrated Waveguide Re-Entrant Cavity for Complex Permittivity Measurement of Liquids. *Sensors*, 18(11), 4005.
- Wiltshire, B. D. & Zarifi, M. H. (2019) 3D Printing Microfluidic Channels with Embedded Planar Microwave Resonators for RFID and Liquid Detection. *IEEE Microwave and Wireless Components Letters* 29(1), 65-67.
- Wolkersdorfer, C. (2008) *Water Management at Abandoned Flooded Underground Mines — Fundamentals, Tracer Tests, Modelling, Water Treatment*. Heidelberg: Springer.
- Wolkersdorfer, C. & Bowell, R. (2005) Contemporary Reviews of Mine Water Studies in Europe, Part 2. *Mine Water and the Environment*, 24(1), 2-37.
- Wolkersdorfer, C., Bowell, R., O'Sullivan, A. D., Diels, L., Grmela, A., Rapantová, N. a., Pfeifer, H.-R., Dold, B., Midžić, S., Silajdžić, I., Cabral Pinto, M. M. S. & Silva, M. M. V. G. (2012) Erratum to: Contemporary Reviews of Mine Water Studies in Europe, Part 3. *Mine Water and the Environment*, 31(3), 239-239.
- Wong, D., Yesiloz, G., Boybay, M. S. & Ren, C. L. (2016) Microwave temperature measurement in microfluidic devices. *Lab on a Chip*, 16(12), 2192-2197.

- Wooseok, J., Am, J., Bishop, P. L. & Ahn, C. H. (2011) A polymer lab chip sensor with microfabricated planar silver electrode for continuous and on-site heavy metal measurement. *Sensors and Actuators: B Chemical*, 155(1), 145-53.
- Yaroshenko, I., Kirsanov, D., Marjanovic, M., Lieberzeit, P. A., Korostynska, O., Mason, A., Frau, I. & Legin, A. (2020) Real-Time Water Quality Monitoring with Chemical Sensors. *Sensors*, 20(12), 3432.
- Yarur, F., Macairan, J.-R. & Naccache, R. (2019) Ratiometric detection of heavy metal ions using fluorescent carbon dots. *Environmental Science: Nano*, 6(4), 1121-1130.
- Younger, P. L., Banwart, S. A. & Hedin, R. S. (2002) *Hydrology, Pollution, Remediation*. Dordrecht.: Kluwer Academic Publishers.
- Yuan, Y., Feng, S., Alahi, M., Nag, A., Afsarimanesh, N., Zhang, H. & He, S. (2018) Development of an Internet of Things Based Electrochemical Microfluidic System for Free Calcium Detection. *Applied Sciences*, 8(8), 1357.
- Zarifi, M. H. & Daneshmand, M. (2016) Liquid sensing in aquatic environment using high quality planar microwave resonator. *Sensors and Actuators B: Chemical*, 225(Supplement C), 517-521.
- Zarifi, M. H., Deif, S., Abdolrazzaghi, M., Chen, B., Ramsawak, D., Amyotte, M., Vahabisani, N., Hashisho, Z., Chen, W. & Daneshmand, M. (2018a) A Microwave Ring Resonator Sensor for Early Detection of Breaches in Pipeline Coatings. *IEEE Transactions on Industrial Electronics*, 65(2), 1626-1635.
- Zarifi, M. H., Farsinezhad, S., Abdolrazzaghi, M., Daneshmand, M. & Shankar, K. (2016) Selective microwave sensors exploiting the interaction of analytes with trap states in TiO₂ nanotube arrays. *Nanoscale*, 8(14), 7466-7473.
- Zarifi, M. H., Gholidoust, A., Abdolrazzaghi, M., Shariaty, P., Hashisho, Z. & Daneshmand, M. (2018b) Sensitivity enhancement in planar microwave active-resonator using metal organic framework for CO₂ detection. *Sensors and Actuators B: Chemical*, 255, 1561-1568.
- Zhang, K., K Amineh, R., Dong, Z. & Nadler, D. (2019) Microwave Sensing of Water Quality. *IEEE Access*, 7, 69481 - 69493.
- Zhao, W., Gan, H., He, L., Liu, Q., Wang, D., Xu, K., Chen, S., Dong, L. & Wang, G. (2020) Microwave Planar Sensors for Fully Characterizing Magneto-Dielectric Materials. *IEEE Access*, 8, 41985 - 41999.
- Zhou, F., Li, C., Zhu, H. & Li, Y. (2019) A novel method for simultaneous determination of zinc, nickel, cobalt and copper based on UV-vis spectrometry. *Optik*, 182, 58-64.

Zubiarrain-Laserna, A. & Kruse, P. (2020) Review—Graphene-Based Water Quality Sensors. *Journal of The Electrochemical Society*, 167(3), 037539.

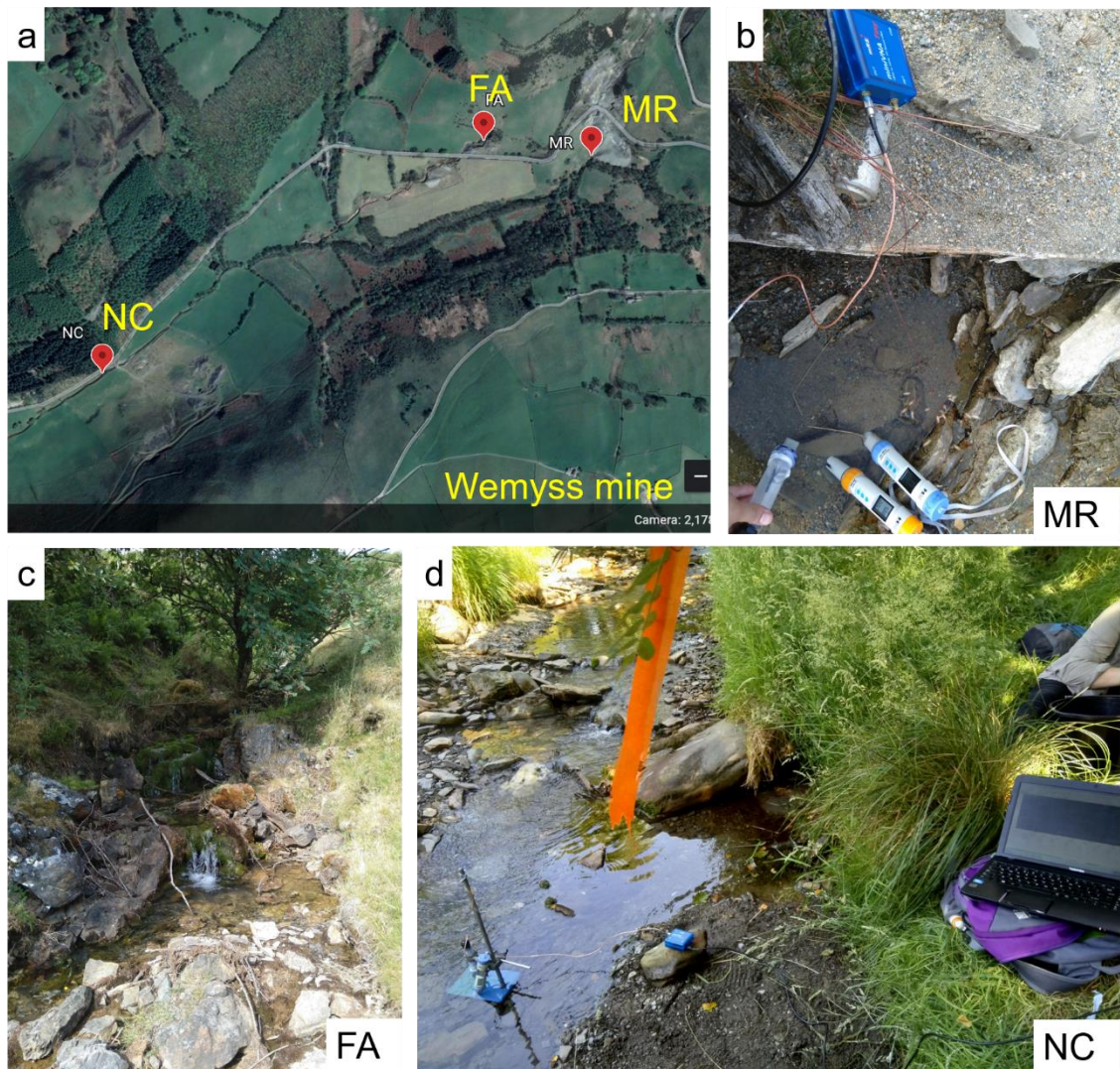
Appendix 1

Smart chart which summarises the progression of the work decided depending on the 1) achievements and the 2) limitations that were identified performing specific experiments.



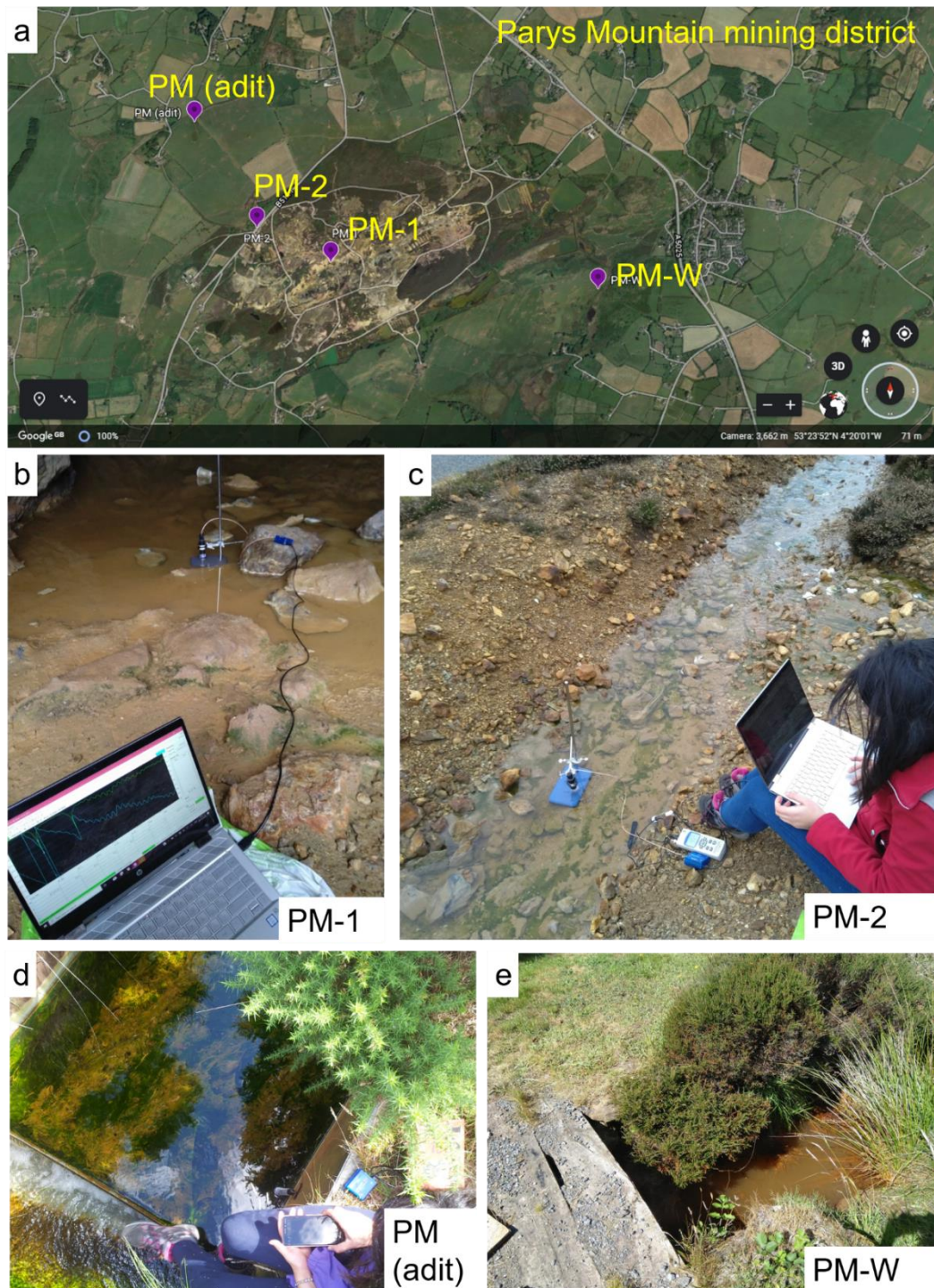
Appendix 2a

Aerial image from GoogleEarth which appoints water sample site in Wemyss mine area (a) and the image of selected samples, MR (b), FA (c) and NC (d), showing some configuration for *in situ* measurements using microwaves and planar immersed f-EM sensors.



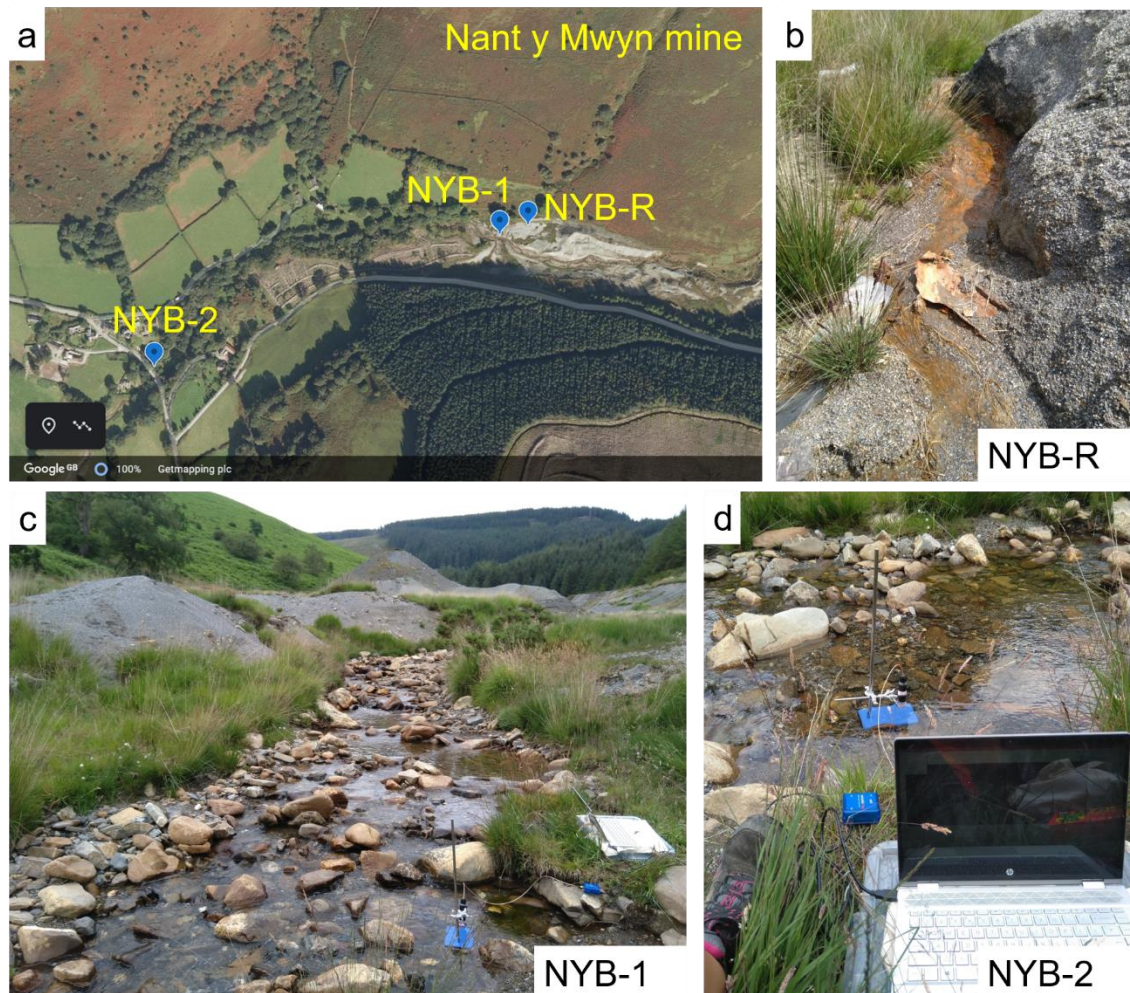
Appendix 2b

Aerial image from GoogleEarth which appoints water sample site in Parys Mountain mining district (a) and the image of selected samples, PM-1 (b), PM-2 (c), PM (d) and PM-W (e), showing some configuration for *in situ* measurements using microwaves and planar immersed f-EM sensors.



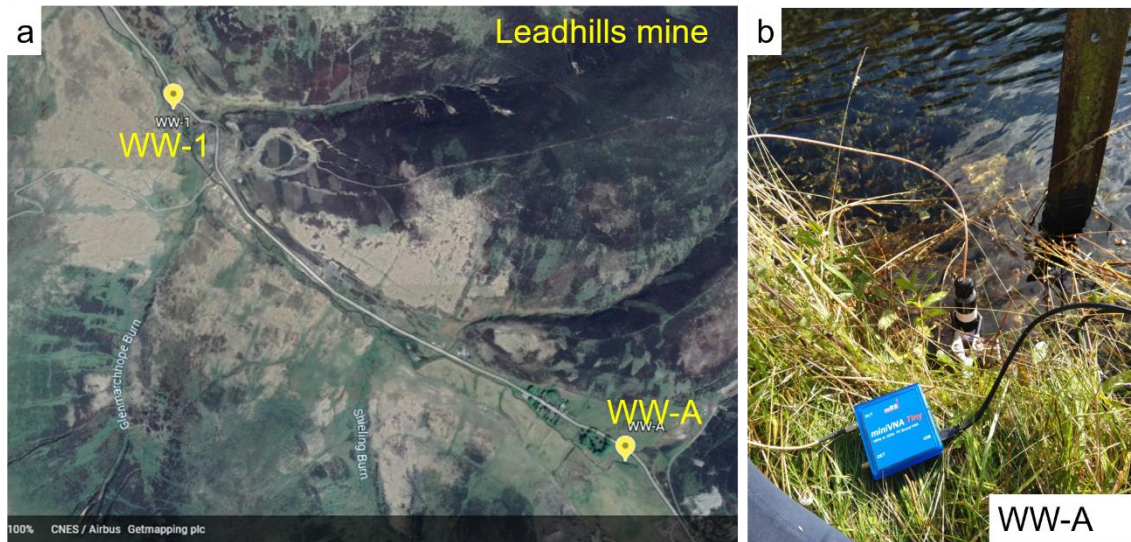
Appendix 2c

Aerial image from GoogleEarth which appoints water sample site in Nant y Mwyn mine (a) and the image of selected samples, NYB-R (b), NYB-1 (c) and NYB-2 (d), showing some configuration for *in situ* measurements using microwaves and planar immersed f-EM sensors.



Appendix 2d

Aerial image from GoogleEarth which appoints water sample site in Leadhills mine (a) and the image of a selected sample, WW-A (b), showing the configuration for *in situ* measurements using microwaves and a planar immersed sensor.



Appendix 3

Table which illustrates physicochemical parameters (EC, pH, T) for mining-impacted water samples measured in both field and lab, when were performed microwave and impedance measurements.

Sample	Mining area	<i>In situ</i>			In lab		
		EC	pH	T	EC	pH	T
		$\mu\text{S/cm}$		$^{\circ}\text{C}$	$\mu\text{S/cm}$		$^{\circ}\text{C}$
FA	Wemyss mine	210	6.65	15	175.1	6.65	19.0
MR	Wemyss mine	89.6	5.94	23	90.6	5.98	19.1
NC	Wemyss mine	115	6.26	19.6	118.0	6.33	19.0
PM	Parys Mountain	3,200	2.44	13.4	3,300	2.45	19.1
PM-1	Parys Mountain	1,634	2.78	10.2	1,715	2.46	19.1
PM-2	Parys Mountain	7,570	1.80	10.8	6,030	1.94	19.0
PM-W	Parys Mountain	249	5.9	18.9	280	6.2	19.0
NYB-1	Nant y Mwyn	87.9	6.62	18.7	87.5	7.12	19.2
NYB-2	Nant y Mwyn	76.1	6.67	14.7	77.0	6.84	19.0
NYB-R	Nant y Mwyn	109.3	6.60	14.8	110.2	6.18	18.9
WW-A	Leadhills mine	162.0	7.52	12.3	183.6	7.6	18/9
WW-1	Leadhills mine	132.0	7.46	10.8	157.7	7.22	19.0

In red: values which should indicate extremely polluted water

Appendix 4

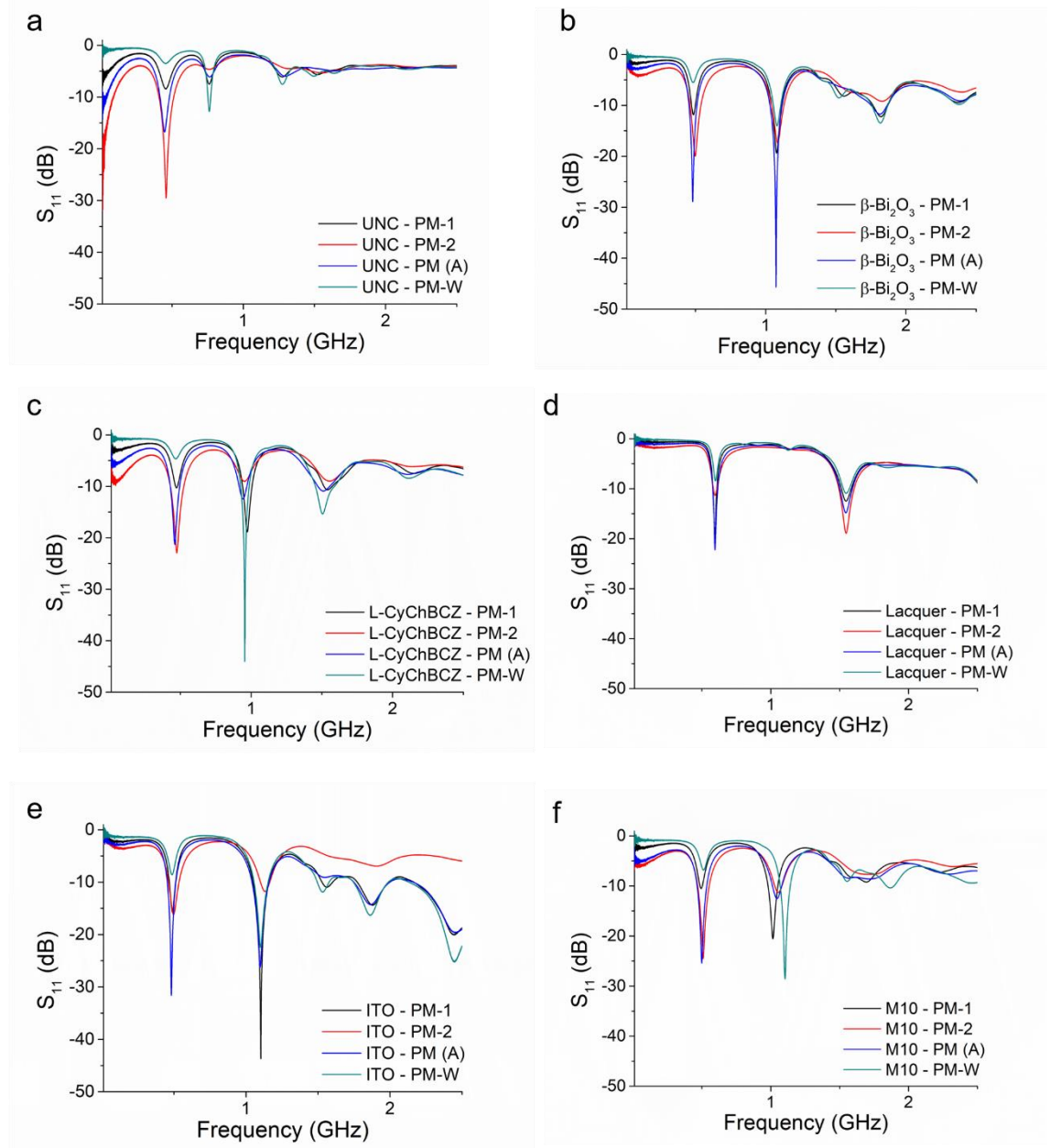
Table which illustrates toxic metal and major cations concentrations for the collected mining-impacted water samples using ICP-MS and/or ICP-OES.

Sample	Zn	Cu	Pb	Cd	Fe	Mn
	µg/L	µg/L	µg/L	µg/L	µg/L	µg/L
FA	9,266.805	<0.0001	229.455	9.719	5.200	1.849
MR	5,876.962	0.0025	2,499.514	6.683	6.073	<0.0001
NC	2,935.171	<0.0001	48.01	<0.0001	5.61	<0.0001
PM	10,640.051	9,657.249	20.897	116.021	44,115.083	10,153.337
PM-1	12,453	7,029.993.	888.582	69.632	86,232.687	52.048
PM-2	13,542.031	25,008.	210.852	48.668	511,223.3	2,594.671
PM-W	1,231.423	1,131.653	12.342	20.993	3,210.617	300.582
NYB-1	951.624	8.116	417.507	5.225	46.708	3.752
NYB-2	754.438	7.856	331.159	3.915	70.577	8.076
NYB-R	1,729.217	68.981	1,970.48	10.685	148.068	8.753
WW-A	109.032	1.002	12.104	1.552	5.002	2.5
WW-1	273.813	3.375	61.949	2.88	54.031	17.00

All values measured using a ICP-MS were accurate (DL<0.0001 µg/L for all measurements).
All values measured using a ICP-MS were accurate precise (CV<0.5%).

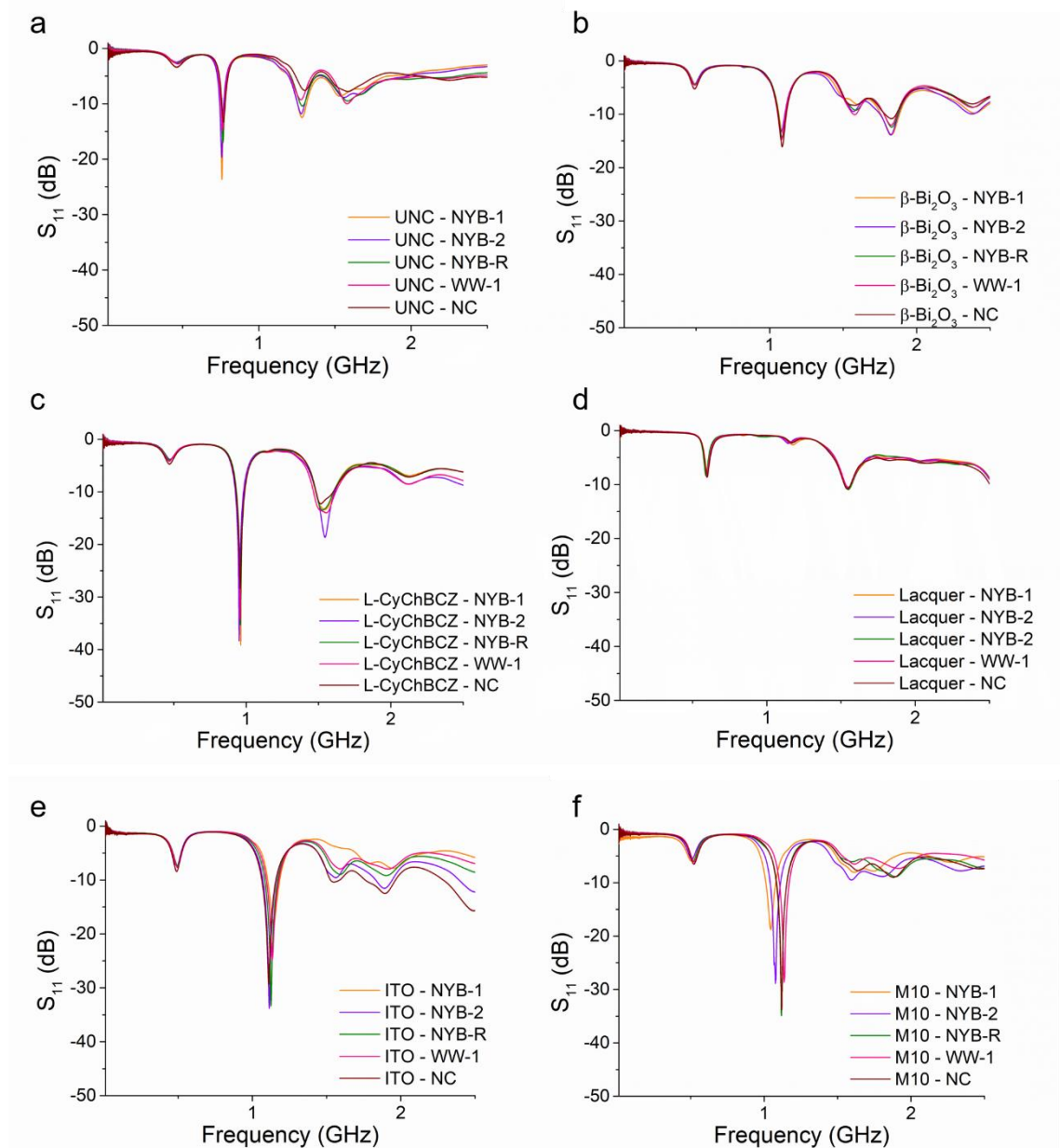
Appendix 5a

Spectral response of the collected mining-impacted water samples in Parys Mountain mining district measured in the laboratory using the ZVA 24 and various developed sensors: uncoated sensor (a) and f-EM sensor based on β - Bi_2O_3 (b), L-CyChBCZ (c), lacquered (d), ITO (e) and M10 (f).



Appendix 5b

Spectral response of the collected mining-impacted water samples in Nant y Mwyn, Leadhills and Wemyss mines measured in the laboratory using the ZVA 24 and various developed sensors: uncoated sensor (a), f-EM sensor based on β - Bi_2O_3 (b), L-CyChBCZ (c), lacquered (d), ITO (e) and M10 (f).



List of publications

The following journal and conference articles, and a book chapter, arose from work presented in this thesis.

Journal articles

Yaroshenko, I., Kirsanov, D., Marjanovic, M., Lieberzeit, P. A., Korostynska, O., Mason, A., Frau, I. & Legin, A. (2020) Real-Time Water Quality Monitoring with Chemical Sensors. *Sensors*, 20(12), 3432.

Frau, I., Wylie, S. R., Byrne, P., Cullen, J. D., Korostynska, O. & Mason, A. (2020) Functionalised microwave sensors for real-time monitoring of copper and zinc concentration in mining-impacted water. *International Journal of Environmental Science and Technology*, 17(4), 1861-1876

Frau, I., Wylie, S., Byrne, P., Cullen, J., Korostynska, O. & Mason, A. (2019) Detection of Zn in water using novel functionalised planar microwave sensors. *Materials Science and Engineering: B*, 247, 114382

Frau, I., Korostynska, O., Mason, A. & Byrne, P. (2018) Comparison of Electromagnetic Wave Sensors with Optical and Low-frequency Spectroscopy Methods for Real-time Monitoring of Lead Concentrations in Mine Water. *Mine Water and the Environment*, 37(3), 617-624.

Book Chapters

Frau, I., Wylie, S., Cullen, J., Korostynska, O., Byrne, P. & Mason, A. (2019) Microwaves and Functional Materials: A Novel Method to Continuously Detect Metal Ions in Water, in Mukhopadhyay, S. C., Jayasundera, K. P. & Postolache, O. A. (eds), *Modern Sensing Technologies*. Cham: Springer International Publishing, 179-201.

Conference Proceedings

Frau, I., Wylie, S., Byrne, P., Cullen, J., Korostynska, O. & Mason, A. (2019). F-EM sensors for monitoring continuously trace metals in mine-impacted water. FET LJMU Research week 2019.

Frau, I., Wylie, S., Byrne, P., Cullen, J., Korostynska, O. & Mason, A. (2018) Continuous Detection of Copper and Bromide in Polluted Water using f-EM Sensors, 2018 12th International Conference on Sensing Technology (ICST). 4-6 Dec. 2018.

Frau, I., Wylie, S., Byrne, P., Cullen, J., Korostynska, O. & Mason, A. (2018) Screen-printed thick films based on L-cysteine-chitosan-ruthenium oxide on planar IDE sensors for EM detection of Cu ions in water. FET LJMU Research week 2018.

Frau, I., Wylie, S., Byrne, P., Cullen, J., Korostynska, O. & Mason, A. (2018) Screen-Printed f-EM Sensors Based on Two Chelating-Polymers and a Metal Oxide for the Continuous Detection of Cu Ions in Surface Water. *Proceedings*, 2(13), 828.

Frau, I., Wylie, S., Byrne, P., Cullen, J., Korostynska, O. & Mason, A. (2018) New sensing system based on electromagnetic waves and functionalised EM sensors for continuous monitoring of Zn in freshwater 11th ICARD | IMWA | MWD Conference – “Risk to Opportunity”. Pretoria, South Africa (Tshwane University of Technology).

Frau, I., Korostynska, O., Byrne, P. & Mason, A. (2017) Continuous monitoring of Zn in water with bismuth oxide thick-film using microwave and electric techniques, 2017 Eleventh International Conference on Sensing Technology (ICST). 4-6 Dec. 2017.

Frau, I., Korostynska, O., Byrne, P. & Mason, A. (2017) Real-time assessment of zinc-polluted water using optical, electrical and microwave techniques, FET LJMU Research week 2017. (Best paper – Third place).

Frau, I., Korostynska, O., Byrne, P. & Mason, A. (2017) Feasibility of in-situ quality assessment of zinc contamination in water, 2017 IEEE First Ukraine Conference on Electrical and Computer Engineering (UKRCON). 29 May-2 June 2017.

Awards

- Excellent paper Presentation, awarded by ICST2018 (Dec 2018) “Continuous detection of copper and bromide in polluted water using f-EM sensors” (Limerick, Ireland).
- Winner of the 2018 SWIG Early Career Researcher poster competition, awarded by Sensors for water interest group (SWIG) at the WWEN Conference (Nov 2018) “Microwaves and Functional Materials: a Novel Method to Continuously Detect Zinc Ions in Water” <http://www.swig.org.uk/announcing-the-winner-of-the-swig-2018-early-career-researcher-prize/> (Telford, UK).
- Third place in FET 3MT competition, awarded by FET, LJMU (Mar 2018) “Monitoring water for healthy living” (Liverpool, UK).
- Third place in Best paper category, awarded by in FET Research week 2017, LJMU (May 2017) “Real-time assessment of zinc pollution of water using optical, electrical and microwave techniques” (Liverpool, UK)